Title

Low-Coordinate Silylarylamido Complexes of Early First-Row Transition Metals

Author

Cai, Irene Chu

Publication Date

2018

Peer reviewed|Thesis/dissertation

Low-Coordinate Silylarylamido Complexes of Early First-Row Transition Metals

by

Irene Chu Cai

A dissertation submitted in partial satisfaction of the requirements

for the degree of

Doctor of Philosophy

in

Chemistry

in the

Graduate Division

of the

University of California, Berkeley

Committee in charge:
Professor T. Don Tilley, Chair
Professor Richard A. Andersen
Professor Alexis T. Bell

Summer 2018

ABSTRACT

Low-Coordinate Silylarylamido Complexes of Early First-Row Transition Metals

by

Irene Chu Cai
Doctor of Philosophy in Chemistry
University of California, Berkeley
Professor T. Don Tilley, Chair

Chapter 1. The amido ligand –N(Si^{i}Pr$_3$)DIPP (DIPP = 2,6-diisopropylphenyl) was used to prepare two-coordinate complexes of Cr^{I}, Cr^{II}, and Cr^{III}. The two-coordinate Cr^{II} complex was employed to prepare a three-coordinate Cr^{III} iodide complex, which then afforded access to a stable Cr^{III} methyl species.

Chapter 2. Products resulting from the reduction of various Cr^{III} complexes supported by the silylarylamido ligand –N(SiMe$_3$)DIPP (DIPP = 2,6-diisopropylphenyl) were synthesized and characterized. The solid state structure of a dimeric chromium species, in which the ligands have undergone C–H bond activation, is also reported.

Chapter 3. Products from reduction and attempted oxidations of low-coordinate manganese complexes supported by silylarylamido ligands –N(SiR$_3$)DIPP$_2$ (R = Me or ^{i}Pr; DIPP = 2,6-diisopropylphenyl) were synthesized and characterized. Steric differences were found to have a noticeable effect on structure and even coordination number. In addition, the reduction of Mn[N(SiMe$_3$)DIPP]$_2$ under nitrogen afforded a dinitrogen-bound dimeric species.

Chapter 4. Divalent complexes of vanadium were synthesized employing bulky silyl(aryl)amido ligands –N(Si^{i}Pr$_3$)DIPP and –N(Si^{t}Bu$_2$Me)DIPP (DIPP = 2,6-diisopropylphenyl). Solid-state structural characterization revealed that although the ligand –N(Si^{i}Pr$_3$)DIPP supports a rare two-coordinate complex of vanadium, its constitutional isomer –N(Si^{t}Bu$_2$Me)DIPP affords a homoleptic complex in which the vanadium center is sandwiched between the arene rings, an unusual binding mode for arylamido ligands. Magnetometry studies indicate that V[N(Si^{i}Pr$_3$)DIPP]$_2$ and V[(η^5-DIPP)N(Si^{t}Bu$_2$Me)]$_2$ have similar high-spin d^3 electron configurations. However, spectroscopic methods, including electron paramagnetic resonance, nuclear magnetic resonance, infrared, and UV-visible spectroscopies, suggest that V[N(Si^{i}Pr$_3$)DIPP]$_2$ is stereochemically nonrigid in solution while V[(η^5-DIPP)N(Si^{t}Bu$_2$Me)]$_2$ is not. This nonrigidity explicitly impacts the reactivity of V[N(Si^{i}Pr$_3$)DIPP]$_2$, which can be used to access both amido-bound and arene-bound complexes. In addition, these divalent complexes exhibit rich reduction and oxidation chemistry. Both vanadium(II) complexes can be reduced to anionic vanadium(I) species, {V[(η^5-DIPP)N(Si^{i}Pr$_3$)]$_2$}$^-$ and {V[(η^5-DIPP)N(Si^{t}Bu$_2$Me)]$_2$}$^-$. Moreover, treatment of V[N(Si^{i}Pr$_3$)DIPP]$_2$ with single and multi-electron oxidants reveals a range of transformations including an intramolecular C–H bond activation.

Low-Coordinate Silylarylamido Complexes of Early First-Row Transition Metals

TABLE OF CONTENTS

TABLE OF CONTENTS i

INTRODUCTION iii

DEDICATION vi

ACKNOWLEDGEMENTS vii

Chapter 1: A Bis(amido) Ligand Set that Supports Two-Coordinate Chromium in the +1, +2, and +3 Oxidation States 1

- Introduction 1
- Results and Discussion 2
- Conclusions 6
- References 7
- Experimental Details 9
- Supplementary Figures 14
- Single-Crystal X-ray Diffraction Crystal Structure Details 16
- References for Experimental Details, Supplementary Figures, and Single-Crystal X-ray Diffraction Crystal Structure Details 27

Chapter 2: Low-Coordinate Chromium in Various Oxidation States Supported by –N(SiMe$_3$)DIPP 28

- Introduction 28
- Results and Discussion 29
- Conclusions 37
- References 38
- Experimental Details 39
- Supplementary Figure 44
- Single-Crystal X-ray Diffraction Crystal Structure Details 45
- References for Experimental Details, Supplementary Figures, and Single-Crystal X-ray Diffraction Crystal Structure Details 62

Chapter 3: Coordination Chemistry of Low-Coordinate Manganese Bis(amido) Complexes 63

Introduction 63

Results and Discussion 64

Conclusions 69

References 70

Experimental Details 71

Single-Crystal X-ray Diffraction Crystal Structure Details 76

References for Experimental Details and Single-Crystal X-ray Diffraction Crystal Structure Details 92

Chapter 4: Divalent Vanadium Complexes Supported by Bulky Silyl(aryl)amido Ligands: Linkage Isomerism and Reactivity of a Two-Coordinate Species 93

Introduction 93

Divalent Vanadium Complexes 94

Electronic Properties and Isomerism 97

Reduced Vanadium Amido Complexes 102

Oxidations of Vanadium Amido Complexes 106

C–H Activation Resulting from Oxidation of Vanadium(II) 108

Concluding Remarks 110

References 111

Experimental Details 113

Supplementary Figures 127

Single-Crystal X-ray Diffraction Crystal Structure Details 144

Computational Details 167

References for Experimental Details, Supplementary Figures, Single-Crystal X-ray Diffraction Crystal Structure Details, and Computational Details 174

CONCLUSION 176

INTRODUCTION

Two-coordinate, open-shell (d^1 – d^9) complexes of first-row transition metals are known to undergo reactions typical of expensive noble metals, due to coordinative unsaturation and electron deficiency at the metal center. Recent work from our group and others has shown that two-coordinate complexes of nickel and iron not only exhibit well-defined stoichiometric reactivity and stability in multiple oxidation states, but can even catalyze bond transformations such as C–C bond formation, alkyne trimerization, and nitrogen reduction.[1–4] Notably, this work on paramagnetic, low-coordinate complexes has benefitted from the scalability and low cost of silyl(aryl)amido ligands of the form –N(SiR$_3$)DIPP (Figure 1, DIPP = 2,6-diisopropylphenyl), which can be used to synthesize low-coordinate species on large scales.

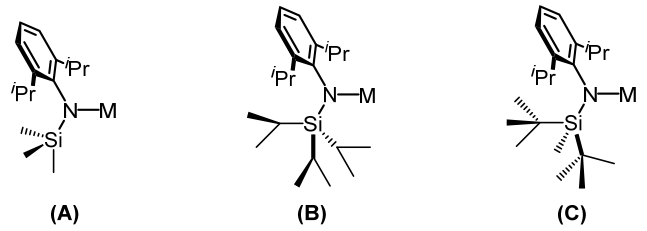

Figure 1: Various silylarylamido ligands. **(A)** –N(SiMe$_3$)DIPP, **(B)** –N(Si^{i}Pr$_3$)DIPP, **(C)** –N(Si^{t}Bu$_2$Me)DIPP.

In particular, the two-coordinate complex Ni[N(SiMe$_3$)DIPP]$_2$, which is stable as both a neutral and anionic species, catalyzes the cross-coupling of aryl halides with Grignard reagents.[2] This catalysis leverages the redox space afforded by the bis(silyl(aryl)amido) framework, which can also be used to support two-coordinate complexes of manganese, iron, cobalt, and copper in both the +1 and +2 oxidation states (Figure 2).[5–8]

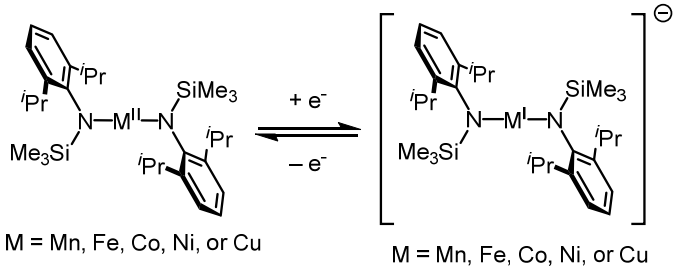

Figure 2: Two-coordinate first-row transition metal complexes supported by –N(SiMe$_3$)DIPP.[5–8]

In contrast to this previous work, my efforts have been geared toward exploring the synthesis and reactivity of two-coordinate complexes of early first-row transition metals, which are more generally more challenging to access than their late transition metal analogs. Prior to the start of my graduate work in October 2013, only two two-coordinate vanadium complexes had been reported[9] and fewer than ten mononuclear two-coordinate chromium species had been structurally characterized.[10] A previously reported attempt to incorporate the –N(SiMe$_3$)DIPP ligand (Figure 1, **A**) into a homoleptic two-coordinate chromium(II) complex resulted in a tetrameric species featuring C–H bond activation of the ligand.[5] Given that –N(SiMe$_3$)DIPP appeared unsuitable for supporting two-coordinate chromium, we hypothesized that by increasing

the steric bulk of the silyl(aryl)amido ligand motif (Figure 1, **B** and **C**), two-coordinate complexes of early transition metals might be isolable and stable in multiple oxidation states.

By using the more sterically demanding silyl(aryl)amido ligand –N(Si^{i}Pr$_3$)DIPP, a two-coordinate complex of chromium(II) was isolated. Further investigation by cyclic voltammetry revealed two-coordinate anionic chromium(I) and cationic chromium(III) analogs, both chemically accessible and isolable, demonstrating the ability of silyl(aryl)amido ligands to support two-coordinate complexes of an early first-row transition metal in three different oxidation states. Oxidation of Cr[N(Si^{i}Pr$_3$)DIPP]$_2$ with iodine followed by addition of methyl Grignard afforded a chromium(III) alkyl complex, demonstrating the viability of using silylarylamido ligands to support various low-coordinate complexes of chromium (Chapter 1).

The synthesis of various two- and three-coordinate chromium complexes supported by the bulky ligand –N(Si^{i}Pr$_3$)DIPP encouraged studies of –N(SiMe$_3$)DIPP as a supporting ligand for both chromium (Chapters 2) and manganese systems (Chapter 3). In spite of previous reports, the ligand –N(SiMe$_3$)DIPP was found to support a range of various low-coordinate chromium complexes, some of which were even capable of polymerizing ethylene without the use of an activator.[11] As a supplement to work on chromium, comparisons of manganese species supported by –N(Si^{i}Pr$_3$)DIPP versus its less sterically demanding analog –N(SiMe$_3$)DIPP also provided insight into the effects of steric bulk on the coordination chemistry of coordinatively unsaturated species.

Gratifyingly, the bulky ligand –N(Si^{i}Pr$_3$)DIPP was also found to readily support a nominally two-coordinate vanadium(II) species. Although both the chromium and manganese analogs retain a two-coordinate structure in both the +2 and the +1 oxidation states, interestingly, the complex V[N(Si^{i}Pr$_3$)DIPP]$_2$ was found to adopt multiple coordination modes, rearranging upon 1 e$^-$ reduction to a vanadium(I) bis(pentadienyl) complex (Figure 3). The linkage isomerism of this rare two-coordinate vanadium species prompted an in-depth spectroscopic investigation of its binding modes, as well as an exploration of oxidation chemistry, including the observation of an intriguing C–H bond activation (Chapter 4).

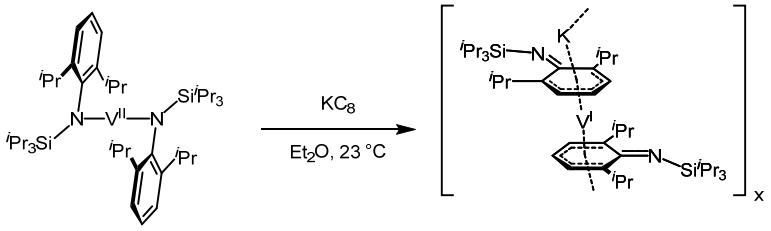

Figure 3: Linkage isomerism of the {V[N(Si^{i}Pr$_3$)DIPP]$_2$} fragment, as a function of oxidation state.

Despite the general challenges associated with working with highly air-sensitive paramagnetic complexes, I have developed several strategies to access two-coordinate early first-row transition metal complexes supported by silyl(aryl)amido ligands. These two-coordinate species and their low-coordinate intermediates have all been characterized by X-ray crystallography, in conjunction with various other techniques such as the Evans method, elemental analysis, UV-visible spectroscopy, cyclic voltammetry, NMR spectroscopy, EPR spectroscopy, and SQUID magnetometry. We expect these studies to inspire further work on two- and three-coordinate systems containing early transition metal centers.

INTRODUCTION REFERENCES

(1) Lipschutz, M. I., Tilley, T. D. *Chem. Commun.* **2012**, *48* (57), 7146–7148.
(2) Lipschutz, M. I., Tilley, T. D. *Angew. Chem. Int. Ed.* **2014**, *53* (28), 7290–7294.
(3) Lipschutz, M. I., Chantarojsiri, T., Dong, Y., Tilley, T. D. *J. Am. Chem. Soc.* **2015**, *137* (19), 6366–6372.
(4) Ung, G., Peters, J. C. *Angew. Chem. Int. Ed.* **2015**, *54* (2), 532–535.
(5) Lin, C.-Y., Guo, J.-D., Fettinger, J. C., Nagase, S., Grandjean, F., Long, G. J., Chilton, N. F., Power, P. P. *Inorg. Chem.* **2013**, *52* (23), 13584–13593.
(6) Lin, C.-Y., Fettinger, J. C., Grandjean, F., Long, G. J., Power, P. P. *Inorg. Chem.* **2014**, *53* (17), 9400–9406.
(7) Werncke, C. G., Suturina, E., Bunting, P. C., Vendier, L., Long, J. R., Atanasov, M., Neese, F., Sabo-Etienne, S., Bontemps, S. *Chem. – Eur. J.* **2016**, *22* (5), 1668–1674.
(8) Wagner, C. L., Tao, L., Thompson, E. J., Stich, T. A., Guo, J., Fettinger, J. C., Berben, L. A., Britt, R. D., Nagase, S., Power, P. P. *Angew. Chem. Int. Ed.* **2016**, *55* (35), 10444–10447.
(9) Boynton, J. N., Guo, J.-D., Fettinger, J. C., Melton, C. E., Nagase, S., Power, P. P. *J. Am. Chem. Soc.* **2013**, *135* (29), 10720–10728.
(10) Bruno, I. J., Cole, J. C., Edgington, P. R., Kessler, M., Macrae, C. F., McCabe, P., Pearson, J., Taylor, R. *Acta Crystallogr. B* **2002**, *58* (3), 389–397.
(11) Liu, H., Cai, I. C., Fedorov, A., Ziegler, M. S., Copéret, C., Tilley, T. D. *Helv. Chim. Acta* **2016**, *99* (11), 859–867.

DEDICATION

To my family

ACKNOWLEDGEMENTS

Over the past five years, I have learned how to be a scientist. Much of that learning did not occur in isolation, and throughout my graduate career, a number of people have provided their support.

First and foremost, my graduate career would not have been possible without the constant support of my advisor, Professor T. Don Tilley. Don provided me with the opportunity to pursue science as an organometallic chemist and helped me to forge indispensable tools which will accompany me in my future career. His motivation and encouragement have pushed me to grow and develop as an independent researcher, and for that, I cannot thank him enough.

I thank Professor Richard A. Andersen, for his help throughout my graduate studies, at the board and at the bench.

I thank Dr. Michael I. Lipschutz, who was a central resource during my first year in the Tilley Group. He introduced me to a viable platform for low-coordinate early transition metal chemistry, from which I was able to develop my work further.

I thank all of my collaborators; their efforts have helped to develop my studies in ways which I might not have considered. I thank Dr. Micah Ziegler for all of his input, especially with regards to EPR spectroscopy, for whom I also thank Professor K. V. Lakshmi. The vanadium project was a massive undertaking; I thank Phil Bunting, Amélie Nicolay, and Dr. Daniel Levine for their help with SQUID magnetometry, cyclic voltammetry, and DFT, respectively. With regards to my studies on organochromium complexes, I thank Dr. Hsueh-Ju Liu, whose work helped me explore more applied aspects of my work. I thank Allison Devitt, for her enthusiasm and dedication as an undergraduate student in the Tilley Group; mentoring her was also a gratifying and enjoyable learning experience for myself.

In addition to those listed above, I thank past and present members of the Tilley Group. I thank Patrick Smith for being an excellent guide on various spectroscopic techniques. Dr. Andy Nguyen, Dr. James Dombrowski, Gavin Kiel, and Rex Handford have all been great colleagues and positive sources of encouragement. I thank Dr. Christopher Letko, Dr. Wenjun Liu, and Jaruwan "Jom" Amtawong for their assistance with cyclic voltammetry. A special thanks to Dr. Raúl Huerta-Lavorie, for helping to cultivate a good group dynamic and for writing the group's first proposal for time at the ALS, which has been an invaluable resource for many of my single-crystal X-ray diffraction studies.

I thank various people around the department and those affiliated with the Lawrence Berkeley National Lab. Rosemary Tilley, administrative guru, has been helpful in so many ways. I thank Dante Valdez, who was an excellent resource both during and after my teaching assignments for CHEM 108. Dr. Miao Zhang took excellent care of the Catalysis Center, for which I am grateful. Single-crystal X-ray crystallography has been an essential component of my work; I thank Nicholas Settineri, Dr. Simon Teat and Dr. Laura McCormick for their assistance.

I thank Steven Hager for being a constant source of support during our time in Berkeley. Both his humor and friendship have helped to make my experience here unforgettable and all the more enjoyable.

Lastly, I thank my family for their undying love and support. As a fellow chemist, my father instilled in me a passion for science, which has propelled me to where I am now. As my junior, my brother has always been a source of youthful inspiration. And to my mother, I thank her for all of her encouragement throughout these years.

Chapter 1: A Bis(amido) Ligand Set that Supports Two-Coordinate Chromium in the +1, +2, and +3 Oxidation States[a]

INTRODUCTION

The first-row transition metals are unique in their ability to support very low coordination numbers over a wide range of d^n configurations. The interest in such compounds has largely been driven by attempts to understand structure and bonding for these unusual coordination geometries, and this has led to the isolation and characterization of fewer than one hundred two-coordinate, open-shell complexes.[1–11] Recently, the silyl(aryl)amido ligand –N($SiMe_3$)DIPP (DIPP = 2,6-diisopropylphenyl) has been shown to allow access to multiple oxidation states for two-coordinate nickel, iron and cobalt complexes.[4–7] Interestingly, this silylamido ligand cannot be used to support a strictly two-coordinate chromium complex; attempts to synthesize Cr[N($SiMe_3$)DIPP]$_2$ led to C–H bond activation of the ligand and formation of a remarkable tetra-chromium complex containing bridging –CH_2($SiMe_2$) groups (**A**, Figure 1.1).[6] Also, although the silylamido ligand –N($SiMe_2Ph$)$_2$ can be used to support a two-coordinate chromium complex in the solid state, the bis(THF) adduct of the complex is also isolated from the same reaction mixture (**B**, Figure 1.1).[8]

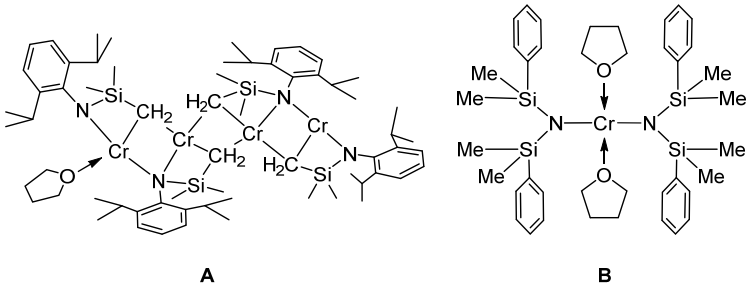

Figure 1.1: Previous examples of chromium complexes supported by silylamido ligands, **A**[6] and **B**.[8]

[a] This chapter was reproduced with permission from Cai, I. C.; Lipschutz, M. I.; Tilley, T. D. A bis(amido) ligand set that supports two-coordinate chromium in the +1, +2, and +3 oxidation states. *Chem. Commun.* **2014**, *50* (86), 13062–13065. DOI: 10.1039/C4CC06615D.

The stabilization of low-coordinate complexes is more challenging for the earlier first-row transition metals, due to their larger atomic radii and lower d^n counts. Notably, only two two-coordinate vanadium complexes have been reported and both require stabilization by extremely bulky terphenyl amido ligands.[2] Similar requirements for exceptional steric bulk seem to hold for open-shell, two-coordinate chromium complexes, which have been obtained with bulky supporting borylamido,[12,13] arylamido,[3,14] thiolato,[15] and terphenyl[16–19] ligands.[1] Although the aforementioned –N(SiMe$_3$)DIPP ligand cannot stabilize a two-coordinate Cr^{II} species, it seemed that an increase of the steric bulk for this type of ligand would allow for isolation of such a complex. Herein, we describe the synthesis and characterization of a two-coordinate Cr^{II} complex with the sterically demanding –N(Si^{i}Pr$_3$)DIPP ligand, which also allows access to low-coordinate complexes of Cr^{I} and Cr^{III}.

RESULTS AND DISCUSSION

Cr[N(Si^{i}Pr$_3$)DIPP]$_2$ (**1.1**) was synthesized by a salt metathesis reaction of $CrCl_2$ with 2 equiv of K[N(Si^{i}Pr$_3$)DIPP] in THF at ambient temperature. Workup of the red reaction mixture and recrystallization from pentane and hexamethyldisiloxane (HMDSO) afforded green crystals of **1.1** in 60% yield. The X-ray structure of **1.1** (Figure 1.2) reveals a linear geometry about chromium with a crystallographically imposed 180° N–Cr–N bond angle and a Cr–N bond length of 2.0036(12) Å, which falls within the 1.94-2.00 Å range of distances previously reported for two-coordinate chromium bis(amido) complexes.[1,8] The solid state structure also indicates a close interaction between the chromium atom and the *ipso* carbon of the adjacent aryl ring, with a Cr–N–C$_{ipso}$ angle of 81.59(8)° and a Cr–C$_{ipso}$ distance of 2.2709(14) Å. This distance is shorter than Cr-C$_{ipso}$ interactions observed for related chromium bis(amido) complexes, with Cr[N(Ph)BMes$_2$]$_2$ (Mes = C$_6$H$_2$-2,4,6-Me$_3$) having the shortest distance of 2.328(2) Å between the chromium atom and an *ipso* carbon from a –BMes$_2$ group.[1,13] The solution magnetic moment of **1.1**, determined by the Evans method,[20,21] is 4.9 μ_B and consistent with a high-spin d^4 configuration. Correspondingly, broad, unintegrable signals are observed in the ^{1}H NMR spectrum of **1.1**, due to its paramagnetism.

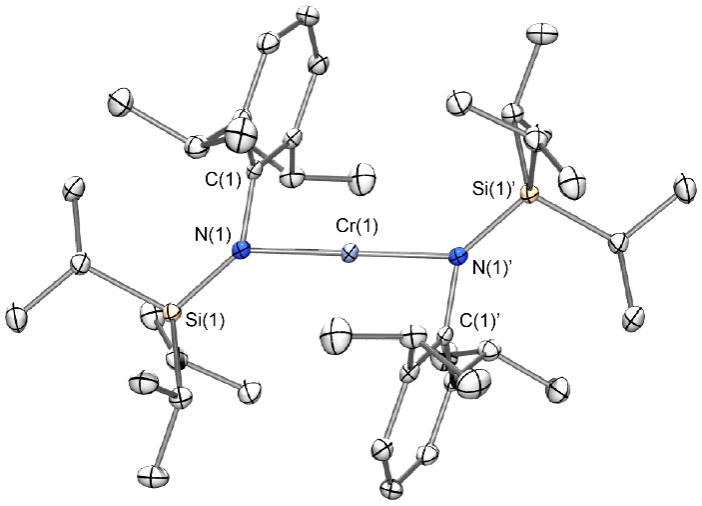

Figure 1.2: Solid-state structure of **1.1** as determined by single-crystal X-ray diffraction. Thermal ellipsoids shown at 50% probability. Hydrogen atoms are omitted for clarity.

A previous report on the ability of the –N(SiMe$_3$)DIPP ligand to stabilize multiple d^n configurations and oxidation states of nickel[5] prompted an investigation of **1.1** by cyclic voltammetry (CV). The cyclic voltammogram of **1.1** reveals reversible Cr(I/II) and Cr(II/III) couples at −2.04 V ($E_{1/2}$ vs Fc/Fc^+, ip_a/ip_c = 0.95) and −0.38 V ($E_{1/2}$ vs Fc/Fc^+, ip_a/ip_c = 1.09), respectively (see Figure S1.1). The reversibility of these redox events suggested that the analogous two-coordinate complexes of Cr^I and Cr^{III} would be stable and chemically accessible.

Reduction of **1.1** with 1.1 equiv of KC_8 in diethyl ether over 30 min at ambient temperature, followed by recrystallization from dimethoxyethane (DME) and pentane, afforded orange crystals which were dried under reduced pressure to provide $[K(DME)_n]\{Cr[N(Si^iPr_3)DIPP]_2\}$ (**1.2a**) in 97% yield (Scheme 1.1, n = 1.5, determined by ^1H NMR integration against an internal standard). The X-ray structure of **1.2a** before desolvation under vacuum (Figure 1.3) reveals that the linear coordination environment of the complex is maintained, with a N–Cr–N bond angle of 175.02(13)° and Cr–N bond lengths of 2.054(3) and 2.061(3) Å, which are slightly longer than that of **1.1**, as expected. Interestingly, the *ipso* carbon of **1.2a** interacts less strongly with Cr^I than with Cr^{II} (in **1.1**), with a Cr–C*ipso* distance greater than 2.8 Å and Cr–N–C*ipso* angles of 108.4(2)° and 108.5(2)° for **1.2a**. Additionally, unlike the analogous Ni^I species $K\{Ni[N(SiMe_3)DIPP]_2\}$,[5] the potassium is not coordinated to the aryl groups of the amido ligands and is instead complexed by four equivalents of DME to give the outer-sphere $[K(DME)_4]^+$ cation. The solution magnetic moment of **1.2a**, 5.2 μ_B (Evans method), is lower than the expected spin-only value of 5.9 μ_B but consistent with a high-spin d^5 configuration.

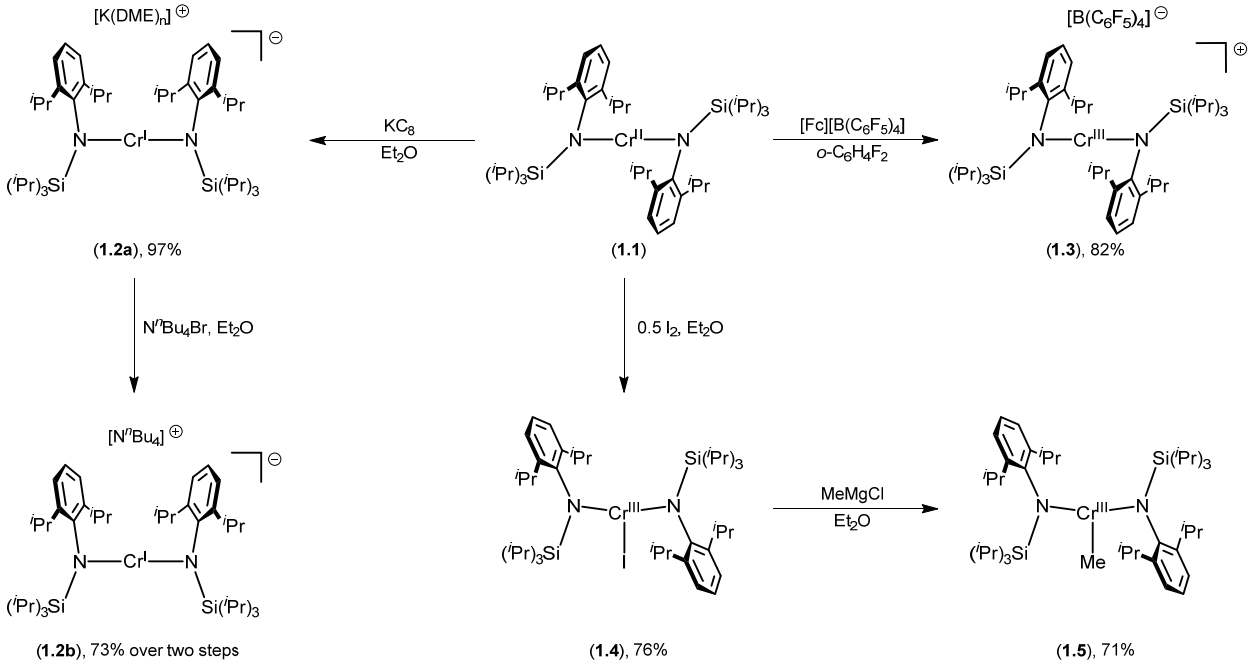

Scheme 1.1: Reactions of chromium bis(amido) complexes.

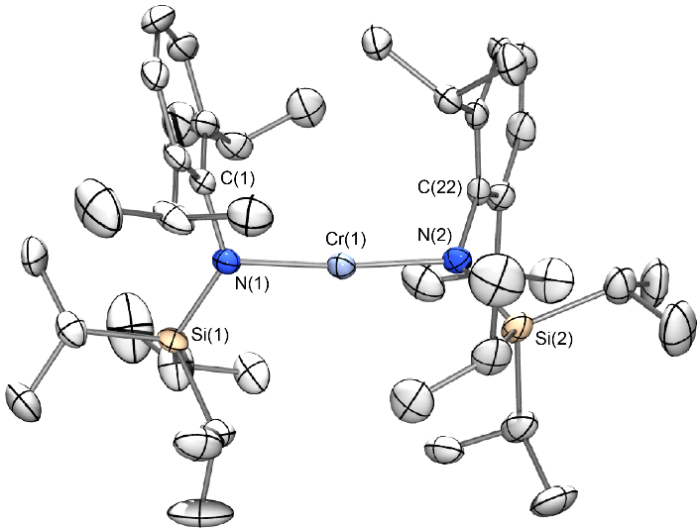

Figure 1.3: Solid-state structure of **1.2a** as determined by single-crystal X-ray diffraction. Thermal ellipsoids shown at 50% probability. Hydrogen atoms, cation, and solvent are omitted for clarity.

Compound **1.2a** reacted with tetrabutylammonium bromide to provide $[N^nBu_4]\{Cr[N(Si^iPr_3)DIPP]_2\}$ (**1.2b**), which has a geometry consistent with that of **1.2a** (Scheme 1.1, see Figure S1.2). The solution magnetic moment of **1.2b** is 5.7 μ_B, also consistent with a high-spin d^5 configuration. The UV-vis spectra of **1.2a** and **1.2b** in DME are consistent with each other; despite being high-spin, the Cr^I species displays several intense absorptions with molar absorptivities ranging from 5200 to 18000 mol^{-1} L cm^{-1}, likely corresponding to ligand-to-metal charge transfer.

Reaction of **1.1** with ferrocenium tetrakis(pentafluorophenyl)borate over 1 h at ambient temperature afforded dark red crystals of $\{Cr[N(Si^iPr_3)DIPP]_2\}[B(C_6F_5)_4]$ (**1.3**) from 1,2-difluorobenzene and HMDSO in 82% yield (Scheme 1.1). The complex co-crystallizes with 1,2-difluorobenzene and contains two crystallographically independent molecules of **1.3** within the unit cell. Both molecules are linear, having a N–Cr–N bond angle of 180.000(1)° (Figure 1.4). Due to a smaller atomic radius, the Cr–N bond lengths for each of the molecules of **1.3** are 1.872(2) and 1.869(2) Å, respectively, and notably shorter than comparable distances observed for **1.1**. Correspondingly, the Cr–C_{ipso} interaction is increased, such that relatively short Cr–C_{ipso} distances of 2.225(2) and 2.217(2) Å are observed. The solution magnetic moment of **1.3**, determined by the Evans method, is 3.8 μ_B and most consistent with a high-spin d^3 configuration. Assuming a $(d_{xy}, d_{x2-y2})^2(d_{xz}, d_{yz})^1(d_{z2})^0$ electronic configuration based on $D_{\infty h}$ symmetry, **1.3** might be expected to be anisotropic. However, despite being isoelectronic to the linear two-coordinate complex $V\{N(H)(C_6H_3\text{-}2,6\text{-}(C_6H_2\text{-}2,4,6\text{-}^iPr_3)_2)\}_2$,[2] **1.3** does not exhibit significant spin-orbit coupling. Calculations on a similar complex, $Fe[N(SiMe_3)DIPP]_2$, have shown that the nitrogen lone pairs can interact with the metal center, breaking degeneracy of the (d_{xz}, d_{yz}) pair and quenching orbital angular momentum.[22,23] In contrast to the isoelectronic vanadium complex, the cationic charge on **1.3** is expected to increase further the strength of the ligand field and such degeneracy-breaking interactions, such that isotropic magnetic properties would be observed for **1.3**.

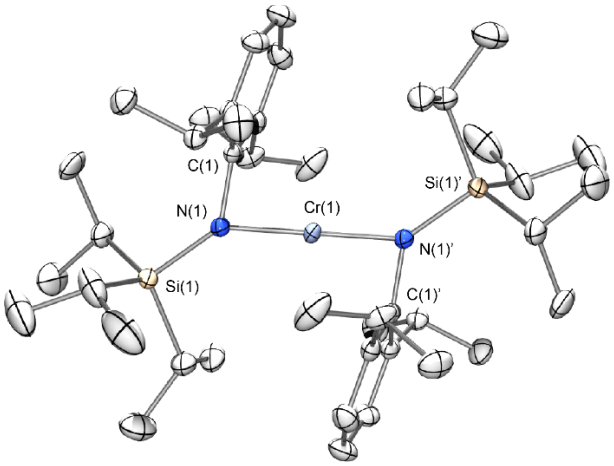

Figure 1.4: Solid-state structure of **1.3** as determined by single-crystal X-ray diffraction. The second crystallographically independent molecule of **1.3** has been omitted. Thermal ellipsoids shown at 50% probability. Hydrogen atoms, anions, and solvent are omitted for clarity.

Similar to what is observed for later first row transition metals supported by –N(SiMe$_3$)DIPP,[4,6] both **1.1** and **1.3** exhibit an eclipsed configuration of the two amido ligands, with C$_{ipso}$–NCrN–C$_{ipso}$ dihedral angles of 180.0(1)° and 180.0(2)°, respectively. In contrast, the aryl groups on the ligands of **1.2a** and **1.2b** adopt a *syn* conformation and are approximately staggered, with C$_{ipso}$–NCrN–C$_{ipso}$ dihedral angles of 44.1(3)° and 39.8(2)°, respectively.

To further explore the oxidation chemistry associated with **1.1**, 0.5 equivalents of I$_2$ were added to **1.1**, to afford dark red crystals of (I)Cr[N(Si^{i}Pr$_3$)DIPP]$_2$ (**1.4**) from pentane in 76% yield (Scheme 1.1). Addition of the iodo ligand to **1.1** results in a trigonal planar geometry with a N–Cr–N bond angle of 139.49(17)° and shorter Cr–N bond lengths of 1.906(4) and 1.889(4) Å (Figure 1.5). There is no significant interaction of the aryl *ipso* carbons with the chromium center, as indicated by Cr–N–C$_{ipso}$ angles of 120.2(3) and 123.8(3)° for **1.4**. The solution magnetic moment of **1.4**, determined by the Evans method, is 3.35 μ_B and lower than the expected spin-only value of 3.87 μ_B but consistent with a d^3 configuration.

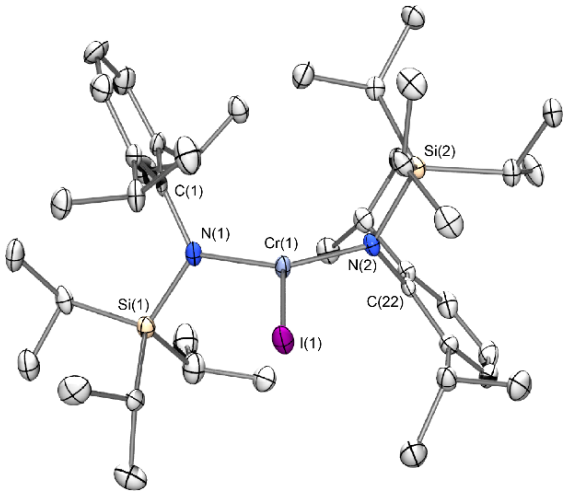

Figure 1.5: Solid-state structure of **1.4** as determined by single-crystal X-ray diffraction. Thermal ellipsoids shown at 50% probability. Hydrogen atoms are omitted for clarity.

Given the long-standing interest in Cr^{III} alkyl complexes,[24–27] **1.4** was examined as a possible synthetic entry to such species. Addition of methylmagnesium chloride in THF to a dark red solution of **1.4** in diethyl ether resulted in a color change to red-orange after five minutes. Workup of the reaction mixture and recrystallization from pentane afforded red crystals of (Me)Cr[N(Si^{i}Pr$_3$)DIPP]$_2$ (**1.5**) in 71% yield (Scheme 1.1). Complex **1.5** crystallizes in a unit cell nearly identical to that of **1.4**. The N–Cr–N bond angle of 142.89(11)° is slightly wider than that for **1.4**, but comparable Cr–N bond lengths of 1.906(2) and 1.893(2) Å are observed (Figure 1.6). Similarly, there is no significant interaction of the *ipso* carbon with the chromium center, with Cr–N–C$_{ipso}$ angles of 122.71(19) and 118.75(19)°. The Cr–C$_{Me}$ bond length of 2.058(3) Å is comparable to the Cr-C$_{Me}$ distance of 2.081(3) Å observed in the β-ketiminate Cr^{II} methyl complex reported by Mindiola and coworkers, one of the few three-coordinate chromium alkyl complexes to be fully characterized.[28] The solution magnetic moment of **1.5** (3.57 μ_B, Evans method) is consistent with a d^3 configuration.

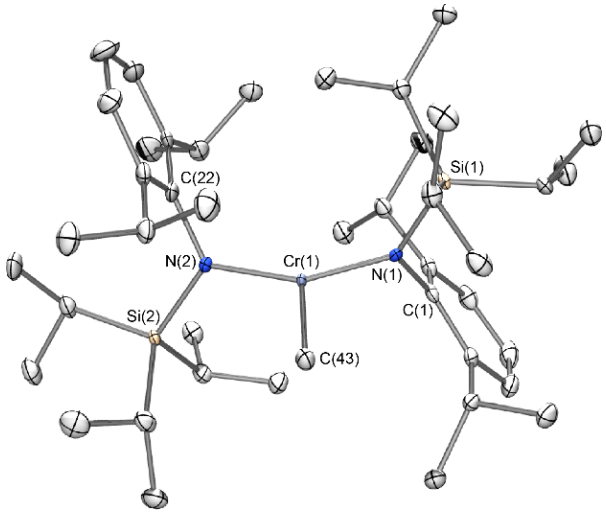

Figure 1.6: Solid-state structure of **1.5** as determined by single-crystal X-ray diffraction. Thermal ellipsoids shown at 50% probability. Hydrogen atoms are omitted for clarity. Disordered chromium and silicon atoms have been excluded.

CONCLUSIONS

In summary, a series of two-coordinate chromium complexes has been isolated and characterized. The ability of the –N(Si^{i}Pr$_3$)DIPP ligand to support a monomeric Cr^{II} complex, in contrast to the less bulky –N(SiMe$_3$)DIPP ligand, highlights the role of sterics in maintaining linearity for two-coordinate complexes. Furthermore, isolation of these chromium species continues to demonstrate the ability of silyl(aryl)amido ligands to support two-coordinate species of first row transition metals in a variety of oxidation states. Studies further examining the reactivity of this chromium series are currently ongoing.

REFERENCES

(1) Power, P. P. *Chem. Rev.* **2012**, *112* (6), 3482–3507.
(2) Boynton, J. N., Guo, J.-D., Fettinger, J. C., Melton, C. E., Nagase, S., Power, P. P. *J. Am. Chem. Soc.* **2013**, *135* (29), 10720–10728.
(3) Huang, Y.-L., Lu, D.-Y., Yu, H.-C., Yu, J.-S. K., Hsu, C.-W., Kuo, T.-S., Lee, G.-H., Wang, Y., Tsai, Y.-C. *Angew. Chem. Int. Ed.* **2012**, *51* (31), 7781–7785.
(4) Lipschutz, M. I., Tilley, T. D. *Chem. Commun.* **2012**, *48* (57), 7146–7148.
(5) Lipschutz, M. I., Yang, X., Chatterjee, R., Tilley, T. D. *J. Am. Chem. Soc.* **2013**, *135* (41), 15298–15301.
(6) Lin, C.-Y., Guo, J.-D., Fettinger, J. C., Nagase, S., Grandjean, F., Long, G. J., Chilton, N. F., Power, P. P. *Inorg. Chem.* **2013**, *52* (23), 13584–13593.
(7) Lin, C.-Y., Fettinger, J. C., Grandjean, F., Long, G. J., Power, P. P. *Inorg. Chem.* **2014**, *53* (17), 9400–9406.
(8) König, S. N., Schädle, C., Maichle-Mössmer, C., Anwander, R. *Inorg. Chem.* **2014**, *53* (9), 4585–4597.
(9) Ung, G., Rittle, J., Soleilhavoup, M., Bertrand, G., Peters, J. C. *Angew. Chem. Int. Ed.* **2014**, *53* (32), 8427–8431.
(10) Mondal, K. C., Roy, S., De, S., Parameswaran, P., Dittrich, B., Ehret, F., Kaim, W., Roesky, H. W. *Chem. – Eur. J.* **2014**, *20* (37), 11646–11649.
(11) Samuel, P. P., Mondal, K. C., Amin Sk, N., Roesky, H. W., Carl, E., Neufeld, R., Stalke, D., Demeshko, S., Meyer, F., Ungur, L., Chibotaru, L. F., Christian, J., Ramachandran, V., van Tol, J., Dalal, N. S. *J. Am. Chem. Soc.* **2014**, *136* (34), 11964–11971.
(12) Bartlett, R. A., Chen, H., Power, P. P. *Angew. Chem. Int. Ed. Engl.* **1989**, *28* (3), 316–317.
(13) Chen, H., Bartlett, R. A., Olmstead, M. M., Power, P. P., Shoner, S. C. *J. Am. Chem. Soc.* **1990**, *112* (3), 1048–1055.
(14) Boynton, J. N., Merrill, W. A., Reiff, W. M., Fettinger, J. C., Power, P. P. *Inorg. Chem.* **2012**, *51* (5), 3212–3219.
(15) Nguyen, T., Panda, A., Olmstead, M. M., Richards, A. F., Stender, M., Brynda, M., Power, P. P. *J. Am. Chem. Soc.* **2005**, *127* (23), 8545–8552.
(16) Nguyen, T., Sutton, A. D., Brynda, M., Fettinger, J. C., Long, G. J., Power, P. P. *Science* **2005**, *310* (5749), 844–847.
(17) Wolf, R., Ni, C., Nguyen, T., Brynda, M., Long, G. J., Sutton, A. D., Fischer, R. C., Fettinger, J. C., Hellman, M., Pu, L., Power, P. P. *Inorg. Chem.* **2007**, *46* (26), 11277–11290.
(18) Wolf, R., Brynda, M., Ni, C., Long, G. J., Power, P. P. *J. Am. Chem. Soc.* **2007**, *129* (19), 6076–6077.
(19) Lei, H., Guo, J.-D., Fettinger, J. C., Nagase, S., Power, P. P. *J. Am. Chem. Soc.* **2010**, *132* (49), 17399–17401.
(20) Evans, D. F. *J. Chem. Soc. Resumed* **1959**, No. 0, 2003–2005.
(21) Live, D. H., Chan, S. I. *Anal. Chem.* **1970**, *42* (7), 791–792.
(22) Zadrozny, J. M., Atanasov, M., Bryan, A. M., Lin, C.-Y., Rekken, B. D., Power, P. P., Neese, F., Long, J. R. *Chem. Sci.* **2013**, *4* (1), 125–138.
(23) Atanasov, M., Zadrozny, J. M., Long, J. R., Neese, F. *Chem. Sci.* **2013**, *4* (1), 139–156.
(24) Theopold, K. H. *Acc. Chem. Res.* **1990**, *23* (8), 263–270.
(25) Liang, Y., Yap, G. P. A., Rheingold, A. L., Theopold, K. H. *Organometallics* **1996**, *15* (25), 5284–5286.

(26) Heintz, R. A., Leelasubcharoen, S., Liable-Sands, L. M., Rheingold, A. L., Theopold, K. H. *Organometallics* **1998**, *17* (25), 5477–5485.
(27) MacAdams, L. A., Buffone, G. P., Incarvito, C. D., Rheingold, A. L., Theopold, K. H. *J. Am. Chem. Soc.* **2005**, *127* (4), 1082–1083.
(28) Fan, H., Adhikari, D., Saleh, A. A., Clark, R. L., Zuno-Cruz, F. J., Sanchez Cabrera, G., Huffman, J. C., Pink, M., Mindiola, D. J., Baik, M.-H. *J. Am. Chem. Soc.* **2008**, *130* (51), 17351–17361.

EXPERIMENTAL DETAILS

General Considerations. Unless otherwise noted, all experiments were conducted with dry, oxygen-free solvents using standard Schlenk techniques or in a N_2 atmosphere glovebox. Benzene-d_6 was purchased from Cambridge Isotope Laboratories and dried by vacuum distillation from Na/K alloy. Dimethoxyethane (DME) was purchased from Sigma Aldrich, dried by vacuum distillation from K/benzophenone, and stored over 3 Å molecular sieves. Unless otherwise noted, reagents were obtained from commercial suppliers and used as received. Potassium hydride was purchased as a dispersion in mineral oil from Sigma Aldrich and washed with pentane before use. Tetrabutylammonium tetrakis(pentafluorophenyl)borate,[1] potassium graphite,[2] and ferrocenium tetrakis(pentafluorophenyl)borate[3] were prepared by standard literature procedures. The abbreviation "DIPP" refers to a 2,6-diisopropylphenyl moiety and "DME" refers to dimethoxyethane.

Analytical Methods. All ^{1}H NMR spectra were collected at ambient temperature (ca. 21 °C) on Bruker AVB-400, AVQ-400, AV-500, or AV-600 NMR spectrometers, each equipped with a 5 mm BB probe, and referenced to the residual proteo-solvent signals. Solution magnetic susceptibilities were determined by ^{1}H NMR spectroscopy using the Evans method.[4,5] For Evans method measurements using only proteo-solvent, a sealed insert containing DMSO-d_6 was also included for a lock signal. IR spectra were collected on a Bruker Alpha-P FR-IR Spectrometer equipped with a "Platinum" Attenuated Total Reflection sample module. Solution UV-Vis spectra were collected using a Varian Cary 300 series spectrophotometer. Melting points were determined on a Mel-Temp II melting point apparatus. Elemental analyses were performed by the UC Berkeley College of Chemistry Microanalytical Facility.

Cyclic Voltammetry Experiments. Cyclic voltammetry experiments were conducted at ambient temperature in a Vacuum Atmospheres glovebox. Measurements employed a Bio-Logic SP-200 potentiostat with a standard three-electrode configuration. The working electrode was a 3mm diameter glassy carbon electrode purchased from ALS. Silver wire was used as a quasi-reference electrode and sublimed ferrocene was used as an internal potential reference. The counter electrode was a 1/8 inch diameter graphite rod purchased from Electron Microscopy Sciences. The glassy carbon electrode was polished with 1 μm alumina prior to each use. The graphite rod was cleaned with acetone and dried prior to each use. Analyses of **1.1** were performed in a 0.1 M solution of tetrabutylammonium tetrakis(pentafluorophenyl)borate in 1,2-difluorobenzene with an analyte concentration of 1 mM at a scan rate of 100 mV/s. Solution resistance was corrected by applying *i*R compensation for each measurement. All potential values are reported as $E_{1/2}$ for reversible events and E_p for irreversible events.

X-ray Diffraction Experiments. Single crystal X-ray diffraction experiments were carried out at the UC Berkeley CHEXRAY crystallographic facility. Measurements of all compounds were performed on a Bruker APEX-II CCD area detector using Mo Kα radiation (λ = 0.71073 Å) monochromated using QUAZAR multilayer mirrors. Crystals were kept at 100(2) K throughout collection. Data collection, refinement, and reduction were performed with Bruker APEX2 software (v. 2013.4). All structures were solved using SIR97.[6] Structures **1.1**, **1.2a**, **1.3**, **1.4**, and **1.5** were refined with SHELXL-97[7] with refinement of F^2 against all reflections by full-matrix least squares, while structures **1.2b** was refined with SHELXL-2013[8] with refinement of F^2 against all reflections by full-matrix least squares. In all models, non-hydrogen atoms were refined anisotropically, and hydrogen atoms were included at the geometrically-calculated positions and refined using a riding model. Specific details can be found below (Table E1.1) and in the crystallographic information files.

Table E1.1: X-ray Crystallography Experimental Details:

Compound	Detector Distance (mm)	Image Width (°)	Exposure Time (s)
1.1	40	0.5	10
1.2a	50	0.5	20
1.2b	40	0.5	30
1.3	40	0.5	10
1.4	60	0.5	30
1.5	40	0.5	30

Synthesis of HN(Si^{i}Pr$_3$)DIPP. To a 250 mL Chemglass Air-Free Teflon-stoppered flask was added 2,6-diisopropylaniline (5.3 mL, 28 mmol) and 30 mL of THF. The solution was placed in an ice bath, and to the stirred solution was added *n*BuLi (1.6 M in hexanes, 18.4 mL, 29.4 mmol), dropwise *via* syringe. The yellow solution was removed from the ice bath and stirred for 20 minutes. To the stirred solution was then slowly added a solution of triisopropylsilyl chloride (6.0 mL, 28 mmol) in 10 mL of THF, *via* syringe. The solution was stirred for 23 h in a 75 °C oil bath. After allowing the reaction to cool to ambient temperature, the volatile materials were removed under reduced pressure. The resulting residue was distilled under 90 °C/ 0.05 mmHg to give a clear, light orange oil (7.3 g, 78%). ^{1}H NMR (400 MHz, C_6D_6, 20 °C) δ 1.10 (d, J_{HH} = 7.1 Hz, 18 H, CH(C*H*$_3$)$_2$), 1.17-1.26 (m, 3 H, C*H*(CH$_3$)$_2$), 1.23 (d, 12 H, CH(C*H*$_3$)$_2$), 2.43 (br s, 1 H, N-*H*), 3.56 (sep, 2 H, C*H*(CH$_3$)$_2$), 7.05-7.16 (m, 3 H, C$_6$*H*$_3$). ^{13}C NMR data in C_6D_6 were consistent with values reported in the literature.[9]

K[N(Si^{i}Pr$_3$)DIPP]. To a 20 mL scintillation vial was added benzyl potassium (0.351, 2.7 mmol) and 6 mL of diethyl ether. To a 4 mL, 1 dram vial was added HN(Si^{i}Pr$_3$)DIPP (0.900 g, 2.7 mmol), and 2 mL of diethyl ether. Both vials were placed in a -30 °C freezer and allowed to cool for 30 min. Upon removal of both vials from the freezer, the suspension of benzyl potassium was stirred and the solution of HN(Si^{i}Pr$_3$)DIPP] was added dropwise. The contents of 4 mL vial were washed with an additional 2 mL of diethyl ether and the resulting solution in diethyl ether was then added to the 20 mL scintillation vial. The reaction mixture was stirred at ambient temperature for 70 min. The mixture was filtered and concentrated to a solid. The solid was washed with pentane (3 x 5 mL) and dried *in vacuo* to give an off-white powder (0.725, 72%), which was used without further purification.

Cr[N(Si^{i}Pr$_3$)DIPP]$_2$ (1.1). To a 20 mL scintillation vial was added chromium(II) chloride (0.100 g, 0.81 mmol) and 4 mL of THF. To a 4 mL, 1 dram vial was added K[N(Si^{i}Pr$_3$)DIPP] (0.610 g, 1.64 mmol) and 2 mL of THF, forming a clear, light yellow solution. Both vials were placed in a -30 °C freezer and allowed to cool for 10 min. Upon removal of both vials from the freezer, the suspension of chromium(II) chloride was stirred and the solution of K[N(Si^{i}Pr$_3$)DIPP] was added dropwise. The contents of 4 mL vial were washed with an additional 2 mL of THF and the resulting solution in THF was then added to the 20 mL scintillation vial. The reaction mixture was stirred at ambient temperature for 1 h. The red solution was concentrated under reduced pressure to a green and orange solid, which was extracted into 10 mL of pentane. The pentane extract was filtered, then concentrated under reduced pressure to a volume of 4 mL, and placed in a -30 °C freezer for several hours, to yield 0.263 g (45%) of Cr[N(Si^{i}Pr$_3$)DIPP]$_2$ (**1.1**) as green, block-like crystals which were isolated by decantation and dried *in vacuo*. The supernatant was collected and the volatile components were removed under reduced pressure. A second crystallization was set up in an identical fashion using the resulting residue with a minimal amount of hexamethyldisiloxane, yielding an additional 0.096 g of **1.1**. Total yield: 0.349 g (60%). The ^{1}H NMR spectrum of **1.1** in C_6D_6 contains non-distinctive, broad and unintegrable signals, attributed to the paramagnetism of **1.1**; μ_{eff} = 4.92 μ_B (C_6D_6, 19.2 °C, Evans method). IR (neat solid, cm^{-1}) 2863 m, 929 m, 879 s, 766 s, 766 s, 722 m, 669 m. UV-vis (DME) λ_{max} (ε): 437 nm (5.4×10^3 mol^{-1} L cm^{-1}). Mp: 77-80 °C (color change from green to red), 137-140 °C (decomposition). Anal. Calcd. for $C_{42}H_{76}N_2CrSi_2$: C, 70.33%, H, 10.68%, N, 3.91%. Found: C, 70.55%, H, 10.42%, N, 3.81%. Crystals suitable for single crystal X-ray diffraction studies were obtained from the workup described above.

[K(DME)$_n$]{Cr[N(Si^{i}Pr$_3$)DIPP]$_2$} (1.2a). To a 20 mL scintillation vial was added **1.1** (0.200 g, 0.279 mmol) and 10 mL of diethyl ether. The solution was placed in a -30 °C freezer and allowed to cool for 20 minutes. Upon removal of the vial from the freezer, the solution was stirred and potassium graphite (0.042 g, 0.307 mmol) was added as a solid. The reaction mixture was stirred at ambient temperature for 30 min. The mixture was filtered and concentrated to a red solid under reduced pressure. The solid was dissolved in 1 mL of DME, upon which was layered 9 mL of pentane. The layered solution was placed in a -30 °C freezer overnight, yielding orange crystals which were isolated by decantation and dried in vacuo, resulting in a 0.242 g (0.270 mmol, 97%) of [K(DME)$_{1.5}$]{Cr[N(Si^{i}Pr$_3$)DIPP]$_2$} (MW 891.53) as an orange solid. The relative amount of residual DME was determined after each workup by ^{1}H NMR spectroscopy, using hexamethylbenzene as an internal standard. Apart from residual DME, the ^{1}H NMR spectrum of **1.2a** in C_6D_6 contains non-distinctive, broad and unintegrable signals, attributed to the paramagnetism of **1.2a**; μ_{eff} = 5.2 μ_B (C_6D_6, 20 °C, Evans method). UV-vis (DME) λ_{max} (ε): 244 (1.8×10^4), 282 (7.2×10^3), 330 (5.7×10^3), 429 (5.2×10^3) nm (mol^{-1} L cm^{-1}). Anal. Calcd. for $C_{42}H_{76}N_2CrKSi_2 \cdot 1.4C_4H_{10}O_2$: C, 64.78%, H, 10.30%, N, 3.17%. Found: C, 64.46%, H, 10.41%, N, 2.96%. Crystals suitable for single crystal X-ray diffraction studies were obtained from the workup described above.

[N^{n}Bu$_4$]{Cr[N(Si^{i}Pr$_3$)DIPP]$_2$} (1.2b). To a 20 mL scintillation vial was added **1.1** (0.200 g, 0.279 mmol) and 8 mL of diethyl ether. The solution was placed in a -30 °C freezer and allowed to cool for 30 minutes. Upon removal of the vial from the freezer, the solution was stirred and potassium graphite (0.042 g, 0.307 mmol) was added as a solid. The reaction mixture was stirred at ambient temperature for 30 min. Tetrabutylammonium bromide (0.090 g, 0.279 mmol) was then added

directly to the stirring reaction. The mixture was stirred for an additional 1 h at ambient temperature. The mixture was filtered, and the filtrate was concentrated to a volume of 4 mL. The solution was placed in a -30 °C freezer for two days, affording 0.196 g (73%) of $[N^nBu_4]\{Cr[N(Si^iPr_3)DIPP]_2\}$ (**1.2b**) as orange crystals, which were isolated by decantation and dried *in vacuo*. The ^1H NMR spectrum of **1.2b** in C_6D_6 contains non-distinctive, broad and unintegrable signals, attributed to the paramagnetism of **1.2b**; $\mu_{eff} = 5.74\ \mu_B$ (THF, 20 °C, Evans method). UV-vis (DME) λ_{max} (ε): 243 (1.8×10^4), 282 (8.8×10^3), 330 (7.4×10^3), 427(6.3×10^3) nm (mol^{-1} L cm^{-1}). UV-vis (toluene) λ_{max} (ε): 327 (1.0×10^4), 424 (7.2×10^3) nm (mol^{-1} L cm^{-1}). Anal. Calcd. for $C_{58}H_{112}N_3CrSi_2$: C, 72.59%, H, 11.76%, N, 4.38%. Found: C, 72.32%, H, 11.90%, N, 4.25%. Crystals suitable for single crystal X-ray diffraction studies were obtained from the workup described above.

$\{Cr[N(Si^iPr_3)DIPP]_2\}[B(C_6F_5)_4]$ (1.3). To a 20 mL scintillation vial was added **1.1** (0.100 g, 0.140 mmol) and 4 mL of 1,2-difluorobenzene, to produce an orange solution. The solution was placed in a -30 °C freezer and allowed to cool for 50 min. Upon removal of the vial from the freezer, the solution was stirred and ferrocenium tetrakis(pentafluorphenyl)borate) (0.121 g, 0.140 mmol) in 4 mL of 1,2-difluorobenzene was added dropwise. The reaction was stirred at ambient temperature for 1 h. The volatile components of the reaction mixture were removed under reduced pressure and the resulting residue was washed with 5 portions of 2 mL of pentane, until the pentane from washing was no longer visibly yellow. The residue was dissolved in 1,2-difluorobenzene, and the resulting solution was filtered and then concentrated to a volume of 2 mL, upon which was layered 8 mL of hexamethyldisiloxane. The layered solution was placed in a -30 °C freezer for two days, yielding 0.161 g (82%) of $\{Cr[N(Si^iPr_3)DIPP]_2\}[B(C_6F_5)_4]$ (**1.3**) as very dark red crystals, which were isolated by decantation and dried in vacuo. The ^1H NMR spectrum of **1.3** in C_6D_6 contains non-distinctive, broad and unintegrable signals, attributed to the paramagnetism of **1.3**; $\mu_{eff} = 3.83\ \mu_B$ (THF, 20 °C, Evans method). UV-vis (DME) λ_{max} (ε): 355 (5.1×10^3), 391 (5.1×10^3) nm (mol^{-1} L cm^{-1}). Anal. Calcd. for $C_{66}H_{76}N_2BCrF_{20}Si_2$: C, 56.77%, H, 5.49%, N, 2.01%. Found: C, 56.49%, H, 5.38%, N, 1.75%. Crystals suitable for single crystal X-ray diffraction studies were obtained from the workup described above.

(I)$Cr[N(Si^iPr_3)DIPP]_2$ (1.4). To a stirred solution of **1.1** (0.389 g, 0.542 mmol) in 10 mL of diethyl ether was added dropwise a solution of iodine (0.069 g, 0.271 mmol) in 4 mL of diethyl ether. The reaction was stirred for 2 h at ambient temperature and then concentrated to a solid under reduced pressure. The solid was dissolved in pentane, and the resulting solution was filtered and the pentane was removed under reduced pressure to afford a red solid. Crystallization from pentane at -30 °C afforded 0.264 g (58%) of $(I)Cr[N(Si^iPr_3)DIPP]_2$ (**1.4**) as dark red crystals, which were isolated by decantation and dried *in vacuo*. The supernatant was collected and the volatile components were removed under reduced pressure. Subsequent recrystallizations were set up in an identical fashion, yielding an additional 0.084 g of **1.4**. Total yield: 0.348 g (76%). The ^1H NMR spectrum of **1.4** in C_6D_6 contains non-distinctive, broad and unintegrable signals, attributed to the paramagnetism of **1.4**; $\mu_{eff} = 3.35\ \mu_B$ (C_6D_6, 26 °C, Evans method). UV-vis (DME) λ_{max} (ε): 286 (1.5×10^4), 355 (6.5×10^3), 480 (1.4×10^4) nm (mol^{-1} L cm^{-1}). Anal. Calcd. for $C_{42}H_{76}N_2CrISi_2$: C, 59.76%, H, 9.08%, N, 3.32%. Found: C, 59.92%, H, 9.34%, N, 3.41%. Crystals suitable for single crystal X-ray diffraction studies were obtained from the workup described above.

(Me)Cr[N(Si^{i}Pr$_3$)DIPP]$_2$ (1.5). To a 20 mL scintillation vial was added **1.4** (0.084 g, 0.100 mmol) and 4 mL of diethyl ether. The solution was placed in a -30 °C freezer allowed to cool for 10 min. Upon removal of the vial from the freezer, the solution was stirred and methylmagnesium chloride (0.1 M in THF, 1.00 mL, 0.100 mmol) was added dropwise *via* syringe. The reaction was stirred for 2 h at ambient temperature and then concentrated to a red-orange solid under reduced pressure. The solid was triturated with 6 mL of pentane and dried *in vacuo*. The solid was dissolved in pentane, and the resulting solution was filtered and re-concentrated to a solid. Recrystallization from pentane at -30 °C afforded 0.052 g (71%) of (Me)Cr[N(Si^{i}Pr$_3$)DIPP]$_2$ (**1.5**) as red crystals, which were isolated by decantation and dried *in vacuo*. The ^{1}H NMR spectrum of **1.5** in C_6D_6 contains non-distinctive, broad and unintegrable signals, attributed to the paramagnetism of **1.5**; μ_{eff} = 3.57 μ_B (C_6D_6, 26 °C, Evans method). UV-vis (DME) λ_{max} (ε): 244 (1.7×10^4), 340 (7.6×10^3), 450 (4.7×10^3) nm (mol^{-1} L cm^{-1}). Anal. Calcd. for $C_{43}H_{79}N_2CrSi_2$: C, 70.53%, H, 10.87%, N, 3.83%. Found: C, 70.27%, H, 11.21%, N, 3.69%. Crystals suitable for single crystal X-ray diffraction studies were obtained from the workup described above.

SUPPLEMENTARY FIGURES

Figure S1.1: Cyclic voltammogram of **1.1** in 1,2-difluorobenzene

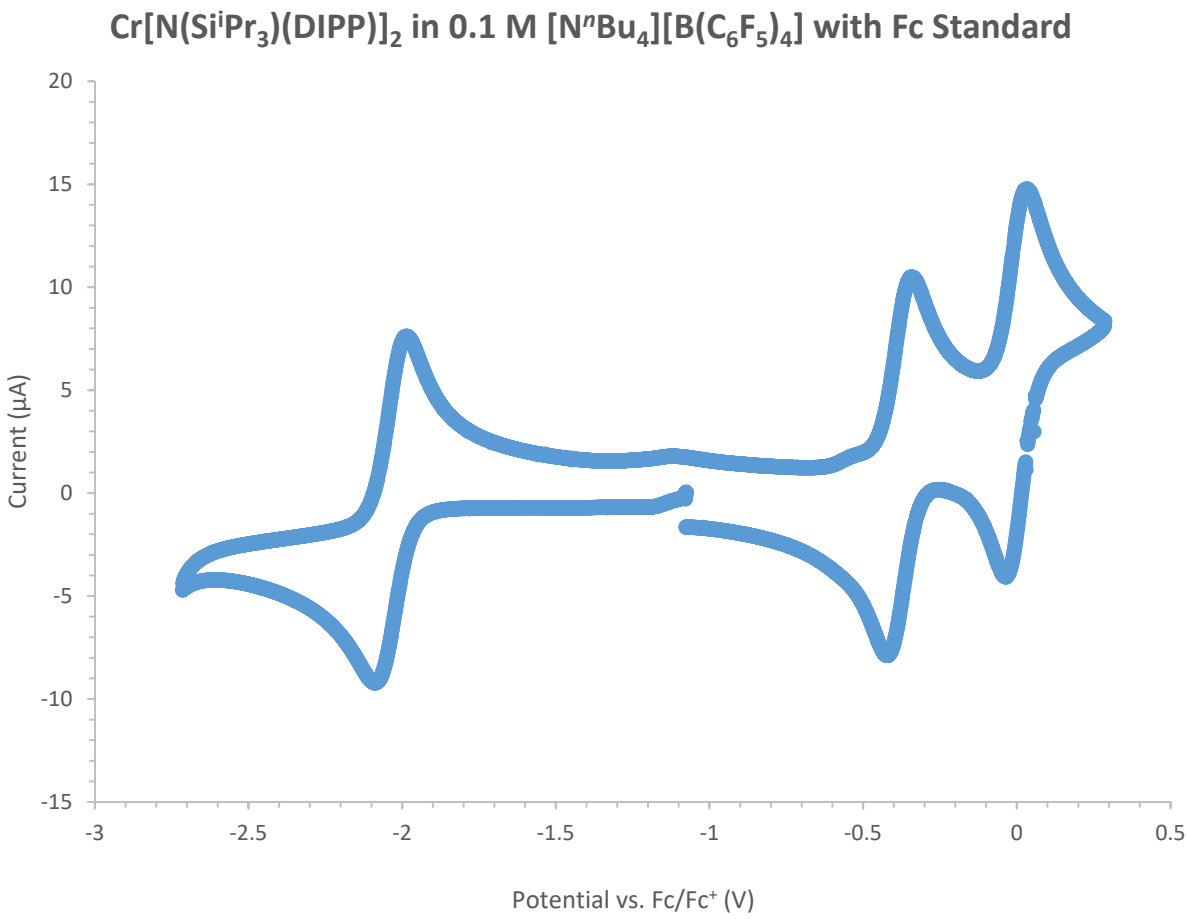

Figure S1.2: Solid-state structure of **1**.**2b** as determined by single-crystal X-ray diffraction.

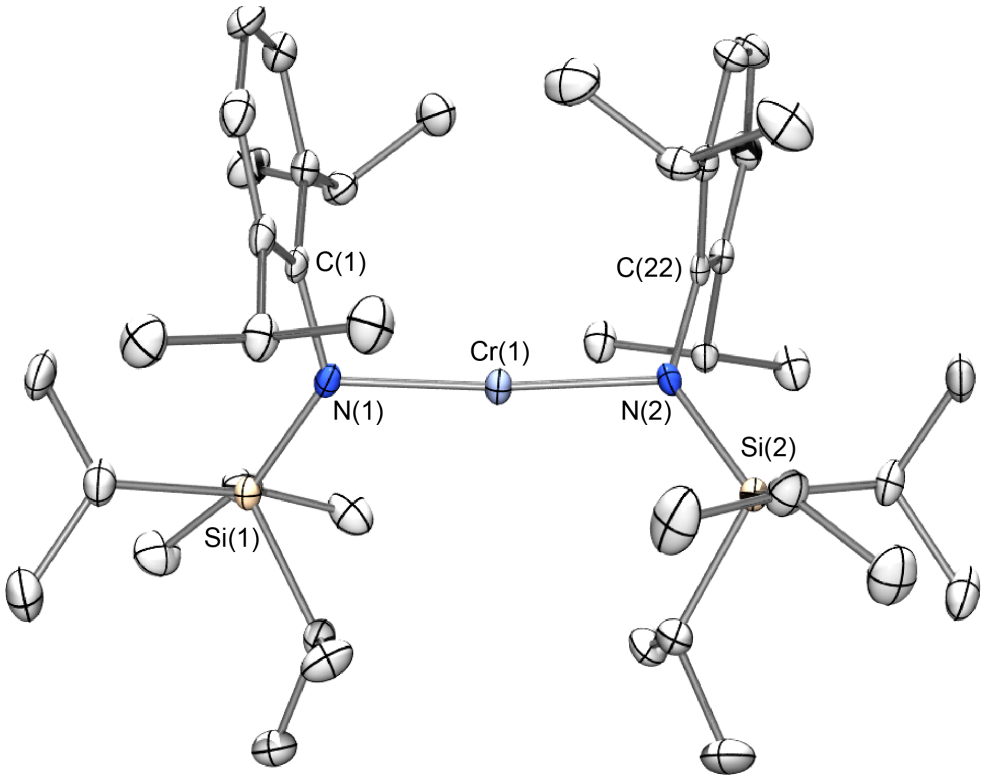

Notes: Thermal ellipsoids shown at 50% probability. Hydrogen atoms and tetrabutylammonium cation have been omitted for clarity. Selected bond distances [Å], angles [°], and torsions [°]: Cr(1)–N(1): 2.051(2), Cr(1)–N(2): 2.047(2), C(1)–N(1): 1.405(3), C(22)–N(2): 1.407(3), N(1)–Si(1): 1.699(2), N(2)–Si(2): 1.703(2), Cr(1)–C(1): 2.836(3), Cr(1)–C(22): 2.789(3), N(1)–Cr(1)–N(2): 175.63(9), C(1)–N(1)–Cr(1): 108.86(16), C(22)–N(2)–Cr(1): 106.19(16), Si(1)–N(1)–Cr(1): 122.64(12), Si(2)–N(2)–Cr(1): 123.86(12), C(1)–N(1)–N(2)–C(22): ±39.8(2).

SINGLE-CRYSTAL X-RAY DIFFRACTION CRYSTAL STRUCTURE DETAILS

Carbon atoms are shown in light gray, chromium in light blue, silicon in yellow and nitrogen in dark blue in all of the following diagrams.

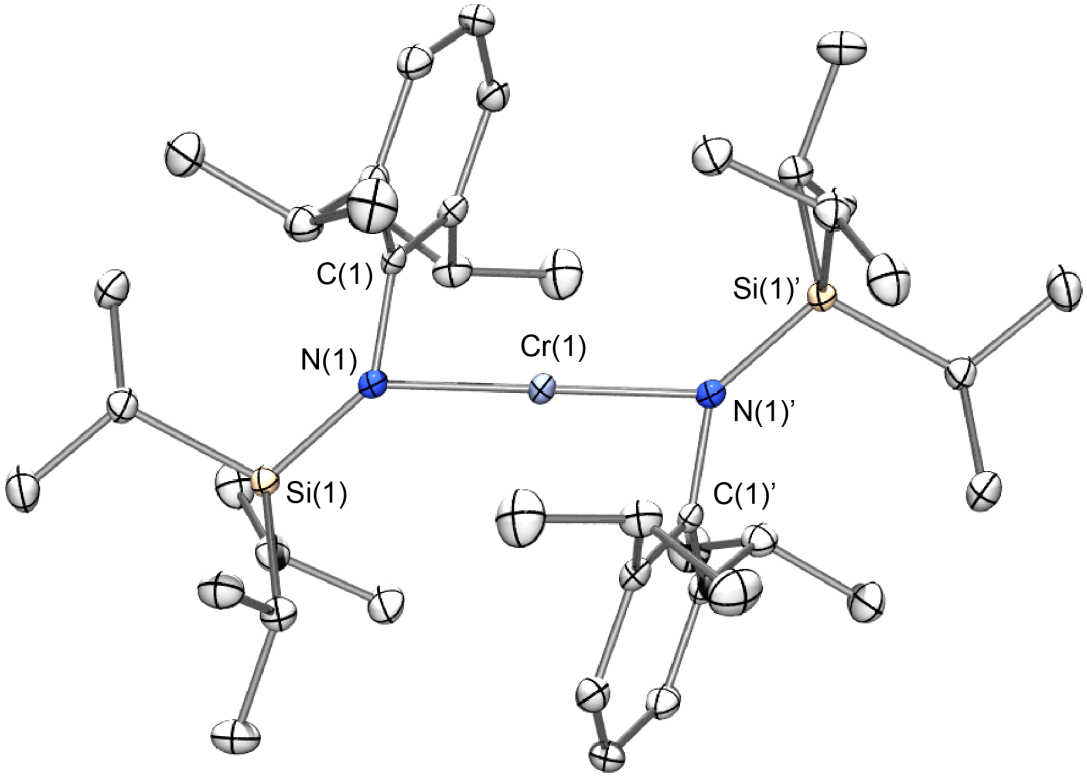

Solid-state structure of Cr[N(Si^{i}Pr$_3$)DIPP]$_2$ (**1.1**) as determined by single-crystal X-ray diffraction. Hydrogen atoms have been omitted for clarity. Thermal ellipsoids shown at 50% probability. Selected bond distances [Å], angles [°], and torsions [°]: Cr(1)–N(1): 2.0036(12), C(1)–N(1): 1.402(2), N(1)–Si(1): 1.7146(13), Cr(1)–C(1): 2.2709(14), N(1)–Cr(1)–N(1)': 180.00(8), C(1)–N(1)–Cr(1): 81.59(8), Si(1)–N(1)–Cr(1): 137.87(8), C(1)–N(1)–N(1)'–C(1)': 180.0(1).

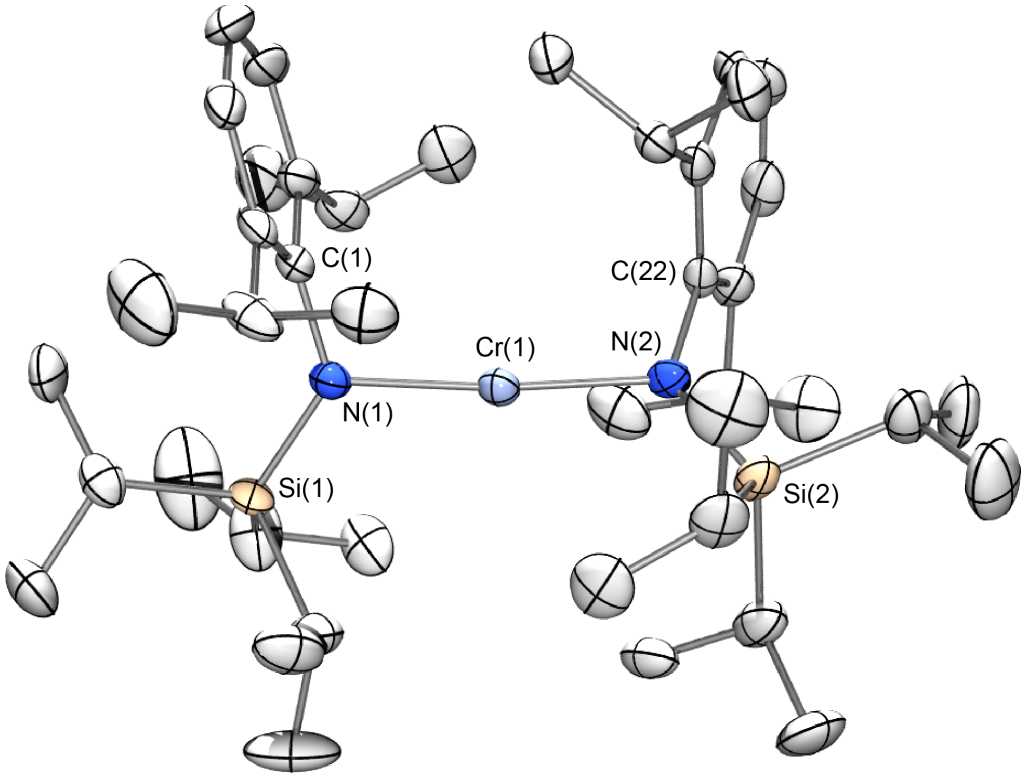

Solid-state structure of [K(DME)$_4$]{Cr[N(Si^{i}Pr$_3$)DIPP]$_2$} (**1.2a**) as determined by single-crystal X-ray diffraction. Hydrogen atoms and potassium cation coordinated by DME have been omitted for clarity. Thermal ellipsoids shown at 50% probability. Selected bond distances [Å], angles [°], and torsions [°]: Cr(1)–N(1): 2.054(3), Cr(1)–N(2): 2.061(3), C(1)–N(1): 1.416(5), C(22)–N(2): 1.425(5), N(1)–Si(1): 1.703(3), N(2)–Si(2): 1.697(3), Cr(1)–C(1): 2.840(5), Cr(1)–C(22): 2.854(3), N(1)–Cr(1)–N(2): 175.02(13), C(1)–N(1)–Cr(1): 108.4(2), C(22)–N(2)–Cr(1): 108.5(2), Si(1)–N(1)–Cr(1): 123.67(18), Si(2)–N(2)–Cr(1): 125.79(17), C(1)–N(1)–N(2)–C(22): ±44.1(3).

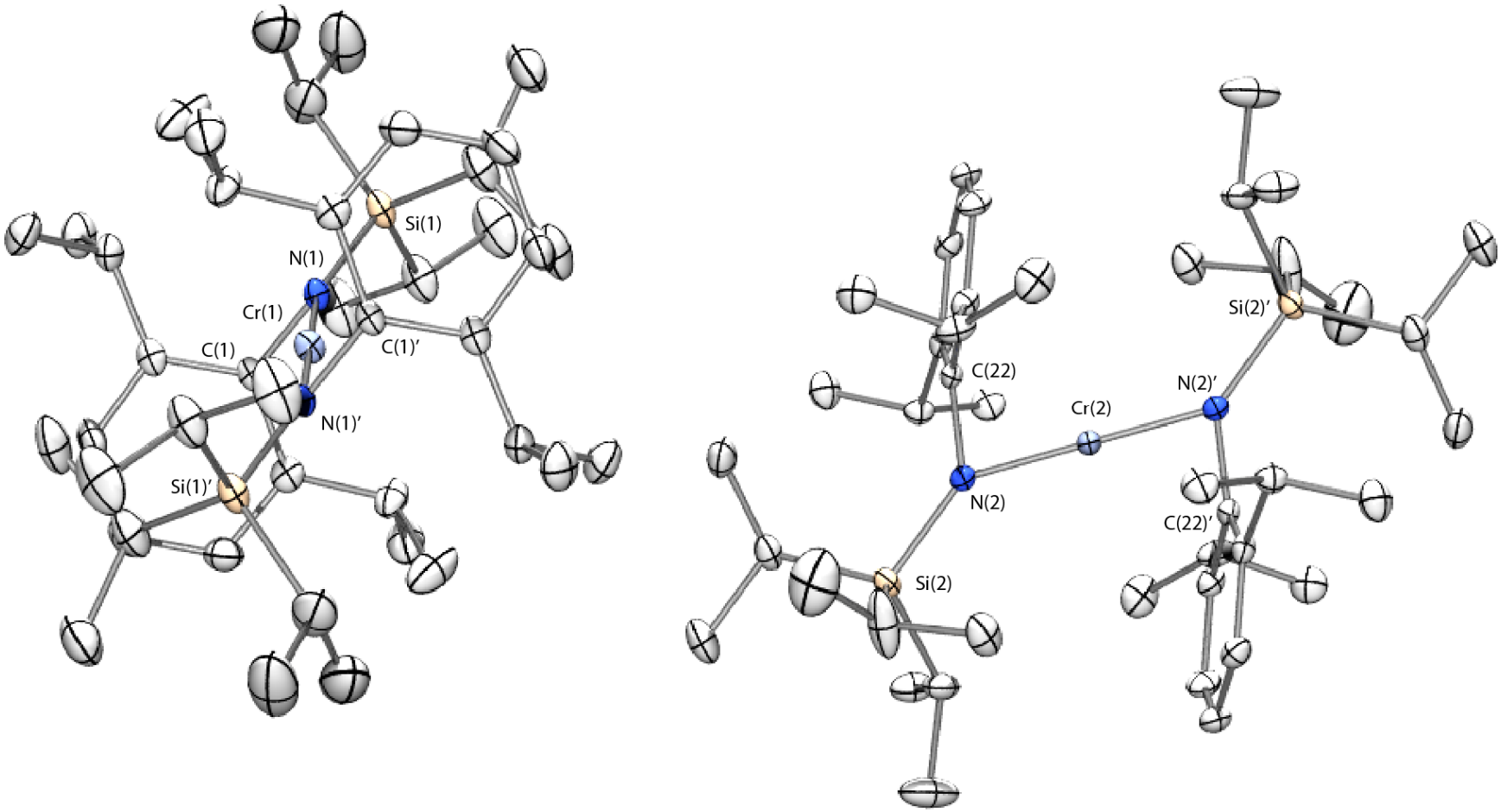

Solid-state structure of {Cr[N(Si^{i}Pr$_3$)DIPP]$_2$}[B(C$_6$F$_5$)$_4$] (**1.3**) as determined by single-crystal X-ray diffraction. Hydrogen atoms have been omitted for clarity. Solvent and B(C$_6$F$_5$)$_4$ anions have been excluded. Thermal ellipsoids shown at 50% probability. Selected bond distances [Å], angles [°], and torsions [°]: Cr(1)–N(1): 1.872(2), Cr(2)–N(2): 1.869(2), C(1)–N(1): 1.433(3), C(22)–N(2): 1.433(3), N(1)–Si(1): 1.796(2), N(2)–Si(2): 1.785(2), Cr(1)–C(1): 2.225(2), Cr(2)–C(22): 2.217(2), N(1)–Cr(1)–N(1)': 180.000(1), N(2)–Cr(2)–N(2)': 180.0, C(1)–N(1)–Cr(1): 83.48(14), C(22)–N(2)–Cr(2): 83.24(13), Si(1)–N(1)–Cr(1): 142.58(12), Si(2)–N(2)–Cr(2): 141.09(12), C(1)–N(1)–N(1)'–C(1)': 180.0(2), C(22)–N(2)–N(2)'–C(22)': 180.0(2).

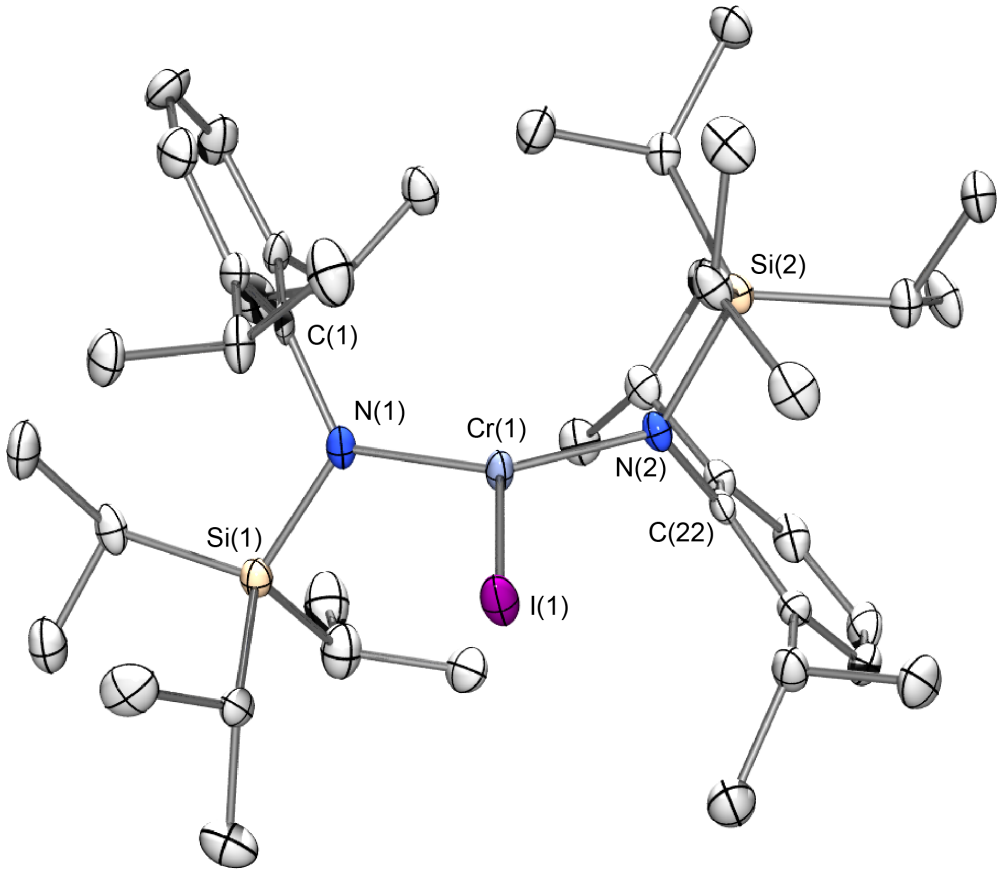

Solid-state structure of (I)Cr[N(Si^{i}Pr$_3$)DIPP]$_2$ (**1.4**) as determined by single-crystal X-ray diffraction. Hydrogen atoms have been omitted for clarity. Thermal ellipsoids shown at 50% probability. Selected bond distances [Å], angles [°], and torsions [°]: Cr(1)–N(1): 1.906(4), Cr(1)–N(2): 1.889(4), Cr(1)–I(1): 2.5929(8), C(1)–N(1): 1.457(6), C(22)–N(2): 1.465(6), N(1)–Si(1): 1.808(4), N(2)–Si(2): 1.815(4), Cr(1)–C(1): 2.924(5), Cr(1)–C(22): 2.965(5), N(1)–Cr(1)–N(2): 139.49(17), N(1)–Cr(1)–I(1): 110.31(12), N(2)–Cr(1)–I(1): 110.19(12), C(1)–N(1)–Cr(1): 120.2(3), C(22)–N(2)–Cr(1): 123.8(3), Si(1)–N(1)–Cr(1): 121.2(2), Si(2)–N(2)–Cr(1): 120.1(2), C(1)–N(1)–N(2)–C(22): ±136.5(4).

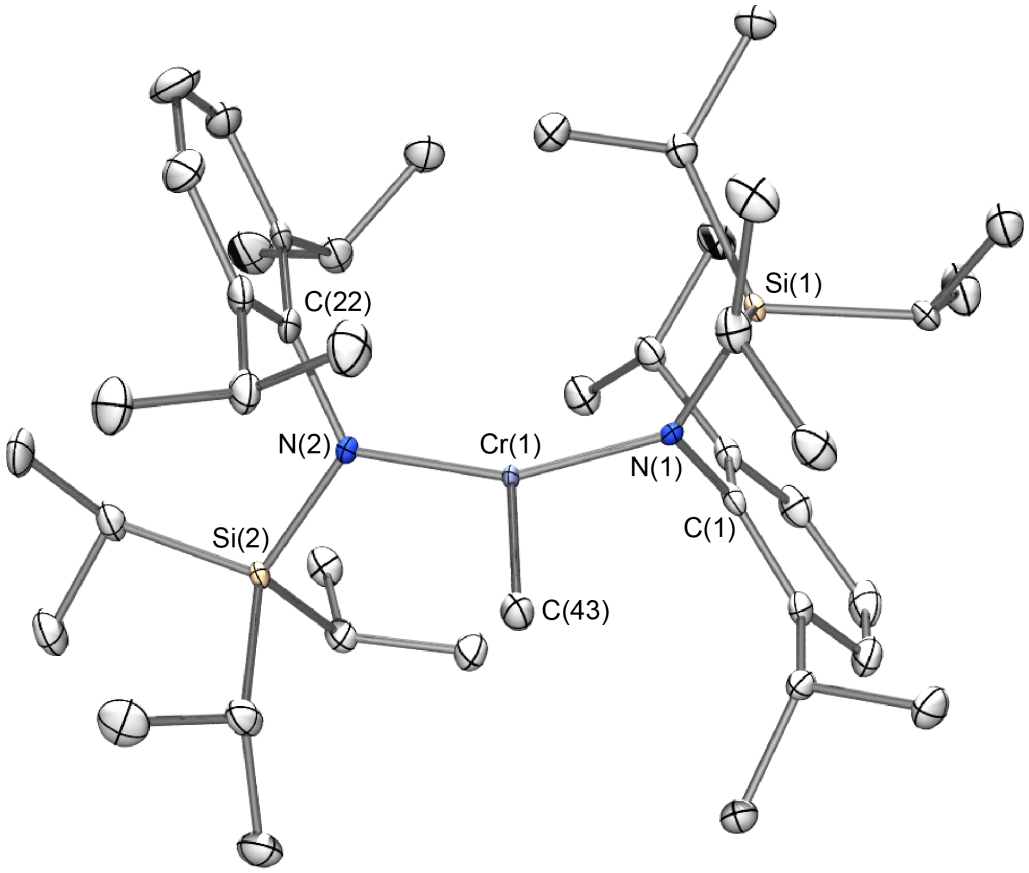

Solid-state structure of (Me)Cr[N(Si^{i}Pr$_3$)DIPP]$_2$ (**1.5**) as determined by single-crystal X-ray diffraction. Hydrogen atoms have been omitted for clarity. Disordered chromium and silicon atoms have been excluded. Thermal ellipsoids shown at 50% probability. Selected bond distances [Å], angles [°], and torsions [°]: Cr(1)–N(1): 1.893(2), Cr(1)–N(2): 1.906(2), Cr(1)–C(43): 2.058(3), C(1)–N(1): 1.458(4), C(22)–N(2): 1.460(4), N(1)–Si(1): 1.793(3), N(2)–Si(2): 1.783(3), Cr(1)–C(1): 2.949(3), Cr(1)–C(22): 2.905(3), N(1)–Cr(1)–N(2): 142.89(11), N(1)–Cr(1)–C(43): 107.92(12), N(2)–Cr(1)–C(43): 109.14(12), C(1)–N(1)–Cr(1): 122.71(19), C(22)–N(2)–Cr(1): 118.75(19), Si(1)–N(1)–Cr(1): 120.45(14), Si(2)–N(2)–Cr(1): 121.61(13), C(1)–N(1)–N(2)–C(22): ±138.2(2).

Crystal data and structure refinement for complex **1.1**:

Empirical formula	C42 H76 Cr N2 Si2	
Formula weight	717.23	
Temperature	100(2) K	
Wavelength	0.71073 Å	
Crystal system	Triclinic	
Space group	P-1	
Unit cell dimensions	a = 10.6605(3) Å	α = 98.9810(10)°.
	b = 10.8266(3) Å	β = 104.6850(10)°.
	c = 11.4767(3) Å	γ = 118.9100(10)°.
Volume	1059.18(5) $Å^3$	
Z	1	
Density (calculated)	1.124 Mg/m^3	
Absorption coefficient	0.356 mm^{-1}	
F(000)	394	
Crystal size	0.09 x 0.09 x 0.06 mm^3	
Theta range for data collection	1.94 to 31.24°.	
Index ranges	-13<=h<=15, -15<=k<=13, -14<=l<=16	
Reflections collected	24671	
Independent reflections	5882 [R(int) = 0.0420]	
Completeness to theta = 25.00°	99.4 %	
Absorption correction	Semi-empirical from equivalents	
Max. and min. transmission	0.9790 and 0.9687	
Refinement method	Full-matrix least-squares on F^2	
Data / restraints / parameters	5882 / 0 / 224	
Goodness-of-fit on F^2	1.021	
Final R indices [I>2sigma(I)]	R1 = 0.0405, wR2 = 0.0852	
R indices (all data)	R1 = 0.0675, wR2 = 0.0950	
Largest diff. peak and hole	0.365 and -0.302 $e.Å^{-3}$	

Crystal data and structure refinement for complex **1.2a**:

Empirical formula	C58 H116 Cr K N2 O8 Si2	
Formula weight	1116.81	
Temperature	100(2) K	
Wavelength	0.71073 Å	
Crystal system	Orthorhombic	
Space group	P2(1)2(1)2(1)	
Unit cell dimensions	a = 15.8187(7) Å	a= 90°.
	b = 17.0756(8) Å	b= 90°.
	c = 25.0015(13) Å	g = 90°.
Volume	6753.2(6) $Å^3$	
Z	4	
Density (calculated)	1.098 Mg/m^3	
Absorption coefficient	0.313 mm^{-1}	
F(000)	2452	
Crystal size	0.11 x 0.10 x 0.01 mm^3	
Theta range for data collection	1.44 to 30.70°.	
Index ranges	-10<=h<=22, -19<=k<=22, -31<=l<=32	
Reflections collected	54941	
Independent reflections	16443 [R(int) = 0.0409]	
Completeness to theta = 25.00°	100.0 %	
Absorption correction	Semi-empirical from equivalents	
Max. and min. transmission	0.9969 and 0.9664	
Refinement method	Full-matrix least-squares on F^2	
Data / restraints / parameters	16443 / 158 / 677	
Goodness-of-fit on F^2	1.037	
Final R indices [I>2sigma(I)]	R1 = 0.0729, wR2 = 0.1814	
R indices (all data)	R1 = 0.0961, wR2 = 0.1995	
Absolute structure parameter	0.00	
Largest diff. peak and hole	1.261 and -0.615 e.$Å^{-3}$	

Crystal data and structure refinement for complex **1.2b**:

Empirical formula	C58 H112 Cr N3 Si2	
Formula weight	959.68	
Temperature	100(2) K	
Wavelength	0.71073 Å	
Crystal system	Monoclinic	
Space group	P 21/n	
Unit cell dimensions	a = 14.7215(4) Å	α = 90°.
	b = 28.4194(8) Å	β = 90.949(2)°.
	c = 14.8687(4) Å	γ = 90°.
Volume	6219.9(3) $Å^3$	
Z	4	
Density (calculated)	1.025 Mg/m^3	
Absorption coefficient	0.257 mm^{-1}	
F(000)	2132	
Crystal size	0.100 x 0.100 x 0.040 mm^3	
Theta range for data collection	1.558 to 25.376°.	
Index ranges	-17<=h<=17, -30<=k<=34, -17<=l<=17	
Reflections collected	36473	
Independent reflections	11368 [R(int) = 0.0567]	
Completeness to theta = 25.000°	99.8 %	
Absorption correction	Semi-empirical from equivalents	
Max. and min. transmission	0.942 and 0.828	
Refinement method	Full-matrix least-squares on F^2	
Data / restraints / parameters	11368 / 0 / 601	
Goodness-of-fit on F^2	1.013	
Final R indices [I>2sigma(I)]	R1 = 0.0574, wR2 = 0.1120	
R indices (all data)	R1 = 0.1036, wR2 = 0.1308	
Extinction coefficient	n/a	
Largest diff. peak and hole	1.353 and -0.480 $e.Å^{-3}$	

Crystal data and structure refinement for complex **1.3**:

Empirical formula	C69 H77 B Cr F21 N2 Si2	
Formula weight	1452.32	
Temperature	100(2) K	
Wavelength	0.71073 Å	
Crystal system, space group	Triclinic	
Space group	P-1	
Unit cell dimensions	a = 13.4838(8) Å	α = 67.150(3) deg.
	b = 15.8748(9) Å	β = 89.637(3) deg.
	c = 18.4544(10) Å	γ = 69.398(3) deg.
Volume	3368.3(3) $Å^3$	
Z	2	
Calculated density	1.432 Mg/m^3	
Absorption coefficient	0.307 mm^{-1}	
F(000)	1502	
Crystal size	0.13 x 0.06 x 0.02 mm	
Theta range for data collection	1.49 to 25.45 deg.	
Limiting indices	-16<=h<=15, -19<=k<=19, -22<=l<=22	
Reflections collected / unique	55268 / 12395 [R(int) = 0.0321]	
Completeness to theta = 25.00	100.0 %	
Absorption correction	None	
Max. and min. transmission	0.9939 and 0.9612	
Refinement method	Full-matrix least-squares on F^2	
Data / restraints / parameters	12395 / 0 / 897	
Goodness-of-fit on F^2	1.032	
Final R indices [I>2sigma(I)]	R1 = 0.0494, wR2 = 0.1204	
R indices (all data)	R1 = 0.0600, wR2 = 0.1282	
Largest diff. peak and hole	2.339 and -0.829 $e.Å^{-3}$	

Crystal data and structure refinement for complex **1.4**:

Empirical formula	C42 H76 Cr I N2 Si2	
Formula weight	844.13	
Temperature	100(2) K	
Wavelength	0.71073 Å	
Crystal system	Monoclinic	
Space group	P2(1)/c	
Unit cell dimensions	a = 11.0285(5) Å	α= 90°.
	b = 23.0870(10) Å	β= 90.515(3)°.
	c = 17.0353(7) Å	γ = 90°.
Volume	4337.3(3) $Å^3$	
Z	4	
Density (calculated)	1.293 Mg/m^3	
Absorption coefficient	1.061 mm^{-1}	
F(000)	1788	
Crystal size	0.04 x 0.03 x 0.01 mm^3	
Theta range for data collection	1.76 to 25.43°.	
Index ranges	-13<=h<=13, 0<=k<=27, 0<=l<=20	
Reflections collected	7912	
Independent reflections	7912 [R(int) = 0.0808]	
Completeness to theta = 25.00°	99.1 %	
Absorption correction	Semi-empirical from equivalents	
Max. and min. transmission	0.9895 and 0.9588	
Refinement method	Full-matrix least-squares on F^2	
Data / restraints / parameters	7912 / 0 / 453	
Goodness-of-fit on F^2	1.050	
Final R indices [I>2sigma(I)]	R1 = 0.0523, wR2 = 0.0978	
R indices (all data)	R1 = 0.0854, wR2 = 0.1047	
Largest diff. peak and hole	0.977 and -0.583 e.$Å^{-3}$	

Crystal data and structure refinement for complex **1.5**:

Empirical formula	C43 H79 Cr N2 Si2	
Formula weight	732.26	
Temperature	100(2) K	
Wavelength	0.71073 Å	
Crystal system	Monoclinic	
Space group	P2(1)/c	
Unit cell dimensions	a = 11.0453(7) Å	a= 90°.
	b = 23.1010(16) Å	b= 90.156(3)°.
	c = 16.8139(10) Å	g = 90°.
Volume	4290.2(5) $Å^3$	
Z	4	
Density (calculated)	1.134 Mg/m^3	
Absorption coefficient	0.353 mm^{-1}	
F(000)	1612	
Crystal size	0.09 x 0.09 x 0.02 mm^3	
Theta range for data collection	1.50 to 25.41°.	
Index ranges	-13<=h<=13, -27<=k<=27, -20<=l<=20	
Reflections collected	47476	
Independent reflections	7802 [R(int) = 0.0811]	
Completeness to theta = 25.00°	99.4 %	
Absorption correction	Semi-empirical from equivalents	
Max. and min. transmission	0.9930 and 0.9689	
Refinement method	Full-matrix least-squares on F^2	
Data / restraints / parameters	7802 / 0 / 468	
Goodness-of-fit on F^2	1.067	
Final R indices [I>2sigma(I)]	R1 = 0.0515, wR2 = 0.1176	
R indices (all data)	R1 = 0.0607, wR2 = 0.1222	
Largest diff. peak and hole	0.517 and -0.375 $e.Å^{-3}$	

REFERENCES FOR EXPERIMENTAL DETAILS, SUPPLEMENTARY FIGURES, AND SINGLE-CRYSTAL X-RAY DIFFRACTION CRYSTAL STRUCTURE DETAILS

(1) LeSuer, R. J., Buttolph, C., Geiger, W. E. *Anal. Chem.* **2004**, *76* (21), 6395–6401.
(2) Bergbreiter, D. E., Killough, J. M. *J. Am. Chem. Soc.* **1978**, *100* (7), 2126–2134.
(3) O'Connor, A. R., Nataro, C., Golen, J. A., Rheingold, A. L. *J. Organomet. Chem.* **2004**, *689* (14), 2411–2414.
(4) Evans, D. F. *J. Chem. Soc. Resumed* **1959**, No. 0, 2003–2005.
(5) Live, D. H., Chan, S. I. *Anal. Chem.* **1970**, *42* (7), 791–792.
(6) Altomare, A., Burla, M. C., Camalli, M., Cascarano, G. L., Giacovazzo, C., Guagliardi, A., Moliterni, A. G. G., Polidori, G., Spagna, R. *J. Appl. Crystallogr.* **1999**, *32* (1), 115–119.
(7) Sheldrick, G. M., Schneider, T. R. In *Methods in Enzymology*, Macromolecular Crystallography Part B, Academic Press, 1997, Vol. 277, pp 319–343.
(8) Sheldrick, G. M. *Acta Crystallogr. Sect. C Struct. Chem.* **2015**, *71* (1), 3–8.
(9) Shen, B., Ying, L., Chen, J., Luo, Y. *Inorganica Chim. Acta* **2008**, *361* (5), 1255–1260.

Chapter 2: Low-Coordinate Chromium in Various Oxidation States Supported by –N(SiMe$_3$)DIPP

INTRODUCTION

The silylarylamido ligand –N(SiMe$_3$)DIPP (DIPP = 2,6-diisopropylphenyl) has been used to support various low-coordinate bis(amido) complexes of late first-row transition metals. This specific ligand platform has provided neutral, two-coordinate complexes of iron, cobalt, and nickel,[1,2] which can be coordinated by Lewis bases[1,3] or reduced to their anionic two-coordinate analogues.[4,5] Derivatives of Ni[N(SiMe$_3$)DIPP]$_2$, including an anionic three-coordinate nickel(II) methyl species, have also been investigated in the context of catalytic C–C bond formation.[6]

In contrast, use of –N(SiMe$_3$)DIPP with earlier metals such as chromium has received less attention. A previously reported attempt to access a chromium(II) species supported by –N(SiMe$_3$)DIPP *via* salt metathesis with CrCl$_2$(THF)$_2$ resulted in a tetrameric complex formed by C–H activation of the ligand (Figure 2.1, **A**).[2] One approach to deconvolution of this complex reaction sequence is implementation of a bulkier silylarylamido ligand, –N(Si^{i}Pr$_3$)DIPP, which enables the facile synthesis of two-coordinate chromium in multiple oxidation states, as well as three-coordinate bis(amido) chromium(III) iodide and methyl complexes.[7]

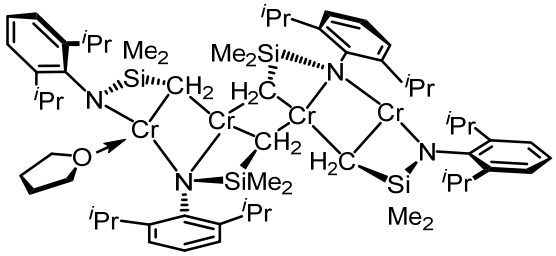

A

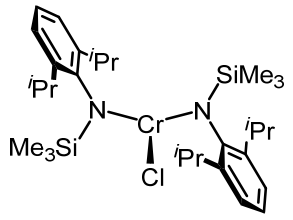

2.1

Figure 2.1. Previously reported chromium complexes supported by –N(SiMe$_3$)DIPP, (**A**) C–H activated tetrameric Cr(II) species[2] and (**2.1**) (Cl)Cr[N(SiMe$_3$)DIPP]$_2$.[8]

A more recent investigation has shown that the Cr[N(SiMe$_3$)DIPP]$_2$ fragment is more stable with chromium in the formally +3 oxidation state.[8] In contrast to the analogous reaction with CrCl$_2$(THF)$_2$, which leads to C–H activation chemistry, CrCl$_3$(THF)$_3$ readily reacts with LiN(SiMe$_3$)DIPP to give (Cl)Cr[N(SiMe$_3$)DIPP]$_2$ (**2.1**; Figure 2.1), which was converted to three-coordinate chromium(III) alkyl complexes such as Me–Cr[N(SiMe$_3$)DIPP]$_2$ (**2.2**) and the benzyl complex Bn–Cr[N(SiMe$_3$)DIPP]$_2$ (**2.3**).[8] Although these three-coordinate bis(amido) chromium complexes have been investigated in the context of ethylene polymerization and can produce ultra-high molecular weight polyethylene in the absence of an external activator, the redox reactivity of these species has not been investigated.[8]

Given the rarity of mononuclear chromium(II) and chromium(I) species supported by silylarylamido ligands,[7] and the previously reported redox chemistry of (Me)Ni[N(SiMe$_3$)DIPP]$_2$[6] it seemed that anionic analogues of **2.2** and **2.3** might be accessible, and of interest as low-coordinate chromium species that might exhibit novel reactivity modes. Furthermore, various Lewis-base adducts of M[N(SiMe$_3$)DIPP]$_2$ (M = Fe, Co, Ni)[3] indicated that neutral donor-stabilized chromium(II) complexes of the Cr[N(SiMe$_3$)DIPP]$_2$ moiety could be isolable, assuming such species could be generated. Here, we report stoichiometric reactions of the previously characterized mononuclear chromium(III) bis(amido) species, **2.1**, **2.2**, and **2.3**, in an effort to more broadly define the structural and chemical properties of chromium species in exceedingly low coordination numbers supported by the –N(SiMe$_3$)DIPP ligand.

RESULTS AND DISCUSSION

Reduction of **2.2** with 1.04 equiv of KC$_8$ in diethyl ether at -116 °C, followed by washing the crude solid with pentane and crystallization from diethyl ether layered with pentane afforded a coordination polymer of K{(Me)Cr[N(SiMe$_3$)DIPP]$_2$} (**2.4**) as teal crystals in 24% yield (Scheme 2.1). Similarly, reduction of **2.3** with 1.04 equiv of KC$_8$ in diethyl ether at -116 °C afforded the dimer of K{(Bn)Cr[N(SiMe$_3$)DIPP]$_2$} (**2.5**) as green crystals in 88% yield, from diethyl ether layered with pentane (Scheme 2.1). The solution magnetic moments of **2.4** and **2.5** in THF, determined by the Evans method,[9–11] are 4.5 and 4.9 μ_B, respectively, both consistent with a high-spin d^4 configuration.

The average Cr–N bond length in the solid-state structure of **2.4** is 2.038(14) Å (Figure 2.2), noticeably longer than the corresponding average Cr–N distance in **2.2** (1.872(4) Å). Moreover, **2.4** has an average Cr–C$_{Me}$ bond length of 2.092(11) Å, longer than the corresponding Cr–C$_{Me}$ bond length in the neutral chromium(III) methyl analogue **2.2** (2.036(6) Å), as expected for the increase in charge. The Cr–C$_{Me}$ bond length in **2.4** is also comparable to the Cr–C$_{SiMe3}$ distance in the dimeric chromium(II) bis(amido) alkyl species {K(TMEDA)$_3$}[{[(Me$_3$Si)$_2$N]Cr[μ-N(SiMe$_3$)$_2$](μ-CH$_2$SiMe$_3$)}$_2$(K)] (*cf.* Cr–C$_{SiMe3}$: 2.112(4) Å), formed from the addition of KCH$_2$SiMe$_3$ to Cr[N(SiMe$_3$)$_2$]$_2$(THF)$_2$.[12]

Similar to the trends observed for **2.4**, complex **2.5** has a Cr–C$_{CH2Ph}$ distance of 2.168(2) Å, longer than the 2.094(3) Å distance reported for the neutral chromium(III) benzyl analogue **2.3**.[8] The average Cr–N bond length in **2.5** is 2.023(3) Å, consistent with that of **2.4** and also longer than the corresponding average Cr–N distance in **2.3** (1.874(3) Å).

The extended structures of complexes **2.4** and **2.5** contain K$\cdots$C$_{alkyl}$ and K$\cdots$C$_{SiMe3}$ contacts similar to that of {K(TMEDA)$_3$}[{[(Me$_3$Si)$_2$N]Cr[μ-N(SiMe$_3$)$_2$](μ-CH$_2$SiMe$_3$)}$_2$(K)][12] (see Table 2.1), although there are no bridging amido interactions. Instead, the potassium cations in **2.4** and **2.5** are primarily coordinated through the more favorable aromatic DIPP moieties.

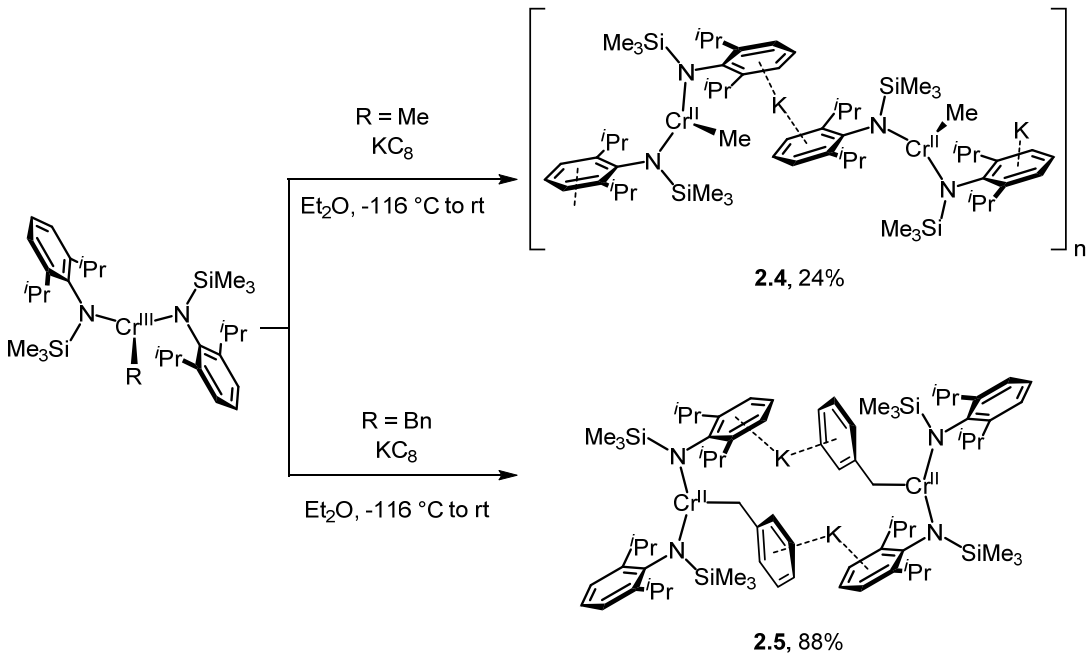

Scheme 2.1: Reduction of chromium(III) alkyl complexes.

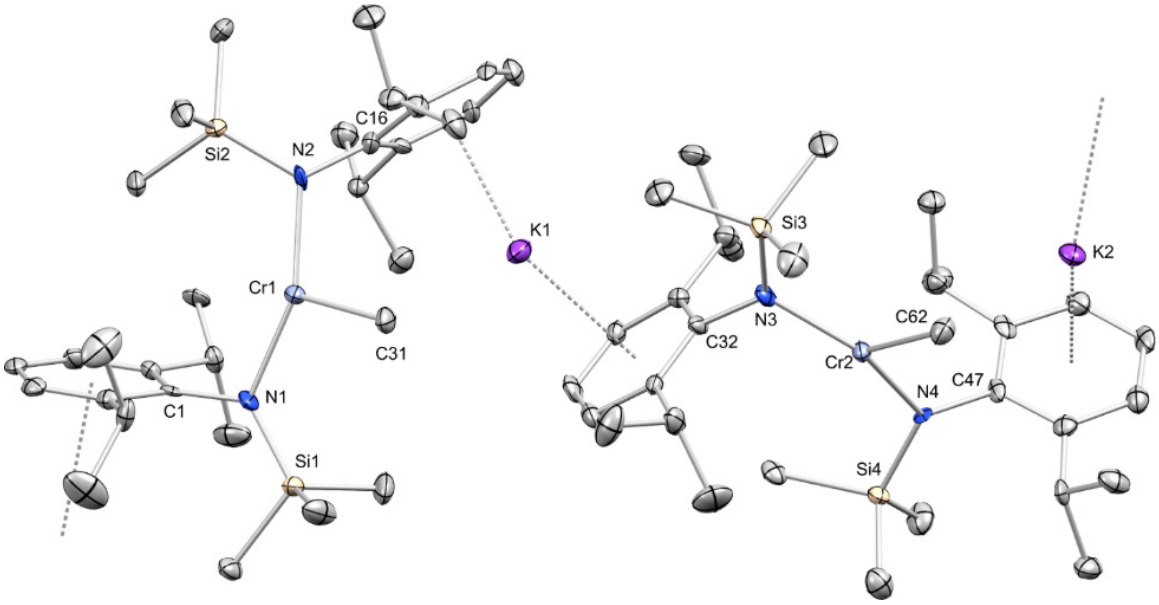

Figure 2.2. Solid-state structure of **2.4** determined by single-crystal X-ray crystallography. Thermal ellipsoids are shown at 50% probability. Hydrogen atoms have been omitted for clarity.

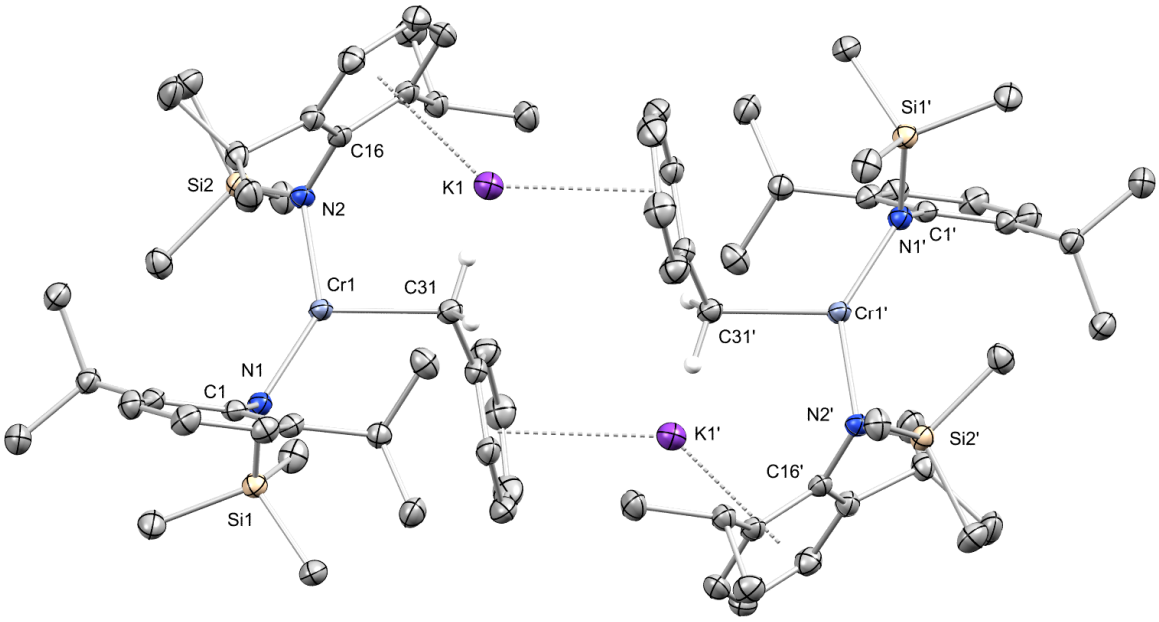

Figure 2.3. Solid-state structure of **2.5** determined by single-crystal X-ray crystallography. Thermal ellipsoids are shown at 50% probability. Hydrogen atoms have been omitted for clarity, with the exception of hydrogens on C31, which have been located from the electron density difference map.

Table 2.1. Bond lengths and close contact distances in complexes **2.4**, **2.5**, and {K(TMEDA)$_3$}[{[(Me$_3$Si)$_2$N]Cr{μ-N-(SiMe$_3$)$_2$}(μ-CH$_2$SiMe$_3$)}$_2$(K)].[12]

	2.4	**2.5**	{K(TMEDA)$_3$}[{[(Me$_3$Si)$_2$N]Cr [μ-N-(SiMe$_3$)$_2$](μ-CH$_2$SiMe$_3$)}$_2$(K)]
Cr–C$_{alkyl}$ (Å)	2.085(8), 2.099(8)	2.1685(19)	2.112(4)
K–C$_{alkyl}$ (Å)	3.079(9), 3.040(9)	3.051(2)	3.050(4)
K–C$_{SiMe3}$ (Å)	3.23(1), 3.220(9)	3.374(2)	3.420(4), 3.456(4)

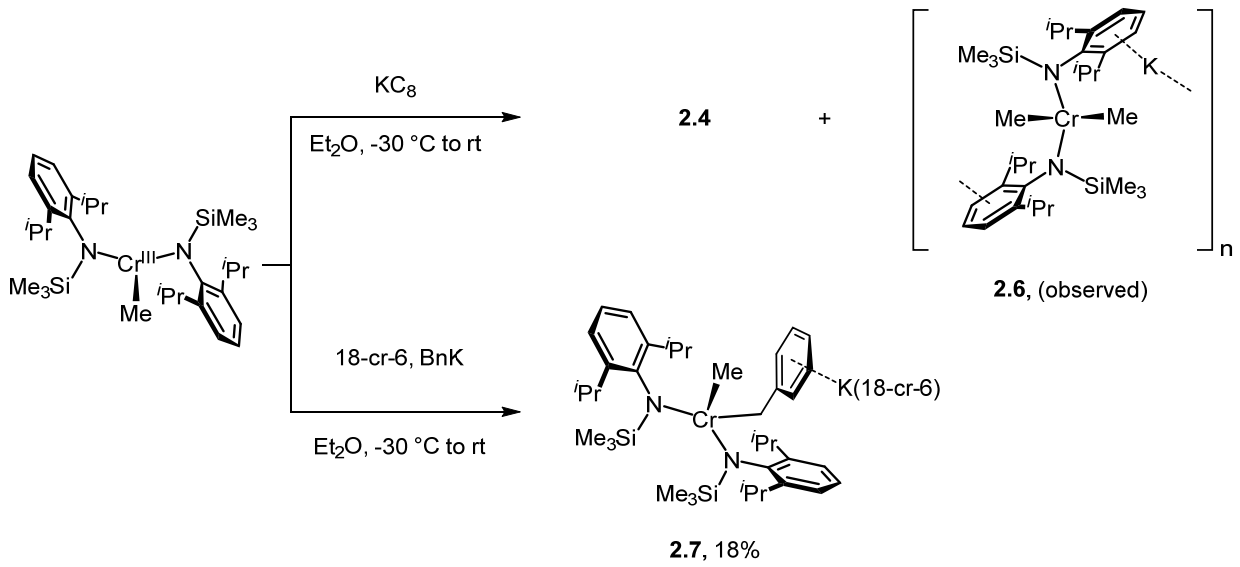

Scheme 2.2: Formation of chromium dialkyl complexes from **2.2**.

Interestingly, reduction of **2.2** with 1.1 equiv of KC_8 in diethyl ether at -30 °C, followed by crystallization of the filtered reaction mixture layered with pentane afforded crystals of primarily **2.4** but also of the anionic chromium(III) dialkyl species, $K\{(Me)_2Cr[N(SiMe_3)DIPP]_2\}$ (**2.6**, Scheme 2.2). The solid-state structure of **2.6** has an average $Cr–C_{Me}$ bond length of 2.074(4) Å, only slightly longer than the previously reported $Cr–C_{Me}$ bond length in the three-coordinate monoalkyl complex **2.2** (2.036(6) Å). The average Cr–N bond length in **2.6** is 2.004(5) Å, noticeably longer than the corresponding average Cr–N distance in **2.2** (1.872(4) Å), likely due to the higher coordination number of the metal center. Similar to **2.4** and **2.5**, **2.6** also coordinates the potassium cation via the aryl rings of the amido ligand and possesses an average $K–C_{Me}$ contact distance of 3.287(9) Å.

An analogue of **2.6** was synthesized by addition of benzyl potassium to a solution of **2.2** and 18-crown-6 (18-cr-6) in diethyl ether. Crystallization from diethyl ether afforded purple needles of $\{K(18\text{-cr-}6)\}\{(Bn)(Me)Cr[N(SiMe_3)DIPP]_2\}$ (**2.7**) in 18% yield. The solid-state structure of **2.7** contains average $Cr–C_{Me}$ and $Cr–C_{CH_2Ph}$ bond lengths of 2.043(3) Å and 2.116(3) Å, similar in length to the $Cr–C_{Me}$ and $Cr–C_{CH_2Ph}$ distances for **2.2** and **2.3** (*vida supra*). The average Cr–N bond length in **2.7** is 2.010(3) Å, similar to that of **2.6**. The solution magnetic moment of **2.7** in THF is 3.5 μ_B, consistent with a high-spin d^3 configuration.

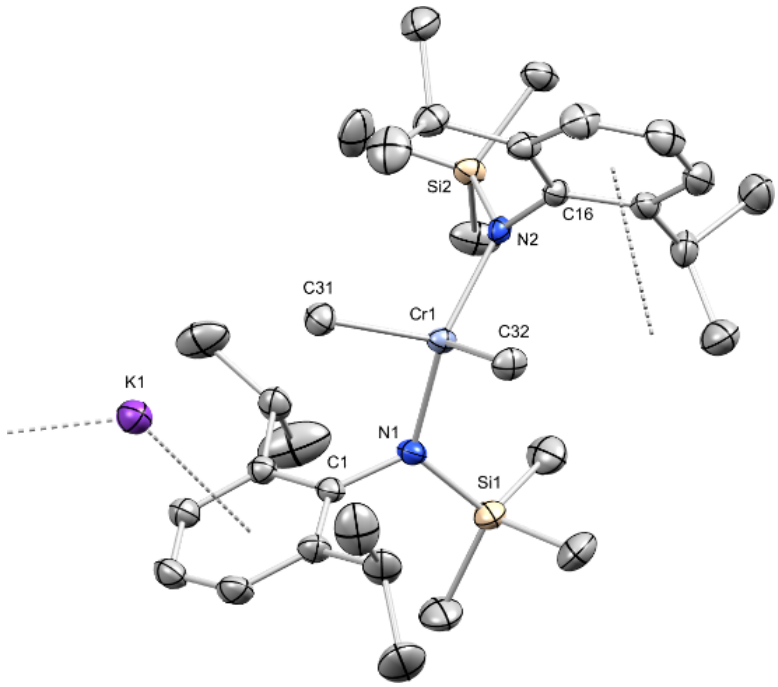

Figure 2.4. Solid-state structure of **2.6** determined by single-crystal X-ray crystallography. The second crystallographically independent unit of **2.6** has been omitted. Thermal ellipsoids are shown at 50% probability. Hydrogen atoms and diethyl ether molecule coordinated to the potassium cation have been omitted for clarity.

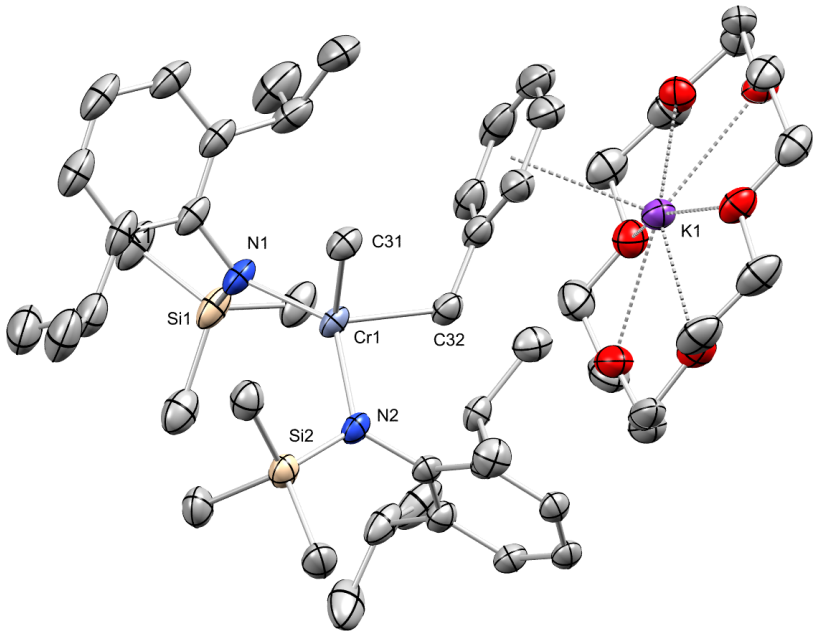

Figure 2.5. Solid-state structure of **2.7** determined by single-crystal X-ray crystallography. The second crystallographically independent unit of **2.7** has been omitted. Thermal ellipsoids are shown at 50% probability. Hydrogen atoms and diethyl ether molecule coordinated to the potassium cation have been omitted for clarity. Oxygen atoms shown in red.

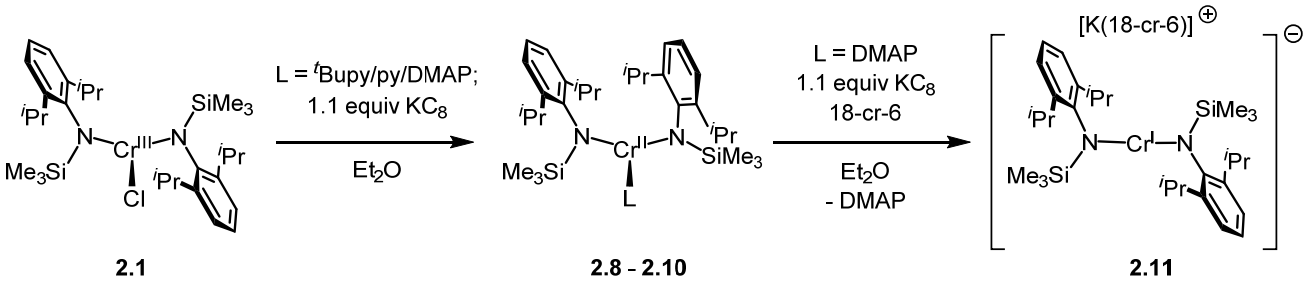

Scheme 2.3: Synthesis of low-valent, low-coordinate chromium complexes supported by –N(SiMe$_3$)DIPP.

Given that access to anionic, monomeric chromium(II) complexes supported by –N(SiMe$_3$)DIPP is possible, as indicated by the syntheses of **2.4** and **2.5**, it seemed that it might be possible to generate *neutral* chromium(II) complexes supported by –N(SiMe$_3$)DIPP. In fact, reduction of **2.1** with 1.1 equiv of KC_8 in the presence of 1 equiv of 4-*tert*-butylpyridine (^{t}Bupy) in diethyl ether afforded the three-coordinate chromium(II) complex (tBupy)Cr[N(SiMe$_3$)DIPP]$_2$ (**2.8**) in 55% yield (Scheme 2.3). Similarly, both the pyridine (py) and dimethylaminopyridine (DMAP) analogues (py)Cr[N(SiMe$_3$)DIPP]$_2$ (**2.9**) and (DMAP)Cr[N(SiMe$_3$)DIPP]$_2$ (**2.10**) were synthesized in 48 and 56% yield, respectively.

The solid-state structure of **2.8** reveals a distorted trigonal planar geometry (Figure 2.6) and contains a N1–Cr1–N2 bond angle of 143.12(6) Å. Comparable to the Cr–N bond length in the two-coordinate chromium(II) complex Cr[N(Si^{i}Pr$_3$)DIPP]$_2$ (2.0036(1) Å), **2.8** has Cr–N1 and Cr–N2 distances of 1.9559(11) and 2.0102(12) Å. Complex **2.10** is similar to **2.8** in structure, with a slightly less obtuse N1–Cr1–N2 bond angle of 139.59(8) Å (Figure S2.1). In complexes **2.8** and **2.10**, the plane of the pyridine core intersects the N1–Cr1–N2 plane by 55.78(3)° and 53.68(7)°, respectively. The geometries of these complexes are also similar to previously reported pyridine and DMAP complexes of later first-row transition metal complexes supported by –N(SiMe$_3$)DIPP.[1,3]

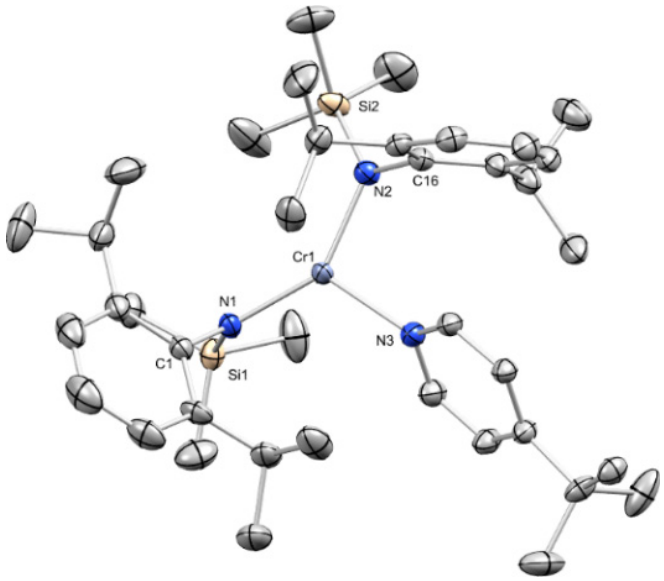

Figure 2.6. Solid-state structure of **2.8** determined by single-crystal X-ray crystallography. Thermal ellipsoids are shown at 50% probability. Hydrogen atoms and disordered *tert* butyl group have been omitted for clarity.

Previous work by Sylviane Sabo-Etienne and co-workers indicated that one-electron reduction to a two-coordinate metal(I) complex does not require a rigorously two-coordinate metal(II) precursor.[13,14] Reduction of **2.10** with KC_8 in the presence of 18-crown-6 (18-cr-6) resulted in an orange solution. Crystallization of the filtered reaction mixture layered with pentane, followed by recrystallization of the resulting solid from diethyl ether resulted in orange needles of {K(18-cr-6)}{Cr[N(SiMe$_3$)DIPP]$_2$} (**2.11**, Scheme 2.3), identified by single-crystal X-ray crystallography. In the solid-state structure of **2.11**, the chromium atom sits on an inversion center, with a crystallographically imposed linear N–Cr–N bond angle. The Cr–N bond distance is 2.0519(11) Å, similar in length to the two-coordinate chromium(I) complex [K(DME)$_{1.5}$]{Cr[N(Si^{i}Pr$_3$)DIPP]$_2$} (Cr–N: 2.054(3), 2.061(3) Å).[7] Although the tetrametallic complex resulting from addition of Li[N(SiMe$_3$)DIPP] to $CrCl_2(THF)_2$ (Figure 2.1, **A**) demonstrates the difficulties of directly accessing a two-coordinate species supported by –N(SiMe$_3$)DIPP *via* salt metathesis, the structure of **2.11** suggests that the ligand is sufficiently bulky to support a two-coordinate chromium(I) species.

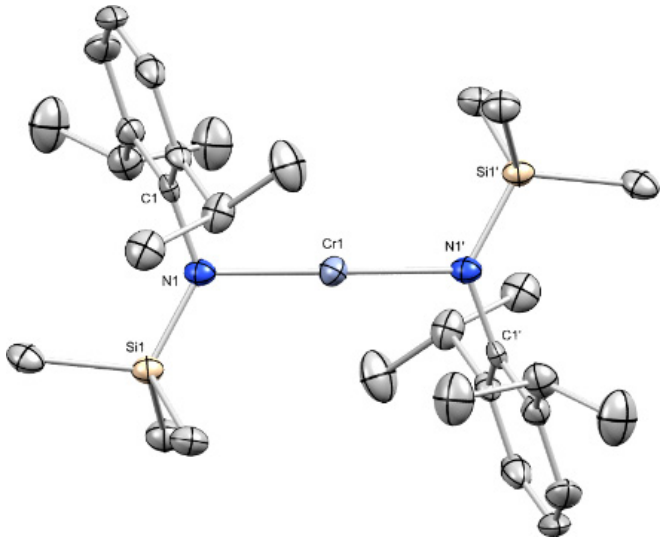

Figure 2.7. Solid-state structure of **2.11** determined by single-crystal X-ray crystallography. Thermal ellipsoids are shown at 50% probability. Hydrogen atoms and K(18-cr-6) have been omitted for clarity.

In an effort to examine other adducts of the Cr[N(SiMe$_3$)DIPP]$_2$ moiety, both trimethylphosphine and triethylamine were examined as potential donor ligands. Reduction of **2.1** with 1.05 equiv of KC_8 in the presence of 3 equiv of trimethylphosphine readily yielded (Me$_3$P)Cr[N(SiMe$_3$)DIPP]$_2$ (**2.12**). Complex **2.12** features a distorted trigonal planar geometry similar to that of **2.8** and **2.10**, with a wider N1–Cr1–N2 bond angle of 151.70(5) Å and Cr–N bond lengths of 1.9912(13) and 2.0132(13) Å. To date, no other three-coordinate chromium complexes containing any type of Cr–P bond have been structurally characterized,[15] although the two-coordinate chromium(I) complex (Me$_3$P)Cr[C$_6$H$_1$-2,6-(C$_6$H$_2$-2,4,6-^{i}Pr$_3$)2-3,5-^{i}Pr$_2$] is known.[16] The M–P bond distance in **2.12** is 2.4288(5) Å; shorter in length than the corresponding distances in both the iron(II) analogue (Me$_3$P)Fe[N(SiMe$_3$)DIPP]$_2$ (Fe–P: 2.4970(7) Å)[3] and the low-coordinate chromium(I) complex (Me$_3$P)Cr[C$_6$H$_1$-2,6-(C$_6$H$_2$-2,4,6-^{i}Pr$_3$)2-3,5-^{i}Pr$_2$] (Cr–P: 2.4646(5) Å),[16] as expected.

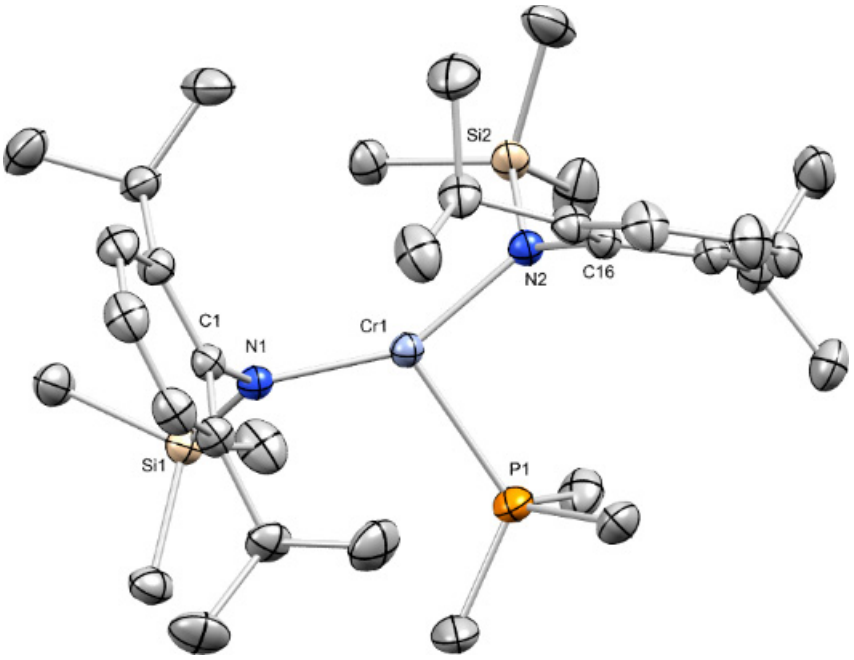

Figure 2.8. Solid-state structure of **2.12** determined by single-crystal X-ray crystallography. Thermal ellipsoids are shown at 50% probability. Hydrogen atoms have been omitted for clarity.

In contrast to its reactivity with trimethylphosphine, reduction of **2.1** with KC_8 in the presence of triethylamine afforded crystals of the dimeric chromium species $Cr[N(SiMe_2CH_2)DIPP]_2Cr[N(SiMe_3)DIPP]$ (**2.13**). Complex **2.13** features C–H activation of the $–SiMe_3$ methyl groups, similar to what has been observed for other chromium complexes supported by trimethylsilylamido ligands.[2,8,17] However, unlike previous species featuring this type of cyclometallation, the solid-state structure of **2.13** indicates a mixed valent species (Figure 2.9). The Cr1 metal center features Cr–N bond lengths of 1.8794(10) and 1.8841(11) Å, consistent with the average Cr–N distance in the chromium(III) methyl complex **2.2** (1.872(4) Å) but notably shorter than the Cr2–N3 distance of 1.9809(11) Å. Likely due to the lower coordination number compared to that of the Cr1 center, the Cr2 atom features a close interaction with the *ipso* carbon of the DIPP moiety (Cr2–C31: 2.2787(12) Å), similar to what is observed for both $Cr[N(Si^iPr_3)DIPP]_2$ and $\{Cr[N(Si^iPr_3)DIPP]_2\}\{B(C_6F_5)_4\}$.[7] The Cr1···Cr2 distance in **2.13** is 2.6629(3) Å, comparable to Cr···Cr distances of 2.727 and 2.662 Å in the previously reported tetrametallic complex resulting from addition of $Li[N(SiMe_3)DIPP]$ to $CrCl_2(THF)_2$ (Figure 2.1, **A**).[2]

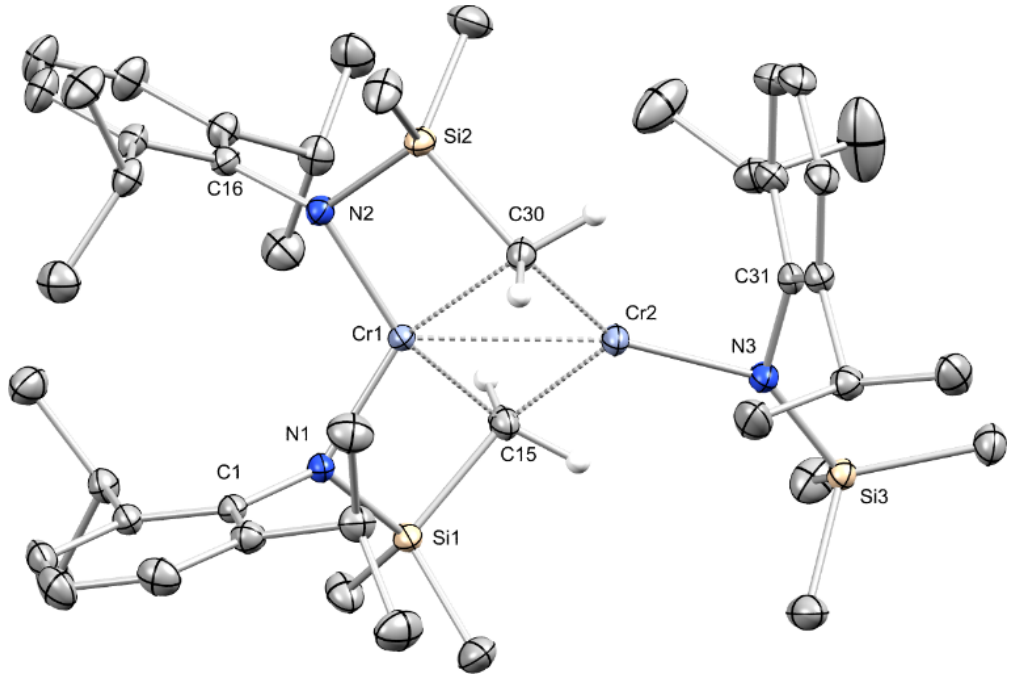

Figure 2.9. Solid-state structure of **2.13** determined by single-crystal X-ray crystallography. Thermal ellipsoids are shown at 50% probability. Hydrogen atoms have been omitted for clarity, with the exception of hydrogen atoms on C15 and C30, which were located using the electron density difference map.

CONCLUSIONS

This work extends the family of chromium complexes supported by –N(SiMe$_3$)DIPP. Both anionic and neutral chromium(II) species have been synthesized via reduction of their chromium(III) analogues. While –N(SiMe$_3$)DIPP is sterically deficient enough to enable isolation of a range of both chromium(III) and chromium(II) complexes, the observation of a two-coordinate chromium(I) species also provides evidence that this ligand is still sterically demanding enough to enable two-coordination. Moreover, reduction of **2.1** in the presence of triethylamine, resulting in the formation of dimeric species **2.13**, appears to enable C–H activation in an intermolecular fashion. Despite the synthetic challenges associated with accessing lower-valent derivatives of Cr[N(SiMe$_3$)DIPP]$_2$, this work demonstrates a range of species which can be supported by this bis(silylarylamido) ligand set.

REFERENCES

(1) Lipschutz, M. I., Tilley, T. D. *Chem. Commun.* **2012**, *48* (57), 7146–7148.
(2) Lin, C.-Y., Guo, J.-D., Fettinger, J. C., Nagase, S., Grandjean, F., Long, G. J., Chilton, N. F., Power, P. P. *Inorg. Chem.* **2013**, *52* (23), 13584–13593.
(3) Lin, C.-Y., Fettinger, J. C., Power, P. P. *Inorg. Chem.* **2017**, *56* (16), 9892–9902.
(4) Lipschutz, M. I., Yang, X., Chatterjee, R., Tilley, T. D. *J. Am. Chem. Soc.* **2013**, *135* (41), 15298–15301.
(5) Lin, C.-Y., Fettinger, J. C., Grandjean, F., Long, G. J., Power, P. P. *Inorg. Chem.* **2014**, *53* (17), 9400–9406.
(6) Lipschutz, M. I., Tilley, T. D. *Angew. Chem. Int. Ed.* **2014**, *53* (28), 7290–7294.
(7) Cai, I. C., Lipschutz, M. I., Tilley, T. D. *Chem. Commun.* **2014**, *50* (86), 13062–13065.
(8) Liu, H., Cai, I. C., Fedorov, A., Ziegler, M. S., Copéret, C., Tilley, T. D. *Helv. Chim. Acta* **2016**, *99* (11), 859–867.
(9) Evans, D. F. *J. Chem. Soc. Resumed* **1959**, No. 0, 2003–2005.
(10) Sur, S. K. *J. Magn. Reson. 1969* **1989**, *82* (1), 169–173.
(11) Grant, D. H. *J. Chem. Educ.* **1995**, *72* (1), 39–40.
(12) Carrella, L. M., Förster, C., Kennedy, A. R., Klett, J., Mulvey, R. E., Rentschler, E. *Organometallics* **2010**, *29* (21), 4756–4758.
(13) Werncke, C. G., Bunting, P. C., Duhayon, C., Long, J. R., Bontemps, S., Sabo-Etienne, S. *Angew. Chem. Int. Ed.* **2015**, *54* (1), 245–248.
(14) Werncke, C. G., Suturina, E., Bunting, P. C., Vendier, L., Long, J. R., Atanasov, M., Neese, F., Sabo-Etienne, S., Bontemps, S. *Chem. – Eur. J.* **2016**, *22* (5), 1668–1674.
(15) Bruno, I. J., Cole, J. C., Edgington, P. R., Kessler, M., Macrae, C. F., McCabe, P., Pearson, J., Taylor, R. *Acta Crystallogr. B* **2002**, *58* (3), 389–397.
(16) Wolf, R., Brynda, M., Ni, C., Long, G. J., Power, P. P. *J. Am. Chem. Soc.* **2007**, *129* (19), 6076–6077.
(17) Messere, R., Spirlet, M.-R., Jan, D., Demonceau, A., Noels, A. F. *Eur. J. Inorg. Chem. 2000* (6), 1151–1153.

EXPERIMENTAL DETAILS

General Considerations. Unless otherwise noted, all experiments were conducted with dry, oxygen-free solvents using standard Schlenk techniques or in a nitrogen atmosphere glovebox. Pentane, toluene, diethyl ether, and tetrahydrofuran were dried and deaerated using a JC Meyers Phoenix SDS solvent purification system. Deuterated solvents were purchased from Cambridge Isotope Laboratories, degassed by three freeze-pump-thaw cycles and stored under nitrogen over activated 3 Å molecular sieves prior to use.

Potassium graphite[1] benzyl potassium,[2] and previously reported compounds (Cl)Cr[N(SiMe$_3$)DIPP]$_2$ (**2.1**), (Me)Cr[N(SiMe$_3$)DIPP]$_2$ (**2.2**), and (Bn)Cr[N(SiMe$_3$)DIPP]$_2$ (**2.3**)[3] were prepared according to literature procedure. Pyridine was dried by distillation from calcium hydride. From Sigma Aldrich, 18-crown-6 was purchased and dried by distillation under reduced pressure before use. All other reagents were obtained from commercial suppliers and used as received.

The abbreviation "DIPP" refers to a 2,6-diisopropylphenyl moiety.

Analytical Method Details. Elemental analyses were performed by the College of Chemistry Microanalytical Facility at the University of California, Berkeley.

NMR Spectroscopy. All NMR spectra were collected at ambient temperature (ca. 22 °C) on Bruker AV-300, AVB-400, AVQ-400, AV-500, or AV-600 MHz spectrometers. ^{1}H NMR spectra were referenced to tetramethylsilane calibrated *via* residual proteo-solvent signals.[4] All NMR spectra were analyzed with MestReNova (v. 12.0.3). Solution magnetic susceptibilities were determined by ^{1}H NMR spectroscopy using the Evans method.[5–7]

X-ray Diffraction Experiments. Data for **2.4**, **2.5**, **2.6**, **2.7**, **2.8**, **2.11**, **2.12**, and **2.13** were collected at Beamline 11.3.1/12.2.1 (Small Molecule Crystallography) of the Advanced Light Source at Lawrence Berkeley National Laboratory (LBNL). Measurements of **2.10** were performed on a Bruker APEX-II CCD area detector using Mo Kα radiation (λ = 0.71073 Å) monochromated using QUAZAR multilayer mirrors. All crystals were kept at 100(2) K throughout collection.

Data collection, refinement, and reduction were performed with Bruker APEX2 or APEX3 software (v. 2013.4-0 or v. 2016.9-0). Structure solution, modeling, and refinement was performed using Olex2.[8] All structures were solved using SHELXT-2014[9] and refined with SHELXL-2018[10], with refinement of F^2 on all data by full-matrix least squares. In all models, non-hydrogen atoms were refined anisotropically, and hydrogen atoms were included at the geometrically-calculated positions and refined using a riding model, unless otherwise specified.

For complex **2.5**, hydrogen atoms on C31 were located using the electron density difference map. For complex **2.13**, hydrogen atoms on C15 and C30 were located using the electron density difference map.

Specific details can be found below (Table E2.1) and in the crystallographic information files.

Table E2.1: X-ray Crystallography Experimental Details:

Compound	Detector Distance (mm)	Image Width (°)	Exposure Time (s)
2.4	50	1	1
2.5	50	1 or 4	1
2.6	50	1 or 4	1
2.7	50	1 or 4	1
2.8	50	1 or 4	1
2.10	60	0.5	20
2.12	50	1 or 4	1
2.11	50	1 or 4	1
2.13	50	1 or 4	1

K{(Me)Cr[N(SiMe$_3$)DIPP]$_2$} (2.4). To a 20 mL scintillation vial was added **2.2** (0.074 g, 0.131 mmol) and diethyl ether (10 mL); the resulting solution was frozen in a coldwell chilled externally with liquid nitrogen. The cooled solution of **2.2** was briefly thawed and potassium graphite (0.0184 g, 0.136 mmol, 1.04 equiv) was added directly in a single aliquot. The reaction mixture was stirred at ambient temperature for 40 min. The resulting green reaction mixture was filtered, then concentrated *in vacuo* a green foam, which was triturated with pentane (2 mL). The resulting solid was washed with pentane (5 x 1.5 mL), until pentane washes were colorless. The blue pentane-insoluble solid was dissolved in diethyl ether (3 mL). The resulting solution was filtered, then concentrated *in* vacuo to 2 mL, upon which pentane (8 mL) was layered. The layered solution was stored overnight at −30 °C to yield 0.019 g (0.032 mmol, 24%) of **2.4** as teal crystals, which were isolated by decanting the supernatant and removing residual volatile compounds *in vacuo*.

Crystals of **2.4** sufficient for single crystal X-ray diffraction studies were obtained from the crystallization procedure described above.

Effective magnetic moment (Evans method, 500.23 MHz, THF, 21 °C): μ_{eff} = 4.5 μ_B.

Anal. Calcd for $C_{31}H_{55}N_2CrKSi_2$: C, 61.74; H, 9.19; N, 4.65. Found: C, 61.82; H, 9.34; N, 4.80.

K{(Bn)Cr[N(SiMe$_3$)DIPP]$_2$} (2.5). To a 20 mL scintillation vial was added potassium graphite (0.022 g, 0.163 mmol, 1.04 equiv) and diethyl ether (8 mL); the resulting mixture was frozen in a coldwell chilled externally with liquid nitrogen. The cooled mixture of potassium graphite was briefly thawed and a solution of **2.3** (0.100 g, 0.156 mmol) in diethyl ether (3 mL) was added directly in a single aliquot. The reaction mixture was stirred at ambient temperature for 20 min. The resulting green reaction mixture was filtered, then concentrated *in* vacuo to 2 mL, upon which pentane (8 mL) was layered. The layered solution was stored overnight at −30 °C to yield 0.093 g (0.137 mmol, 88%) of **2.5** as green crystals, which were isolated by decanting the supernatant and removing residual volatile compounds *in vacuo*.

Crystals of **2.5** sufficient for single crystal X-ray diffraction studies were obtained from the crystallization procedure described above.

Effective magnetic moment (Evans method, 600.13 MHz, THF, 23 °C): μ_{eff} = 4.9 μ_B.

Anal. Calcd for $C_{37}H_{59}N_2CrKSi_2$: C, 65.44; H, 8.76; N, 4.12. Found: C, 65.46; H, 8.43; N, 4.36.

Alternative synthesis of 2.4, with formation of K{(Me)$_2$Cr[N(SiMe$_3$)DIPP]$_2$} (2.6). To a 20 mL scintillation vial was added **2.2** (0.040 g, 0.071 mmol) and diethyl ether (1.5 mL); the resulting solution was cooled to -30 °C. The cooled mixture of **2.2** was stirred and potassium graphite (0.0101 g, 0.075 mmol, 1.05 equiv) was added directly in a single aliquot. The reaction mixture was stirred at ambient temperature for 5 min. The resulting green reaction mixture was filtered, upon which pentane (4 mL) was layered. The layered solution was stored overnight at −30 °C to yield predominantly teal blocks of **2.4**, interspersed with trace amounts of blue needles of K{(Me)$_2$Cr[N(SiMe$_3$)DIPP]$_2$} (**2.6**), independently identified by single-crystal X-ray diffraction. Yields could not be determined.

K{(Bn)(Me)Cr[N(SiMe$_3$)DIPP]$_2$} (2.7). To a 20 mL scintillation vial was added **2.2** (0.0215 g, 0.038 mmol), 18-crown-6 (0.010 g, 0.038 mmol, 1 equiv), and diethyl ether (3 mL); the resulting solution was cooled to -30 °C. The cooled solution of **2.2** and 18-crown-6 was stirred and benzyl potassium (0.005 g, 0.038 mmol, 1 equiv) was added directly in a single aliquot. The reaction mixture was stirred at ambient temperature for 1 h. The resulting blue reaction mixture was filtered, and the blue filtride was collected. The solid was dissolved in diethyl ether (10 mL), and the resulting solution was stored overnight at −30 °C to yield 0.0068 g (0.007 mmol, 18%) of **2.7** as purple needles, which were isolated by decanting the supernatant and removing residual volatile compounds *in vacuo*.

Crystals of **2.7** sufficient for single crystal X-ray diffraction studies were obtained from the crystallization procedure described above.

Effective magnetic moment (Evans method, 500.23 MHz, THF, 21 °C): μ_{eff} = 3.5 μ_B.

Anal. Calcd for $C_{50}H_{86}CrKN_2O_6Si_2$: C, 62.65; H, 9.04; N, 2.92. Found: C, 62.49; H, 8.83; N, 2.74.

(^{t}Bupy)Cr[N(SiMe$_3$)DIPP]$_2$ (2.8). To a 20 mL scintillation vial was added **2.1** (0.050 g, 0.086 mmol), diethyl ether (5 mL), and 4-*tert*-butylpyridine (0.0116, 0.086 mmol); the resulting solution was cooled to -30 °C. The cooled mixture of **2.1** and 4-*tert*-butylpyridine was stirred and potassium graphite (0.013 g, 0.096 mmol, 1.1 equiv) was added directly in a single aliquot. The reaction mixture was stirred at ambient temperature for 1 h. The resulting reaction mixture was concentrated *in vacuo* to a solid, which was triturated with pentane (1.5 mL). The resulting solid was extracted with pentane (10 mL total). The combined pentane extracts were filtered, concentrated *in vacuo* to 3 mL, and stored overnight at -30 °C, to yield 0.032 g (0.047 mmol, 55%) of **2.8** as dark red blocks, which were isolated by decanting the supernatant and removing residual volatile compounds *in vacuo*.

Crystals of **2.8** suitable for single crystal X-ray diffraction studies were obtained from the crystallization procedure described above.

Effective magnetic moment (Evans method, 600.13 MHz, C_6D_6, 22 °C): μ_{eff} = 4.6 μ_B.

Anal. Calcd for $C_{39}H_{65}N_3CrSi_2$: C, 68.47; H, 9.58; N, 6.14. Found: C, 68.16; H, 9.51; N, 6.24.

(py)Cr[N(SiMe$_3$)DIPP]$_2$ (2.9). To a Schlenk flask fitted with a solid addition funnel was added **2.1** (0.688 g, 1.18 mmol), diethyl ether (40 mL), and pyridine (0.1 mL, 1.24 mmol, 1.05 mmol); the resulting solution was cooled to 0 °C using an ice bath. The solution was stirred, and potassium graphite (0.175 g, 1.29 mmol, 1.1 equiv) was added directly in a single aliquot *via* the solid addition funnel. The reaction mixture was stirred at ambient temperature for 45 min. The resulting reaction mixture was concentrated *in vacuo* to a solid, which was extracted with pentane (70 mL total). The combined pentane extracts were filtered, concentrated *in vacuo* to 25 mL, and stored overnight at -30 °C, to yield 0.358 g (0.057 mmol, 48%) of **2.9** as dark red needles, which were isolated by decanting the supernatant and removing residual volatile compounds *in vacuo*.

Effective magnetic moment (Evans method, 600.13 MHz, C_6D_6, 23 °C): μ_{eff} = 5.0 μ_B.

Anal. Calcd for $C_{35}H_{57}N_3CrSi_2$: C, 66.94; H, 9.15; N, 6.69. Found: C, 67.21; H, 9.00; N, 6.51.

(DMAP)Cr[N(SiMe$_3$)DIPP]$_2$ (2.10). To a 20 mL scintillation vial was added **2.1** (0.051 g, 0.087 mmol), diethyl ether (6 mL), and 4-(dimethylamino)pyridine (0.011, 0.090 mmol, 1.0 equiv); the resulting solution was cooled to -30 °C. The cooled mixture of **2.1** and 4-(dimethylamino)pyridine was stirred and potassium graphite (0.013 g, 0.096 mmol, 1.07 equiv) was added directly in a single aliquot. The reaction mixture was stirred at ambient temperature for 50 min. The resulting reaction mixture was concentrated *in vacuo* to a solid, which was extracted with toluene (5 mL total). The combined toluene extracts were filtered, then concentrated *in vacuo* to 2 mL, upon which pentane (8 mL) was layered. The layered solution was stored at -30 °C over several days, to yield 0.033 g (0.049 mmol, 56%) of **2.10** as green blocks, which were isolated by decanting the supernatant and removing residual volatile compounds *in vacuo*.

Crystals of **2.10** suitable for single crystal X-ray diffraction studies were obtained from the crystallization procedure described above.

Effective magnetic moment (Evans method, 300.13 MHz, C_6D_6, 21 °C): μ_{eff} = 4.5 μ_B.

Anal. Calcd for $C_{37}H_{62}N_4CrSi_2$: C, 66.22; H, 9.31; N, 8.35. Found: C, 65.60; H, 9.19; N, 8.17.

{K(18-cr-6)}{Cr[N(SiMe$_3$)DIPP]$_2$} (2.11). To a 20 mL scintillation vial was added **2.10** (0.020 g, 0.030 mmol) and diethyl ether (3 mL). The solution of **2.10** was stirred and potassium graphite (0.0044 g, 0.033 mmol, 1.1 equiv) was added directly in a single aliquot, followed by a solution of 18-crown-6 (0.0079, 0.030 mmol, 1.0 equiv) in diethyl ether (1 mL), which was added dropwise. The reaction mixture was stirred at ambient temperature for 5 min. The reaction mixture was filtered, and pentane (10 mL) was layered on top of the orange diethyl ether filtrate. The layered solution was stored overnight at -30 °C to yield orange needles, which were isolated by decanting

the supernatant and removing residual volatile compounds *in vacuo*. The resulting orange solid was recrystallized from diethyl ether (1.5 mL) at -30 °C to yield 0.0026 g (0.003 mmol, 10%) of **2.11** as orange needles, which were isolated by decanting the supernatant and removing residual volatile compounds *in vacuo*.

Crystals of **2.10** suitable for single crystal X-ray diffraction studies were obtained from recrystallization of **2.10** from diethyl ether, stored overnight at −30 °C.

Anal. Calcd for $C_{42}H_{76}N_2CrO_6Si_2$: C, 59.19; H, 8.99; N, 3.29. Found: C, 59.08; H, 8.78; N, 3.25.

$(Me_3P)Cr[N(SiMe_3)DIPP]_2$ (2.12). To a Schlenk flask was added potassium graphite (0.054 g, 0.40 mmol, 1.05 equiv) and diethyl ether (10 mL); the resulting mixture was frozen using a liquid nitrogen bath. The potassium graphite mixture was removed from the liquid nitrogen bath, and to the flask was added *via* cannula a pre-combined solution of **2.1** (0.222 g, 0.38 mmol), diethyl ether (6 mL), and trimethylphosphine (0.14 M in diethylether, 8 mL, 1.12 mmol, 3 equiv). The resulting reaction mixture was stirred at ambient temperature for 45 min. The resulting reaction mixture was concentrated *in vacuo* to a solid, which was extracted with pentane (15 mL total). The combined pentane extracts were filtered, concentrated *in vacuo* to 4 mL, and stored at -30 °C over several days, allowing for slow evaporation of the solvent, to yield 0.063 g (0.10 mmol, 26%) of **2.12** as teal needles, which were isolated by decanting the supernatant and removing residual volatile compounds *in vacuo*.

Crystals of **2.12** suitable for single crystal X-ray diffraction studies were obtained from the crystallization procedure described above.

Effective magnetic moment (Evans method, 600.13 MHz, C_6D_6, 23 °C): $\mu_{eff} = 5.2\ \mu_B$.

Anal. Calcd for $C_{33}H_{61}N_2CrPSi_2$: C, 63.42; H, 9.84; N, 4.48. Found: C, 63.10; H, 9.43; N, 4.40.

$Cr[N(SiMe_2CH_2)DIPP]_2Cr[N(SiMe_3)DIPP]$ (2.13). To a Schlenk flask was added **2.1** (0.141 g, 0.24 mmol), diethyl ether (9 mL), and triethylamine (0.05 mL, 0.36 mmol, 1.5 mmol). The solution was stirred, and potassium graphite (0.036 g, 0.27 mmol, 1.1 equiv) was added directly in a single aliquot from a second Schlenk flask, under a counter-flow of nitrogen. The reaction mixture was stirred at ambient temperature for 25 min. The resulting reaction mixture was concentrated *in vacuo* to a solid, which was triturated with pentane (20 mL) to remove any residual volatile compounds. The resulting solid was extracted with pentane (10 mL total). The combined pentane extracts were filtered, and concentrated *in vacuo* to a solid. The solid was dissolved in a 1:2 hexamethyldisiloxane:pentane solution (3 mL), filtered, and stored at -30 °C for one month, allowing for slow evaporation of the solvent, to yield 0.0024 g (0.0028 mmol, 1%) of **2.13** as dark brown needles, which were identified by single-crystal X-ray diffraction.

Effective magnetic moment (Evans method, 600.13 MHz, C_6D_6, 22 °C): $\mu_{eff} = 2.2\ \mu_B$.

SUPPLEMENTARY FIGURE

Figure S2.1: Solid-state structure of complex **2.10**, as determined by single-crystal X-ray diffraction

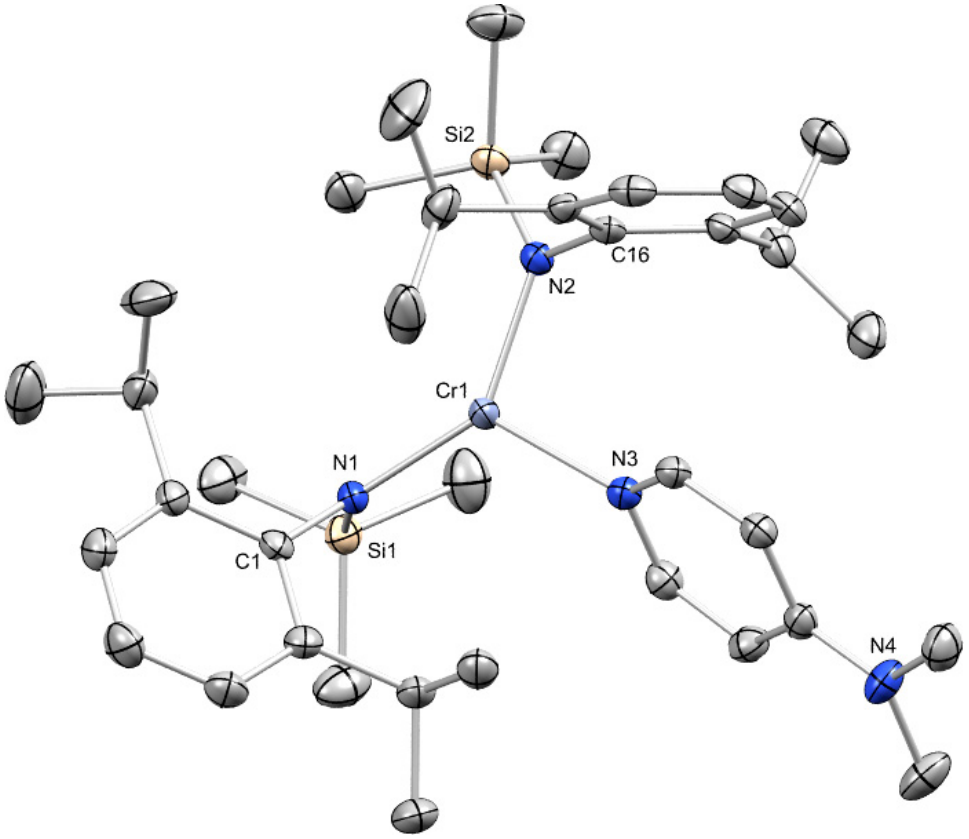

Notes: Thermal ellipsoids are shown at 50% probability. Hydrogen atoms have been omitted for clarity. Selected bond distances [Å], angles [°], and torsions [°]:Cr1–N1: 1.9649(19), Cr1–N2: 2.0064(19), Cr1–N3: 2.0842(19), N1–C1: 1.434(3), N2–C16: 1.417(3), N1–Si1: 1.730(2), N2–Si2: 1.714(2); N1–Cr1–N2: 139.59(8); C1–N1---N2–C16: ±46.7(3).

SINGLE-CRYSTAL X-RAY DIFFRACTION CRYSTAL STRUCTURE DETAILS

Figure SX2.1. Solid-state structure of complex **2.4**, as determined by single-crystal X-ray diffraction

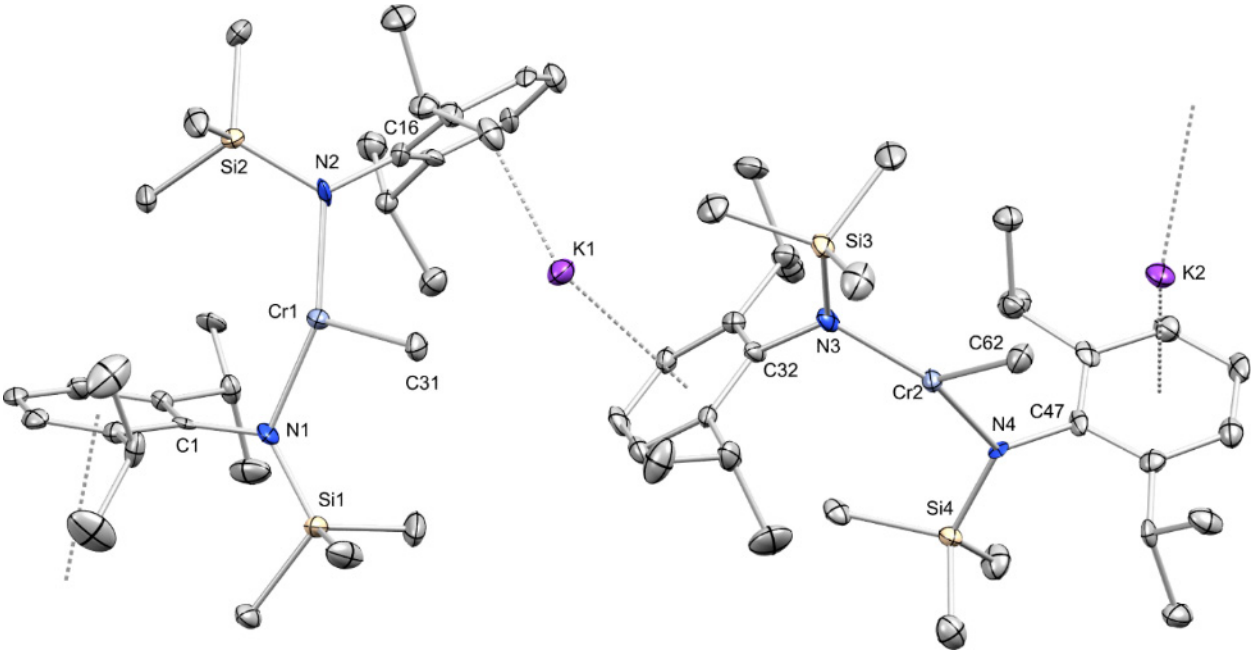

Notes: Thermal ellipsoids are shown at 50% probability. Hydrogen atoms have been omitted for clarity. Selected bond distances [Å], angles [°], and torsions [°]: Cr1–C31: 2.085(8), Cr2–C62: 2.099(8), K1–C31: 3.079(9), K2–C62: 3.040(9), Cr1–N1: 2.051(7), Cr1–N2: .039(7), Cr2–N3: 2.027(7), Cr2–N4: 2.035(6), N1–C1: 1.407(10), N2–C16: 1.395(9), N3–C32: 1.410(9), N4–C47: 1.410(9), N1–Si1: 1.692(8), N2–Si2: 1.708(7), N3–Si3: 1.724(7), N4–Si4: 1.719(7); N1–Cr1–N2: 153.1(3), N3–Cr2–N4: 153.1(3); C1–N1---N2–C16: ±144.1(7), C32–N3---N4–C47: ±145.4(7).

Table SX2.1. Crystal data and structure refinement for complex **2.4**

Empirical formula	$C_{31}H_{55}CrKN_2Si_2$
Formula weight	603.05
Temperature (K)	100(2)
Crystal system	triclinic
Space group	P-1
a (Å)	11.7323(7)
b (Å)	16.1627(10)
c (Å)	18.2461(11)
α (°)	96.666(3)
β (°)	90.033(3)
γ (°)	92.622(3)
Volume ($Å^3$)	3432.9(4)
Z	4
ρ_{calc} (g/cm^3)	1.167
μ (mm^{-1})	0.581
F(000)	1304.0
Crystal size (mm^3)	0.157 × 0.15 × 0.143
Radiation (Å)	synchrotron (λ = 0.7288)
2Θ range for data collection (°)	3.27 to 54.794
Index ranges	$-14 \leq h \leq 14$, $-20 \leq k \leq 19$, $0 \leq l \leq 22$
Reflections collected	14642
Independent reflections	14642 [R_{sigma} = 0.1182]
Data/restraints/parameters	14642/748/698
Goodness-of-fit on F^2	1.025
Final R indexes [I>=2σ (I)]	R_1 = 0.1005, wR_2 = 0.2574
Final R indexes [all data]	R_1 = 0.1519, wR_2 = 0.3015
Largest diff. peak/hole ($e/Å^3$)	2.44/-0.72

Figure SX2.2. Solid-state structure of complex **2.5**, as determined by single-crystal X-ray diffraction

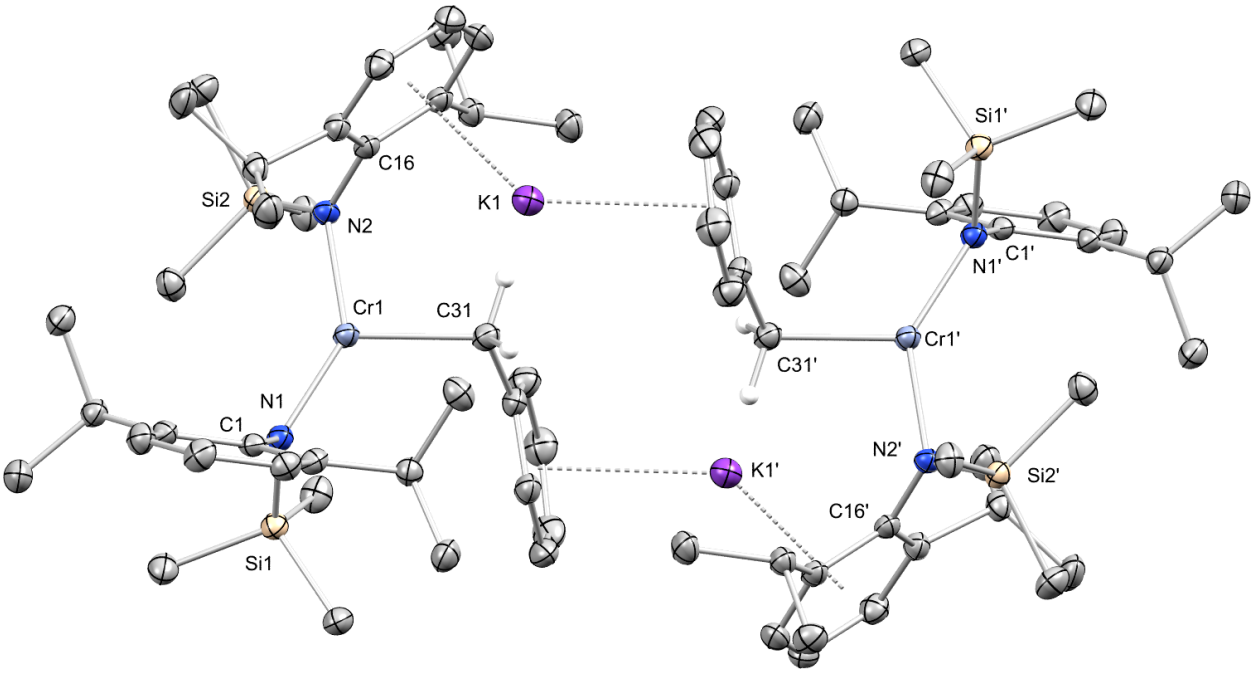

Notes: Thermal ellipsoids are shown at 50% probability. Hydrogen atoms have been omitted for clarity, with the exception of hydrogens on C31, which have been located from the electron density difference map. Selected bond distances [Å], angles [°], and torsions [°]: Cr1–C31: 2.1685(19), K1–C31: 3.051(2), Cr1–N1: 2.0034(15), Cr1–N2: 2.0417(15), N1–C1: 1.426(2), N2–C16: 1.408(2), N1–Si1: 1.7231(17), N2–Si2: 1.7071(16); N1–Cr1–N2: 140.48(6); C1–N1---N2–C16: ±38.5(2).

Table SX2.2. Crystal data and structure refinement for complex **2.5**

Empirical formula	$C_{37}H_{59}CrKN_2Si_2$
Formula weight	679.14
Temperature (K)	100(2)
Crystal system	triclinic
Space group	P-1
a (Å)	9.5108(8)
b (Å)	12.3852(11)
c (Å)	16.7426(14)
α (°)	80.394(5)
β (°)	88.937(5)
γ (°)	74.056(5)
Volume ($Å^3$)	1868.9(3)
Z	2
ρ_{calc} (g/cm^3)	1.207
μ (mm^{-1})	0.641
F(000)	732.0
Crystal size (mm^3)	0.1 × 0.1 × 0.1
Radiation (Å)	synchrotron (λ = 0.7749)
2Θ range for data collection (°)	4.858 to 45.656
Reflections collected	3932
Independent reflections	3932 [R_{sigma} = 0.0777]
Data/restraints/parameters	3932/332/402
Goodness-of-fit on F^2	1.537
Final R indexes [I>=2σ (I)]	R_1 = 0.1425, wR_2 = 0.3527
Final R indexes [all data]	R_1 = 0.1682, wR_2 = 0.3726
Largest diff. peak/hole ($e/Å^3$)	1.08/-1.08

Figure SX2.3. Solid-state structure of complex **2.6**, as determined by single-crystal X-ray diffraction

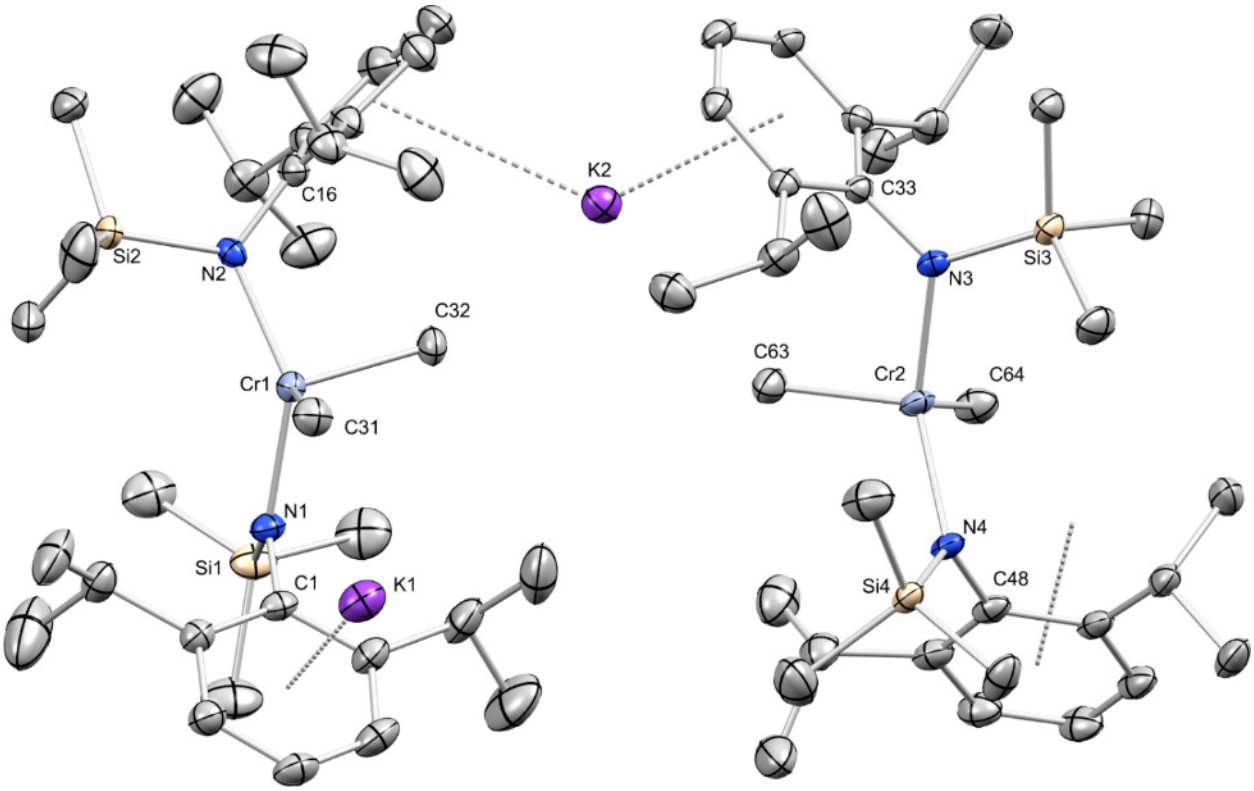

Notes: Thermal ellipsoids are shown at 50% probability. Hydrogen atoms and disordered diethyl ether molecules coordinated to the potassium cations have been omitted for clarity. Selected bond distances [Å], angles [°], and torsions [°]: Cr1–C31: 2.071(4), Cr1–C32: 2.065(4), Cr2–C63: 2.073(4), Cr2–C64: 2.087(4), K1–C31: 3.351(4), K1–C64: 3.249(4), K2–C32: 3.194(5), K2–C63: 3.353(4), Cr1–N1: 1.997(3), Cr1–N2: 1.993(3), Cr2–N3: 2.015(3), Cr2–N4: 2.011(3), N1–C1: 1.417(5), N2–C16: 1.418(5), N3–C33: 1.422(4), N4–C48: 1.430(5), N1–Si1: 1.732(3), N2–Si2: 1.725(3), N3–Si3: 1.726(3), N4–Si4: 1.722(3); N1–Cr1–N2: 140.50(13), N3–Cr2–N4: 144.14(13); C1–N1---N2–C16: ±109.0(4), C33–N3---N4–C48: ±110.4(4).

Table SX2.3. Crystal data and structure refinement for complex **2.6**

Empirical formula	$C_{36}H_{68}CrKN_2OSi_2$
Formula weight	692.20
Temperature (K)	100(2)
Crystal system	monoclinic
Space group	Cc
a (Å)	18.9506(9)
b (Å)	19.3825(9)
c (Å)	23.5313(11)
α (°)	90
β (°)	109.058(2)
γ (°)	90
Volume ($Å^3$)	8169.5(7)
Z	8
ρ_{calc} (g/cm^3)	1.126
μ (mm^{-1})	0.498
F(000)	3016.0
Crystal size (mm^3)	0.129 × 0.129 × 0.064
Radiation (Å)	synchrotron (λ = 0.7288)
2Θ range for data collection (°)	3.174 to 58.292
Index ranges	$-25 \leq h \leq 25$, $-25 \leq k \leq 25$, $-31 \leq l \leq 31$
Reflections collected	67163
Independent reflections	20359 [R_{int} = 0.0549, R_{sigma} = 0.0618]
Data/restraints/parameters	20359/2/860
Goodness-of-fit on F^2	1.052
Final R indexes [I>=2σ (I)]	R_1 = 0.0453, wR_2 = 0.1052
Final R indexes [all data]	R_1 = 0.0570, wR_2 = 0.1111
Largest diff. peak/hole ($e/Å^3$)	1.34/-0.47
Flack parameter	0.306(15)

Figure SX2.4. Solid-state structure of complex **2.7**, as determined by single-crystal X-ray diffraction

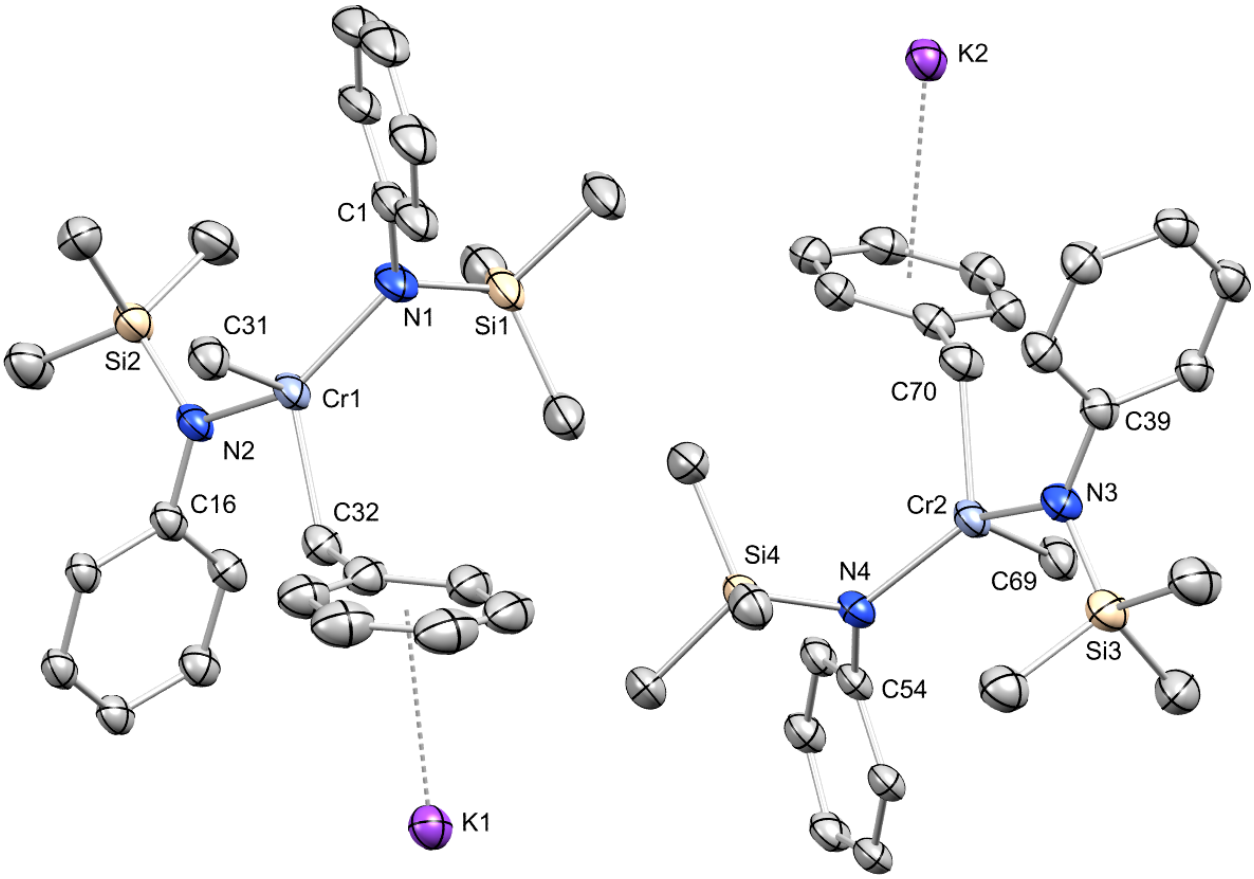

Notes: Thermal ellipsoids are shown at 50% probability. Hydrogen atoms, isopropyl groups, 18-crown-6 and disordered diethyl ether molecules have been omitted for clarity. Selected bond distances [Å], angles [°], and torsions [°]: Cr1–C31: 2.043(3), Cr1–C32: 2.116(3), Cr2–C69: 2.037(3), Cr2–C70: 2.107(3), Cr1–N1: 2.009(2), Cr1–N2: 2.010(2), Cr2–N3: 2.005(2), Cr2–N4: 2.001(2), N1–C1: 1.440(4), N2–C16: 1.425(4), N3–C39: 1.430(4), N4–C54: 1.433(4), N1–Si1: 1.733(3), N2–Si2: 1.722(3), N3–Si3: 1.732(3), N4–Si4: 1.733(2); N1–Cr1–N2: 131.09(11), N3–Cr2–N4: 134.36(10); C1–N1---N2–C16: ±141.4(4), C39–N3---N4–C54: ±133.2(4).

Table SX2.4. Crystal data and structure refinement for complex **2.7**

Empirical formula	$C_{107.92}H_{191.79}Cr_2K_2N_4O_{13.98}Si_4$
Formula weight	2063.65
Temperature (K)	100(2)
Crystal system	triclinic
Space group	P-1
a (Å)	16.9347(11)
b (Å)	18.6711(11)
c (Å)	20.9392(12)
α (°)	64.376(2)
β (°)	85.064(3)
γ (°)	88.015(3)
Volume ($Å^3$)	5947.5(6)
Z	2
ρ_{calc} (g/cm^3)	1.152
μ (mm^{-1})	0.371
F(000)	2242.0
Crystal size (mm^3)	0.136 × 0.064 × 0.05
Radiation (Å)	synchrotron (λ = 0.7288)
2Θ range for data collection (°)	2.218 to 52.3
Index ranges	$-20 \leq h \leq 20$, $-22 \leq k \leq 22$, $-25 \leq l \leq 25$
Reflections collected	77472
Independent reflections	21962 [R_{int} = 0.0619, R_{sigma} = 0.0676]
Data/restraints/parameters	21962/0/1289
Goodness-of-fit on F^2	1.022
Final R indexes [I>=2σ (I)]	R_1 = 0.0536, wR_2 = 0.1345
Final R indexes [all data]	R_1 = 0.0824, wR_2 = 0.1501
Largest diff. peak/hole ($e/Å^3$)	0.72/-0.54

Figure SX2.5. Solid-state structure of complex **2.8**, as determined by single-crystal X-ray diffraction

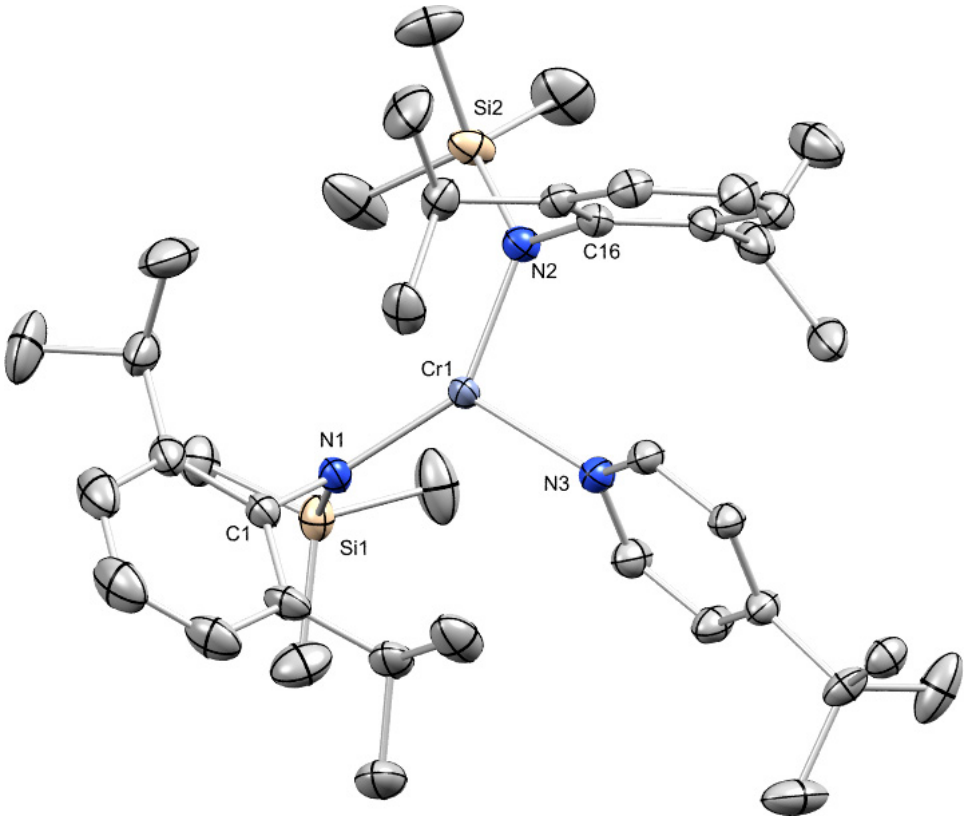

Notes: Thermal ellipsoids are shown at 50% probability. Hydrogen atoms, disordered *tert*-butyl group, and disordered chromium atom have been omitted for clarity. Selected bond distances [Å], angles [°], and torsions [°]: Cr1–N1: 1.9559(11), Cr1–N2: 2.0102(12), Cr1–N3: 2.0930(12), N1–C1: 1.4312(13), N2–C16: 1.4207(12), N1–Si1: 1.7351(10), N2–Si2: 1.7154(9); N1–Cr1–N2: 143.12(6); C1–N1---N2–C16: ±50.8(1).

Table SX2.5. Crystal data and structure refinement for complex **2.8**

Empirical formula	$C_{39}H_{65}CrN_3Si_2$
Formula weight	684.12
Temperature (K)	100(2)
Crystal system	orthorhombic
Space group	Pbca
a (Å)	20.1406(8)
b (Å)	18.9037(7)
c (Å)	21.2282(8)
α (°)	90
β (°)	90
γ (°)	90
Volume ($Å^3$)	8082.3(5)
Z	8
ρ_{calc} (g/cm^3)	1.124
μ (mm^{-1})	0.466
F(000)	2976.0
Crystal size (mm^3)	0.339 × 0.339 × 0.136
Radiation (Å)	synchrotron (λ = 0.7749)
2Θ range for data collection (°)	4.41 to 80.71
Index ranges	$-33 \leq h \leq 33$, $-31 \leq k \leq 31$, $-35 \leq l \leq 34$
Reflections collected	149357
Independent reflections	19691 [R_{int} = 0.0358, R_{sigma} = 0.0225]
Data/restraints/parameters	19691/0/473
Goodness-of-fit on F^2	1.088
Final R indexes [I>=2σ (I)]	R_1 = 0.0455, wR_2 = 0.1309
Final R indexes [all data]	R_1 = 0.0588, wR_2 = 0.1395
Largest diff. peak/hole ($e/Å^3$)	1.61/-0.83

Table SX2.6. Crystal data and structure refinement for complex **2.10**

Empirical formula	$C_{37}H_{62}CrN_4Si_2$
Formula weight	671.08
Temperature (K)	100(2)
Crystal system	orthorhombic
Space group	Pbca
a (Å)	20.0402(15)
b (Å)	18.7134(14)
c (Å)	21.0537(15)
α (°)	90
β (°)	90
γ (°)	90
Volume ($Å^3$)	7895.6(10)
Z	8
ρ_{calc} (g/cm^3)	1.129
μ (mm^{-1})	0.379
F(000)	2912.0
Crystal size (mm^3)	0.1 × 0.1 × 0.1
Radiation (Å)	MoKα (λ = 0.71073)
2Θ range for data collection (°)	3.55 to 50.83
Index ranges	$-24 \leq h \leq 23$, $-21 \leq k \leq 22$, $-25 \leq l \leq 25$
Reflections collected	64926
Independent reflections	7252 [R_{int} = 0.0484, R_{sigma} = 0.0299]
Data/restraints/parameters	7252/0/413
Goodness-of-fit on F^2	1.043
Final R indexes [I>=2σ (I)]	R_1 = 0.0433, wR_2 = 0.0979
Final R indexes [all data]	R_1 = 0.0628, wR_2 = 0.1092
Largest diff. peak/hole ($e/Å^3$)	0.95/-0.80

Figure SX2.6. Solid-state structure of complex **2.11**, as determined by single-crystal X-ray diffraction

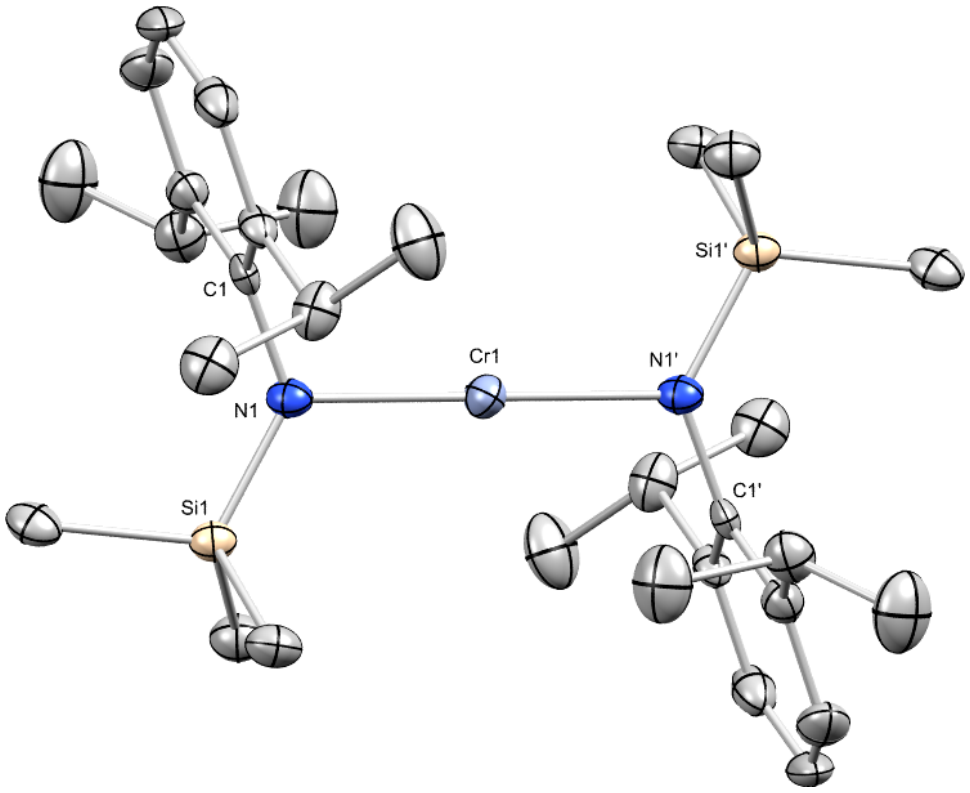

Notes: Thermal ellipsoids are shown at 50% probability. Hydrogen atoms and {K(18-crown-6)} cation have been omitted for clarity. Selected bond distances [Å], angles [°], and torsions [°]: Cr1–N1: 2.0519(11), N1–C1: 1.4048(17), N1–Si1: 1.6895(12); N1–Cr1–N1': 180.00(6); C1–N1---N1'–C1': ±180.0(1).

Table SX2.7. Crystal data and structure refinement for complex **2.11**

Empirical formula	$C_{42}H_{76}CrKN_2O_6Si_2$
Formula weight	852.32
Temperature (K)	100(2)
Crystal system	monoclinic
Space group	$P2_1/n$
a (Å)	10.5097(6)
b (Å)	14.4250(8)
c (Å)	16.1249(9)
α (°)	90
β (°)	90.036(2)
γ (°)	90
Volume ($Å^3$)	2444.6(2)
Z	2
ρ_{calc} (g/cm^3)	1.158
μ (mm^{-1})	0.437
F(000)	922.0
Crystal size (mm^3)	0.094 × 0.087 × 0.07
Radiation (Å)	synchrotron (λ = 0.7288)
2Θ range for data collection (°)	3.884 to 58.192
Index ranges	$-14 \leq h \leq 13$, $-19 \leq k \leq 19$, $-21 \leq l \leq 21$
Reflections collected	39151
Independent reflections	6053 [R_{int} = 0.0532, R_{sigma} = 0.0363]
Data/restraints/parameters	6053/0/254
Goodness-of-fit on F^2	1.043
Final R indexes [I>=2σ (I)]	R_1 = 0.0347, wR_2 = 0.0812
Final R indexes [all data]	R_1 = 0.0466, wR_2 = 0.0881
Largest diff. peak/hole ($e/Å^3$)	0.34/-0.36

Figure SX2.7. Solid-state structure of complex **2.12**, as determined by single-crystal X-ray diffraction

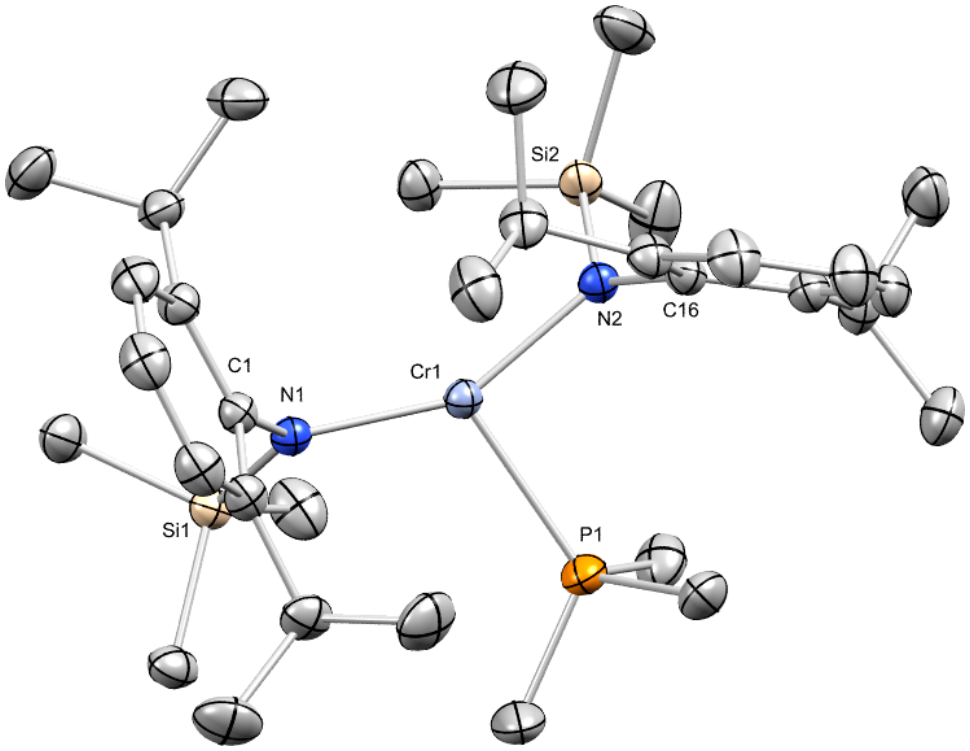

Notes: Thermal ellipsoids are shown at 50% probability. Hydrogen atoms have been omitted for clarity. Selected bond distances [Å], angles [°], and torsions [°]: Cr1–P1: 2.4288(5), Cr1–N1: 1.9912(13), Cr1–N2: 2.0132(13), N1–C1: 1.4290(19), N2–C16: 1.4180(18), N1–Si1: 1.7253(13), N2–Si2: 1.7148(13); N1–Cr1–N2: 151.70(5); C1–N1---N2–C16: ±40.4(1).

Table SX2.8. Crystal data and structure refinement for complex **2.12**

Empirical formula	$C_{33}H_{61}CrN_2PSi_2$
Formula weight	624.98
Temperature (K)	100(2)
Crystal system	monoclinic
Space group	$P2_1/n$
a (Å)	11.7634(6)
b (Å)	19.6124(10)
c (Å)	16.7178(9)
α (°)	90
β (°)	107.035(3)
γ (°)	90
Volume ($Å^3$)	3687.7(3)
Z	4
ρ_{calc} (g/cm^3)	1.126
μ (mm^{-1})	0.556
F(000)	1360.0
Crystal size (mm^3)	0.174 × 0.116 × 0.116
Radiation (Å)	synchrotron (λ = 0.7749)
2Θ range for data collection (°)	4.108 to 72.118
Index ranges	$-17 \leq h \leq 17$, $-29 \leq k \leq 29$, $-25 \leq l \leq 25$
Reflections collected	54134
Independent reflections	13476 [R_{int} = 0.0581, R_{sigma} = 0.0539]
Data/restraints/parameters	13476/0/369
Goodness-of-fit on F^2	1.059
Final R indexes [I>=2σ (I)]	R_1 = 0.0473, wR_2 = 0.1135
Final R indexes [all data]	R_1 = 0.0655, wR_2 = 0.1218
Largest diff. peak/hole ($e/Å^3$)	0.48/-0.93

Figure SX2.8. Solid-state structure of complex **2.13**, as determined by single-crystal X-ray diffraction

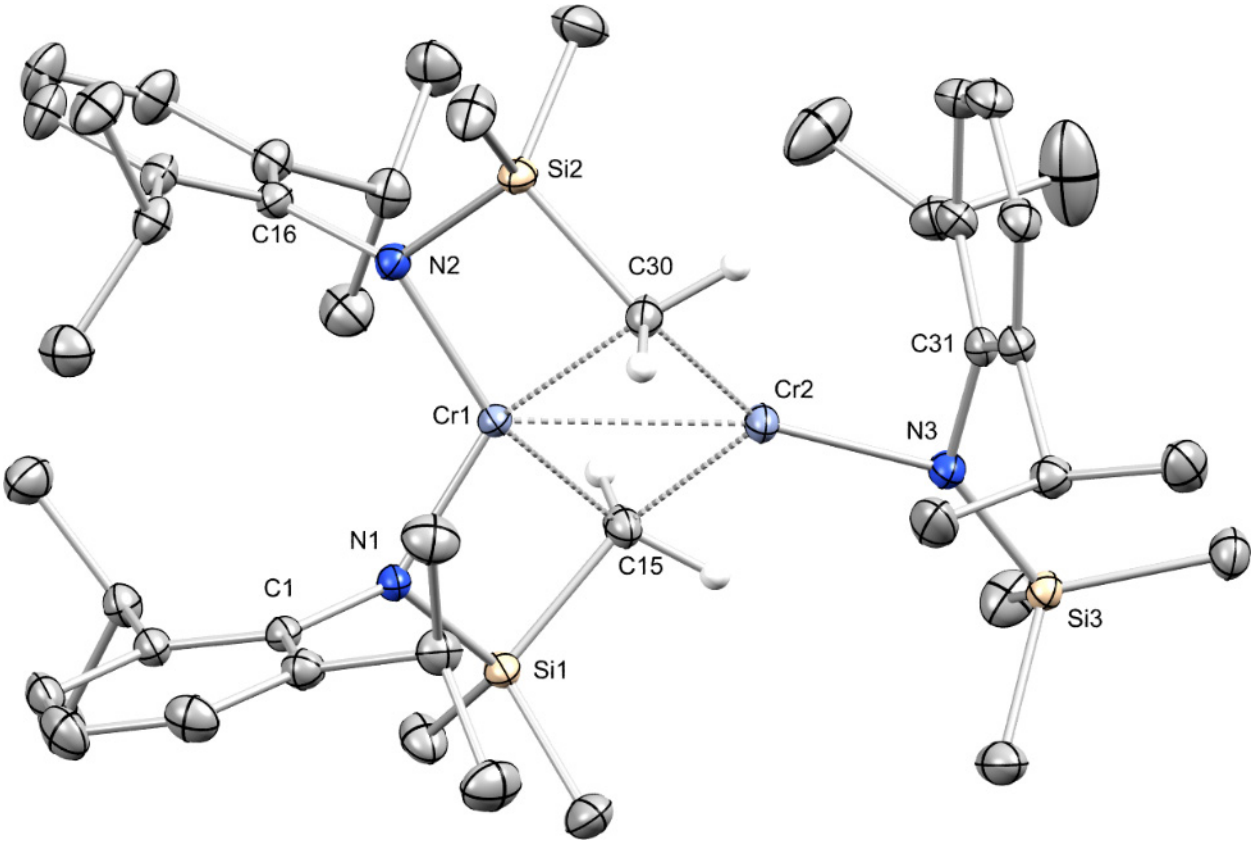

Notes: Thermal ellipsoids are shown at 50% probability. Hydrogen atoms have been omitted for clarity, with the exception of hydrogen atoms on C15 and C30, which were located using the electron density difference map. Selected bond distances [Å], angles [°], and torsions [°]: Cr1–Cr2: 2.6229(3), Cr1–N1: 1.8794(10), Cr1–N2: 1.8841(11), Cr2–N3: 1.9809(11), Cr1–C15: 2.2469(13), Cr1–C30: 2.2306(12), Cr2–C15: 2.1777(13), Cr2–C30: 2.1742(13), Cr2–C31: 2.2787(12), N1–C1: 1.4195(15), N2–C16: 1.4202(16), N3–C31: 1.4055(16), N1–Si1: 1.7388(10), N2–Si2: 1.7382(11), N3–Si3: 1.7055(11); N1–Cr1–N2: 115.95(5); C1–N1---N2–C16: ±67.5(1).

Table SX2.9. Crystal data and structure refinement for complex **2.13**

Empirical formula	$C_{45}H_{76}Cr_2N_3Si_3$
Formula weight	847.35
Temperature (K)	100(2)
Crystal system	triclinic
Space group	P-1
a (Å)	11.8688(9)
b (Å)	12.8612(9)
c (Å)	17.1626(12)
α (°)	74.129(4)
β (°)	78.187(4)
γ (°)	74.071(4)
Volume ($Å^3$)	2399.3(3)
Z	2
ρ_{calc} (g/cm^3)	1.173
μ (mm^{-1})	0.707
F(000)	914.0
Crystal size (mm^3)	0.598 × 0.299 × 0.15
Radiation (Å)	synchrotron (λ = 0.7749)
2Θ range for data collection (°)	3.69 to 82.332
Index ranges	$-20 \leq h \leq 19$, $-21 \leq k \leq 20$, $-27 \leq l \leq 29$
Reflections collected	43184
Independent reflections	23316 [R_{int} = 0.0421, R_{sigma} = 0.0764]
Data/restraints/parameters	23316/0/513
Goodness-of-fit on F^2	1.032
Final R indexes [I>=2σ (I)]	R_1 = 0.0457, wR_2 = 0.1078
Final R indexes [all data]	R_1 = 0.0801, wR_2 = 0.1238
Largest diff. peak/hole ($e/Å^3$)	0.57/-1.10

REFERENCES FOR EXPERIMENTAL DETAILS, SUPPLEMENTARY FIGURE, AND SINGLE-CRYSTAL X-RAY DIFFRACTION CRYSTAL STRUCTURE DETAILS

(1) Bergbreiter, D. E., Killough, J. M. *J. Am. Chem. Soc.* **1978**, *100* (7), 2126–2134.
(2) Bailey, P. J., Coxall, R. A., Dick, C. M., Fabre, S., Henderson, L. C., Herber, C., Liddle, S. T., Loroño-González, D., Parkin, A., Parsons, S. *Chem. – Eur. J.* **2003**, *9* (19), 4820–4828.
(3) Liu, H., Cai, I. C., Fedorov, A., Ziegler, M. S., Copéret, C., Tilley, T. D. *Helv. Chim. Acta* **2016**, *99* (11), 859–867.
(4) Fulmer, G. R., Miller, A. J. M., Sherden, N. H., Gottlieb, H. E., Nudelman, A., Stoltz, B. M., Bercaw, J. E., Goldberg, K. I. *Organometallics* **2010**, *29* (9), 2176–2179.
(5) Evans, D. F. *J. Chem. Soc. Resumed* **1959**, No. 0, 2003–2005.
(6) Sur, S. K. *J. Magn. Reson. 1969* **1989**, *82* (1), 169–173.
(7) Grant, D. H. *J. Chem. Educ.* **1995**, *72* (1), 39–40.
(8) Dolomanov, O. V., Bourhis, L. J., Gildea, R. J., Howard, J. a. K., Puschmann, H. *J. Appl. Crystallogr.* **2009**, *42* (2), 339–341.
(9) Sheldrick, G. M. *Acta Crystallogr. Sect. Found. Adv.* **2015**, *71* (1), 3–8.
(10) Sheldrick, G. M. *Acta Crystallogr. Sect. C Struct. Chem.* **2015**, *71* (1), 3–8.

Chapter 3: Coordination Chemistry of Low-Coordinate Manganese Bis(amido) Complexes

INTRODUCTION

Two-coordinate manganese complexes provide an intriguing platform for exploring the limits of coordinative-unsaturation in a wide range of potential oxidation states. While more than twenty two-coordinate manganese complexes have been reported,[1–7] descriptions of homogeneous reaction chemistry with these species has been primarily limited to ligand exchange studies.[1] To the best of our knowledge, there have been few reported efforts to examine the redox chemistry of two-coordinate manganese species. In terms of accessing higher oxidation states, although low-coordinate bridging oxo manganese complexes have been observed,[8,9] three-coordinate terminal oxo manganese complexes remain elusive.

With regards to low-valent chemistry of two-coordinate manganese complexes, both $Mn[C(SiMe_3)_3]_2$ and $Mn[N(SiMe_3)DIPP]_2$ (**3.1**, DIPP = 2,6-diisopropylphenyl) have been reduced to form the corresponding anionic analogs, although the reactivity of these resulting species remains largely unexplored.[5,7] For anionic first-row transition metal species of the form $\{M[N(SiMe_3)DIPP]_2\}^-$, reported complexes containing a potassium cation, such as $[K(18\text{-cr-}6)][Mn[N(SiMe_3)DIPP]_2]$ (**3.2**), have primarily been isolated in conjunction with a chelating agent such as 18-crown-6 (Figure 3.1, **A**).[7,10,11] An exception is $K\{Ni[N(SiMe_3)DIPP]_2\}$, in which the potassium is bound between the two arene rings in the solid state (Figure 3.1, **B**).[12] Although arene coordination of potassium ions appears to play an important role in nitrogen activation by low-coordinate iron species,[13–15] the effect of arene-bound potassium anions on the reactivity of two-coordinate bis(amido) species is not well defined.

Since **3.1** has also been isolated as a THF adduct in the solid state,[16] it seemed that a rigorously two-coordinate species enforced by steric bulk might more readily coordinate potassium in a fashion analogous to that of $K\{Ni[N(SiMe_3)DIPP]_2\}$, without the use of a chelating agent. Here, we report the synthesis of a manganese species bearing a highly sterically demanding bis(amido) ligand set, and a comparison of its redox reactivity to complex **3.1**.

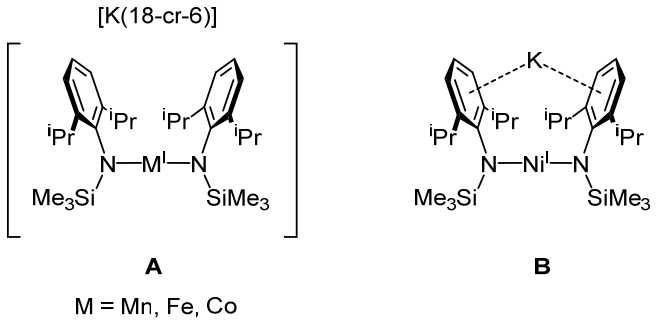

Figure 3.1. Previously reported anionic two-coordinate complexes supported by –N(SiMe$_3$)DIPP, (**A**) [K(18-cr-6)][M[N(SiMe$_3$)DIPP]$_2$] and (**B**) K{Ni[N(SiMe3)DIPP]$_2$}

RESULTS AND DISCUSSION

Complex **3.3**, Mn[N(Si^{i}Pr$_3$)DIPP]$_2$, was synthesized in a fashion similar to that reported for the synthesis of **3.1**. Addition of Li[N(Si^{i}Pr$_3$)DIPP] to a suspension of manganese dichloride in diethyl ether afforded **3.3** as yellow blocks in 65% yield. In contrast to the solid-state structure of **3.1**, the manganese center in **3.3** does not lie on an inversion center and consequently has a C$_{ipso}$–N---N–C$_{ipso}$ dihedral angle of 40.5(2)° (Figure 3.2). However, **3.3** possesses a linear N–Mn–N bond angle of 177.15(8)° and Mn–N bond lengths of 1.9344(18) Å and 1.9386(19) Å, only slightly elongated compared to that of **3.1** (1.9181(6) Å), as might be expected by the increase in steric bulk. Consistent with the high- spin d^5 configuration of **3.1**, the solution magnetic moment of **3.3**, measured by the Evans method,[17–19] is 5.6 μ_B.

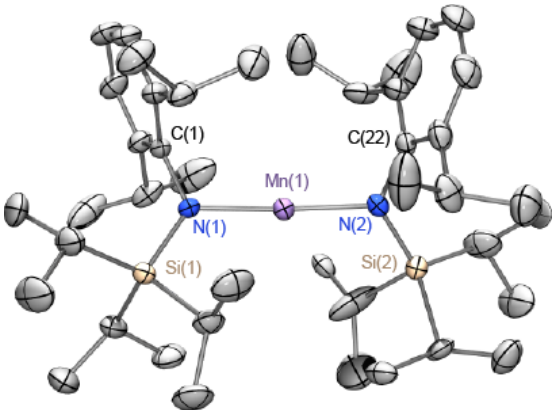

Figure 3.2. Solid-state structure of **3.3** as determined by single-crystal X-ray diffraction. Thermal ellipsoids are shown at 50% probability. Hydrogen atoms and disordered atoms have been omitted for clarity.

In an attempt to access a low-coordinate manganese oxo complex, 1 equiv of pyridine N-oxide (pyO) was added to **3.3** in diethyl ether at -30 °C. Recrystallization of the resulting product afforded the pyridine N-oxide adduct (pyO)Mn[N(Si^{i}Pr$_3$)DIPP]$_2$ (**3.4**), as yellow-green needles from pentane in 61% yield. In the solid state, the axis defined by the manganese center and the nitrogen of the pyridine ring is collinear with a C_2 axis (Figure 3.3). In contrast to hexakis(pyridine N-oxide) manganese(II) bis(triflate), in which the Mn–O–N bond angles range from 116.07(18)° to 128.76(19)°, the Mn–O–N(2) bond angle in **3.4** is nearly linear at 167.8(11)°. This linearity of

the Mn–O–N bond angle in **3.4** can be attributed to severe steric crowding imposed by the triisopropylsilyl group, consistent with the fact that the smaller trimethylsilyl moiety is bulky enough to support the two coordinate bis(silyl(aryl)amido) manganese complex **3.1**. Despite this linearity, the pyridine N-oxide O–N(2) bond length of **3.4** is 1.314(3) Å, comparable to that of free pyNO (1.33 Å) and does not appear to indicate significant activation.[20] The Mn–N(1) bond length of **3.4** is 2.0159(11) Å, noticeably longer than that of **3.3**, but expected given the higher coordination number.

Similarly, pyridine N-oxide can be added to **3.1** in diethyl ether at -30 °C to afford the analogous pyridine N-oxide adduct (pyO)Mn[N(SiMe$_3$)DIPP]$_2$ (**3.5**) in 85% yield. The smaller amido ligand provides relatively more steric relief; the Mn–O–N(3) bond angle in **3.5** is significantly more bent at 129.56(10)° (Figure 3.4) and the manganese amido bond lengths (1.9834(14) Å, 1.9927(14) Å) are shorter than that of **3.4**.

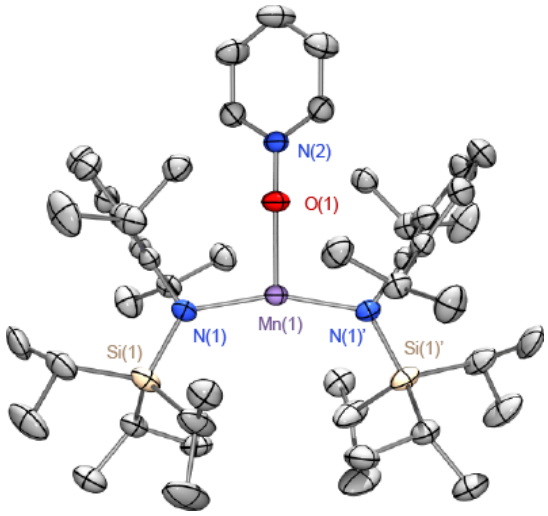

Figure 3.3. Solid-state structure of **3.4** as determined by single-crystal X-ray diffraction. Thermal ellipsoids are shown at 50% probability. Hydrogen atoms and disordered atoms have been omitted for clarity.

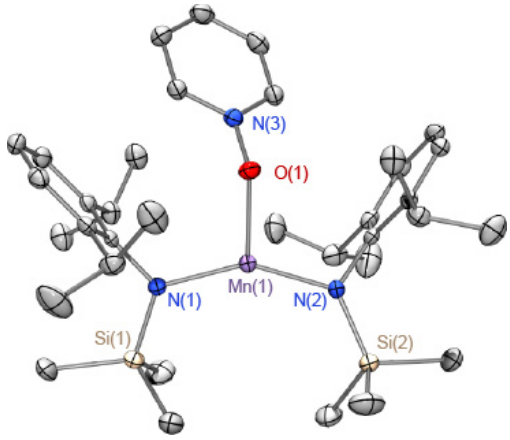

Figure 3.4. Solid-state structure of **3.5** as determined by single-crystal X-ray diffraction. Thermal ellipsoids are shown at 50% probability. Hydrogen atoms have been omitted for clarity.

To examine the effect of a stronger oxidizing agent, trimethylamine N-oxide (Me_3NO) was added to **3.1** in diethyl ether at ambient temperature to afford the N-oxide adduct, $(Me_3NO)Mn[N(SiMe_3)DIPP]_2$ (**3.6**) in 21% yield. Complex **3.6** contains a Mn–O–N(3) bond angle of 152.25(10)° (Figure 3.5), which is slightly more linear than that of the iron(III) tris(alkoxy) trimethylamine N-oxide adduct $(Me_3NO)Fe(OCMe^tBu_2)_3$ (137.24(13)°).[21] However, **3.6** contains an O–N(3) distance of 1.3928(16) Å, which is similar to that of free Me_3NO (1.404(5) Å),[22] indicating very little activation of the N-oxide. Although sterically demanding silylarylamido ligands help to enforce two-coordination of both **3.1** and **3.3**, these ligands also appear to prevent formation of higher-valent oxo species with these stoichiometric oxidants.

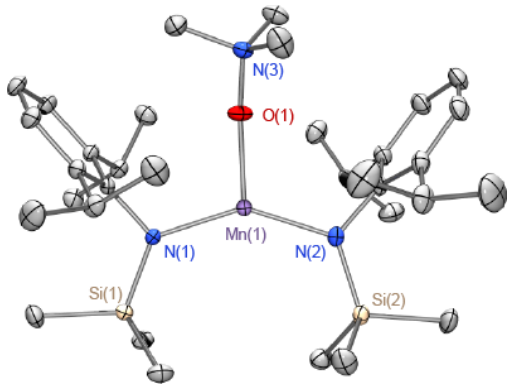

Figure 3.5. Solid-state structure of **3.6** as determined by single-crystal X-ray diffraction. Thermal ellipsoids are shown at 50% probability. Hydrogen atoms have been omitted for clarity.

Given the difficulty associated with isolating stable manganese(IV) bis(amido) oxo complexes, the reduction chemistry of **3.1** and **3.3** was investigated. Reduction of **3.3** with 1.1 equiv of KC_8 in diethyl ether at -30 °C, followed by recrystallization from pentane, afforded $K\{Mn[N(Si^iPr_3)DIPP]_2\}$ (**3.7**) as purple crystals in 45% yield. The conformation of **3.7**, with a N−Mn−N bond angle of 177.89(7)°, is similar to that of **3.3**, albeit with the potassium cation coordinated to the aryl rings of both amido ligands (Figure 3.6). The Mn−N bond lengths of the anionic complex **3.7** (1.9850(18) Å, 1.9699(18) Å) are also longer than that of **3.3**, as expected.

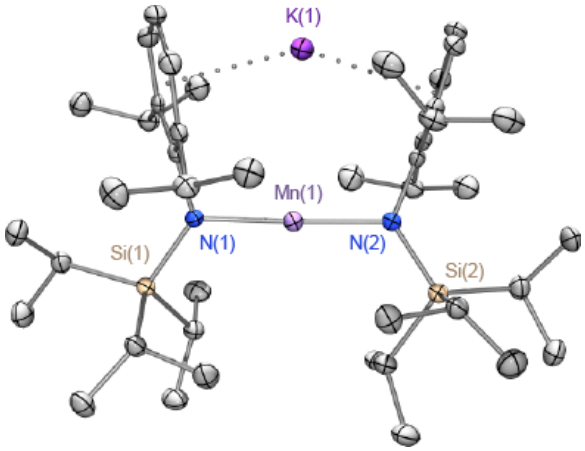

Figure 3.6. Solid-state structure of **3.7** as determined by single-crystal X-ray diffraction. Thermal ellipsoids are shown at 50% probability. Hydrogen atoms have been omitted for clarity.

Formation of **3.7** *in situ* followed by salt metathesis with tetrabutylammonium bromide gave $[NBu_4]\{Mn[N(Si^iPr_3)DIPP]_2\}$ (**3.8**) as blue-green needles from diethyl ether in 50% yield. The Mn−N bond lengths (1.9636(17) Å, 1.9649(17) Å) and N−Mn−N bond angle of 174.75(7)° of **3.8** (Figure 3.7) are very similar to that of **3.7**, indicating that coordination of potassium does not have a significant effect on the structure of the manganese(I) anionic $\{Mn[N(Si^iPr_3)DIPP]_2\}^-$ fragment. The solution magnetic moments of **3.7** and **3.8** are 4.9 and 4.5 μ_B respectively, both consistent with a high-spin d^6configuration.

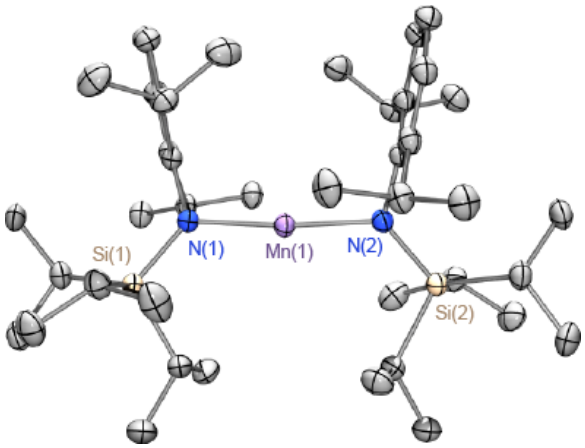

Figure 3.7. Solid-state structure of **3.8** as determined by single-crystal X-ray diffraction. Thermal ellipsoids are shown at 50% probability. Hydrogen atoms and tetrabutylammonium cation have been omitted for clarity.

Although the anionic manganese(I) complex **3.2** was previously reported, the isolation of **3.7** prompted a reexamination of the structure of **3.1** in the absence of chelating agents such as 18-crown-6. Reduction of **3.1** with 1.1 equiv of KC_8 in toluene at 0 °C under an atmosphere of argon, followed by recrystallization from toluene layered with pentane afforded dark red needles of $K\{Mn[N(SiMe_3)DIPP]_2\}$ (**3.9**) in 17% yield. In contrast to **3.7**, the potassium cations in **3.9** are bound intermolecularly between the aryl groups of adjacent molecules, resulting in a coordination polymer (Figure 3.8). Comparable to the Mn−N bond lengths of **3.7** and **3.8**, as well as that of **3.2** (*cf.* 1.954(3) Å, 1.961(3) Å),[7] **3.9** contains Mn−N bond lengths of (1.966(2) Å, 1.967(2) Å). Consistent with the N−Mn−N bond angle of **3.2** (167.13(15)°), **3.9** possesses a N−Mn−N bond angle of 165.44(10)°. However, in contrast to **3.2**, **3.7**, and **3.8**, which all feature a slightly staggered conformation of the DIPP moieties, the solid-state structure of **3.9** reveals an obtuse C_{ipso}–N1---N2–C_{ipso} torsion angle of 161.9(3)°.

Interestingly, reduction of **3.1** with 1 equiv of KC_8 in pentane at -30 °C under an atmosphere of nitrogen, in the absence of chelating agents, followed by recrystallization from pentane, affords the bridging dinitrogen complex **3.10** as dark green crystals in 33% yield. Although arene-bound, the potassium cations in **3.10** are collinear with a 2-fold screw axis and enforce a dimeric species in which dinitrogen is bound between the two manganese centers. The N−N bond length is 1.240(5) Å, indicating slight activation with respect to free dinitrogen (1.0975 Å).[23] This dinitrogen distance is longer than any of the few structurally characterized manganese complexes with an end-on bound dinitrogen reported to date,[24–27] including the four-coordinate complex $([N_2P_2]Mn)_2(\mu\text{-}N_2)$ (N_2P_2 = $(^tBuN^{(-)}SiMe_2)N(CH_2CH_2P^iPr_2)_2$), which has an N–N bond length of 1.208(6) Å.[26] The activation of the N–N bond in $([N_2P_2]Mn)_2(\mu\text{-}N_2)$, due to π back-bonding into the π* orbital of dinitrogen, is attributed to the low-coordination number of the metal

center. Given that **3.10** is only three-coordinate at each metal center, a similar argument is consistent with the slightly longer N–N bond distance in **3.10**.

Due to higher coordination number of the metal center compared to that of **3.9**, **3.10** contains elongated Mn−N_{amido} bonds (2.070(2) Å, 2.063(2) Å) and a N−Mn−N bond angle of 123.03(9)° (Figure 3.9). Unlike in complex **3.7**, arene-bound potassium cations, promoted by the absence of coordinating solvents or chelating agents, in conjunction with the smaller silylarylamido ligand in **3.10** appear to allow for the coordination of a small molecule (dinitrogen).

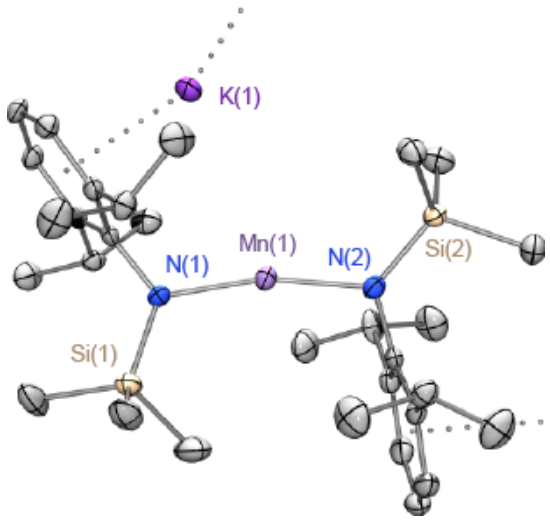

Figure 3.8. Solid-state structure of **3.9** as determined by single-crystal X-ray diffraction. Thermal ellipsoids are shown at 50% probability. Hydrogen atoms have been omitted for clarity.

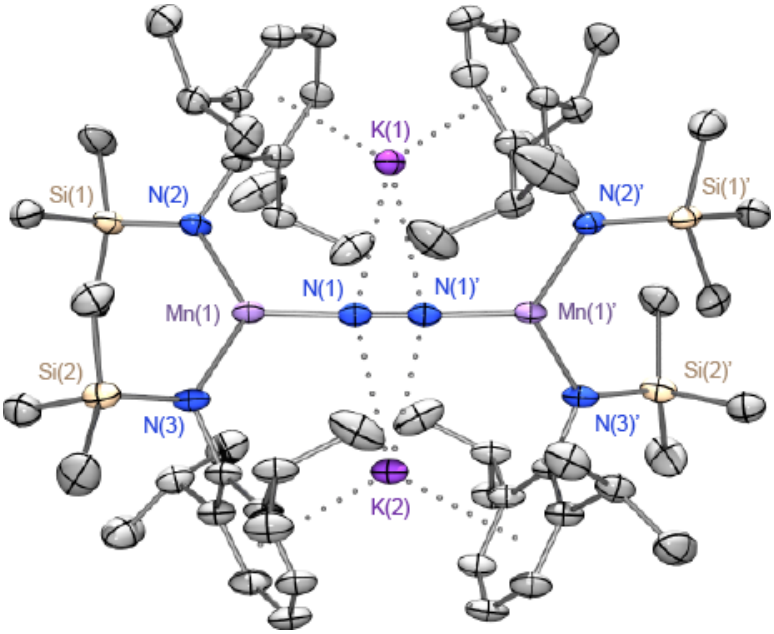

Figure 3.9. Solid-state structure of **3.10** as determined by single-crystal X-ray diffraction. Thermal ellipsoids are shown at 50% probability. Hydrogen atoms and disordered solvent molecules have been omitted for clarity.

CONCLUSIONS

These comparisons of the coordination chemistry of **3.1** and **3.3** illustrate the effects of ligand modification on the structure of derivatives arising from two-coordinate complexes. Both manganese bis(amido) complexes have been used to synthesize the corresponding pyridine N-oxide adducts, with the products having subtle differences in structure. Surprisingly, attempts to oxidize **3.1** with trimethylamine N-oxide also results in a manganese N-oxide adduct, rather than expected oxo complex. Further efforts to access higher valent derivatives of **3.1** and **3.3** are underway.

Reduction of **3.3** affords the corresponding mononuclear anionic species, which can be isolated as either its potassium (**3.7**) or tetrabutylammonium salt (**3.8**). Although reduction of **3.1** under an atmosphere of argon yields the coordination polymer **3.9**, reduction under nitrogen in the absence of a chelating agent affords the dinitrogen-bound dimeric complex **3.10**. In the +1 oxidation state, the difference in steric bulk is significant enough to not only effect changes in bond lengths and bond angles, but also the coordination of additional ligands. These complexes demonstrate the potential chemistry available to low-coordinate anionic manganese complexes containing arene-bound cations. Although many advances have been made on the forefront of synthesizing two-coordinate complexes, differences in steric bulk between ligands that are otherwise electronically similar can have a noticeable impact on low-coordinate reactivity.

REFERENCES

(1) Power, P. P. *Chem. Rev.* **2012**, *112* (6), 3482–3507.
(2) Ni, C., Fettinger, J. C., Long, G. J., Power, P. P. *Dalton Trans.* **2010**, *39* (44), 10664–10670.
(3) Samuel, P. P., Mondal, K. C., Roesky, H. W., Hermann, M., Frenking, G., Demeshko, S., Meyer, F., Stückl, A. C., Christian, J. H., Dalal, N. S., Ungur, L., Chibotaru, L. F., Pröpper, K., Meents, A., Dittrich, B. *Angew. Chem. Int. Ed.* **2013**, *52* (45), 11817–11821.
(4) König, S. N., Schädle, C., Maichle-Mössmer, C., Anwander, R. *Inorg. Chem.* **2014**, *53* (9), 4585–4597.
(5) Lin, C.-Y., Fettinger, J. C., Chilton, N. F., Formanuik, A., Grandjean, F., Long, G. J., Power, P. P. *Chem. Commun.* **2015**, *51* (68), 13275–13278.
(6) Kreye, M., Freytag, M., Daniliuc, C. G., Jones, P. G., Walter, M. D. *Z. Für Anorg. Allg. Chem.* **2015**, *641* (12–13), 2109–2114.
(7) Werncke, C. G., Suturina, E., Bunting, P. C., Vendier, L., Long, J. R., Atanasov, M., Neese, F., Sabo-Etienne, S., Bontemps, S. *Chem. – Eur. J.* **2016**, *22* (5), 1668–1674.
(8) Al-Juaid, S. S., Eaborn, C., El-Hamruni, S. M., Hitchcock, P. B., Smith, J. D., Sözerli Can, S. E. *J. Organomet. Chem.* **2002**, *649* (2), 121–127.
(9) R. Kennedy, A., Klett, J., E. Mulvey, R., Newton, S., S. Wright, D. *Chem. Commun.* **2008**, *0* (3), 308–310.
(10) Cai, I. C., Lipschutz, M. I., Tilley, T. D. *Chem. Commun.* **2014**, *50* (86), 13062–13065.
(11) Lin, C.-Y., Fettinger, J. C., Grandjean, F., Long, G. J., Power, P. P. *Inorg. Chem.* **2014**, *53* (17), 9400–9406.
(12) Lipschutz, M. I., Yang, X., Chatterjee, R., Tilley, T. D. *J. Am. Chem. Soc.* **2013**, *135* (41), 15298–15301.
(13) Smith, J. M., Sadique, A. R., Cundari, T. R., Rodgers, K. R., Lukat-Rodgers, G., Lachicotte, R. J., Flaschenriem, C. J., Vela, J., Holland, P. L. *J. Am. Chem. Soc.* **2006**, *128* (3), 756–769.
(14) Rodriguez, M. M., Bill, E., Brennessel, W. W., Holland, P. L. *Science* **2011**, *334* (6057), 780–783.
(15) Chiang, K. P., Bellows, S. M., Brennessel, W. W., Holland, P. L. *Chem. Sci.* **2013**, *5* (1), 267–274.
(16) Kennepohl, D. K., Brooker, S., Sheldrick, G. M., Roesky, H. W. *Z. Für Naturforschung B* **1992**, *47*, 9–16.
(17) Evans, D. F. *J. Chem. Soc. Resumed* **1959**, No. 0, 2003–2005.
(18) Sur, S. K. *J. Magn. Reson. 1969* **1989**, *82* (1), 169–173.
(19) Grant, D. H. *J. Chem. Educ.* **1995**, *72* (1), 39–40.
(20) Marsh, R. E., Kapon, M., Hu, S., Herbstein, F. H. *Acta Crystallogr. B* **2002**, *58* (1), 62–77.
(21) Chambers, M. B., Groysman, S., Villagrán, D., Nocera, D. G. *Inorg. Chem.* **2013**, *52* (6), 3159–3169.
(22) Caron, A., Palenik, G. J., Goldish, E., Donohue, J. *Acta Crystallogr.* **1964**, *17* (2), 102–108.
(23) Hazari, N. *Chem. Soc. Rev.* **2010**, *39* (11), 4044–4056.
(24) Weidenhammer, K., Herrmann, W. A., Ziegler, M. L. *Z. Für Anorg. Allg. Chem.* **2004**, *457* (1), 183–188.
(25) Perthuisot, C., Fan, M., Jones, W. D. *Organometallics* **1992**, *11* (11), 3622–3629.
(26) Chomitz, W. A., Arnold, J. *Chem. Commun.* **2007**, *0* (45), 4797–4799.
(27) Cummins, D. C., Yap, G. P. A., Theopold, K. H. *Eur. J. Inorg. Chem.* **2016**, *2016* (15–16), 2349–2356.

EXPERIMENTAL DETAILS

General Considerations. Unless otherwise noted, all experiments were conducted with dry, oxygen-free solvents using standard Schlenk techniques or in a nitrogen atmosphere glovebox. Pentane, toluene, diethyl ether, and tetrahydrofuran were dried and deaerated using a JC Meyers Phoenix SDS solvent purification system. Deuterated solvents were purchased from Cambridge Isotope Laboratories, degassed by three freeze-pump-thaw cycles and stored under nitrogen over activated 3 Å molecular sieves prior to use.

$HN(Si^iPr_3)DIPP$[1], $Mn[N(SiMe_3)DIPP]_2$ (**3.1**),[2] and potassium graphite[3] were prepared according to literature procedures. From Sigma Aldrich, *n*-butyllithium solution (1.6 M in hexanes) was purchased and used as received. Pyridine N-oxide was dried by sublimation under reduced pressure.[4] Trimethylamine N-oxide was dried by azeotropic distillation with toluene, followed by removal of solvent *in vacuo*.[5] Ultra high purity argon (99.999%) was purchased from Praxair Technology, Inc. All other reagents were obtained from commercial suppliers and used as received.

The abbreviation "DIPP" refers to a 2,6-diisopropylphenyl moiety.

Analytical Method Details. Elemental analyses were performed by the College of Chemistry Microanalytical Facility at the University of California, Berkeley.

NMR Spectroscopy. All NMR spectra were collected at ambient temperature (ca. 22 °C) on Bruker AVB-400, AVQ-400, AV-500, or AV-600 MHz spectrometers. ^{1}H NMR spectra were referenced to tetramethylsilane calibrated *via* residual proteo-solvent signals.[6] All NMR spectra were analyzed with MestReNova (v. 12.0.3). Solution magnetic susceptibilities were determined by ^{1}H NMR spectroscopy using the Evans method.[7–9]

X-ray Diffraction Experiments. Data for **3.3**, **3.4**, **3.6**, **3.8**, and **3.9** were collected at Beamline 11.3.1/12.2.1 (Small Molecule Crystallography) of the Advanced Light Source at Lawrence Berkeley National Laboratory (LBNL). Measurements of **3.5**, **3.7**, and **3.10** were performed on a Bruker APEX-II CCD area detector using Mo Kα radiation (λ = 0.71073 Å) monochromated using QUAZAR multilayer mirrors. All crystals were kept at 100(2) K throughout collection.

Data collection, refinement, and reduction were performed with Bruker APEX2 or APEX3 software (v. 2013.4-0 or v. 2016.9-0). Structure solution, modeling, and refinement was performed using Olex2.[10] All structures were solved using SHELXT-2014[11] and refined with SHELXL-2018[12], with refinement of F^2 on all data by full-matrix least squares. In all models, non-hydrogen atoms were refined anisotropically, and hydrogen atoms were included at the geometrically-calculated positions and refined using a riding model. Disordered isopropyl groups and co-crystallizing solvent molecules were modeled atomistically.

Specific details can be found below (Table **E3.1**) and in the crystallographic information files.

Table E3.1: X-ray Crystallography Experimental Details:

Compound	*Detector Distance (mm)*	*Image Width (°)*	*Exposure Time (s)*
3.3	50	1 or 4, depending on angle	1
3.4	50	1 or 4, depending on angle	1
3.5	40	0.5	5
3.6	50	1 or 4, depending on angle	1
3.7	48	0.5	15
3.8	50	1 or 4, depending on angle	1
3.9	50	1 or 4, depending on angle	1
3.10	50	0.4	30

Synthesis of Li[N(Si^{i}Pr$_3$)DIPP]. To a Schlenk flask was added HN(Si^{i}Pr$_3$)DIPP (5.34 g, 16.0 mmol) and pentane (ca. 40 mL). The resulting solution was stirred at 0 °C, and *n*-butyllithium in hexanes (10 mL, 1.6 M, 16.0 mmol) was added slowly *via* syringe. The reaction mixture was allowed to warm up to ambient temperature and stirred for 1 h. The resulting mixture was concentrated under reduced pressure to a solid. Residual volatile compounds were removed *in vacuo* to yield an off-white powder (5.23 g, 15.4 mmol, 96%), which was used without further purification.

Mn[N(Si^{i}Pr$_3$)DIPP]$_2$ (3.3). To a 100 mL Teflon-stoppered flask was added manganese dichloride (0.456 g, 3.62 mmol) and diethyl ether (15 mL). The resulting suspension was stirred at room temperature, and a solution of Li[N(Si^{i}Pr$_3$)DIPP] (2.46 g, 7.24 mmol, 2.0 equiv) in diethyl ether (20 mL) was added slowly. The reaction was stirred at ambient temperature for 12 h. The reaction mixture was concentrated under reduced pressure to a yellow solid, which was extracted with pentane (30 mL total). The combined pentane extracts were filtered, concentrated *in vacuo* to 12 mL, and stored overnight at -30 °C, to yield 1.09 g (1.51 mmol, 42%) of **3.3** as yellow blocks, which were isolated by decanting the supernatant and removing residual volatile compounds *in vacuo*. The supernatant was collected and concentrated to a volume of 6 mL. Storage of the resulting solution at -30 °C yielded an additional 0.61 g (0.85 mmol) of **3.3**. Total yield: 1.70 g (2.36 mmol, 65%).

Crystals suitable for single crystal X-ray diffraction studies were obtained from the crystallization procedure described above.

Effective magnetic moment (Evans method, C_6D_6): μ_{eff} = 5.4 μ_B.

Anal. Calcd for $C_{42}H_{76}N_2MnSi_2$: C, 70.05; H, 10.64; N, 3.89. Found: C, 69.67; H, 10.51; N, 3.92.

(pyO)Mn[N(Si^{i}Pr$_3$)DIPP]$_2$ (3.4). To a 20 mL scintillation vial was added **3.3** (0.098 g, 0.136 mmol) and diethyl ether (5 mL); the resulting solution was cooled to -30 °C. The cooled solution of **3.3** was stirred, and pyridine N-oxide (0.013 g, 0.136 mmol, 1.0 equiv) was added directly in a single aliquot. The reaction was stirred at ambient temperature for 25 min, until solids were no longer visible. The resulting solution was concentrated under reduced pressure to a residue, which was triturated with pentane (2 x 1.5 mL) to remove any remaining volatile components. The resulting residue was extracted with pentane (5 mL total). The combined pentane extracts were

filtered, concentrated *in vacuo* to 3 mL, and stored overnight at -30 °C, to yield 0.048 g (0.059 mmol, 43%) of **3.4** as yellow needles, which were isolated by decanting the supernatant and removing residual volatile compounds *in vacuo*.

Crystals suitable for single crystal X-ray diffraction studies were obtained from the crystallization procedure described above.

Effective magnetic moment (Evans method, C_6D_6): μ_{eff} = 5.9 μ_B.

Anal. Calcd for $C_{47}H_{81}N_3MnOSi_2$: C, 69.24; H, 10.01; N, 5.15. Found: C, 68.83; H, 9.78; N, 4.99.

(pyO)Mn[N(SiMe$_3$)DIPP]$_2$ (3.5). To a 20 mL scintillation vial was added **3.1** (0.200 g, 0.362 mmol) and diethyl ether (8 mL); the resulting solution was cooled to -30 °C. The cooled mixture of **3.1** was stirred, and pyridine N-oxide (0.036 g, 0.379 mmol, 1.05 equiv) was added directly in a single aliquot. The reaction was stirred at ambient temperature for 30 min, until solids were no longer visible. The resulting solution was concentrated under reduced pressure to a residue, which was triturated with pentane (2 x 1.5 mL) to remove any remaining volatile components. The resulting residue was extracted with pentane (5 mL total). The combined pentane extracts were filtered, concentrated *in vacuo* to 3 mL, and stored overnight at -30 °C, to yield 0.110 g (0.170 mmol, 47%) of **3.5** as yellow needles, which were isolated by decanting the supernatant and removing residual volatile compounds *in vacuo*.

Crystals suitable for single crystal X-ray diffraction studies were obtained from the crystallization procedure described above.

Effective magnetic moment (Evans method, C_6D_6): μ_{eff} = 5.6 μ_B.

Anal. Calcd for $C_{35}H_{57}N_3MnOSi_2$: C, 64.98; H, 8.88; N, 6.50. Found: C, 64.98; H, 8.86; N, 6.72.

(Me$_3$NO)Mn[N(SiMe$_3$)DIPP]$_2$ (3.6). To a 20 mL scintillation vial was added **3.1** (0.100 g, 0.181 mmol) and diethyl ether (6 mL). The mixture of **3.1** was stirred, and trimethylamine N-oxide (0.0136 g, 0.181 mmol, 1.0 equiv) was added directly in a single aliquot. The reaction was stirred at ambient temperature for 5 min. The resulting reaction mixture was concentrated under reduced pressure to 0.5 mL, filtered, and stored overnight at -30 °C, to yield 0.024 g (0.038 mmol, 21%) of **3.6** as colorless blocks, which were isolated by decanting the supernatant and removing residual volatile compounds *in vacuo*.

Crystals suitable for single crystal X-ray diffraction studies were obtained from the crystallization procedure described above.

Effective magnetic moment (Evans method, C_6D_6): μ_{eff} = 5.7 μ_B.

Anal. Calcd for $C_{33}H_{61}N_3MnOSi_2$: C, 63.22; H, 9.81; N, 6.70. Found: C, 62.85; H, 9.50; N, 6.59.

K{Mn[N(Si^{i}Pr$_3$)DIPP]$_2$} (3.7). To a 20 mL scintillation vial was added **3.3** (0.200 g, 0.278 mmol) and toluene (8 mL); the resulting solution was cooled to -30 °C. The cooled mixture of **3.3** was stirred, and potassium graphite (0.038 g, 0.281 mmol, 1.0 equiv) was added directly in a single aliquot. The reaction was stirred at ambient temperature for 30 min. The resulting reaction mixture was filtered, then concentrated under reduced pressure. The resulting residue was triturated with pentane (2 x 1.5 mL) to remove any residual toluene. The resulting solid was extracted with pentane (20 mL total). The combined pentane extracts were extracts were filtered, then stored overnight in a -30 °C freezer, to yield 0.094 g (0.124 mmol, 45%) of **3.7** as dark purple crystals, which were isolated by decanting the supernatant and removing residual volatile compounds *in vacuo*.

Crystals suitable for single crystal X-ray diffraction studies were obtained from the crystallization procedure described above.

Effective magnetic moment (Evans method, C_6D_6): μ_{eff} = 4.9 μ_B.

Anal. Calcd for $C_{42}H_{76}N_2MnKSi_2$: C, 66.44; H, 10.09; N, 3.69. Found: C, 66.21; H, 9.76; N, 3.58.

[NBu$_4$]{Mn[N(Si^{i}Pr$_3$)DIPP]$_2$} (3.8). To a 20 mL scintillation vial was added **3.3** (0.100 g, 0.139 mmol) and diethyl ether (6 mL); the resulting solution was cooled to -30 °C. The cooled mixture of **3.3** was stirred, and potassium graphite (0.021 g, 0.155 mmol, 1.1 equiv) was added directly in a single aliquot. The reaction was stirred at ambient temperature for 1 h. To the resulting purple reaction mixture was added tetrabutylammonium bromide (0.045 g, 0.140 mmol, 1.0 equiv) in a single aliquot. The reaction was stirred at ambient temperature for an additional 30 min. The resulting dark blue reaction mixture was filtered, then concentrated under reduced pressure to 4 mL and stored in a -30 °C freezer for two days, to yield 0.067 g (0.070 mmol, 50%) of **3.8** as blue-green needles, which were isolated by decanting the supernatant and removing residual volatile compounds *in vacuo*.

Crystals suitable for single crystal X-ray diffraction studies were obtained from the crystallization procedure described above.

Effective magnetic moment (Evans method, THF): μ_{eff} = 4.5 μ_B.

Anal. Calcd for $C_{58}H_{112}N_3MnSi_2$: C, 72.37; H, 11.73; N, 4.37. Found: C, 72.30; H, 11.45; N, 4.26.

K{Mn[N(SiMe$_3$)DIPP]$_2$} (3.9). In a nitrogen-filled glovebox, to a Schlenk tube was added **3.1** (0.112 g, 0.203 mmol) and potassium graphite (0.030 g, 0.222 mmol, 1.1 equiv). The remaining steps were conducted under an atmosphere of ultra high purity argon and with nitrogen-free solvent: The Schlenk tube was evacuated and re-filled with argon three times. The solids were cooled to 0 °C using an ice bath, and toluene (10 mL) was added. The reaction was stirred at ambient temperature for 30 min. The resulting reaction mixture was cannula filtered, then concentrated under reduced pressure to 2 mL, upon which pentane (10 mL) was layered. The layered solution was stored at -30 °C over several days, to yield 0.020 g (0.034 mmol, 17%) of **3.9** as dark purple needles, which were isolated by decanting the supernatant and removing residual volatile compounds *in vacuo*.

Crystals suitable for single crystal X-ray diffraction studies were obtained from the crystallization procedure described above.

Anal. Calcd for $C_{30}H_{52}N_2MnKSi_2$: C, 60.97; H, 8.87; N, 4.74. Found: C, 56.10; H, 8.31; N, 4.25.

$(K\{Mn[N(SiMe_3)DIPP]_2\})_2(N_2)$ (3.10). To a 20 mL scintillation vial was added **3.1** (0.200 g, 0.362 mmol) and pentane (10 mL); the resulting solution was cooled to -30 °C. The cooled mixture of **3.1** was stirred, and potassium graphite (0.049 g, 0.362 mmol, 1.0 equiv) was added directly in a single aliquot. The reaction was stirred at ambient temperature for 30 min. The resulting reaction mixture was filtered, then concentrated under reduced pressure to 3 mL and stored overnight in a -30 °C freezer, to yield 0.072 g (0.060 mmol, 33%) of **3.10** as dark green crystals, which were isolated by decanting the supernatant and removing residual volatile compounds *in vacuo*.

Crystals suitable for single crystal X-ray diffraction studies were obtained from the crystallization procedure described above.

Effective magnetic moment (Evans method, C_6D_6): μ_{eff} = 8.0 μ_B.

Anal. Calcd for $C_{60}H_{104}N_6Mn_2K_2Si_4$: C, 59.56; H, 8.66; N, 6.95. Found: C, 59.61; H, 8.46; N, 6.42.

SINGLE-CRYSTAL X-RAY DIFFRACTION CRYSTAL STRUCTURE DETAILS

Figure SX1. Solid-state structure of complex **3.3** as determined by single-crystal X-ray diffraction.

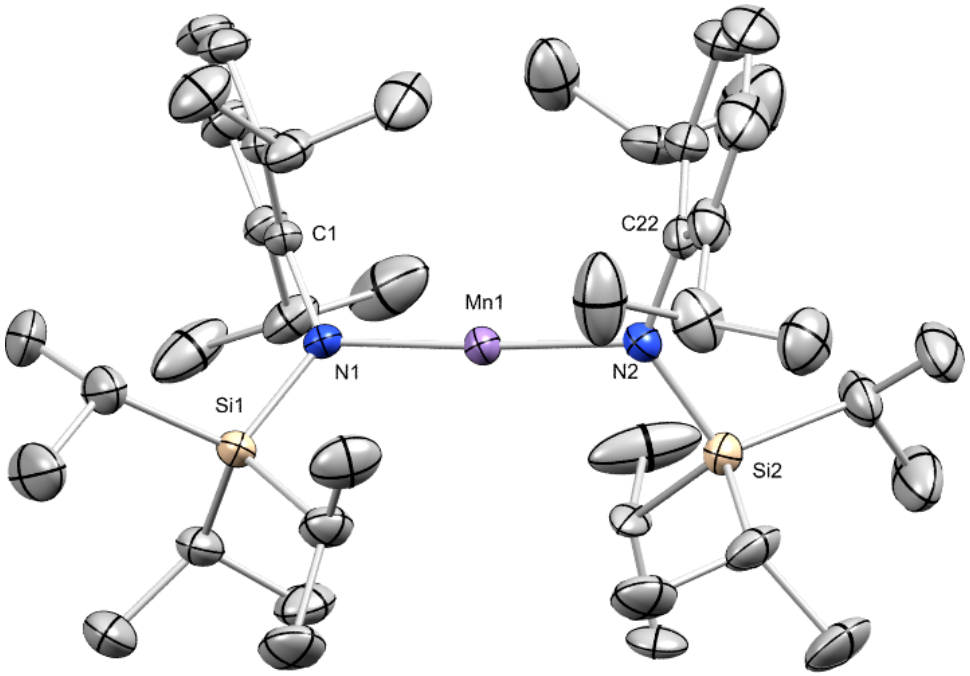

Notes: Thermal ellipsoids are shown at 50% probability. Hydrogen atoms and disordered –Si^{i}Pr$_3$ group have been omitted for clarity. Selected bond distances [Å], angles [°], and torsions [°]: Mn1–N1: 1.9344(18), Mn1–N2: 1.9386(19), N1–C1: 1.435(3), N2–C22: 1.434(3), N1–Si1: 1.7310(19), N2–Si2: 1.730(2); N1–Mn1–N2: 177.15(8); C1–N1---N2–C22: ±40.5(2).

Table SX1. Crystal data and structure refinement for complex **3.3**

Empirical formula	$C_{42}H_{76}MnN_2Si_2$
Formula weight	720.16
Temperature (K)	100(2)
Crystal system	monoclinic
Space group	$P2_1/n$
a (Å)	10.6645(6)
b (Å)	23.2765(13)
c (Å)	17.7904(10)
α (°)	90
β (°)	99.164(3)
γ (°)	90
Volume ($Å^3$)	4359.8(4)
Z	4
ρ_{calc} (g/cm^3)	1.097
μ (mm^{-1})	0.484
F(000)	1580.0
Crystal size (mm^3)	0.339 × 0.113 × 0.113
Radiation (Å)	synchrotron (λ = 0.7749)
2Θ range for data collection (°)	4.56 to 63.364
Index ranges	$-14 \leq h \leq 14$, $-31 \leq k \leq 31$, $-24 \leq l \leq 24$
Reflections collected	49811
Independent reflections	11334 [R_{int} = 0.0636, R_{sigma} = 0.0545]
Data/restraints/parameters	11334/0/532
Goodness-of-fit on F^2	1.131
Final R indexes [I>=2σ (I)]	R_1 = 0.0588, wR_2 = 0.1320
Final R indexes [all data]	R_1 = 0.0724, wR_2 = 0.1376
Largest diff. peak/hole ($e/Å^3$)	0.50/-0.46

Figure SX2. Solid-state structure of complex **3.4** as determined by single-crystal X-ray diffraction.

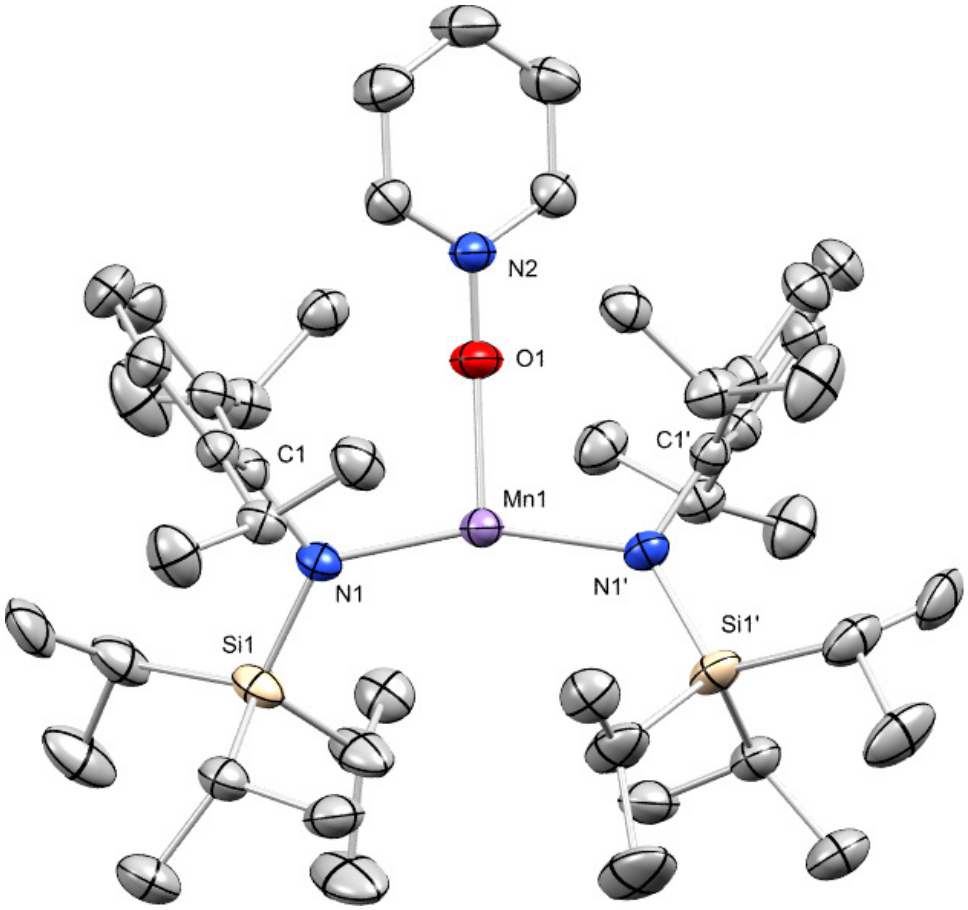

Notes: Thermal ellipsoids are shown at 50% probability. Hydrogen atoms and disordered –Si^{i}Pr$_3$ group have been omitted for clarity. Selected bond distances [Å], angles [°], and torsions [°]: Mn1–N1: 2.0159(11), Mn1–O1: 2.033(2), O1–N2: 1.314(3), N1–C1: 1.4285(17), N1–Si1: 1.7416(11); N1–Mn1–N1': 160.39(7), Mn1–O1–N2: 167.8(11); C1–N1---N1'–C1': ±36.8(1).

Table SX2. Crystal data and structure refinement for complex **3.4**

Empirical formula	$C_{47}H_{81}MnN_3OSi_2$
Formula weight	815.26
Temperature (K)	100(2)
Crystal system	monoclinic
Space group	C2/c
a (Å)	14.7802(6)
b (Å)	18.7761(7)
c (Å)	18.1164(7)
α (°)	90
β (°)	106.243(2)
γ (°)	90
Volume ($Å^3$)	4826.9(3)
Z	4
ρ_{calc} (g/cm^3)	1.122
μ (mm^{-1})	0.448
F(000)	1780.0
Crystal size (mm^3)	0.15 × 0.15 × 0.06
Radiation (Å)	synchrotron (λ = 0.7749)
2Θ range for data collection (°)	4.176 to 67.33
Index ranges	$-21 \leq h \leq 21$, $-26 \leq k \leq 26$, $-25 \leq l \leq 25$
Reflections collected	32420
Independent reflections	7396 [R_{int} = 0.0402, R_{sigma} = 0.0373]
Data/restraints/parameters	7396/0/348
Goodness-of-fit on F^2	1.022
Final R indexes [I>=2σ (I)]	R_1 = 0.0408, wR_2 = 0.1038
Final R indexes [all data]	R_1 = 0.0579, wR_2 = 0.1137
Largest diff. peak/hole ($e/Å^3$)	0.31/-0.36

Figure SX3. Solid-state structure of complex **3.5** as determined by single-crystal X-ray diffraction.

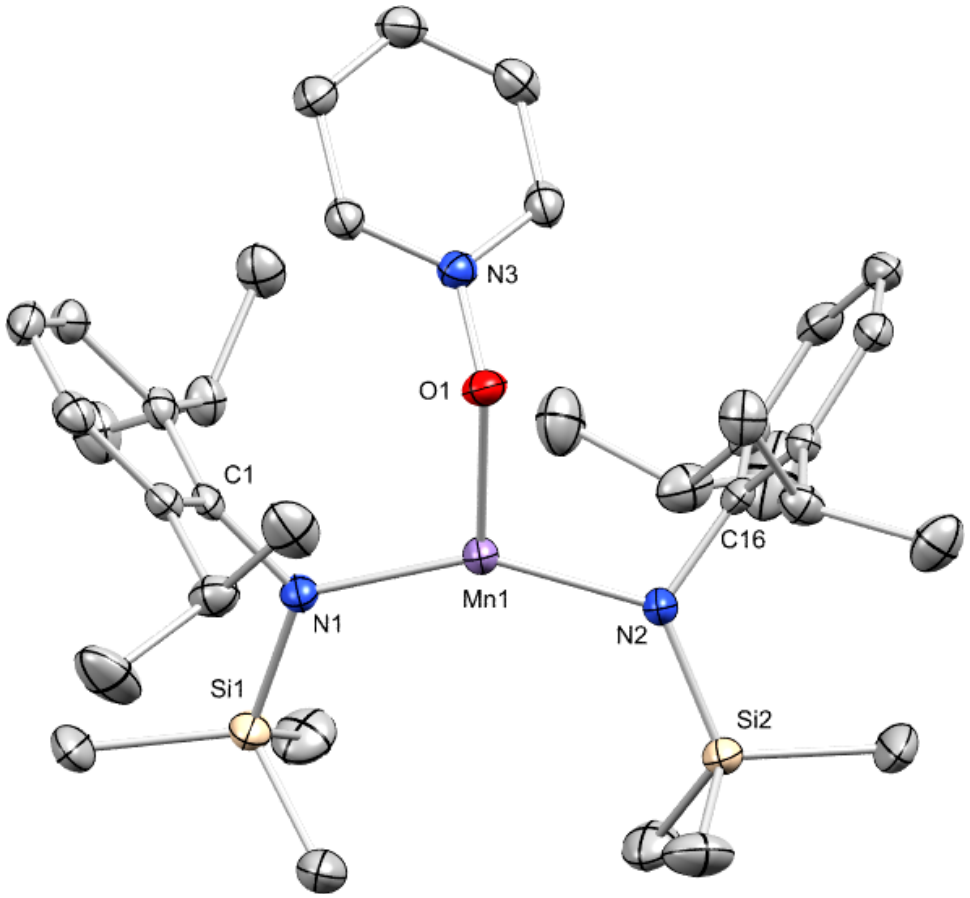

Notes: Thermal ellipsoids are shown at 50% probability. Hydrogen atoms have been omitted for clarity. Selected bond distances [Å], angles [°], and torsions [°]: Mn1–N1: 1.9834(14), Mn1–N2: 1.9927(14), Mn1–O1: 2.0671(12), O1–N3: 1.3346(18), N1–C1: 1.428(2), N2–C16: 1.431(2), N1–Si1: 1.7153(14), N2–Si2: 1.7145(15); N1–Mn1–N2: 146.56(6), Mn1–O1–N3: 129.56(10); C1–N1---N2–C16: ±32.8(2).

Table SX3. Crystal data and structure refinement for complex **3.5**

Empirical formula	$C_{35}H_{57}N_3OSi_2Mn$
Formula weight	646.95
Temperature (K)	100(2)
Crystal system	monoclinic
Space group	$P2_1/c$
a (Å)	9.7989(5)
b (Å)	20.9754(12)
c (Å)	18.6210(10)
α (°)	90
β (°)	100.820(2)
γ (°)	90
Volume ($Å^3$)	3759.2(4)
Z	4
ρ_{calc} (g/cm^3)	1.143
μ (mm^{-1})	0.444
F(000)	1396.0
Crystal size (mm^3)	0.1 × 0.1 × 0.1
Radiation (Å)	MoKα (λ = 0.71073)
2Θ range for data collection (°)	2.954 to 50.856
Index ranges	$-11 \leq h \leq 10$, $-25 \leq k \leq 25$, $-22 \leq l \leq 22$
Reflections collected	88546
Independent reflections	6932 [R_{int} = 0.0384, R_{sigma} = 0.0191]
Data/restraints/parameters	6932/0/393
Goodness-of-fit on F^2	1.049
Final R indexes [I>=2σ (I)]	R_1 = 0.0364, wR_2 = 0.0924
Final R indexes [all data]	R_1 = 0.0418, wR_2 = 0.0959
Largest diff. peak/hole ($e/Å^3$)	0.75/-0.36

Figure SX4. Solid-state structure of complex **3.6** as determined by single-crystal X-ray diffraction.

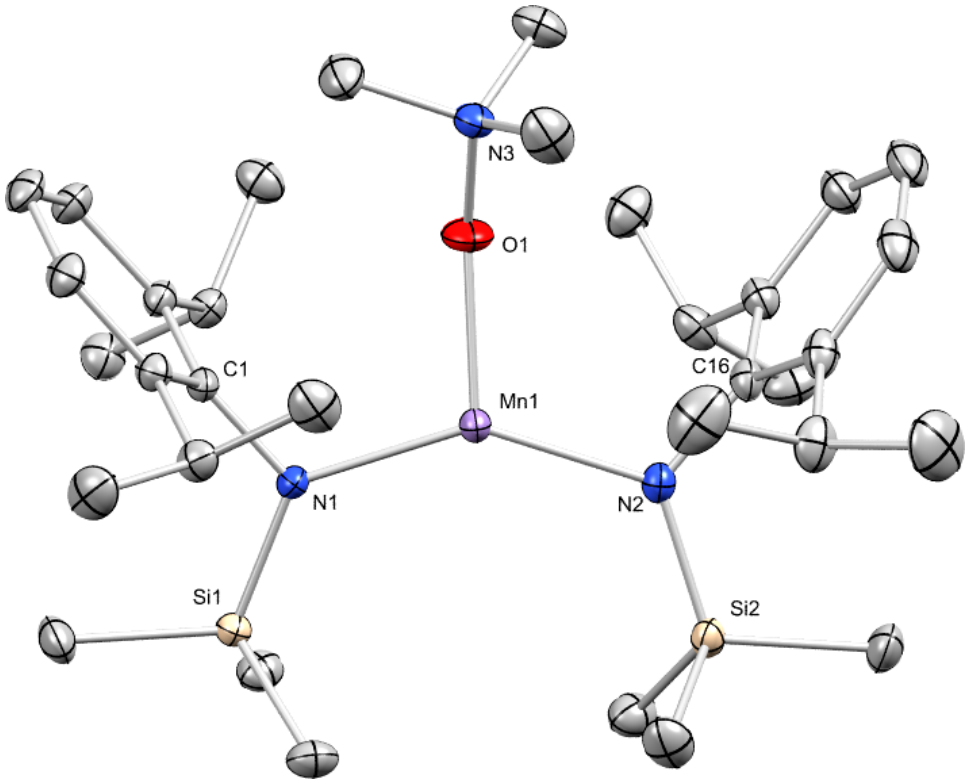

Notes: Thermal ellipsoids are shown at 50% probability. Hydrogen atoms have been omitted for clarity. Selected bond distances [Å], angles [°], and torsions [°]: Mn1–N1: 2.0064(11), Mn1–N2: 2.0177(11), Mn1–O1: 1.9994(10), O1–N3: 1.3928(16), N1–C1: 1.4235(16), N2–C16: 1.4171(17), N1–Si1: 1.7172(11), N2–Si2: 1.7163(12); N1–Mn1–N2: 144.68(4), Mn1–O1–N3: 152.25(10); C1–N1---N2–C16: −15.0(2).

Table SX4. Crystal data and structure refinement for complex **3.6**

Empirical formula	$C_{33}H_{61}MnN_3OSi_2$
Formula weight	626.96
Temperature (K)	100(2)
Crystal system	orthorhombic
Space group	$P2_12_12_1$
a (Å)	12.8836(6)
b (Å)	15.1778(7)
c (Å)	19.4179(9)
α (°)	90
β (°)	90
γ (°)	90
Volume ($Å^3$)	3797.1(3)
Z	4
ρ_{calc} (g/cm^3)	1.097
μ (mm^{-1})	0.464
F(000)	1364.0
Crystal size (mm^3)	0.214 × 0.207 × 0.193
Radiation (Å)	synchrotron (λ = 0.7288)
2Θ range for data collection (°)	3.492 to 74.844
Index ranges	$-21 \leq h \leq 21$, $-25 \leq k \leq 25$, $-32 \leq l \leq 32$
Reflections collected	88091
Independent reflections	18361 [R_{int} = 0.0475, R_{sigma} = 0.0435]
Data/restraints/parameters	18361/0/378
Goodness-of-fit on F^2	1.070
Final R indexes [I>=2σ (I)]	R_1 = 0.0326, wR_2 = 0.0732
Final R indexes [all data]	R_1 = 0.0416, wR_2 = 0.0780
Largest diff. peak/hole ($e/Å^3$)	0.39/-0.38
Flack parameter	0.014(3)

Figure SX5. Solid-state structure of complex **3.7** as determined by single-crystal X-ray diffraction.

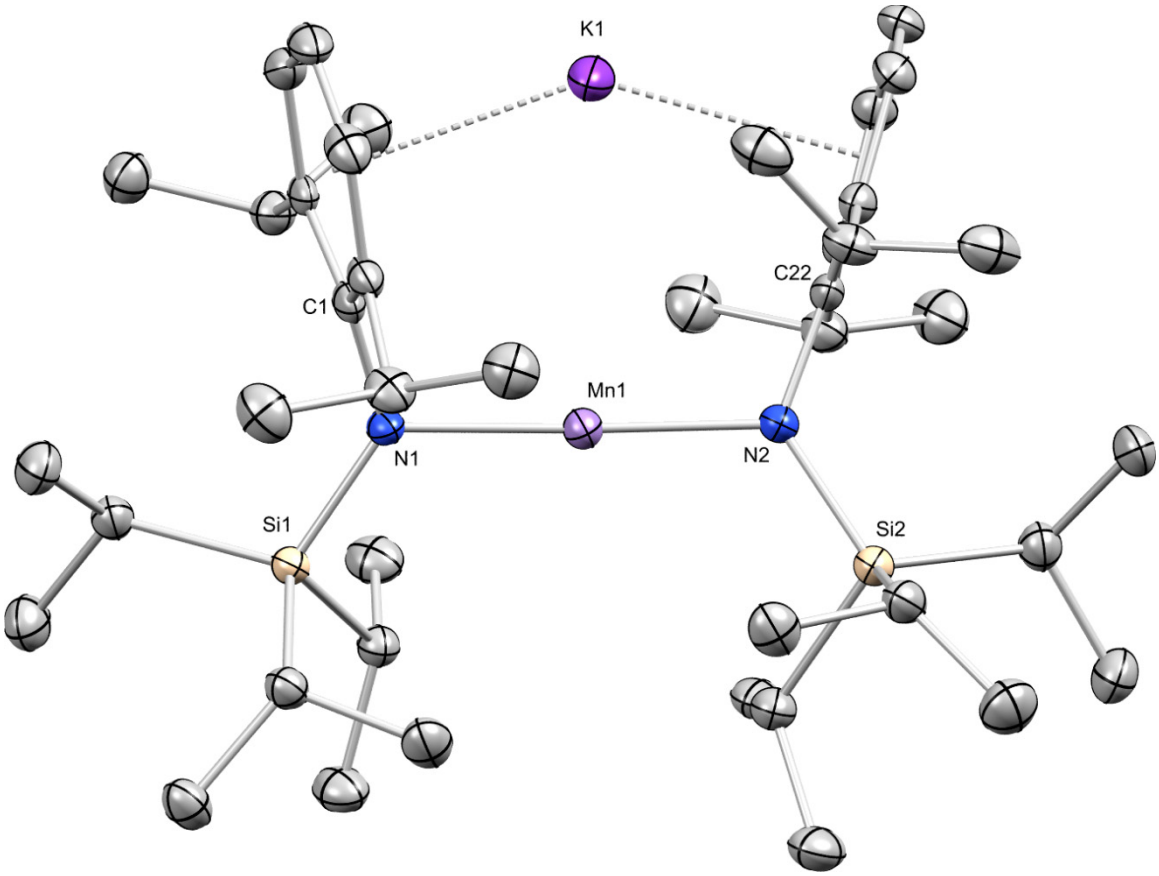

Notes: Thermal ellipsoids are shown at 50% probability. Hydrogen atoms have been omitted for clarity. Selected bond distances [Å], angles [°], and torsions [°]: Mn1–N1: 1.9850(18), Mn1–N2: 1.9699(18), N1–C1: 1.422(3), N2–C22: 1.419(3), N1–Si1: 1.7256(18), N2–Si2: 1.7281(19); N1–Mn1–N2: 177.89(7); C1–N1---N2–C22: ±32.5(2).

Table SX5. Crystal data and structure refinement for complex **3.7**

Empirical formula	$C_{42}H_{76}KMnN_2Si_2$
Formula weight	759.26
Temperature (K)	100(2)
Crystal system	monoclinic
Space group	C2/c
a (Å)	18.8958(4)
b (Å)	11.0243(4)
c (Å)	42.6123(12)
α (°)	90
β (°)	92.102(2)
γ (°)	90
Volume ($Å^3$)	8870.7(4)
Z	8
ρ_{calc} (g/cm^3)	1.137
μ (mm^{-1})	0.474
F(000)	3312.0
Crystal size (mm^3)	0.1 × 0.07 × 0.03
Radiation (Å)	MoKα (λ = 0.71073)
2Θ range for data collection (°)	3.826 to 51.182
Index ranges	$-22 \leq h \leq 22$, $-13 \leq k \leq 13$, $-51 \leq l \leq 51$
Reflections collected	81073
Independent reflections	8296 [R_{int} = 0.0875, R_{sigma} = 0.0665]
Data/restraints/parameters	8296/0/453
Goodness-of-fit on F^2	0.926
Final R indexes [I>=2σ (I)]	R_1 = 0.0427, wR_2 = 0.0957
Final R indexes [all data]	R_1 = 0.0667, wR_2 = 0.1017
Largest diff. peak/hole ($e/Å^3$)	0.70/-0.29

Figure SX6. Solid-state structure of complex **3.8** as determined by single-crystal X-ray diffraction.

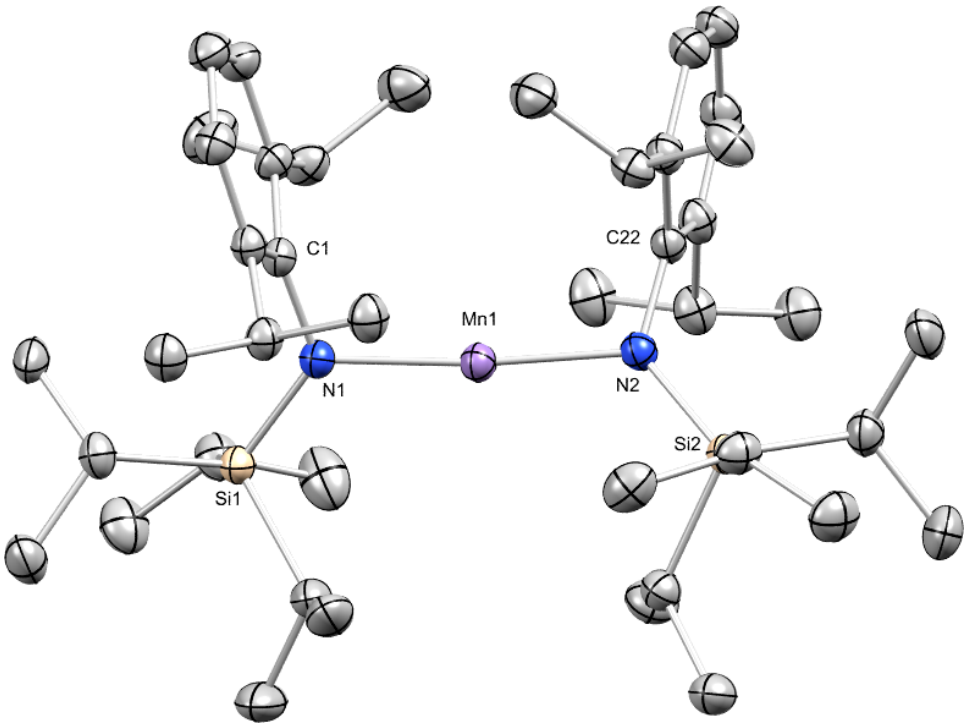

Notes: Thermal ellipsoids are shown at 50% probability. Hydrogen atoms and tetrabutylammonium cation have been omitted for clarity. Selected bond distances [Å], angles [°], and torsions [°]: Mn1–N1: 1.9636(17), Mn1–N2: 1.9649(17), N1–C1: 1.419(3), N2–C22: 1.420(3), N1–Si1: 1.7166(17), N2–Si2: 1.7182(18); N1–Mn1–N2: 174.75(7); C1–N1---N2–C22: ±39.8(2).

Table SX6. Crystal data and structure refinement for complex **3.8**

Empirical formula	$C_{58}H_{112}MnN_3Si_2$
Formula weight	962.62
Temperature (K)	100(2)
Crystal system	monoclinic
Space group	$P2_1/n$
a (Å)	14.6654(6)
b (Å)	28.4308(13)
c (Å)	14.9197(7)
α (°)	90
β (°)	90.834(3)
γ (°)	90
Volume ($Å^3$)	6220.1(5)
Z	4
ρ_{calc} (g/cm^3)	1.028
μ (mm^{-1})	0.356
F(000)	2136.0
Crystal size (mm^3)	0.1 × 0.1 × 0.1
Radiation (Å)	synchrotron (λ = 0.7749)
2Θ range for data collection (°)	4.278 to 67.37
Index ranges	$-20 \leq h \leq 20$, $-40 \leq k \leq 40$, $-21 \leq l \leq 21$
Reflections collected	81139
Independent reflections	19022 [R_{int} = 0.0485, R_{sigma} = 0.0425]
Data/restraints/parameters	19022/0/601
Goodness-of-fit on F^2	1.105
Final R indexes [I>=2σ (I)]	R_1 = 0.0642, wR_2 = 0.1452
Final R indexes [all data]	R_1 = 0.0918, wR_2 = 0.1617
Largest diff. peak/hole ($e/Å^3$)	0.59/-0.74

Figure SX7. Solid-state structure of complex **3.9** as determined by single-crystal X-ray diffraction.

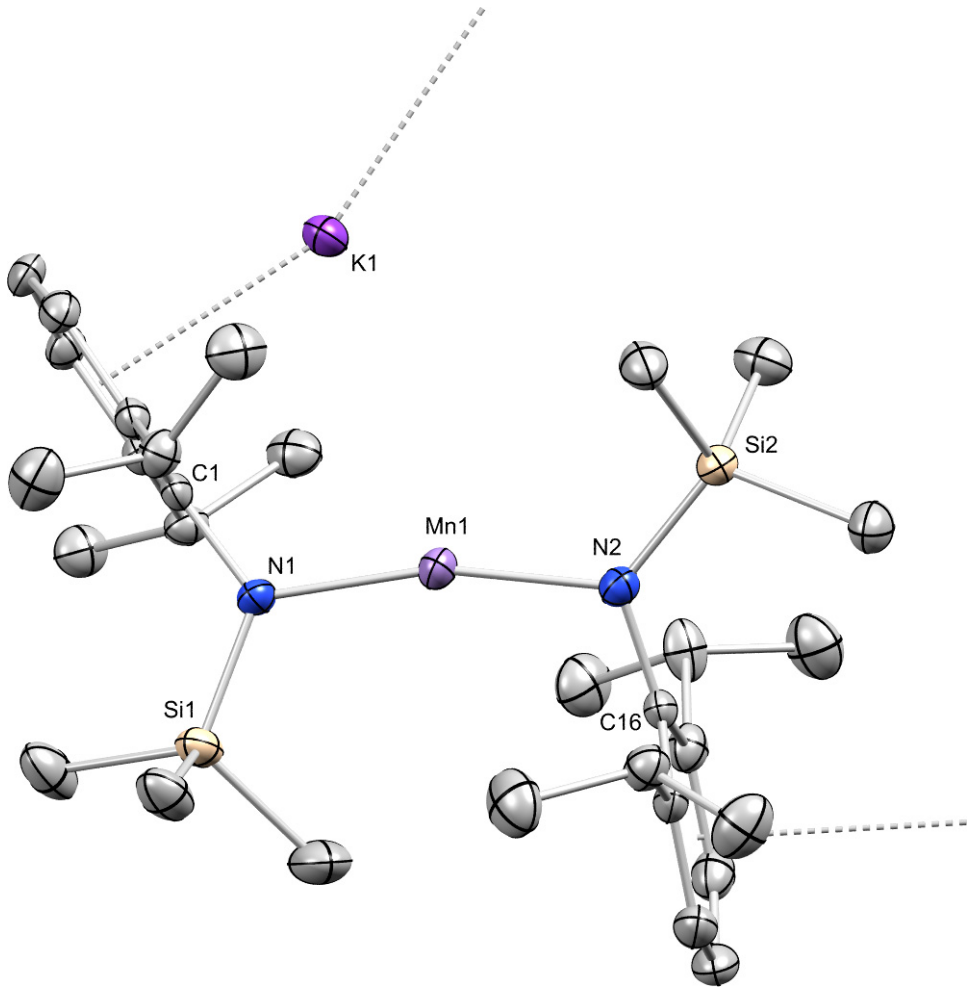

Notes: Thermal ellipsoids are shown at 50% probability. Hydrogen atoms have been omitted for clarity. Selected bond distances [Å], angles [°], and torsions [°]: Mn1–N1: 1.966(2), Mn1–N2: 1.967(2), N1–C1: 1.416(4), N2–C16: 1.406(4), N1–Si1: 1.712(2), N2–Si2: 1.712(3); N1–Mn1–N2: 165.44(10); C1–N1---N2–C16: ±161.9(3).

Table SX7. Crystal data and structure refinement for complex **3.9**

Empirical formula	$C_{30}H_{52}KMnN_2Si_2$
Formula weight	590.95
Temperature (K)	100(2)
Crystal system	monoclinic
Space group	$P2_1/n$
a (Å)	11.6446(15)
b (Å)	17.530(2)
c (Å)	17.876(2)
α (°)	90
β (°)	108.747(5)
γ (°)	90
Volume ($Å^3$)	3455.3(8)
Z	4
ρ_{calc} (g/cm^3)	1.136
μ (mm^{-1})	0.628
F(000)	1272.0
Crystal size (mm^3)	0.137 × 0.082 × 0.069
Radiation (Å)	synchrotron (λ = 0.7288)
2Θ range for data collection (°)	3.43 to 53.638
Index ranges	$-14 \leq h \leq 14$, $-21 \leq k \leq 21$, $-22 \leq l \leq 22$
Reflections collected	44844
Independent reflections	6827 [R_{int} = 0.0760, R_{sigma} = 0.0517]
Data/restraints/parameters	6827/0/339
Goodness-of-fit on F^2	1.078
Final R indexes [I>=2σ (I)]	R_1 = 0.0533, wR_2 = 0.1396
Final R indexes [all data]	R_1 = 0.0709, wR_2 = 0.1514
Largest diff. peak/hole ($e/Å^3$)	1.84/-0.82

Figure SX8. Solid-state structure of complex **3.10** as determined by single-crystal X-ray diffraction.

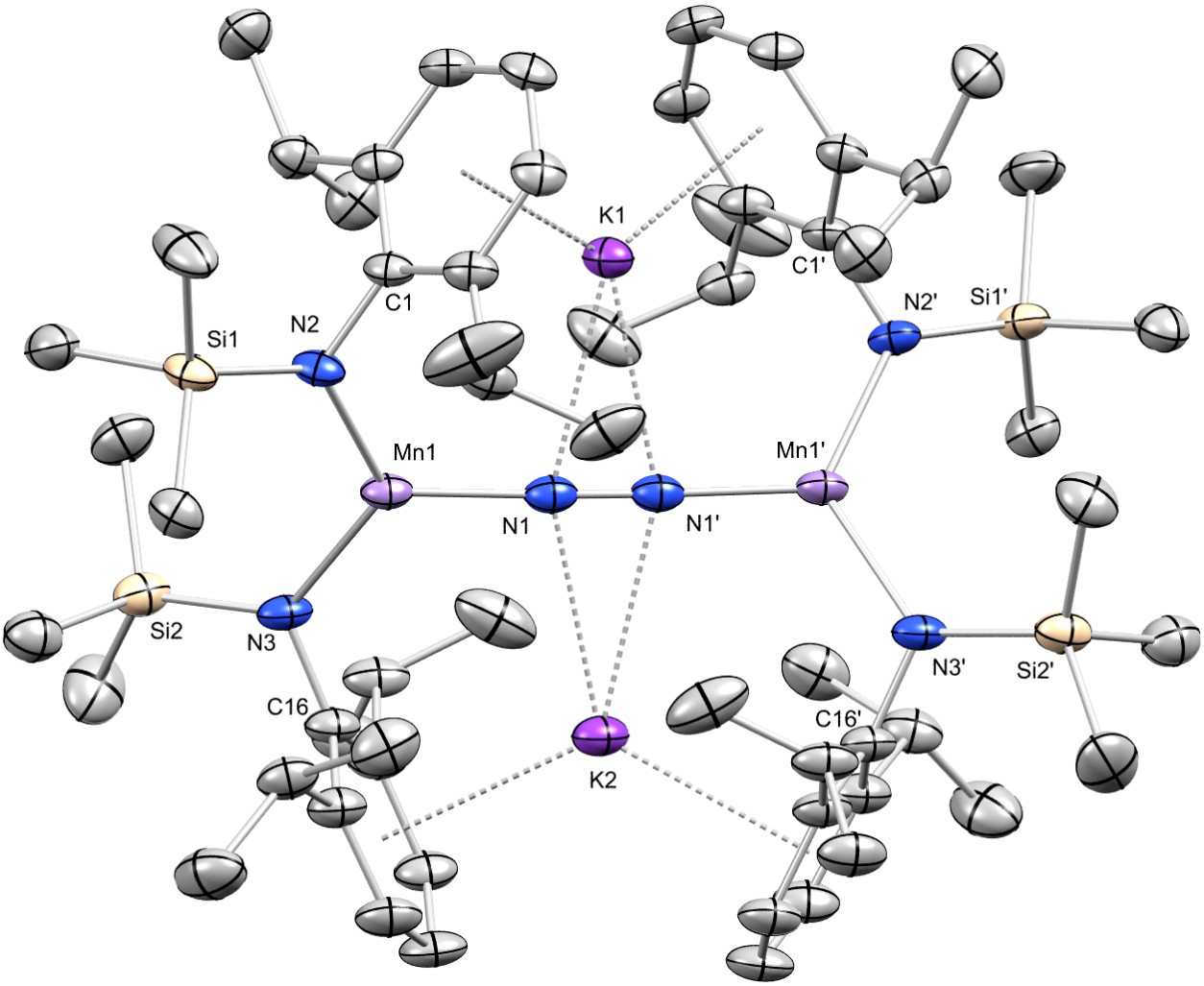

Notes: Thermal ellipsoids are shown at 50% probability. Hydrogen atoms and disordered solvent (pentane) have been omitted for clarity. Selected bond distances [Å], angles [°], and torsions [°]: N1–N1': 1.240(5), Mn1–N1: 1.903(2), Mn1–N2: 2.070(2), Mn1–N3: 2.063(2), N2–C1: 1.421(3), N3–C16: 1.418(3), N2–Si1: 1.734(2), N3–Si2: 1.719(2); N2–Mn1–N3: 123.03(9); C1–N2---N3–C16: ±80.4(3).

Table SX8. Crystal data and structure refinement for complex **3.10**

Empirical formula	C65 H116 K2 Mn2 N6 Si4	
Formula weight	1282.07	
Temperature	100(2) K	
Wavelength	0.71073 Å	
Crystal system	Monoclinic	
Space group	C 2/c	
Unit cell dimensions	a = 15.1643(4) Å	α= 90°.
	b = 21.1646(6) Å	β= 103.9990(10)°.
	c = 23.4439(8) Å	γ = 90°.
Volume	7300.8(4) $Å^3$	
Z	4	
Density (calculated)	1.166 Mg/m^3	
Absorption coefficient	0.565 mm^{-1}	
F(000)	2768	
Crystal size	0.100 x 0.080 x 0.040 mm^3	
Theta range for data collection	1.686 to 27.484°.	
Index ranges	-19<=h<=18, -27<=k<=25, -30<=l<=30	
Reflections collected	31451	
Independent reflections	8375 [R(int) = 0.0486]	
Completeness to theta = 27.484°	100.0 %	
Absorption correction	Semi-empirical from equivalents	
Max. and min. transmission	0.8495 and 0.6805	
Refinement method	Full-matrix least-squares on F^2	
Data / restraints / parameters	8375 / 0 / 414	
Goodness-of-fit on F^2	1.073	
Final R indices [I>2sigma(I)]	R1 = 0.0547, wR2 = 0.1489	
R indices (all data)	R1 = 0.0743, wR2 = 0.1669	
Extinction coefficient	n/a	
Largest diff. peak and hole	2.271 and -0.698 e/$Å^3$	

REFERENCES FOR EXPERIMENTAL DETAILS AND SINGLE-CRYSTAL X-RAY DIFFRACTION CRYSTAL STRUCTURE DETAILS

(1) Cai, I. C., Lipschutz, M. I., Tilley, T. D. *Chem. Commun.* **2014**, *50* (86), 13062–13065.
(2) Werncke, C. G., Suturina, E., Bunting, P. C., Vendier, L., Long, J. R., Atanasov, M., Neese, F., Sabo-Etienne, S., Bontemps, S. *Chem. – Eur. J.* **2016**, *22* (5), 1668–1674.
(3) Bergbreiter, D. E., Killough, J. M. *J. Am. Chem. Soc.* **1978**, *100* (7), 2126–2134.
(4) Junker, M. L., Gilkerson, W. R. *J. Am. Chem. Soc.* **1975**, *97* (3), 493–500.
(5) Pearson, A. J., Yamamoto, Y. In *Encyclopedia of Reagents for Organic Synthesis*, American Cancer Society, 2010.
(6) Fulmer, G. R., Miller, A. J. M., Sherden, N. H., Gottlieb, H. E., Nudelman, A., Stoltz, B. M., Bercaw, J. E., Goldberg, K. I. *Organometallics* **2010**, *29* (9), 2176–2179.
(7) Evans, D. F. *J. Chem. Soc. Resumed* **1959**, No. 0, 2003–2005.
(8) Sur, S. K. *J. Magn. Reson. 1969* **1989**, *82* (1), 169–173.
(9) Grant, D. H. *J. Chem. Educ.* **1995**, *72* (1), 39–40.
(10) Dolomanov, O. V., Bourhis, L. J., Gildea, R. J., Howard, J. a. K., Puschmann, H. *J. Appl. Crystallogr.* **2009**, *42* (2), 339–341.
(11) Sheldrick, G. M. *Acta Crystallogr. Sect. Found. Adv.* **2015**, *71* (1), 3–8.
(12) Sheldrick, G. M. *Acta Crystallogr. Sect. C Struct. Chem.* **2015**, *71* (1), 3–8.

Chapter 4: Divalent Vanadium Complexes Supported by Bulky Silyl(aryl)amido Ligands: Linkage Isomerism and Reactivity of a Two-Coordinate Species

INTRODUCTION

Two-coordinate transition metal complexes can provide insights into fundamental reaction steps for exposed metal centers possessing open coordination sites. Low-coordinate iron, cobalt, and nickel complexes have been studied not only for stoichiometric reactivity[1–8] but also as catalysts for reactions that include C–C bond formation, alkyne trimerization, nitrogen reduction, and hydrosilation.[4,9–12] In contrast, very little is known about the reactivity of two-coordinate complexes containing earlier first-row transition metals. Recently, a few studies demonstrated the reactivity of dinuclear and mononuclear two-coordinate chromium complexes.[1,13,14] For two-coordinate vanadium species, only a single reaction is reported, in which exposure to oxygen produces a lithiated dioxovanadium(V) species.[15] Despite the relevance of low-valent vanadium species in olefin polymerization[16–18] and several studies indicating the range of reactivity afforded by three-coordinate platforms of vanadium,[19–21] the reactivity of two-coordinate and inherently low-valent vanadium complexes remains to be developed.

Investigations of the reactivity of two-coordinate complexes of early metals such as chromium and vanadium are primarily inhibited by the significant challenge in synthesizing such molecules. Although just over 100 mononuclear, two-coordinate, open-shell (d^1-d^9) first-row transition metal species have been structurally characterized,[22,23] only two contain vanadium (Chart 4.1) and to date, no two-coordinate complexes of titanium or scandium have been reported. Generally, open-shell, two-coordinate complexes require stabilization by sterically demanding yet metallation-resistant ligands. The terphenyl amido ligands used to support formally two-coordinate complexes of vanadium, $-NHAr^{Mes2}$ (Ar^{Mes2} = C_6H_3-2,6-(C_6H_2-2,4,6-Me_3)$_2$) and $-NHAr^{Trip2}$ (Ar^{Trip2} = C_6H_3-2,6-(C_6H_2-2,4,6-^{i}Pr$_3$)$_2$) (Chart 4.1), nonetheless result in close metal-aryl interactions in the solid state structure for $V[NHAr^{Mes2}]_2$, and to some extent in $V[NHAr^{Trip2}]_2$.[15] Use of the bulkier terphenyl amido $-NHAr^{Trip2}$ ligand to access low-coordinate species of titanium gave pseudo-low-coordinate complexes with even stronger secondary aryl interactions.[24]

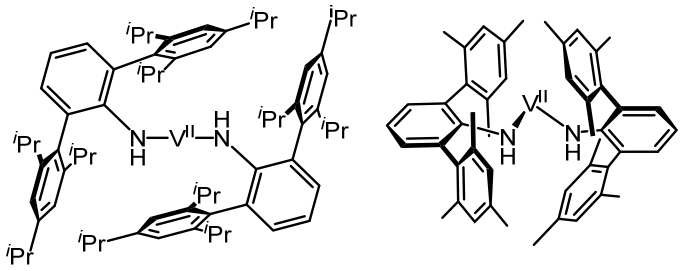

Chart 4.1. Previously reported two-coordinate vanadium complexes.[15]

The –N(SiMe$_3$)DIPP (DIPP = 2,6-diisopropylphenyl) ligand is similarly ubiquitous in two-coordinate chemistry,[4–6,25–27] but a reported attempt to add this ligand directly to $CrCl_2(THF)_2$ produced a tetrameric species derived from C–H activation of the ligand's methyl groups.[26] This result suggests that the Cr(II) center in a putative bis(amido) intermediate may be highly reactive in bond-cleavage reactions. To address the challenge observed with this particular ligand motif, we have employed the more sterically demanding analog –N(Si^{i}Pr$_3$)DIPP to synthesize the two-coordinate chromium complex Cr[N(Si^{i}Pr$_3$)DIPP]$_2$, which supports two-coordination for Cr(I), Cr(II), and Cr(III).[14] On the basis of these results, as described here, attempts were made to synthesize and study comparable two-coordinate V(II) complexes.

DIVALENT VANADIUM COMPLEXES

The complex V[N(Si^{i}Pr$_3$)DIPP]$_2$ (**4.1**) was synthesized by addition of 4 equiv of K[N(Si^{i}Pr$_3$)DIPP] to the vanadium(II) salt $[V_2Cl_3(THF)_6]I$[28] in diethyl ether at ambient temperature (Scheme 4.1). Workup of the purple reaction mixture and crystallization from pentane afforded green blocks of complex **4.1** in 67% overall yield.

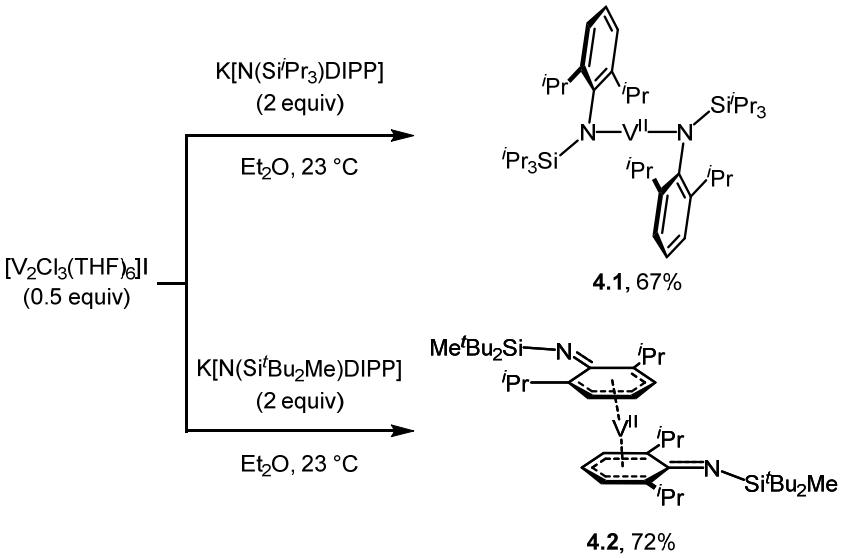

Scheme 4.1. Synthesis of V(II) Complexes

With the vanadium atom sitting on an inversion center, the X-ray structure of **4.1** reveals crystallographically imposed linearity and a V–N bond length of 1.9824(5) Å (Figure 4.1), comparable to the 1.9916(12) Å V–N distance reported for the linear bis(amido) complex V[NHAr^{Trip2}]$_2$ and slightly longer than the V–N distances observed for V[NHAr^{Mes2}]$_2$ (1.976(2) Å, 1.936(2) Å).[15] Complex **4.1** is nearly identical in structure to its neutral chromium analog, Cr[N(Si^{i}Pr$_3$)DIPP]$_2$,[14] crystallizing in the same unit cell with similar bond distances and angles (*cf.* Cr–N: 2.0036(1) Å, N–Cr–N: 180.00(8)°).

Like its chromium(II) analog, **4.1** also features a close interaction between the *ipso* carbon of the aryl ring and the metal center, with a V–C$_{ipso}$ distance of 2.3024(5) Å and a V–N–C$_{ipso}$ bond angle of 83.59(3)° (*cf.* Cr–C$_{ipso}$: 2.2709(14) Å, Cr–N–C$_{ipso}$: 81.59(8)°), likely symptomatic of the electron-deficient metal center. Although longer than the shortest V–C$_{aryl}$ distance observed in the minor disordered component of the solid-state structure of the bent bis(amido) complex V[NHAr^{Mes2}]$_2$ (1.863(3) Å), the V–C$_{ipso}$ distance observed for **4.1** is shorter than any other V–C distance in the structures of either V[NHAr^{Mes2}]$_2$ or V[NHAr^{Trip2}]$_2$.[15] Previously, attractive dispersion interactions have been invoked as a stabilizing influence for two-coordinate complexes of later metals supported by –N(SiMe$_3$)DIPP, in agreement with close SiMe$_3$–^{i}Pr$_2$C$_6$H$_3$ H···H contacts observed in these species (ranging from 2.36 to 2.43 Å).[26] In complex **4.1**, Si^{i}Pr$_3$–^{i}Pr$_2$C$_6$H$_3$ H···H contacts as short as 2.37(2) Å are observed between the two supporting ligands (Figure S4.1), suggesting that similar interactions may help stabilize this low-coordinate structure.

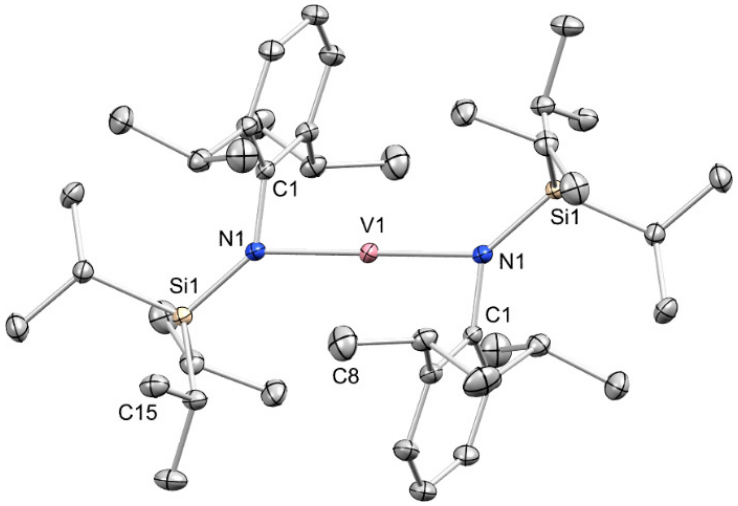

Figure 4.1. Solid-state structure of **4.1** as determined by single-crystal X-ray diffraction. Thermal ellipsoids shown at 50% probability. Hydrogen atoms have been omitted for clarity.

Reaction of 4 equiv of the isomeric ligand K[N(Si^{t}Bu$_2$Me)DIPP] with [V$_2$Cl$_3$(THF)$_6$]I in diethyl ether yielded divalent vanadium complex **4.2** as purple needles crystallized from pentane in 72% yield (Scheme 4.1). In contrast to **4.1** and unlike its neutral chromium analog Cr[N(Si^{t}Bu$_2$Me)DIPP]$_2$ (Figure S4.2, see Experimental Details for synthesis), complex **4.2** in the solid state exhibits a "sandwich" structure in which both silyl(aryl)amido ligands are bound to the vanadium center through the aryl rings (Figure 4.2). Although metallocene complexes are quite common, there are relatively few examples of arylamido ligands binding through the arene.[29–31]

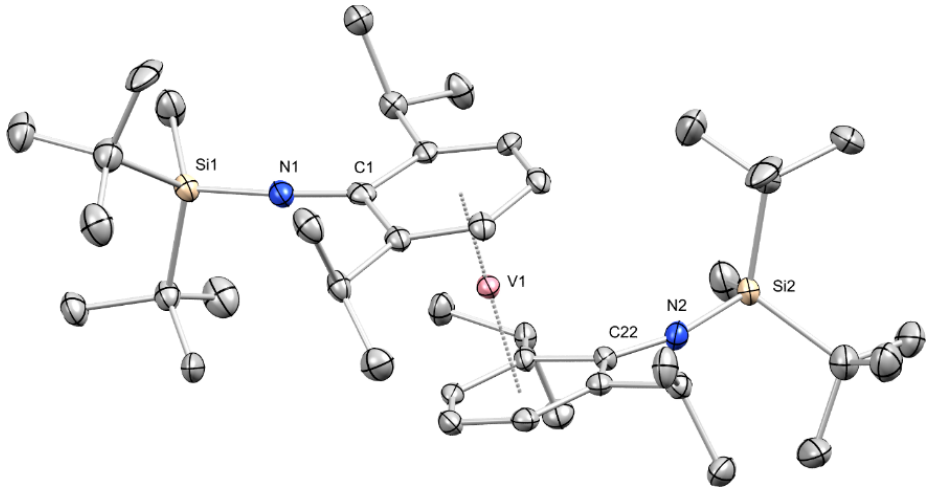

Figure 4.2. Solid-state structure of **4.2** as determined by single-crystal X-ray diffraction. Thermal ellipsoids are shown at 50% probability. Hydrogen atoms and solvent have been omitted for clarity.

Similar to that of vanadocene, the average distance between the vanadium center and the least-squares plane defined by the five coplanar carbons within each arene ring in complex **4.2** is 1.846 Å (versus 1.92 Å for VCp_2).[32] A more nuanced description of the sandwich binding mode observed in complex **4.2** parallels that of the hydrozonyl ligand (η^6-C_6H_5)NN=CHC_6H_4-*p*-NMe_2, which coordinates to CpFe in a manner described as intermediate between that of η^5-iminocyclohexadienyl and η^6-arene ligands.[33]

For well-defined η^5-cyclohexadienyl ligands, the *ipso* carbon is distinctly bent out of the plane defined by the remaining carbons within the ring; in bis(6,6-dimethylcyclohexadienyl)vanadium, the corresponding fold angles are 37° and 38°.[34] In RuH[(η^5-C_6H_5)NPh](PPh_3)$_2$, one of the few structurally characterized complexes containing an arylamido ligand that is not nitrogen-bound, the η^5-iminocyclohexadienyl ring has a fold angle of 24°.[31]

As expected for an η^5-iminocyclohexadienyl ligand, the coordinated arene rings in **4.2** are not planar, with C1 and C22 displaced out of their respective planes, resulting in fold angles of 8° and 10°. However, these values are less than that of the aforementioned hydrozonyl ligand (C_6H_5)NN=CHC_6H_4-*p*-NMe_2 (12.5°),[33] and only slightly more than that of the DIPP moiety in complex **4.1** (2.3°). Furthermore, the V1–C1 and V1–C22 distances (2.556(6) Å and 2.543(5) Å) for **4.2** suggest some interaction with the metal center.

The N–C_{ipso} bond lengths of 1.291(7) Å and 1.298(7) Å in **4.2** indicate partial imine character and are much shorter than the N–C_{ipso} distance observed for **4.1** (1.4132(7) Å). Although the Si1–N1–C1 and Si2–N2–C22 bond angles in **4.2** (164.0(5)°, 162.3(4)°) deviate from the standard 120° bond angle expected for an imine, they are similar to the nearly linear Si–N–C bond angle of 169.5(5) Å observed for the silyl-substituted imine (Me^tBu_2Si)N=(2,6-^{i}Pr_2-C_6H_2)(2,6-*i*Pr_2-C_6H_2)=N(Si ^{t}Bu_2Me).[35]

Given that the compositions of **4.1** and **4.2** are identical, the difference in –SiR_3 groups appears to have a substantial impact on ligand binding to the metal center. In order to better understand the differences in binding in the solid state, calculations were performed on the observed geometries of complexes **4.1** (linear) and **4.2** (sandwich), in addition to their hypothetical constitutional isomers **4.1'** (sandwich) and **4.2'** (linear), using the ωB97X-D functional and the def2-SVP basis set for all atoms. For complex **4.1**, the linear geometry is calculated to be favored

by 19 kcal/mol over the sandwich geometry **4.1'**. For complex **4.2**, the linear geometry **4.2'** is still favored over the sandwich geometry, but only by 9 kcal/mol. These calculations were performed for gas-phase molecules at 0 K; qualitatively, the smaller difference in energy between **4.2** and **4.2'** versus that of **4.1** and **4.1'** is consistent with the different solid state geometries observed for complexes **4.1** and **4.2**.

ELECTRONIC PROPERTIES AND ISOMERISM

Linear coordination environments can give rise to considerable magnetic anisotropy, as electrons may reside in degenerate orbital pairs and exhibit unquenched orbital angular momentum. In a simplified $D_{\infty h}$ crystal-field, linear two-coordinate d^3 transition metal complexes are predicted to have effective magnetic moments (μ_{eff}) as low as 0.77 μ_B.[36–38] However, by the Evans method,[39–41] complexes **4.1** and **4.2** both have μ_{eff} values of 3.7 μ_B, which is higher than that of $V[NHAr^{Trip2}]_2$ (μ_{eff} = 3.41 μ_B)[15] and close to the expected value for an S = 3/2 system with quenched orbital angular momentum (μ_{eff} = 3.87 μ_B). Similarly, SQUID magnetometry gives room temperature values of 3.92 and 3.91 μ_B for **4.1** and **4.2**, respectively. These magnetic moments are temperature invariant (Figure 4.3), which also indicate that **4.1** and **4.2** are magnetically isotropic.

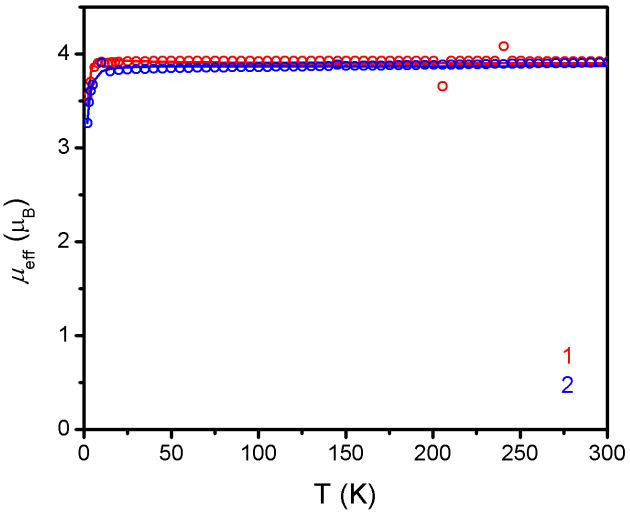

Figure 4.3. Effective magnetic moment (μ_{eff}) versus temperature for **4.1** (red circles) and **4.2** (blue circles) collected under a 1 T dc magnetic field. The red line is a fit of the magnetic data of **4.1** while the blue line is simulated using parameters taken from fits of the EPR data of **4.2**.

Figure 4.4 shows plausible d-orbital splitting diagrams for **4.1** and **4.2**. Configuration **1A** is the expected splitting for a $D_{\infty h}$ geometry with σ-donor ligands. However, previous calculations on a similar complex, $Fe[N(SiMe_3)DIPP]_2$, have shown that the lone-pairs of the nitrogen donor atoms strongly influence d-orbital splitting, breaking the degeneracy of the (d_{xz}, d_{yz}) pair (Figure 4.4, **1B**).[42,43] Given the lack of magnetic anisotropy in **4.1**, it is likely that its d-orbital splitting is similar to that of configuration **1B**. Complex **4.2** likely has a d-orbital splitting which can be approximated as a dicationic bis(benzene) complex (Figure 4.4, configuration **2**), and no magnetic anisotropy is expected.

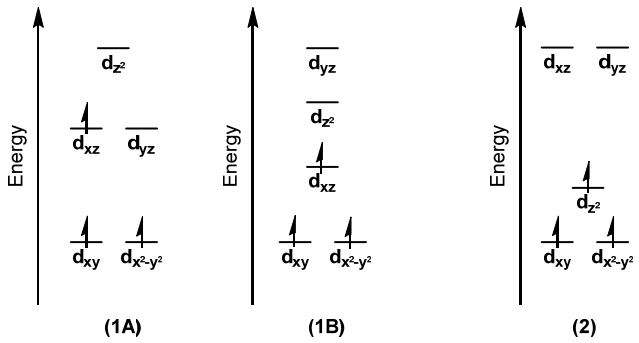

Figure 4.4. Proposed d-orbital splitting diagrams and resulting electronic configurations for **4.1** and **4.2**. **(1A)** d-orbital splitting for a $D_{\infty h}$ geometry with σ-donor ligands. **(1B)** d-orbital splitting for **4.1** assuming d-orbital energies similar to those calculated for Fe[N(SiMe$_3$)DIPP]$_2$.[42,43] **(2)** d-orbital splitting for a dicationic bis(benzene) complex in a D_{6d} geometry.

Despite the fact that both **4.1** and **4.2** are magnetically isotropic, ac magnetic susceptibility measurements under a small dc field reveal peaks in out-of-phase magnetic susceptibility (Figure S4.3-S4.4), indicating that both complexes exhibit slow magnetic relaxation at 2 K. The peaks are temperature dependent but move out of the range of the instrument at 3 K, precluding additional analysis of the origin of this slow magnetic relaxation.

Continuous-wave X-band electron paramagnetic resonance (EPR) spectroscopy allowed for an additional method to explore the electronic structures of complexes **4.1** and **4.2**. The spectrum of finely ground crystalline **4.2** at 10 K reveals two broad features centered around g ≈ 189 and 342 mT with a shoulder feature 120 mT, but no observable hyperfine coupling (Figure S4.5). Dissolving **2** in pentane and freezing the solution provided a significantly more detailed spectrum (Figure 4.5), where hyperfine coupling to the vanadium center is observed. The spectrum suggests a nearly axial geometry, and in particular, is similar to that of vanadocene.[44–47]

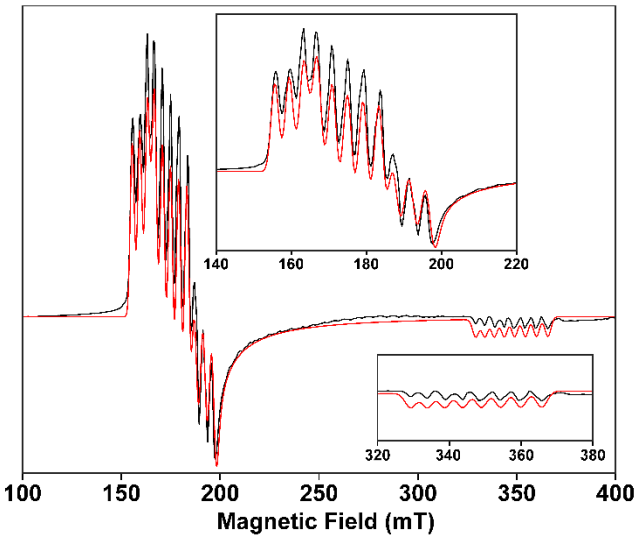

Figure 4.5. Experimental (black trace) and simulated (red trace) *cw* EPR spectrum of **4.2** in pentane, recorded at 9.72 GHz and 10 K. The numerical simulation was obtained with g values of $g_1 = 1.986$, $g_2 = 1.972$, $g_3 = 2.000$, principal hyperfine components of $A_1^V = 42.3$, $A_2^V = 39.7$, $A_3^V = 52.6 \times 10^{-4}$ T, and zero-field splitting parameters of D = 2.6589 and E = 0.0691 cm^{-1}.

A spectral simulation of an S = 3/2 electronic spin with a single vanadium center (nuclear spin I = 7/2, 99.75%) provided a good fit of the experimental spectrum (Figure 5). The calculated g values, principle hyperfine components, and ratio of zero-field splitting parameters ratio (E/D is low) are consistent with a near-axial symmetry for **4.2**, which would be expected given its solid-state structure.

In contrast, the frozen glass and solid-state spectra of **4.1** differ markedly from those of **4.2** (Figures 4.6 and S4.6-S4.8). They are significantly more complex, and exhibit considerable time dependence, suggesting the formation of one or more additional species over time (Figure 4.6). Dissolving **4.1** in pentane at ambient temperature (21 °C), and quickly (<1 min) freezing the sample afforded an EPR spectrum with complex features centered around 176 mT and 345 mT. After thawing the solution, allowing it to stand at 21 °C for 1 h, and then freezing it again, a second spectrum was obtained. The second spectrum reveals that the intensity of the feature at 345 mT had decreased slightly while a feature centered around 482 mT grew in. Meanwhile the feature around 176 mT becomes more complex, with the appearance of additional hyperfine detail. These changes strongly suggest that one or more new species appear upon dissolution of **4.1** in pentane at room temperature.

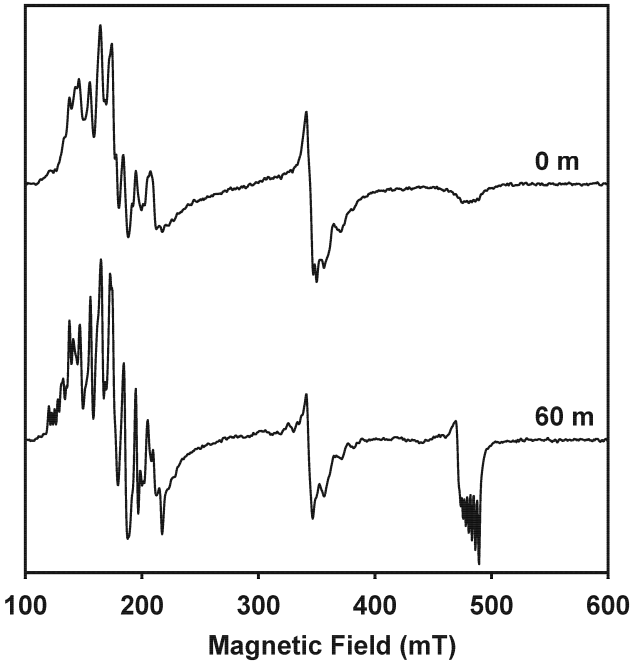

Figure 4.6. Experimental *cw* EPR spectrum of **4.1** in frozen pentane solution upon dissolution (top trace) and after standing at 21 °C for 1 h (bottom trace), recorded at 9.63 GHz and 22 K.

To further investigate this complex behavior in solution, NMR spectroscopy was employed. The ^{1}H NMR spectrum of **4.1** in benzene-d_6 revealed a primary set of broad resonances that can be attributed to the predominant species of **4.1** in solution, as well as secondary features at 3.95 ppm and −7.74 ppm, which noticeably increase in intensity within 30 minutes as a solution of **4.1** is allowed to stand at room temperature (Figure S4.9). Consistent with EPR spectroscopy, these additional NMR shifts appear to indicate the slow transformation to at least one additional complex in solution.

These observations of the magnetic data for complex **4.1** are consistent with changes in the UV-visible spectrum. Upon dissolution of recrystallized complex **4.1**, in a range of non-coordinating or weakly coordinating solvents (pentane, toluene, 1,2-difluorobenzene, diethyl ether), a notable color change of the solution from orange to purple is observed. Initially, the UV-vis spectrum of complex **1** in pentane at 30 °C reveals a single λ_{max} in the visible region at 496 nm (ε ca. 500 M^{-1} cm^{-1} as a function of molar concentration of total **4.1** in solution) and a much weaker feature corresponding to d-d transitions at λ_{max} = 910 nm (ε ca. 70 M^{-1} cm^{-1}). Over the course of 40 minutes, the absorption at λ_{max} = 910 nm decreases and a new feature at 564 nm increases in intensity until the solution reaches equilibrium (ε ca. 800 M^{-1} cm^{-1} after 40 minutes, as a function of total **4.1** in solution, see Figure S4.10).

The absorption that grows in intensity at λ_{max} = 564 nm after dissolution of **4.1** is similar in value to λ_{max} = 577 nm (ε = 6300 M^{-1} cm^{-1}) observed for complex **4.2** under the same conditions (pentane, 30 °C). Given that **4.1** and **4.2** are linkage isomers, their respective transitions at λ_{max} = 564 nm and λ_{max} = 577 nm in UV-Vis solution spectroscopy suggest that complex **4.1** in solution may isomerize to a sandwich species analogous to that of **4.2** (**4.1'**, *vida supra*). In contrast to **4.1**, complex **4.2** remains purple in solution and does not reveal any new features by UV-Vis spectroscopy over the course of an hour following dissolution.

By solid-state IR spectroscopy (KBr pellet), complexes **4.1** and **4.2** have significantly different features (Figure S4.11). The IR spectrum of **4.2** reveals a strong broad peak from 1550 to 1590 cm^{-1}, which can be assigned to the expected ν(C−N) stretch. Although this stretch is absent in the solid-state IR spectrum of **4.1**, it is present in the solution-state spectra of **4.1** in benzene-d_6, consistent with UV-Vis spectroscopy suggesting that **4.1** may isomerize to the sandwich geometry **4.1'** in solution.

Taken together, these various spectroscopic data strongly indicate that **4.1** isomerizes in solution (Scheme 2). Although species **4.1'** is presented as a possible isomer of **4.1**, a mono(amido) half-sandwich isomer would also contain a diagnostic ν(C−N) which would be indistinguishable from **4.1'.** Given that these possible sandwich species have similar spectroscopic handles, the paramagnetism of this system precludes a more detailed assignment of the species present in solution by the aforementioned spectroscopic methods.

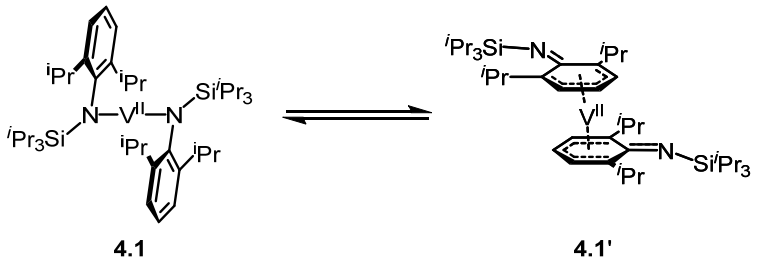

4.1 **4.1'**

Scheme 4.2. Proposed isomerization of complex 1 in solution

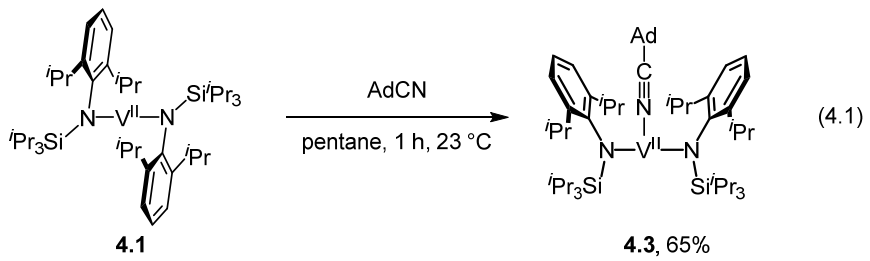

(4.1)

To further probe linkage isomerism in **1** and **2**, the addition of a donor ligand (1-cyanoadamantane, AdCN) was examined. Addition of 1-cyanoadamantane to **4.1** followed by crystallization from pentane resulted in the T-shaped complex (AdCN)V[N(Si^{i}Pr$_3$)DIPP]$_2$ (**4.3**), as dichroic purple-green blocks in 65% yield (eq 4.1). In contrast to **4.1**, complex **4.3** does not have significant V–C$_{ipso}$ interactions and has slightly longer V–N bond lengths of 2.0271(15) and 2.0217(15) Å, as expected for the higher coordination number (Figure 4.7). The solution magnetic moment of **4.3** is 3.8 μ_B (Evans method), consistent with a high-spin d^3 configuration.

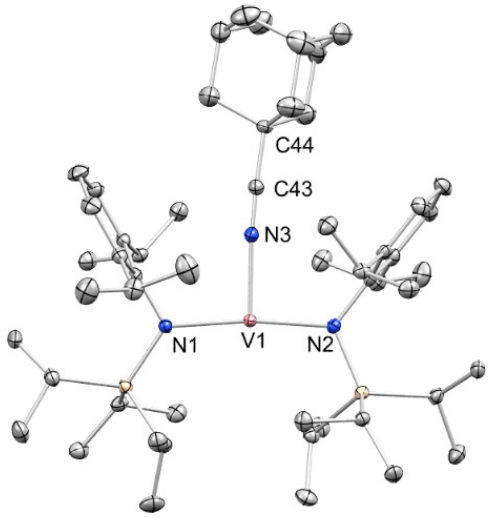

Figure 4.7. Solid-state structure of **4.3** as determined by single-crystal X-ray diffraction. Thermal ellipsoids are shown at 50% probability. Hydrogen atoms have been omitted for clarity.

By ^{1}H NMR spectroscopy, addition of 1-cyanoadamantane to an equilibrated solution of **4.1** in benzene-d_6 at ambient temperature results in fast consumption (< 5 min) giving rise to the formation of **4.3** and simultaneous disappearance of the primary resonances observed for **4.1** (Figure S4.12). However, in addition to a small amount of unconsumed 1-cyanoadamantane, the broadened features at 3.95 ppm and −7.74 ppm attributed to a second isomer of **4.1** (*vida supra*) do not immediately disappear upon the addition of 1-cyanoadamantane. Over the course of 85 minutes, these features slowly disappear, and no peaks attributed to **4.1** reappear during this time. These results suggest that the secondary species observed for **4.1** (presumably **4.1'**) in solution does not readily react with 1-cyanoadamantane, and likely isomerizes to the linear bis(amido) species before coordinating to 1-cyanoadamantane to form **4.3**.

In contrast, addition of 1-cyanoadamantane to complex **4.2** in benzene-d_6 did not result in the consumption of either reactant over the course of 22 h at ambient temperature. Upon heating the reaction mixture to 50 °C for 24 h, 1-cyanoadamantane remained unconsumed (< 1%

conversion) and only minor formation of free amine was observed (~1% conversion of **4.2**). Further heating of the reaction mixture at 70 °C for 24 h resulted in partial consumption of 1-cyanoadamantane (~40%) and an increase in free amine (~10% conversion from **4.2**), but no other additional diamagnetic or paramagnetic products were observed by NMR spectroscopy. Although 1-cyanoadamantane is consumed at higher temperatures, this conversion appears to correspond with the formation of HN(Si^{t}Bu$_2$Me)DIPP from the decomposition of complex **4.2**, rather than formation of a nitrile complex as observed for complex **1**.

REDUCED VANADIUM AMIDO COMPLEXES

Given the ability of –N(SiMe$_3$)DIPP and –N(Si^{i}Pr$_3$)DIPP ligands to stabilize two-coordinate transition metal complexes in multiple oxidation states,[5,14,25–27] we sought to reduce complexes **1** and **2**. Addition of 1.1 equiv of KC_8 to complex **1** in diethyl ether resulted in a magenta solution, and crystallization from a solution of diethyl ether layered with pentane afforded a vanadium(I) compound that was isolated in 30% yield (Scheme 4.3). Surprisingly, X-ray crystallography revealed the product to be a coordination polymer composed of a vanadium sandwich complex, K{V[(η^5-DIPP)N(Si^{i}Pr$_3$)]$_2$} (**4.4**, Figure 4.8), in which the ligands are no longer amido-bound and instead bind in an η^5-iminocyclohexadienyl mode. This change in coordination differs drastically from the reactivity observed for all other first-row transition metal complexes supported by –N(SiR$_3$)DIPP (R = Me or ^{i}Pr), which upon reduction retain their linear bis(amido) geometry.[5,6,14] The average distance between vanadium center and the plane defined by the five coplanar carbons within each DIPP is 1.75 Å, while the average V–C$_{ipso}$ distance is 2.497(4) Å. In addition, a strong IR band corresponding to the ν(C–N) stretch can be observed at 1509 cm^{-1}.

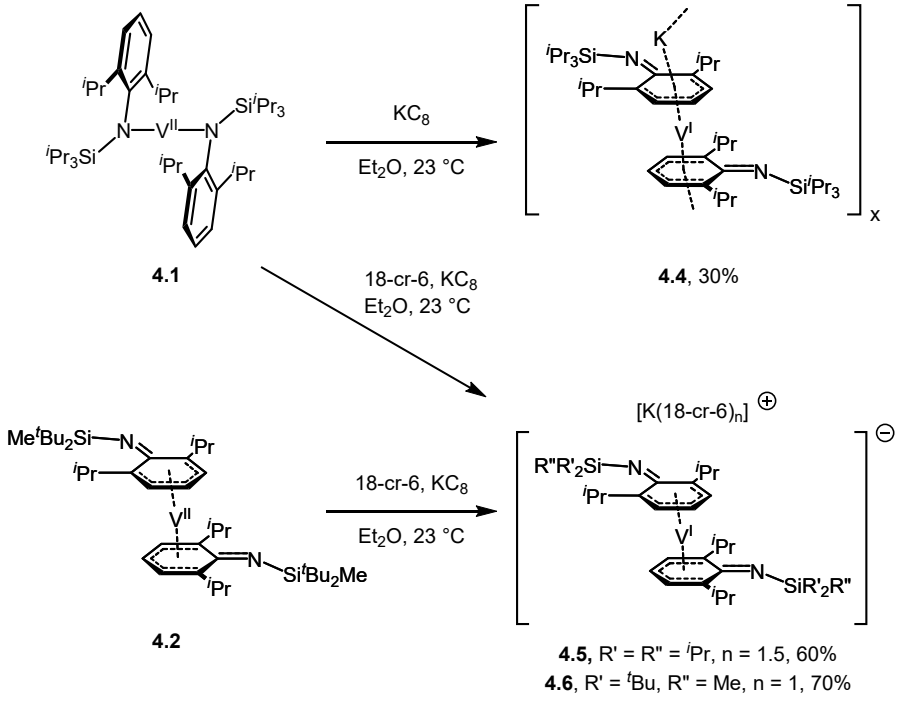

Scheme 4.3. Reductions of 4.1 and 4.2

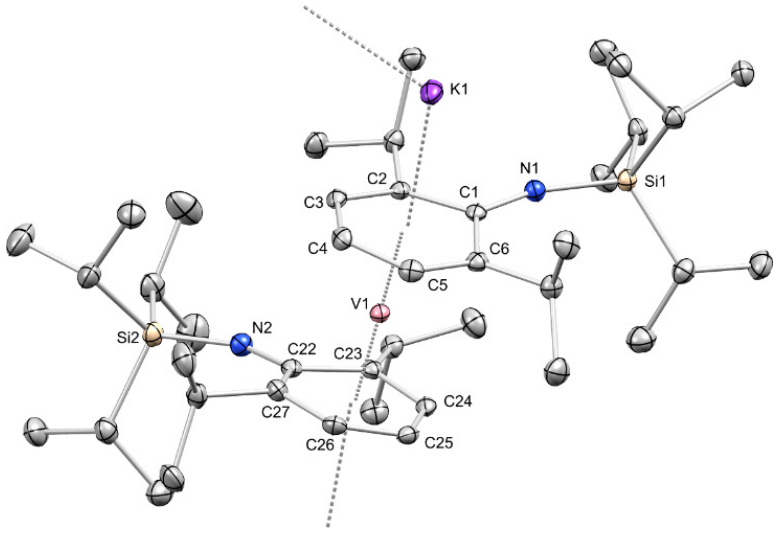

Figure 4.8. Solid-state structure of the anion in **4.4** as determined by single-crystal X-ray diffraction. The second crystallographically independent molecule of **4.4** has been omitted. Thermal ellipsoids are shown at 50% probability. Hydrogen atoms and solvent have also been omitted for clarity.

To determine whether the sandwich structure resulted from interactions with the potassium cation and the resulting polymeric coordination, **1** was also reduced with KC_8 in the presence of 1.5 equiv of 18-crown-6 (18-cr-6). Crystallization from a solution of diethyl ether layered with pentane provided magenta needles of $\{K(18\text{-cr-}6)_{1.5}\}\{V[(\eta^5\text{-DIPP})N(Si^iPr_3)]_2\}$ (**4.5**) in 73% yield (Scheme 4.3). X-ray crystallography confirms that the solid-state structure of **4.5** is also a sandwich complex, (Figure S4.13), indicating that a coordinated potassium cation is not essential to enforce the change to a bis(pentadienyl) geometry upon reduction. Complexes **4.4** and **4.5** exhibit magnetic moments of 2.7 and 2.8 μ_B (Evans method), respectively, corresponding to intermediate-spin d^4 complexes (S = 1), as expected for a V(I) metallocene complex.

Reduction of complex **4.2** by 1.1 equiv of KC_8 in the presence of 18-crown-6 afforded an anionic sandwich analogue $\{K(18\text{-cr-}6)\}\{V[(\eta^5\text{-DIPP})N(Si^tBu_2Me)]_2\}$ (**4.6**), which was isolated as red needles from diethyl ether layered with pentane (70% yield, Scheme 4.3). Layering pentane over a THF solution of **4.6** afforded crystals suitable for X-ray crystallography, which revealed bond distances and angles similar to those of **4.2**, **4.4**, and **4.5**. In the crystal structure of **4.6** (Figure 4.9), the vanadium center sits on an inversion center, and the distance from the vanadium center to the plane defined by the five coplanar DIPP carbon atoms is 1.77 Å while the V1–C1 distance is 2.4727(9) Å. Both of these distances, comparable to that of **4.4**, are shorter than those observed in the neutral complex **4.2**; this contraction is consistent with the population of bonding orbitals with d-character by an additional electron. This effect also manifests in the N–C_{ipso} stretch energies; complex **4.6** has a strong IR band at 1506 cm^{-1}, which is considerably lower in energy than the corresponding band observed for **4.2** (1550–1590 cm^{-1}).

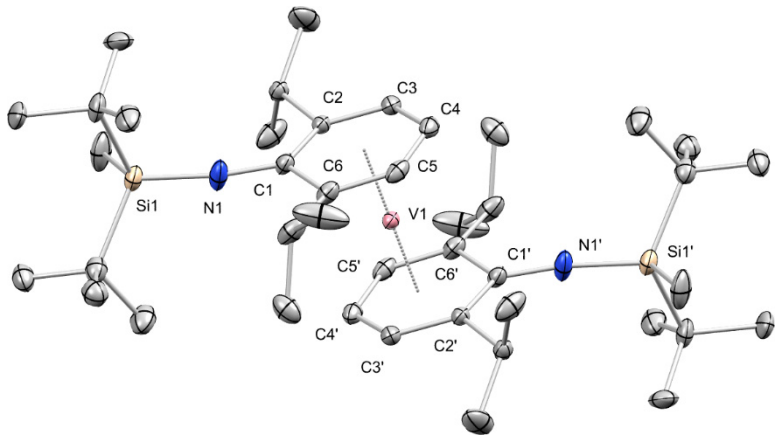

Figure 4.9. Solid-state structure of the anion in **4.6** as determined by single-crystal X-ray diffraction. Thermal ellipsoids are shown at 50% probability. Hydrogen atoms, disordered di-*tert*-butylmethylsilyl group, and cation have been omitted for clarity.

To further investigate the redox behavior of **1** and **2**, cyclic voltammetry studies were performed (Figure 4.10, see also Figures S4.14-S4.17). The cyclic voltammogram of an equilibrated solution of **1** is complex, containing two reversible reduction events at −1.83 V ($E_{1/2}$ vs. Fc/Fc^+, $i_{pa}/i_{pc} = 1.05$) and −2.33 V ($E_{1/2}$ vs. Fc/Fc^+, $i_{pa}/i_{pc} = 0.97$). Meanwhile, a single reversible couple at −1.83 V ($E_{1/2}$ vs. Fc/Fc^+, $i_{pa}/i_{pc} = 1.04$) is observed for **2**. In addition, voltammograms of both **4.1** and **4.2** reveal irreversible oxidation events. While the first reduction event observed for both **1** and **2**, at approximately −1.8 V (vs Fc/Fc+), can be assigned as a V(II/I) couple, the nature of the second reduction feature in the voltammogram of **1** is less clear. Previous work by Power and co-workers[6] suggests that these amido ligand platforms do not readily support a metal(0) oxidation state, making a V(I/0) assignment unlikely.

To further investigate the electrochemical behavior of **4.1**, cyclic voltammograms of **4.5** were also acquired (Figure 4.10c, see also Figures S4.18-S4.20). Complex **4.5** exhibits a reversible oxidation event at −1.79 V (vs Fc/Fc^+), which can be assigned to oxidation of the anionic $\{V[(\eta^5\text{-DIPP})N(Si^iPr_3)]_2\}^-$ species and aligns with the reversible reduction events observed at approximately −1.8 V for both **4.1** and **4.2**. As was observed for **1**, in the voltammogram of **4.5** a second redox event is observed at −2.31 V. However, this event has a significantly smaller peak current than the feature at observed at −1.79 V, which independently suggests that it does not likely correspond to a V(I/0) couple. The difference in relative peak heights between these redox events observed in the voltammograms of **4.1** and **4.5** instead suggest that the event at −2.3 V corresponds to the V(II/I) couple for the linear isomer of **4.1**, with the difference in relative peak heights dependent on the ratio of isomers ($[\mathbf{4.1}]^{-/0}$ *vs*. $[\mathbf{4.1'}]^{-/0}$, linear *vs.* sandwich geometry) in solution.

Consistent with EPR, NMR, and UV-Vis spectroscopy, cyclic voltammetry of **4.1** exhibits time-dependent behavior (Figure **4.11**). Early scans (< 10 min following dissolution of **4.1**) reveal that the reversible reduction event at −2.3 V is the predominant feature, while a second feature at −1.8 V grows in over time. This is consistent with **4.1** converting over time from its linear isomer to the sandwich isomer **4.1'** in solution. Moreover, these results explain the conversion of **4.1** to a sandwich complex upon reduction; the isomers are in equilibrium in solution and sandwich geometry is more easily reduced.

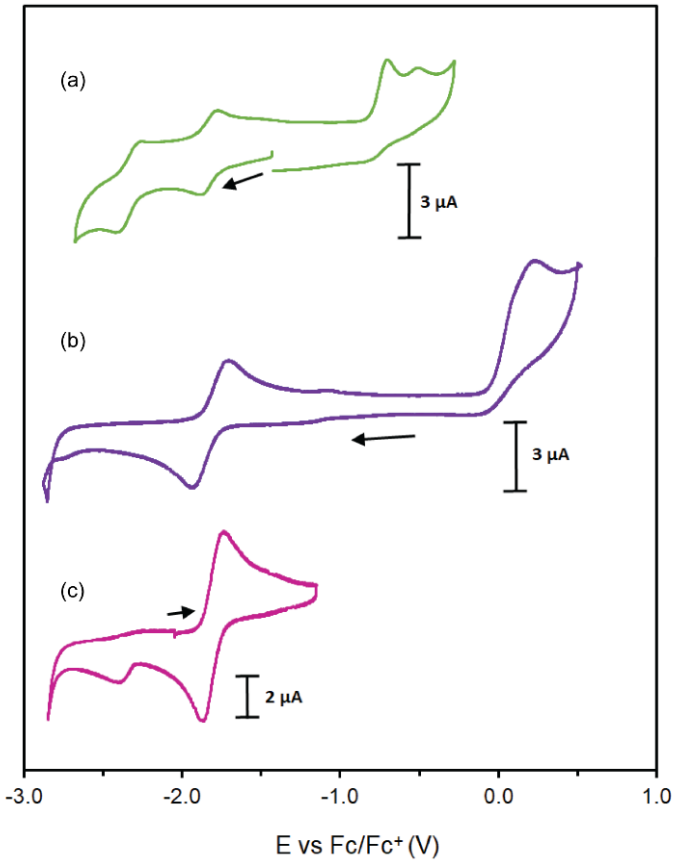

Figure 4.10. Cyclic voltammograms of 1.0 mM solutions of (a) **4.1**, (b) **4.2**, and (c) **4.5** in 1,2-difluorobenzene with 0.1 M [^{n}Bu$_4$N][PF$_6$] supporting electrolyte. The arrows indicate the initial potentials and scanning directions. Scan rate: 100 mV/s.

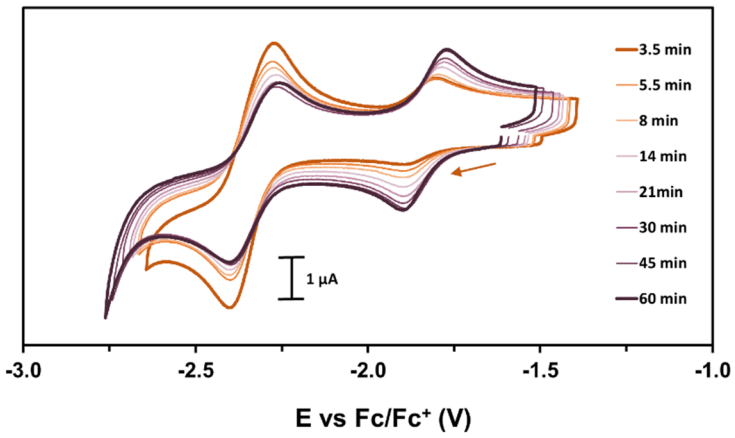

Figure 4.11. Cyclic voltammograms of a 1.0 mM solution of **4.1** in 1,2-difluorobenzene with 0.1 M [^{n}Bu$_4$N][PF$_6$] supporting electrolyte, at various intervals following dissolution. Solution was agitated prior to the collection of each voltammogram. The arrows indicate the initial potentials and scanning directions. Scan rate: 100 mV/s.

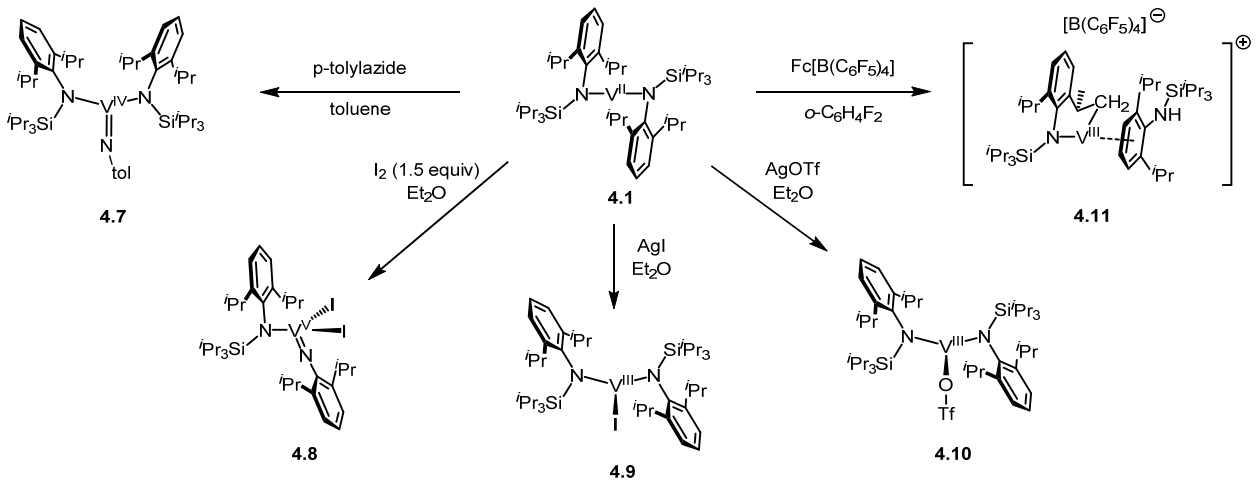

Scheme 4.4. Oxidation chemistry of **4.1**

OXIDATIONS OF VANADIUM AMIDO COMPLEXES

Very few mononuclear three-coordinate vanadium complexes have been structurally characterized and reported in the literature,[19,48,49] likely reflecting the challenges of accessing low-coordinate vanadium species. With a low-coordinate vanadium complex in hand and our knowledge of their one-electron redox chemistry, we sought to explore the reactivity of **4.1** with a range of chemical oxidants. Oxidation of complex **4.1** with 1 equiv of *p*-tolylazide afforded a vanadium(IV) imido complex, (*p*-tolylN)V[N(Si^{i}Pr$_3$)DIPP]$_2$ (**4.7**), isolated in 12% yield[a] as red blocks from pentane (Scheme **4.4**). Complex **4.7** is the first structurally characterized three-coordinate vanadium imido complex;[23] the vanadium-imido bond length (V1–N3: 1.6703(13) Å) is consistent with similar values reported for V(IV) imido complexes.[50–52,20] The V1–N1 and V1–N2 bond lengths in **7** are 1.9175(13) Å and 1.9299(13) Å, respectively, comparable to the V–N distance observed for the cationic three-coordinate tris(amido) vanadium(IV) complex {V[N(SiMe$_3$)$_2$]$_3$}[CN] containing an outer-sphere cyanide anion (1.91(1) Å).[48]

Upon addition of 1 equivalent of I$_2$ to **1**, the imido complex I$_2$V[N(DIPP)][N(Si^{i}Pr$_3$)DIPP] (**4.8**) was initially obtained as green blocks from pentane (19% yield). The highly favorable 1,2 elimination of Me$_3$SiI[53] very likely results in formation of the vanadium-imido bond in **4.8**, the V–N distance of which (1.658(3) Å) is comparable to that of **4.7** (Figure 4.13). Although the ^{1}H NMR spectrum of **4.8** at 370 K in toluene-d_8 is consistent with the solid-state structure, the solution behavior of **4.8** at lower temperatures is complex due to hindered rotation within the molecule (Figure S4.21-S4.22), similar to what is observed for the complex Cl$_2$V[N^{t}Bu][N(^{i}Pr)$_2$].[54] From the aforementioned synthesis, the attempt to obtain a second crop of **8** resulted in isolation of the vanadium(III) iodide complex IV[N(Si^{i}Pr$_3$)DIPP]$_2$ (**4.9**) as orange blocks from pentane.

[a] Complex **4.7**, and all other neutral complexes reported in this paper are highly soluble in unreactive nonpolar solvents, precluding higher yields of the crystallized products.

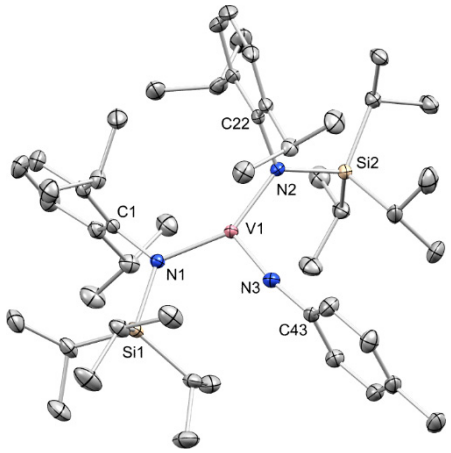

Figure 4.12. Solid-state structure of **4.7** as determined by single-crystal X-ray diffraction. Thermal ellipsoids are shown at 50% probability. Hydrogen atoms have been omitted for clarity.

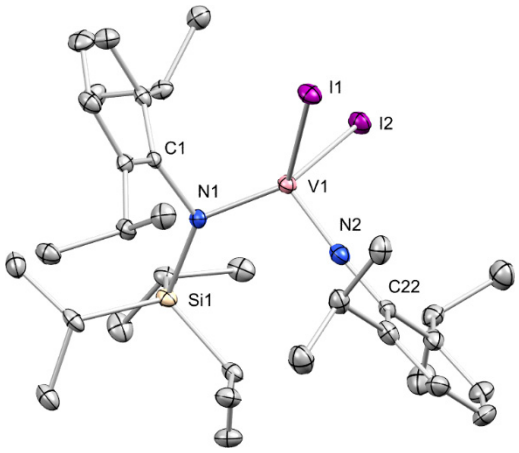

Figure 4.13. Solid-state structure of **4.8** as determined by single-crystal X-ray diffraction. Thermal ellipsoids are shown at 50% probability. Hydrogen atoms have been omitted for clarity.

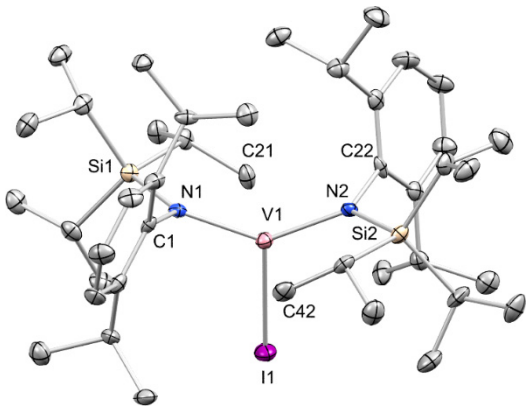

Figure 4.14. Solid-state structure of **4.9** as determined by single-crystal X-ray diffraction. Thermal ellipsoids are shown at 50% probability. Hydrogen atoms have been omitted for clarity.

The yield of complex **8** was increased by addition of more iodine; treatment of **1** with 1.5 equivalents of I_2 affords **8** in 65% yield**.** Meanwhile, complex **4.9** was synthesized without over-oxidation by addition of 1 equiv of silver iodide to **4.1** in diethyl ether, to afford **4.9** in 33% yield (Scheme **4.4**). Similarly, oxidation of complex **4.1** with silver triflate in diethyl ether afforded the vanadium(III) triflate analog (TfO)V[N(Si^{i}Pr$_3$)DIPP]$_2$ (**4.10**) in 36% yield as orange blocks from pentane. The average V–N bond lengths in **4.9** and **4.10** are 1.955(4) Å and 1.9398(8) Å, respectively, and comparable to the V–N distances observed for three-coordinate trivalent vanadium chalcogenolate complexes [(Me$_3$Si)$_2$N]$_2$V(ER) (E = Se, Te; R = Si(SiMe$_3$)$_3$, SiPh$_3$) reported by Gerlach and Arnold (1.92(1) - 1.926(6) Å).[49] Complexes **4.9** and **4.10** are both trivalent (μ_{eff} = 2.6 μ_B and μ_{eff} = 2.7 μ_B, respectively), but they are not strictly three-coordinate; both structures contain close –Si^{i}Pr$_3$ C–H agostic interactions with the metal center (Figures 4.14 and 4.15). In **4.9**, these V···H distances are 2.074 Å and 2.074 Å; similar distances are observed for **4.10** (V···H = 2.098(17) Å, 2.070(17) Å).

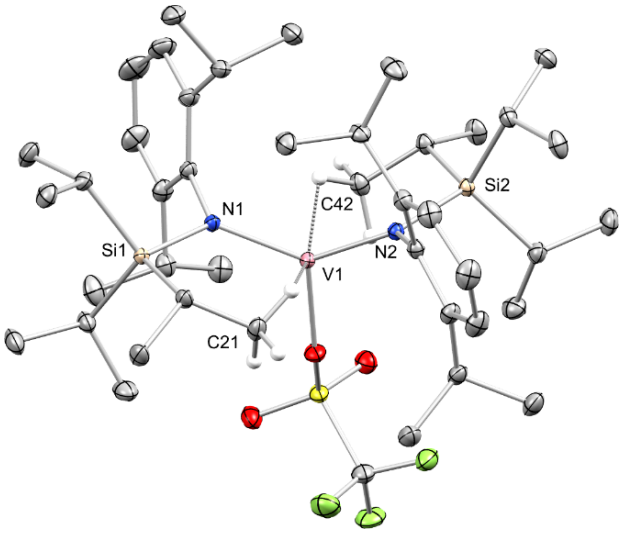

Figure 4.15. X-ray crystal structure of **4.10**. Thermal ellipsoids are shown at 50% probability. Hydrogen atoms have been omitted for clarity, with the exception of hydrogen atoms on C21 and C42, which were located from the electron density difference map. Oxygen atoms shown in red; sulfur atom shown in bright yellow; fluorine atoms shown in green.

C–H ACTIVATION RESULTING FROM OXIDATION OF VANADIUM(II)

In an attempt to characterize the products formed from the irreversible oxidations of the divalent complexes (*vide supra*), **4.1** was treated with Fc[B(C$_6$F$_5$)$_4$] (Fc = ferrocenium) in 1,2-difluorobenzene. Work-up of the reaction mixture and crystallization from 1,2-difluorobenzene and toluene, layered with pentane, afforded complex **4.11** in 29% isolated yield (Scheme 4, Figure 4.16). The formation of **4.11** likely results from cyclometallation and C–H activation of one of the ^{i}Pr groups on the aryl ring and transfer of hydrogen from this activation to the nitrogen atom of the other silyl(aryl)amido ligand. The solid state structure of **4.11** reveals a short V–N bond distance of 1.877(2) Å, and as in complex **4.1** the amido ligand of **4.11** exhibits a close V–C$_{ipso}$ interaction with a distance of 2.314(3) Å.

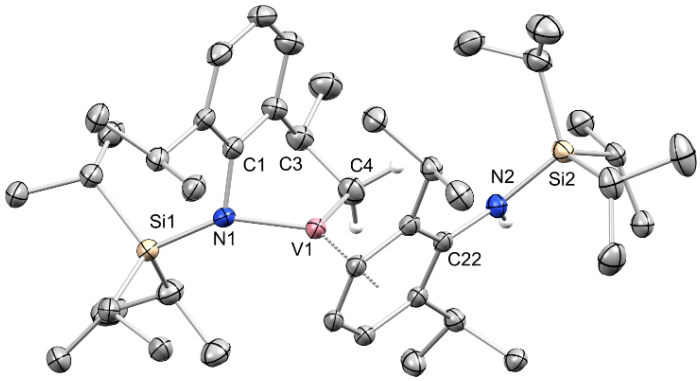

Figure 4.16. Solid-state structure of **4.11** as determined by single-crystal X-ray diffraction. Thermal ellipsoids are shown at 50% probability. Hydrogen atoms, counterion, and solvent have been omitted for clarity, with the exception of hydrogen atoms on C4 and N2, which were located from the electron density difference map.

Solid-state IR spectroscopy of **4.11** reveals a characteristic N–H stretch at 3377 cm^{-1} (KBr pellet), corresponding to the amine bound through the aryl group to the vanadium center and slightly lower in energy than that observed for the free amine HN(Si^{i}Pr$_3$)DIPP (3386 cm^{-1}). Infrared spectroscopy of the crude product prior to crystallization indicates the presence of **4.11**, but also at least two other N–H bonded species (3278 cm^{-1}, 3244 cm^{-1}). Significantly, addition of 1 equiv of Li[B(C$_6$F$_5$)$_4$] to complex **4.10** in 1,2-difluorobenzene afforded a mixture of products consistent with the crude product from the synthesis of **4.11**, as determined by IR spectroscopy (see Experimental Details).

In light of the observed isomerization of **4.1** in solution, multiple pathways are possible for the formation of cationic complex **4.11** upon oxidation of **4.1**. A proposed mechanism for the formation of **4.11** involves the presumed, more reactive (linear) isomer and a concerted C–H activation step (σ-bond metathesis; Scheme **4.5**). Given the evidence that complex **4.10** is a suitable precursor to **4.11**, the close C–H agostic interactions with the metal center in **10** likely play an important role in this C–H activation leading to complex **4.11**.

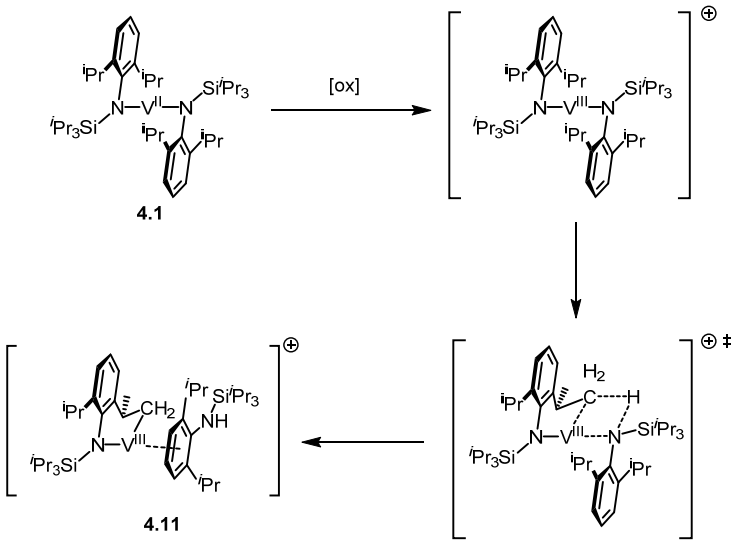

Scheme 4.5. Proposed pathway for the formation of 4.11

CONCLUDING REMARKS

In contrast with previous work on $Cr[N(Si^iPr_3)DIPP]_2$, the divalent silyl(aryl)amido vanadium species reported here do not exist as stable two-coordinate structures. In fact, despite having a composition identical to that of **4.1**, the asymmetric distribution of steric factors within the organosilyl groups in complex **4.2** strongly impacts its geometry, resulting in a "sandwich" conformation in both the +2 and +1 oxidation states. Moreover, while **4.1** exists as a two-coordinate bis(amido) complex in the solid state, EPR, NMR, UV-Vis, and IR spectroscopy suggest the presence of at least two geometries of **4.1** in solution. In addition, the $-N(Si^iPr_3)DIPP$ complex resorts to a sandwich structure upon one-electron reduction of the vanadium center.

Although not strictly two-coordinate, **4.1** can be forced to maintain low-coordination in the presence of a neutral donor such as 1-cyanoadamantane. Coordinative unsaturation at the metal center can also be preserved upon oxidation of **4.1** to higher valent species. However, access to the V(III) bis(amido) triflate complex appears to give rise to a reactive derivative of vanadium that undergoes C–H activation, a presumed property of such highly electron-deficient and low-coordinate metal centers.

These vanadium complexes highlight the challenges of synthesizing two-coordinate complexes of early transition metals and emphasize the possibility that low-coordination environments observed in the solid-state may not always be maintained in solution. Moreover, despite its stereochemically nonrigid behavior, **4.1** can be used to access a range of coordinatively unsaturated species. This work should guide future ligand design, the synthesis of two-coordinate complexes of early metals, and investigations of reactivity accessible at low-coordinate, electron-poor first-row transition metals.

REFERENCES

(1) Power, P. P. *Chem. Rev.* **2012**, *112* (6), 3482–3507.
(2) Ni, C., Power, P. P. *Chem. Commun.* **2009**, No. 37, 5543–5545.
(3) Laskowski, C. A., Miller, A. J. M., Hillhouse, G. L., Cundari, T. R. *J. Am. Chem. Soc.* **2011**, *133* (4), 771–773.
(4) Lipschutz, M. I., Tilley, T. D. *Chem. Commun.* **2012**, *48* (57), 7146–7148.
(5) Lipschutz, M. I., Yang, X., Chatterjee, R., Tilley, T. D. *J. Am. Chem. Soc.* **2013**, *135* (41), 15298–15301.
(6) Lin, C.-Y., Fettinger, J. C., Grandjean, F., Long, G. J., Power, P. P. *Inorg. Chem.* **2014**, *53* (17), 9400–9406.
(7) Lipschutz, M. I., Tilley, T. D. *Organometallics* **2014**, *33* (19), 5566–5570.
(8) Lin, C.-Y., Fettinger, J. C., Power, P. P. *Inorg. Chem.* **2017**, *56* (16), 9892–9902.
(9) Lipschutz, M. I., Tilley, T. D. *Angew. Chem. Int. Ed.* **2014**, *53* (28), 7290–7294.
(10) Lipschutz, M. I., Chantarojsiri, T., Dong, Y., Tilley, T. D. *J. Am. Chem. Soc.* **2015**, *137* (19), 6366–6372.
(11) Ung, G., Peters, J. C. *Angew. Chem. Int. Ed.* **2015**, *54* (2), 532–535.
(12) Liu, Y., Deng, L. *J. Am. Chem. Soc.* **2017**, *139* (5), 1798–1801.
(13) Ni, C., Ellis, B. D., Long, G. J., Power, P. P. *Chem. Commun.* **2009**, No. 17, 2332–2334.
(14) Cai, I. C., Lipschutz, M. I., Tilley, T. D. *Chem. Commun.* **2014**, *50* (86), 13062–13065.
(15) Boynton, J. N., Guo, J.-D., Fettinger, J. C., Melton, C. E., Nagase, S., Power, P. P. *J. Am. Chem. Soc.* **2013**, *135* (29), 10720–10728.
(16) Hagen, H., Boersma, J., Koten, G. van. *Chem. Soc. Rev.* **2002**, *31* (6), 357–364.
(17) Gibson, V. C., Spitzmesser, S. K. *Chem. Rev.* **2003**, *103* (1), 283–316.
(18) Nomura, K., Zhang, S. *Chem. Rev.* **2011**, *111* (3), 2342–2362.
(19) Tran, B. L., Pinter, B., Nichols, A. J., Konopka, F. T., Thompson, R., Chen, C.-H., Krzystek, J., Ozarowski, A., Telser, J., Baik, M.-H., Meyer, K., Mindiola, D. J. *J. Am. Chem. Soc.* **2012**, *134* (31), 13035–13045.
(20) Tran, B. L., Chen, C.-H., Mindiola, D. J. *Inorganica Chim. Acta* **2011**, *369* (1), 215–222.
(21) Tran, B. L., Singhal, M., Park, H., Lam, O. P., Pink, M., Krzystek, J., Ozarowski, A., Telser, J., Meyer, K., Mindiola, D. J. *Angew. Chem. Int. Ed.* **2010**, *49* (51), 9871–9875.
(22) Laskowski, C. A., Hillhouse, G. L. *J. Am. Chem. Soc.* **2008**, *130* (42), 13846–13847.
(23) Bruno, I. J., Cole, J. C., Edgington, P. R., Kessler, M., Macrae, C. F., McCabe, P., Pearson, J., Taylor, R. *Acta Crystallogr. B* **2002**, *58* (3), 389–397.
(24) Boynton, J. N., Guo, J.-D., Grandjean, F., Fettinger, J. C., Nagase, S., Long, G. J., Power, P. P. *Inorg. Chem.* **2013**, *52* (24), 14216–14223.
(25) Wagner, C. L., Tao, L., Thompson, E. J., Stich, T. A., Guo, J., Fettinger, J. C., Berben, L. A., Britt, R. D., Nagase, S., Power, P. P. *Angew. Chem. Int. Ed.* **2016**, *55* (35), 10444–10447.
(26) Lin, C.-Y., Guo, J.-D., Fettinger, J. C., Nagase, S., Grandjean, F., Long, G. J., Chilton, N. F., Power, P. P. *Inorg. Chem.* **2013**, *52* (23), 13584–13593.
(27) Werncke, C. G., Suturina, E., Bunting, P. C., Vendier, L., Long, J. R., Atanasov, M., Neese, F., Sabo-Etienne, S., Bontemps, S. *Chem. – Eur. J.* **2016**, *22* (5), 1668–1674.
(28) Calderazzo, F., De Benedetto, G. E., Pampaloni, G., Mössmer, C. M., Strähle, J., Wurst, K. *J. Organomet. Chem.* **1993**, *451* (1), 73–81.
(29) Helling, J. F., Hendrickson, W. A. *J. Organomet. Chem.* **1977**, *141* (1), 99–105.
(30) Helling, J. F., Hendrickson, W. A. *J. Organomet. Chem.* **1979**, *168* (1), 87–95.
(31) Ireland, B. J., McDonald, R., Fogg, D. E. *Organometallics* **2013**, *32* (17), 4723–4725.

(32) Antipin, M. Y., Boese, R. *Acta Crystallogr. B* **1996**, *52* (2), 314–322.
(33) Figueroa, W., Fuentealba, M., Manzur, C., Carrillo, D., Vega, A. I., Saillard, J.-Y., Hamon, J.-R. *Organometallics* **2004**, *23* (11), 2515–2518.
(34) Ernst, R. D., Basta, R., Arif, A. M. *Z. Für Krist. - New Cryst. Struct.* **2006**, *221* (1–4), 289–290.
(35) Klingebiel, U., Noltemeyer, M., Wand, A. *J. Organomet. Chem.* **2006**, *691* (12), 2657–2665.
(36) Boynton, J. N., Guo, J.-D., Fettinger, J. C., Melton, C. E., Nagase, S., Power, P. P. *J. Am. Chem. Soc.* **2013**, *135* (29), 10720–10728.
(37) Figgis, B. N. *Introduction to Ligand Fields*, Wiley-Interscience, New York, 1966.
(38) Drago, R. S. Harcourt Brace Jovanovich, New York, 1992, p 484.
(39) Evans, D. F. *J. Chem. Soc. Resumed* **1959**, No. 0, 2003–2005.
(40) Sur, S. K. *J. Magn. Reson. 1969* **1989**, *82* (1), 169–173.
(41) Grant, D. H. *J. Chem. Educ.* **1995**, *72* (1), 39–40.
(42) Zadrozny, J. M., Atanasov, M., Bryan, A. M., Lin, C.-Y., Rekken, B. D., Power, P. P., Neese, F., Long, J. R. *Chem. Sci.* **2013**, *4* (1), 125–138.
(43) Atanasov, M., Zadrozny, J. M., Long, J. R., Neese, F. *Chem. Sci.* **2013**, *4* (1), 139–156.
(44) Jackson, T. A., Krzystek, J., Ozarowski, A., Wijeratne, G. B., Wicker, B. F., Mindiola, D. J., Telser, J. *Organometallics* **2012**, *31* (23), 8265–8274.
(45) Ammeter, J. H. *J. Magn. Reson. 1969* **1978**, *30* (2), 299–325.
(46) Prins, R., Voorst, J. D. W. van. *J. Chem. Phys.* **1968**, *49* (10), 4665–4673.
(47) Prins, R., Biloen, P., Voorst, J. D. W. van. *J. Chem. Phys.* **1967**, *46* (3), 1216–1217.
(48) Berno, P., Gambarotta, S. *J. Chem. Soc. Chem. Commun.* **1994**, *0* (20), 2419–2421.
(49) Gerlach, C. P., Arnold, J. *Inorg. Chem.* **1996**, *35* (20), 5770–5780.
(50) Hagen, H., Bezemer, C., Boersma, J., Kooijman, H., Lutz, M., Spek, A. L., van Koten, G. *Inorg. Chem.* **2000**, *39* (18), 3970–3977.
(51) Lorber, C., Choukroun, R., Donnadieu, B. *Inorg. Chem.* **2002**, *41* (16), 4217–4226.
(52) Aharonovich, S., Botoshansky, M., Tumanskii, B., Nomura, K., Waymouth, R. M., Eisen, M. S. *Dalton Trans.* **2010**, *39* (24), 5643–5649.
(53) Braunschweig, H., D. Dewhurst, R., Radacki, K., Wennemann, B., Ye, Q. *Chem. Commun.* **2015**, *51* (84), 15465–15468.
(54) Preuss, F., Steidel, M., Vogel, M., Overhoff, G., Hornung, G., Towae, W., Frank, W., Reiß, G., Müller-Becker, S. *Z. Für Anorg. Allg. Chem. 623* (8), 1220–1228.

EXPERIMENTAL DETAILS

General Considerations. Unless otherwise noted, all experiments were conducted with dry, oxygen-free solvents using standard Schlenk techniques or in a nitrogen atmosphere glovebox. Pentane, toluene, diethyl ether, tetrahydrofuran, and 1,2-difluorobenzene were dried and deaerated using a JC Meyers Phoenix SDS solvent purification system. Deuterated solvents were purchased from Cambridge Isotope Laboratories, degassed by three freeze-pump-thaw cycles and stored under nitrogen over activated 3 Å molecular sieves prior to use.

$[V_2Cl_3(THF)_6]I$[1] was prepared using a modified procedure: the aluminate intermediate $[V_2Cl_3(THF)_6][AlCl_4]$[1] was isolated prior to salt metathesis with 1 equiv of LiI in THF at ambient temperature. HN(Si^{i}Pr$_3$)DIPP,[2] potassium graphite,[3] *p*-tolylazide,[4] and ferrocenium tetrakis(pentafluorophenyl)borate[5] were prepared according to literature procedures. From Sigma Aldrich, *n*-butyllithium solution (1.6 M in hexanes) was purchased and used as received. Di-*tert*-butyl(methyl)silyl chloride was purchased from Gelest and used as received. Potassium hydride was purchased as a dispersion in mineral oil from Sigma Aldrich and washed with pentane before use. 18-crown-6 was purchased from Sigma Aldrich and dried by distillation under reduced pressure before use. Li[$[B(C_6F_5)_4]$] was prepared from $[Li(Et_2O)_3][B(C_6F_5)_4]$ (purchased from Boulder Scientific) according to literature procedure.[6] All other reagents were obtained from commercial suppliers and used as received.

The abbreviation "DIPP" refers to a 2,6-diisopropylphenyl moiety.

Analytical Method Details. Elemental analyses were performed by the College of Chemistry Microanalytical Facility at the University of California, Berkeley.

NMR Spectroscopy. All NMR spectra were collected at ambient temperature (ca. 22 °C) on Bruker AVB-400, AVQ-400, AV-500, or AV-600 MHz spectrometers, each equipped with either a 5 mm QNP or broadband probe. ^{1}H NMR spectra were referenced to tetramethylsilane calibrated *via* residual proteo-solvent signals.[7] All NMR spectra were analyzed with MestReNova (v. 12.0.3). For paramagnetic samples, full-width at half-maximum values ($\nu_{1/2}$) for well-defined features were estimated using the Line Fitting tool and are reported in Hz. Solution magnetic susceptibilities were determined by ^{1}H NMR spectroscopy using the Evans method.[8–10]

IR Spectroscopy. IR spectra were collected on a Thermo Scientific Nicolet iS10 spectrophotometer or a Bruker Vertex 80 FTIR Spectrometer with a room temperature DLaTGS detector. Measurements *via* ATR were collected using an A225/Q Platinum ATR accessory. All measurements were made at 4.0 cm^{-1} resolution.

UV-Vis Spectroscopy. UV-visible spectra of complexes **4.1** and **4.2** were obtained on a Varian Cary 50 UV-Visible spectrophotometer using Cary WinUV software (v. 3.00(182)). Samples for UV-Vis spectra were prepared in a nitrogen-filled glovebox and sealed in 1 cm, air-free quartz cells.

SQUID Magnetometry. Magnetic measurements were carried out in a Quantum Design MPMS-XL SQUID Magnetometer. In an argon atmosphere glovebox, polycrystalline samples of **4.1** and **4.2** were loaded into quartz tubes with either glass wool or eicosane used to restrain the

crystallites. A sealable hose adapter was attached to the tubes and the samples were sealed under vacuum. AC magnetic susceptibility experiments were done using a 6 Oe probe field. All data were corrected for diamagnetic contributions using Pascal's constants.

EPR Spectroscopy. The EPR spectra were obtained on custom-designed continuous-wave (*cw*)/pulsed X-band Bruker Elexsys 580 EPR spectrometers. The *cw* EPR measurements were performed with either a dual-mode ER 4116-DM resonator equipped with a continuous-flow E900 cryostat or a dielectric flexline ER 4118-MD5 resonator equipped with a dynamic continuous-flow CF935 cryostat. Resonators were manufactured by Bruker BioSpin Corporation (Billerica, MA) while cryostats were supplied by Oxford Instruments (Oxfordshire, U.K.). Liquid helium was employed to reach temperatures between 4 and 70 K. Additional experimental details are recorded in Table S4.1.

Table S4.1. EPR spectroscopy details

Complex	Preparation	Mode	Microwave frequency (GHz)	Microwave power (mW)	Modulation amplitude (G)	Modulation frequency (kHz)
4.1	powder	perpendicular	9.635	2.993	2	100.00
4.1 (@ 0 h)	frozen pentane solution	perpendicular	9.634	2.377	2	100.00
4.1 (@ 1 h)	frozen pentane solution	perpendicular	9.634	2.377	2	100.00
4.2	powder	perpendicular	9.645	4.975	2	100.00
4.2	frozen pentane solution	perpendicular	9.718	1.979	1	100.00

All of the samples were prepared under strictly anaerobic conditions in a nitrogen-filled glovebox. Solid-state samples of **4.1** and **4.2** were sealed in 4 mm quartz EPR tubes (Wilmad Labglass, Vineland, NJ). Pentane solutions of **4.1** (ca. 4.0 mM) and **4.2** (ca. 5.6 mM) were sealed in 4 mm quartz EPR tubes with PTFE low pressure/vacuum adapters (Wilmad Labglass, Vineland, NJ).

All of the samples were rapidly frozen at 77 K immediately following transfer to the EPR tubes and kept frozen prior insertion into the resonator that was pre-cooled to liquid helium temperature. Following the collection of the first spectrum of the pentane solution of **4.1**, the sample was allowed to thaw and warm to 21 °C. After standing at 21 °C for a total of 1 h, the pentane solution of **4.1** was refrozen to 77 K and re-inserted into the pre-cooled resonator.

Spectral simulations of **4.2** were performed using the *pepper* function in the EasySpin toolbox (v. 5.2.15) in MATLAB (v 9.3.0.713579, R2017b).

Cyclic Voltammetry Experiments. Cyclic voltammetry experiments were conducted at ambient temperature in a nitrogen atmosphere glovebox. Measurements employed a BASi EC Epsilon potentiostat/galvanostat and a PWR-3 Power Module with a standard three-electrode configuration: a 3mm diameter glassy carbon working electrode (polished with 0.30 then 0.05 μm alumina slurries, rinsed with water, and dried *in vacuo*), a platinum wire counter electrode, and either a silver wire quasi-reference electrode or a $Ag/AgNO_3$ reference electrode (0.1 M $[^nBu_4N][PF_6]$, $AgNO_3$ satd.) in THF, constructed immediately before use). Sublimed ferrocene was used as an internal potential reference.

Cyclic voltammograms were recorded in a 0.1 M solution of tetrabutylammonium hexafluorophosphate in 1,2-difluorobenzene at ca. 23 °C. Sample concentrations, sweep direction, and scan rates are included in the relevant figures or their captions. Solution resistance was corrected by applying software-determined *i*R compensation for each measurement. Data analysis, including peak-finding and baseline determination employing linear regression, was performed with EC-Lab (v. 10.40).

X-ray Diffraction Experiments. Data for **4.1**, **4.2**, **4.6**, **4.5**, **4.7**, **4.8**, **4.9**, **4.10**, and **4.11** were collected at Beamline 11.3.1/12.2.1 (Small Molecule Crystallography) of the Advanced Light Source at Lawrence Berkeley National Laboratory (LBNL). Measurements of **4.3** were performed on a DECTRIS PILATUS3 R 200K-A HPC detector using Mo Kα radiation (λ = 0.71073 Å). Measurements of **4.4** and **$Cr[N(Si^tBu_2Me)DIPP]_2$** were performed on a Bruker APEX-II CCD area detector using Mo Kα radiation (λ = 0.71073 Å) monochromated using QUAZAR multilayer mirrors. All crystals were kept at 100(2) K throughout collection.

Data collection, refinement, and reduction were performed with Bruker APEX2 or APEX3 software (v. 2013.4-0 or v. 2016.9-0). Structure solution, modeling, and refinement was performed using Olex2.[11] All structures were solved using SHELXT-2014[12] and refined with SHELXL-2018[13], with refinement of F^2 on all data by full-matrix least squares. In all models, non-hydrogen atoms were refined anisotropically, and hydrogen atoms were included at the geometrically-calculated positions and refined using a riding model, unless otherwise specified. Disordered solvent molecules were modeled atomistically.

For complex **4.1**, hydrogen atoms on C8 and C15 were located from the electron density difference map. The structural solution of **4.2** in $P2_1/c$ revealed a single organometallic unit, but after refinement, the *R* factor was only reduced to 9.69%. We attribute the high *R* factor to poor crystal quality and the crystal habit of **4.2** (thin needles). For complex **4.10**, hydrogen atoms on C21 and C42 were located from the electron density difference map. For complex **4.11**, hydrogen atoms on C4 and N2 were located from the electron density difference map.

Specific details can be found below (Table **E4.1**) and in the crystallographic information files.

Table E4.1: X-ray Crystallography Experimental Details:

Compound	*Detector Distance (mm)*	*Image Width (°)*	*Exposure Time (s)*
4.1	50	1 or 4, depending on angle	1
4.2	50	1.0	1
4.3	33	0.5	6
4.6	50	1 or 4, depending on angle	0.5 or 1
4.4	40	0.4	20
4.5	50	1 or 4, depending on angle	0.5 or 1
4.7	50	1 or 4, depending on angle	1
4.8	50	1 or 4, depending on angle	0.5 or 1
4.9	50	1.0	1
4.10	50	1 or 4, depending on angle	1
4.11	50	1 or 4, depending on angle	0.5 or 1
$Cr[N(Si^tBu_2Me)DIPP]_2$	40	1.0	20

Synthesis of K[N(Si^{i}Pr$_3$)DIPP]. To a Schlenk flask fitted with a solid addition funnel was added HN(Si^{i}Pr$_3$)DIPP (4.10 g, 12.3 mmol) and THF (ca. 100 mL). The resulting solution was stirred, and potassium hydride (1.47 g, 36.6 mmol, 3.0 equiv) was added slowly *via* the solid addition funnel. The reaction mixture was stirred at ambient temperature for 3.5 h, at which time the mixture was cannula filtered to separate the solution from excess potassium hydride. The resulting filtrate was concentrated under reduced pressure to a residue, which was triturated with 20 mL of pentane to give a solid. The resulting solid was loaded into a medium fritted funnel and then washed with pentane. Residual volatile compounds were removed *in vacuo* to yield an off-white powder (3.75 g, 10.1 mmol, 82%), which was used without further purification.

V[N(Si^{i}Pr$_3$)DIPP]$_2$ (4.1). To a 20 mL scintillation vial was added [$V_2Cl_3(THF)_6$]I (0.500 g, 0.651 mmol) and diethyl ether (5 mL). The resulting suspension was stirred, and a mixture of K[N(Si^{i}Pr$_3$)DIPP] (0.980 g, 2.64 mmol, 4.0 equiv) in diethyl ether (15 mL) was added dropwise. The reaction was stirred at ambient temperature for 14 h. The resulting purple reaction mixture was concentrated under reduced pressure to a solid with both green and purple regions. (Color varied depending on how much solvent had been removed. As more solvent was removed *in vacuo* from the solid, regions of purple solid became green in color.) The solid was triturated with pentane (3 mL) in order to remove any residual diethyl ether, yielding a green solid that was extracted with pentane (25 mL total). (The resulting pentane extracts may range in color from red-brown to purple, depending on the concentration of the extracts and the length of time the complex has been solvated.) The combined pentane extracts were filtered, concentrated *in vacuo* to 17 mL, and stored overnight at –30 °C, to yield 0.536 g (0.748 mmol, 57%) of **4.1** as green blocks, which were isolated by decanting the supernatant and removing residual volatile compounds *in vacuo*. The purple supernatant was collected and concentrated to a residue. A second crystallization using the resulting residue with was set up in a similar fashion using 5 mL of pentane and yielded an additional 0.093 g of **4.1**. Total yield: 0.629 g (0.878 mmol, 67%).

Crystals suitable for single crystal X-ray diffraction studies were obtained from the crystallization procedure described above.

Effective magnetic moment (Evans method, 600.13 MHz, C_6D_6, 23 °C): $\mu_{eff} = 3.7\ \mu_B$.

Effective magnetic moment (SQUID magnetometry, 22 °C): $\mu_{eff} = 3.92\ \mu_B$.

IR (KBr pellet) $\tilde{\nu}_{max}$ (cm^{-1}): 2967 (s), 2948 (s), 2938 (s), 2865 (s), 1460 (s), 1411 (s), 1383 (m), 1361 (m), 1320 (m), 1307 (s), 1256 (s), 1236 (s), 1198(s), 1107 (m), 1098 (m), 1063 (m), 1051 (m), 1040 (m), 997 (m), 917 (vs), 881 (vs), 766 (vs), 720 (s), 673 (vs), 641 (s), 626 (s), 597 (m), 552 (m), 520 (s), 501 (m), 476 (m), 451 (m), 434 (m).

IR (ATR) $\tilde{\nu}_{max}$ (cm^{-1}): 2965 (s), 2946 (s), 2935 (s), 2864 (s), 1459 (s), 1410 (s), 1382 (m), 1361 (m), 1320 (m), 1306 (s), 1255 (s), 1235 (s), 1197(s), 1105 (m), 1099 (m), 1063 (m), 1051 (m), 1040 (m), 996 (m), 915 (vs), 879 (vs), 764 (vs), 718 (s), 671 (vs), 639 (s), 625 (s), 596 (m), 551 (m), 519 (s), 499 (m), 475 (m), 451 (m), 432 (m).

IR (benzene-d_6) $\tilde{\nu}_{max}$ (cm^{-1}): 2960 (s), 2865 (s), 1585 (s), 1563 (s), 1539 (m), 1466 (s), 1458 (s), 1446 (m), 1438 (m), 1382 (m), 1362 (m), 1308(s), 1254 (s), 1237 (s), 1195 (s), 1145 (m), 1133 (m), 1105 (m), 1069 (m), 998 (m), 988 (m), 909 (s), 880 (s), 778 (s), 724 (s), 679 (s), 648 (s).

Anal. Calcd for $C_{42}H_{76}N_2VSi_2$: C, 70.44; H, 10.70; N, 3.91. Found: C, 70.63; H, 10.47; N, 3.85.

For the following solution spectra, * = spectral features appear after dissolution:

> ^{1}H NMR (600.13 MHz, C_6D_6) δ 19.8 ($\nu_{1/2}$ = 400 Hz), 9.9 (sh), 9.2 ($\nu_{1/2}$ = 300 Hz), 3.9* ($\nu_{1/2}$ = 300 Hz), 3.4 ($\nu_{1/2}$ = 210 Hz), 0.5 ($\nu_{1/2}$ = 2200 Hz), –5.4 ($\nu_{1/2}$ = 480 Hz), –7.7* ($\nu_{1/2}$ = 560 Hz), –13.8 ($\nu_{1/2}$ = 1040 Hz).
>
> UV-vis (pentane, 30 °C) λ_{max} (ε calculated based on total concentration of **4.1**):
> 496 nm ($\varepsilon_{initial}$ = ca. 500 M^{-1} cm^{-1}, $\varepsilon_{equilibrium}$ (shoulder peak)= 650 M^{-1} cm^{-1}),
> 564 nm* ($\varepsilon_{equilibrium}$ = 800 M^{-1} cm^{-1}),
> 908 nm. ($\varepsilon_{initial}$ = ca. 100 M^{-1} cm^{-1}, $\varepsilon_{equilibrium}$ = ca. 90 M^{-1} cm^{-1}).

Synthesis of K[N(H)DIPP]. A solution of 2,6-diisopropylaniline (2.98 g, 16.8 mmol, 1.05 equiv) and potassium *tert*-butoxide (1.80 g, 16.0 mmol) in THF (30 mL) was cooled to 0 °C using an ice bath. To the stirring solution was added *n*-butyllithium in hexanes (10 mL, 1.6 M, 16.0 mmol), dropwise, *via* syringe. The yellow solution was removed from the ice bath and stirred for 50 min. Volatile materials were removed under reduced pressure, and the resulting solid was washed with pentane (5 x 20 mL) on a medium fritted funnel. Residual solvent was removed under reduced pressure to yield potassium 2,6-diisopropylanilide as a white powder (3.30 g, 15.3 mmol, 96%), which was used without further purification.

Synthesis of HN(Si^{t}Bu$_2$Me)DIPP. To a 250 mL Chemglass Air-Free Teflon-stoppered flask was added potassium 2,6-diisopropylanilide (3.23 g, 15.0 mmol), di-*tert*-butyl(methyl)silyl chloride (2.89 g, 15.0 mmol), and THF (60 mL). The reaction was heated at 75 °C and stirred. After 17 hours, the reaction mixture was allowed to cool to ambient temperature. An aliquot of the reaction mixture indicated incomplete conversion of di-*tert*-butyl(methyl)silyl chloride to the product by ^{1}H NMR spectroscopy. Additional potassium 2,6-diisopropylanilide (1.15 g, 5.3 mmol) was suspended in toluene (10 mL) and added to the mixture. The reaction mixture was heated at 75 °C and stirred for an additional 15 hours. After allowing the reaction mixture to cool to ambient temperature, the mixture was exposed to air and filtered through Celite in a coarse fritted funnel, and the filtrate was concentrated under reduced pressure. The product was separated from 2,6-diisopropylaniline by fractional distillation under dynamic vacuum to yield a clear, light red oil (2.94 g, 8.8 mmol, 59%). ^{1}H and ^{13}C{^{1}H} NMR data in C_6D_6 were consistent with values reported in the literature.[33]

Synthesis of K[N(Si^{t}Bu$_2$Me)DIPP]. To a 20 mL scintillation vial was added HN(Si^{t}Bu$_2$Me)DIPP (0.646 g, 1.94 mmol) and diethyl ether (6 mL). The solution was placed in a −30 °C freezer and allowed to cool for 30 min. To the stirring solution was added benzyl potassium (0.252 g, 1.94 mmol) in portions. The reaction mixture was stirred for 15 h. The resulting solution was filtered and concentrated *in vacuo* to a solid, which was triturated with pentane (3 mL). The resulting solid was dissolved in diethyl ether (4.5 mL), upon which pentane

(15 mL) was layered. The layered solution was stored at −30 °C for two days to yield 0.471 g (1.27 mmol, 65%) of K[N(Si^{t}Bu$_2$Me)DIPP] as white crystals, which were isolated by decanting the supernatant and removing residual volatile compounds *in vacuo*. The product was used without further purification.

V[(DIPP)N(Si^{t}Bu$_2$Me]$_2$ (4.2). To a 20 mL scintillation vial was added [V$_2$Cl$_3$(THF)$_6$]I (0.100 g, 0.130 mmol) and diethyl ether (1.5 mL). The resulting suspension was stirred, and a mixture of K[N(Si^{t}Bu$_2$Me)DIPP] (0.194 g, 0.522 mmol, 4.0 equiv) in diethyl ether (3 mL) was added dropwise. The reaction mixture was stirred at ambient temperature for 16 h. The resulting purple reaction mixture was concentrated under reduced pressure to a purple solid, which was triturated with pentane (3 mL) in order to remove any residual diethyl ether. The resulting solid was extracted with pentane (20 mL total). The combined pentane extracts were filtered, concentrated *in vacuo* to 10 mL, and stored overnight at -30 °C, to yield 0.134 g (0.187 mmol, 72%) of **4.2** as purple needles, which were isolated by decanting the supernatant and removing residual volatile compounds *vacuo*.

Crystals suitable for single crystal X-ray diffraction studies were obtained from the crystallization procedure described above.

Effective magnetic moment (Evans method, 600.13 MHz, C$_6$D$_6$, 22 °C): μ_{eff} = 3.7 μ_B.

Effective magnetic moment (SQUID magnetometry, 22 °C): μ_{eff} = 3.91 μ_B.

^{1}H NMR (600.13 MHz, C$_6$D$_6$) δ 40-25 (br), 10-5 (br), 4.5 ($\nu_{1/2}$ = 420 Hz), -1.8 ($\nu_{1/2}$ = 220 Hz), -9.6 ($\nu_{1/2}$ = 520 Hz).

UV-vis (pentane, 30 °C) λ_{max} (ε): 577 nm (6300 M^{-1} cm^{-1}).

IR (KBr pellet) $\tilde{\nu}_{max}$ (cm^{-1}): 2959 (vs), 2930 (vs), 2884 (vs), 2856 (vs), 1583 (vs, br, ν_{C-N}), 1564 (vs, br, ν_{C-N}), 1471 (s), 1382 (m), 1362 (s), 1250 (s), 1198 (w), 1132 (m), 1100 (w), 1054 (w), 1032 (m), 1008 (m), 951 (s), 931 (s), 903 (m), 875 (w), 821 (s), 804 (s), 776 (vs), 729 (s), 678 (s), 621 (m), 608 (m), 543 (w), 437 (m), 421 (m).

Anal. Calcd for C$_{42}$H$_{76}$N$_2$VSi$_2$: C, 70.44; H, 10.70; N, 3.91. Found: C, 70.72; H, 10.60; N, 3.67.

Cr[N(Si^{t}Bu$_2$Me)DIPP]$_2$. To a 20 mL scintillation vial was added chromium(II) chloride (0.033 g, 0.269 mmol) and THF (2 mL). To a 4 mL vial was added K[N(Si^{t}Bu$_2$Me)DIPP] (0.204 g, 0.549 mmol, 2.0 equiv) and THF (4 mL). Both vials were placed in a -30 °C freezer and allowed to cool for 10 minutes. Upon removal of the vials from the freezer, the suspension of chromium(II) chloride was stirred and the solution of K[N(Si^{t}Bu$_2$Me)DIPP] was added dropwise. The reaction mixture was stirred at ambient temperature for 1 h. The brown solution was concentrated under reduced pressure, and the resulting orange solid was extracted with diethyl ether (10 mL). The pentane extract was filtered and concentrated *in vacuo* to 9 mL. Slow evaporation of the resulting solution at -30 °C yielded 0.072 g (0.100 mmol, 37%) of Cr[N(Si^{t}Bu$_2$Me)DIPP]$_2$ as orange needles, which were isolated by decanting the supernatant and removing residual volatile compounds *in vacuo*.

Crystals suitable for single crystal X-ray diffraction studies were obtained from the crystallization procedure described above.

Effective magnetic moment (Evans method, 500.23 MHz, 1,2-difluorobenzene with $Si(SiMe_3)_4$ added as a reference, 23°C): $\mu_{eff} = 4.8\ \mu_B$.

IR (ATR) $\tilde{\nu}_{max}$ (cm^{-1}): 2961 (s), 2857 (s), 1467 (s), 1437 (s), 1419 (m), 1383 (m), 1363 (m), 1329 (m), 1306 (m), 1251 (s), 1233 (m), 1194 (m), 1186 (m), 1106 (m), 1043 (w), 1011 (w), 900 (s), 874 (m), 820 (s), 770 (vs), 738 (m), 720 (m), 674 (s), 607 (m), 527 (m).

Anal. Calcd for $C_{42}H_{76}N_2CrSi_2$: C, 70.33; H, 10.68; N, 3.91. Found: C, 69.94; H, 10.52; N, 3.70.

(AdCN)V[N(Si^{i}Pr$_3$)DIPP]$_2$ (4.3). To a 20 mL scintillation vial was added **4.1** (0.050 g, 0.070 mmol) and pentane (3 mL). The mixture was stirred to give a purple solution, and a solution of 1-cyanoadamantane (0.0113 g, 0.070 mmol) in pentane (3 mL) was added dropwise. The reaction was stirred at ambient temperature for 1 h. The resulting red-violet reaction mixture was filtered, concentrated *in vacuo* to 1 mL, and stored overnight at -30 °C, to yield 0.040 g (0.046 mmol, 65%) of **4.3** as dichroic green-purple blocks, which were isolated by decanting the supernatant and removing residual volatile compounds *in vacuo*.

Crystals suitable for single crystal X-ray diffraction studies were obtained from the crystallization procedure described above.

Effective magnetic moment (Evans method, 400.13 MHz, C_6D_6, 22 °C): $\mu_{eff} = 3.8\ \mu_B$.

^{1}H NMR (400.13 MHz, C_6D_6) δ 13.8 ($\nu_{1/2}$ = 200 Hz), 7.9 ($\nu_{1/2}$ = 400 Hz), 1.6 ($\nu_{1/2}$ = 1600 Hz), -0.5 ($\nu_{1/2}$ = 300 Hz), -9.7 ($\nu_{1/2}$ = 600 Hz).

IR (KBr pellet) $\tilde{\nu}_{max}$ (cm^{-1}): 2969 (vs), 2947 (vs), 2925 (vs), 2866 (vs), 1586 (w), 1457 (s), 1420 (s), 1381 (m), 1360 (m), 1308(m), 1252 (m), 1231 (s), 1176 (s), 1101 (m), 1070 (w), 1061 (w), 1052 (w), 1041 (w), 997 (w), 987 (m), 919 (w), 893 (s), 876 (s), 817 (s), 773 (vs), 738 (w), 725 (m), 689 (s), 653 (s), 583 (w), 538 (m).

Anal. Calcd for $C_{53}H_{91}N_3VSi_2$: C, 72.55; H, 10.45; N, 4.79. Found: C, 72.44; H, 10.08; N, 4.68.

Reaction of 4.1 with 1-cyanoadamantane. To a J. Young tube was added a solution of hexamethylbenzene in benzene-d_6 (0.1 mL, 43 mM, 4.3 μmol) as an internal standard, followed by a solution of **4.1** in benzene-d_6 (0.4 mL, 35 mM, 14.0 μmol). The resulting solution was allowed to stand at ambient temperature for 1 h, and then a solution of 1-cyanoadamantane in benzene-d_6 (0.1 mL, 140 mM, 14.0 μmol, 1.0 equiv) was added. The reaction was monitored by ^{1}H NMR spectroscopy at various intervals over the course of 22 h (see Figure S11). The ^{1}H NMR spectra of the product were consistent with that of **4.3**.

Reaction of 4.2 with 1-cyanoadamantane. To a J. Young tube was added a solution of hexamethylbenzene in benzene-d_6 (0.1 mL, 43 mM, 4.3 μmol) as an internal standard, followed

by a solution of **4.2** in benzene-d_6 (0.4 mL, 35 mM, 14.0 μmol). To the resulting purple solution, a solution of 1-cyanoadamantane in benzene-d_6 (0.1 mL, 140 mM, 14.0 μmol, 1.0 equiv) was added. The reaction at ambient temperature was monitored by ^{1}H NMR spectroscopy at various intervals over the course of 22 h; no significant consumption of either **4.2** or 1-cyanoadamantane was observed. The reaction was subsequently heated at 50 °C for 24 h, after which the 1-cyanoadamantane remained primarily unconsumed (< 1% conversion) and a minor formation of HN(Si^{t}Bu$_2$Me)DIPP was observed (ca. 1% conversion of **4.2**). The reaction was heated at 70 °C for 24 h, after which the ^{1}H NMR spectra revealed partial consumption of 1-cyanoadamantane (ca. 40%) and an increase in HN(Si^{t}Bu$_2$Me)DIPP (ca. 10% conversion of **4.2**). No other additional diamagnetic or paramagnetic products between 100 and −100 ppm were observed by ^{1}H NMR spectroscopy.

K{V[(DIPP)N(Si^{i}Pr$_3$)]$_2$} (4.4). To a 20 mL scintillation vial was added **4.1** (0.048 g, 0.067 mmol) and diethyl ether (3 mL); the resulting solution was cooled to -30 °C. The cooled mixture of **4.1** was stirred and potassium graphite (0.0095 g, 0.070 mmol, 1.05 equiv) was added directly in a single aliquot. The reaction mixture was stirred at ambient temperature for 1 h. The resulting magenta reaction mixture was filtered, then concentrated *in vacuo* to 1.5 mL, upon which pentane (8 mL) was layered. The layered solution was stored overnight at −30 °C to yield 0.015 g (0.020 mmol, 30%) of **4.4** as dark magenta crystals, which were isolated by decanting the supernatant and removing residual volatile compounds *in vacuo*.

Crystals suitable for single crystal X-ray diffraction studies were obtained from the crystallization procedure described above.

Effective magnetic moment (Evans method, 400.13 MHz, THF, 20 °C): μ_{eff} = 2.7 μ_B.

^{1}H NMR (600.13 MHz, C_6D_6) δ 2.37 ($\nu_{1/2}$ = 120 Hz), -0.73 ($\nu_{1/2}$ = 700 Hz).

IR (KBr pellet) $\tilde{\nu}_{max}$ (cm^{-1}): 2957 (s), 2944 (s), 2863 (s), 1509 (vs, br, ν_{C-N}), 1466 (s, br), 1381 (m), 1347 (m), 1329 (m), 1272 (m), 1252 (m), 1237 (m), 1197 (m), 1126 (m), 1100 (m), 1072 (m), 1040 (w), 1023 (m), 1008 (m), 990 (m), 946 (s), 917 (m), 900 (m), 880 (s), 842 (w), 973 (s), 768 (m), 735 (s), 653 (s), 639 (s), 615 (m), 560 (m).

Anal. Calcd for $C_{42}H_{76}N_2VKSi_2$: C, 66.79; H, 10.14; N, 3.71. Found: C, 66.79; H, 10.06; N, 3.52.

{K(18-cr-6)$_{1.5}$}{V[(DIPP)N(Si^{i}Pr$_3$)]} (4.5). To a 20 mL scintillation vial was added **4.1** (0.050 g, 0.070 mmol) and diethyl ether (1.5 mL), followed by a solution of 18-crown-6 (0.028 g, 0.106 mmol, 1.5 equiv) in diethyl ether (1.5 mL). The resulting solution was stirred, and potassium graphite (0.0105 g, 0.078 mmol, 1.1 equiv) was added directly in a single aliquot. The reaction mixture was stirred at ambient temperature for 1 h. The resulting magenta reaction mixture was filtered to give a magenta filtrate, upon which pentane (7 mL) was layered. The layered solution was stored overnight at −30 °C to yield 0.059 g (0.051 mmol, 73%) of **4.5** as dark magenta plates, which were isolated by decanting the supernatant and removing residual volatile compounds *in vacuo*.

Crystals suitable for single crystal X-ray diffraction studies were obtained from the crystallization procedure described above.

Effective magnetic moment (Evans method, 400.13 MHz, THF, 21 °C): μ_{eff} = 2.8 μ_B.

IR (KBr pellet) $\tilde{\nu}_{max}$ (cm^{-1}): 2940 (s), 2915 (s), 2857 (s), 1506 (s, br, ν_{C-N}), 1482 (s), 1467 (s, br sh), 1376 (m), 1352 s), 1283 (m), 1250 (m), 1238 (m), 1203 (m), 1109 (s), 1031 (m), 1007 (m), 989 (m), 962 (s), 919 (m), 900 (m), 881 (s), 835 (m), 785 (m), 743 (s), 649 (s), 610 (m), 557 (m).

Anal. Calcd for $C_{60}H_{112}N_2VKO_9Si_2$: C, 62.57; H, 9.80; N, 2.43. Found: C, 62.78; H, 9.83; N, 2.62.

{K(18-cr-6)}{V[(DIPP)N(Si^{t}Bu$_2$Me)]} (4.6). To a 20 mL scintillation vial was added **4.2** (0.051 g, 0.071 mmol) and diethyl ether (1.5 mL), followed by a solution of 18-crown-6 (0.019 g, 0.071 mmol) in diethyl ether (1.5 mL). The resulting solution was stirred, and potassium graphite (0.0106 g, 0.078 mmol, 1.1 equiv) was added directly in a single aliquot. The reaction mixture was stirred at ambient temperature for 1 h. The resulting dark magenta reaction mixture was filtered, then concentrated *in vacuo* to 2 mL, upon which pentane (8 mL) was layered. The layered solution was stored overnight at −30 °C to yield 0.051 g (0.050 mmol, 70%) of **4.6** as dark magenta needles, which were isolated by decanting the supernatant and removing residual volatile compounds *in vacuo*.

Crystals suitable for single crystal X-ray diffraction studies were obtained from a solution of **4.6** in THF layered with pentane stored overnight at −30 °C.

Effective magnetic moment (Evans method, 400.13 MHz, THF, 21 °C): μ_{eff} = 2.7 μ_B.

IR (ATR) $\tilde{\nu}_{max}$ (cm^{-1}): 2948 (s), 2931 (s), 2882 (s), 2857 (s), 1549 (m), 1506 (s, ν_{C-N}), 1470 (vs), 1438 (s), 1379 (m), 1351 (s), 1307 (w), 1281 (w), 1253 (s), 1235 (m), 1199 (w), 1105 (vs), 1057 (w), 1043 (w), 1034 (w), 1009 (w), 962 (s), 934 (m), 900 (s), 873 (m), 835 (w), 819 (s), 784 (s), 768 (vs), 734 (s), 705 (m), 691 (m), 665 (m), 623 (w), 602 (m), 553 (m), 531 (w).

Anal. Calcd for $C_{54}H_{100}N_2VKO_6Si_2$: C, 63.61; H, 9.89; N, 2.75. Found: C, 63.36; H, 9.86; N, 2.65.

(tolN)V[N(Si^{i}Pr$_3$)DIPP]$_2$ (4.7). To a 20 mL scintillation vial was added **4.1** (0.100 g, 0.140 mmol) and toluene (3 mL). The resulting solution was stirred, and a solution of *p*-tolylazide (0.019 g, 0.140 mmol) in toluene (1.5 mL) was added dropwise. The reaction mixture was stirred at ambient temperature for 1 h. The resulting dark brown reaction mixture was concentrated under reduced pressure to a red residue. The residue was triturated with pentane (3 mL) in order to remove any remaining toluene, and the resulting red foam was extracted with pentane (5 mL total). The combined pentane extracts were filtered to give a dark orange-red solution, which was concentrated to 2 mL. Storage of this solution at -30 °C for three days, allowing for slow evaporation of the solvent, yielded 0.013 g (0.016 mmol, 11%) of **4.7** as dark red crystals, which were isolated by decanting the supernatant and removing residual volatile compounds *in vacuo*.

Crystals suitable for single crystal X-ray diffraction studies were obtained from the crystallization procedure described above.

Effective magnetic moment (Evans method, 400.13 MHz, C_6D_6, 21 °C): μ_{eff} = 1.6 μ_B.

The ^{1}H NMR spectrum of **4.7** in C_6D_6 contains non-distinctive, broad signals, attributed to the paramagnetism of **4.7**.

IR (KBr pellet) $\tilde{\nu}_{max}$ (cm^{-1}): 2966 (s), 2955 (s), 2925 (s), 2866 (s), 1489 (m), 1459 (s), 1420 (m), 1383 (m), 1362 (m), 1301 (s), 1251 (m), 1227 (m), 1163 (s), 1103 (s), 1066 (w), 1049 (w), 1011 (m), 987 (m), 920 (w), 882 (s), 842 (s), 819 (s), 784 (vs), 715 (vs), 658 (s), 632 (m), 588 (w), 527 (s).

Anal. Calcd for $C_{49}H_{83}N_3VSi_2$: C, 71.66; H, 10.19; N, 5.12. Found: C, 71.21; H, 10.12; N, 5.18.

[(DIPP)N]V[N(Si^{i}Pr$_3$)DIPP]I$_2$ (4.8).
Method A: To a Schlenk flask was added **4.1** (0.100 g, 0.140 mmol) and diethyl ether (6 mL). The resulting solution was stirred, and a solution of iodine (0.0355 g, 0.140 mmol) in diethyl ether (6 mL) was added dropwise *via* syringe. The reaction was stirred at ambient temperature for 20 min. The volatile components were then removed under reduced pressure, and the resulting residue was extracted with pentane (ca. 6 mL total). The combined pentane extracts were filtered and stored overnight at -30 °C over several days, to yield 0.021 g (0.026 mmol, 19%) of **4.8** as dark green crystals, which were isolated by decanting the supernatant and removing residual volatile compounds *in vacuo*. The brown supernatant was collected and concentrated to a residue. A second crystallization using the resulting residue with was set up in a similar fashion using 3 mL of pentane and yielded 0.014 g of **4.9** (0.017 mmol, 12%, based on **4.1**), confirmed by ^{1}H NMR spectroscopy.

Method B (optimized procedure): To a 20 mL scintillation vial was added **4.1** (0.050 g, 0.070 mmol) and diethyl ether (1.5 mL). The resulting solution was stirred, and a solution of iodine (0.027 g, 0.106 mmol, 1.5 equiv) in diethyl ether (1.5 mL) was added dropwise. The reaction was stirred at ambient temperature for 30 min. The volatile components were then removed under reduced pressure, and the resulting solid was triturated with pentane (3 mL) to remove any residual diethyl ether. The resulting solid was extracted with pentane (10 mL total). The combined pentane extracts were filtered, concentrated *in vacuo* to 6 mL, and stored overnight at -30 °C, to yield 0.037 g (0.046 mmol, 65%) of **4.8** as dark green crystals, which were isolated by decanting the supernatant and removing residual volatile compounds *in vacuo*.

Crystals suitable for single crystal X-ray diffraction studies were obtained from the crystallization procedure described above.

^{1}H NMR (500.23 MHz, C_6D_6, 290 K) δ 7.34 (t, 1 H, Ar-*H*), 7.16 (d, 2 H, Ar-*H*), 7.02 (d, 2 H, Ar-*H*), 6.96 (t, 1 H, Ar-*H*), 4.27 (br, 2 H, *H*C(CH$_3$)$_2$), 3.42 (hept, 2 H, *H*C(CH$_3$)$_2$), 1.82 (br, 3 H, *H*C(CH$_3$)$_2$), 1.47 (d, 6 H, HC(C*H*$_3$)$_2$), 1.33 (d, 12 H, HC(C*H*$_3$)$_2$), 1.26 (6 H, HC(C*H*$_3$)$_2$), 1.13 (d, 18 H, HC(C*H*$_3$)$_2$).

$^{13}C\{^{1}H\}$ NMR (150.93 MHz, C_6D_6, 297 K) δ 148.00, 147.56, 132.93, 126.62, 123.99, 34.02, 29.07, 28.86, 26.47, 26.10, 25.54, 22.30, 20.61 (br), 19.02, 16.41 (br), 13.86

IR (KBr pellet) $\tilde{\nu}_{max}$ (cm^{-1}): 2967 (s), 2868 (s), 1459 (s), 1413 (m), 1383 (s), 1362 (s), 1252 (m), 1225 (m), 1178 (m), 1158 (m), 1145 (m), 1101 (s), 1064 (m), 1049 (m), 1001 (w), 987 (m), 934 (m), 923 (m), 881 (s), 850 (vs), 809 (w), 788 (vs), 752 (s), 728 (s), 698 (m), 666 (s), 583 (m) 529 (w), 511 (s), 498 (s).

Anal. Calcd for $C_{33}H_{55}N_2VI_2Si$: C, 48.77; H, 6.82; N, 3.45. Found: C, 48.88; H, 7.06; N, 3.20.

(I)V[N(Si^{i}Pr$_3$)DIPP]$_2$ (4.9). To a 20 mL scintillation vial was added **4.1** (0.150 g, 0.209 mmol) and toluene (5 mL). The resulting solution was stirred, and silver iodide (0.050 g, 0.213 mmol, 1.02 equiv) was added in a single aliquot. The reaction mixture was stirred at ambient temperature for 3 h. The brown reaction mixture was concentrated under reduced pressure, and the resulting solid was extracted into pentane (10 mL total). The combined pentane extracts were filtered and stored at -30 °C for two days, to yield 0.059 g (0.070 mmol, 33%) of **4.9** as dark orange blocks, which were isolated by decanting the supernatant and removing residual volatile compounds *in vacuo*.

Crystals suitable for single crystal X-ray diffraction studies were obtained from the crystallization procedure described above.

Effective magnetic moment (Evans method, 400.13 MHz, C_6D_6, 22 °C): μ_{eff} = 2.6 μ_B.

^{1}H NMR (400.13 MHz, C_6D_6) δ 15.5 ($\nu_{1/2}$ = 50 Hz), 3.5 to -2.0 (br), 2.95 ($\nu_{1/2}$ = 170 Hz), 2.6 to 1.8 (br).

IR (KBr pellet) $\tilde{\nu}_{max}$ (cm^{-1}): 2951 (s), 2869 (s), 1464 (s), 1420 (s), 1385 (m), 1363 (m), 1302 (m), 1249 (m), 1224 (m), 1159 (s), 1144 (m), 1098 (s), 1065 (w), 1039 (w), 1013 (m), 981 (w), 920 (m), 881 (s), 838 (s), 816 (s), 779 (vs), 702 (vs), 675 (s), 640 (m), 596 (w), 530 (vs).

Anal. Calcd for $C_{42}H_{76}N_2VISi_2$: C, 59.83; H, 9.09; N, 3.32. Found: C, 59.97; H, 8.86; N, 3.15.

(TfO)V[N(Si^{i}Pr$_3$)DIPP]$_2$ (4.10). To a 20 mL scintillation vial was added **4.1** (0.050 g, 0.070 mmol) and toluene (1.5 mL). The resulting solution was stirred, and a solution of silver triflate (0.0187 g, 0.073 mmol, 1.04 equiv) in toluene (1.5 mL) was added dropwise. The reaction mixture was stirred at ambient temperature for 1 h. The brown reaction mixture was concentrated under reduced pressure, and the resulting solid was extracted with pentane (5 mL total). The combined pentane extracts were filtered, concentrated *in vacuo* to 2 mL, and stored at -30 °C for several days, to yield 0.022 g (0.025 mmol, 36%) of **4.10** as orange crystals, which were isolated by decanting the supernatant and removing residual volatile compounds *in vacuo*.

Crystals suitable for single crystal X-ray diffraction studies were obtained from the crystallization procedure described above.

Effective magnetic moment (Evans method, 400.13 MHz, C_6D_6, 21 °C): μ_{eff} = 2.7 μ_B.

^{1}H NMR (400.13 MHz, C_6D_6) δ 17.6 ($\nu_{1/2}$ = 90 Hz), 2.3 ($\nu_{1/2}$ = 170 Hz), -3.6 ($\nu_{1/2}$ = 2000 Hz).

IR (KBr pellet) $\tilde{\nu}_{max}$ (cm^{-1}): 2953 (s), 2870 (s), 1464 (s), 1419 (m), 1386 (m), 1356 (s), 1300 (w), 1238 (s), 1221 (w), 1198 (vs), 1163 (s), 1097 (m), 1067 (w), 1051 (w), 1039 (m), 1015 (m), 990 (s), 920 (w), 883 (m), 836 (s), 815 (m), 780 (vs), 700 (s), 680 (m), 646 (m), 630 (s), 594 (w), 530 (s).

Anal. Calcd for $C_{43}H_{76}N_2VF_3SO_3Si_2$: C, 59.69; H, 8.85; N, 3.24. Found: C, 59.50; H, 8.57; N, 3.23.

{V[κ^2-*N*(Si^{i}Pr$_3$)(2-CH(Me)*C*H-6-isopropylphenyl)][(DIPP)NH(Si^{i}Pr$_3$)]}{B(C$_6$F$_5$)$_4$} (4.11). To a 20 mL scintillation vial was added **4.1** (0.036 g, 0.050 mmol) and 1,2-difluorobenzene (1.5 mL); the resulting solution was cooled to -30 °C. The cooled mixture of **4.1** was stirred, and a solution of ferrocenium tetrakis(pentafluorophenyl)borate (0.043 g, 0.050 mmol) in 1,2-difluorobenzene (1.5 mL) was added dropwise. The reaction mixture was stirred at ambient temperature for 1 h. The dark orange-red reaction mixture was concentrated under reduced pressure, and the resulting residue was triturated with pentane (3 mL) in order to ensure the removal of any remaining volatile components. The resulting residue was washed with six portions of 1.5 mL of pentane, and residual volatile components were removed *in vacuo* to give an orange foam. The orange foam was dissolved in 1,2-difluorobenzene (1.5 mL); the resulting orange solution was filtered and combined with 1.5 mL of toluene, upon which was layered pentane (3 mL). The layered solution was stored at -30 °C for several days to yield 0.020 g (0.014 mmol, 28%) of **4.11** as orange crystals, which were isolated by decanting the supernatant and removing residual volatile compounds *in vacuo*.

Crystals suitable for single crystal X-ray diffraction studies were obtained from the crystallization procedure described above.

Effective magnetic moment (Evans method, 400.13 MHz, 1,2-difluorobenzene with Si(SiMe$_3$)$_4$ added as a reference, 21°C): μ_{eff} = 2.8 μ_B.

IR (KBr pellet) $\tilde{\nu}_{max}$ (cm^{-1}): 3376 (w, ν_{N-H}), 2957 (m), 2872 (m), 1643 (m), 1514 (s), 1463 (s), 1370 (m), 1346 (m), 1304 (w), 1275 (m), 1172 (w), 1088 (s), 981 (vs), 896 (m), 878 (m), 831 (w), 775 (m), 756 (m), 729 (m), 685 (s), 662 (s).

Anal. Calcd for $C_{66}H_{76}N_2VBF_{20}Si_2$: C, 56.82; H, 5.49; N, 2.01. Found: C, 57.02; H, 5.34; N, 1.88.

Crude product from the synthesis of 4.11, prior to crystallization. To a 20 mL scintillation vial was added **4.1** (0.020 g, 0.028 mmol) and 1,2-difluorobenzene (1.5 mL). The solution of **4.1** was stirred, and a solution of ferrocenium tetrakis(pentafluorophenyl)borate (0.024 g, 0.028 mmol) in 1,2-difluorobenzene (1.5 mL) was added dropwise. The reaction was stirred at ambient temperature for 1 h. The dark orange-red reaction mixture was concentrated under reduced pressure, and the resulting residue was washed with ten portions of 0.5 mL of pentane. Residual volatile components were removed *in vacuo*. The resulting orange residue was dissolved in 1,2-difluorobenzene (1.5 mL); the resulting orange solution was filtered, then concentrated under

reduced pressure back to a residue. The residue was triturated with pentane (1.5 mL) to give 0.036 g of an orange foam. The IR spectrum of the crude product contained features consistent with that of crystallized **4.11** (*vide supra*).

IR (KBr pellet) $\tilde{\nu}_{max}$ (cm^{-1}): 3377 (w), 3278 (vw), 3244 (vw), 2962 (m), 2872 (m), 1643 (m), 1514 (s), 1465 (vs), 1370 (m), 1345 (w), 1305 (vw), 1275 (m), 1170 (w), 1088 (s), 892(m), 981 (vs), 881 (m), 858 (m), 828 (vw), 797 (m), 775 (m), 756 (m), 726 (w), 685 (m), 662 (m).

Reaction of 4.10 with Li[B(C_6F_5)$_4$]. To a 20 mL scintillation vial was added **4.10** (0.036 g, 0.042 mmol) and 1,2-difluorobenzene (1.5 mL). The solution of **4.10** was stirred, and a solution of Li[B(C_6F_5)$_4$] (0.029 g, 0.042 mmol) in 1,2-difluorobenzene (1.5 mL) was added dropwise. The reaction was stirred at ambient temperature for 1.5 h. The dark red reaction mixture was concentrated under reduced pressure to a red residue, which was washed with pentane (2 x 1.5 mL). The resulting orange foam was dissolved in 1,2-difluorobenzene (3 mL); the resulting orange solution was filtered, then concentrated under reduced pressure back to a residue. The residue was triturated with pentane (1.5 mL) to give 0.054 g of an orange foam. The IR spectrum of the product contained features consistent with that of the crude product from the synthesis of **4.11** (*vide supra*).

IR (KBr pellet) $\tilde{\nu}_{max}$ (cm^{-1}): 3376 (w), 3277 (vw), 3242 (vw), 2960 (m), 2872 (m), 1643 (m), 1514 (s), 1465 (vs), 1370 (m), 1345 (w), 1308 (w), 1273 (m), 1226 (w), 1198 (w), 1173 (vw), 1087 (s), 980 (vs), 894 (m), 879 (m), 858 (m), 830 (vw), 797 (m), 775 (m), 756 (m), 727 (m), 685 (m), 662 (m).

SUPPLEMENTARY FIGURES

Figure S4.1: Solid-state structure of **4.1** as determined by single-crystal X-ray diffraction.

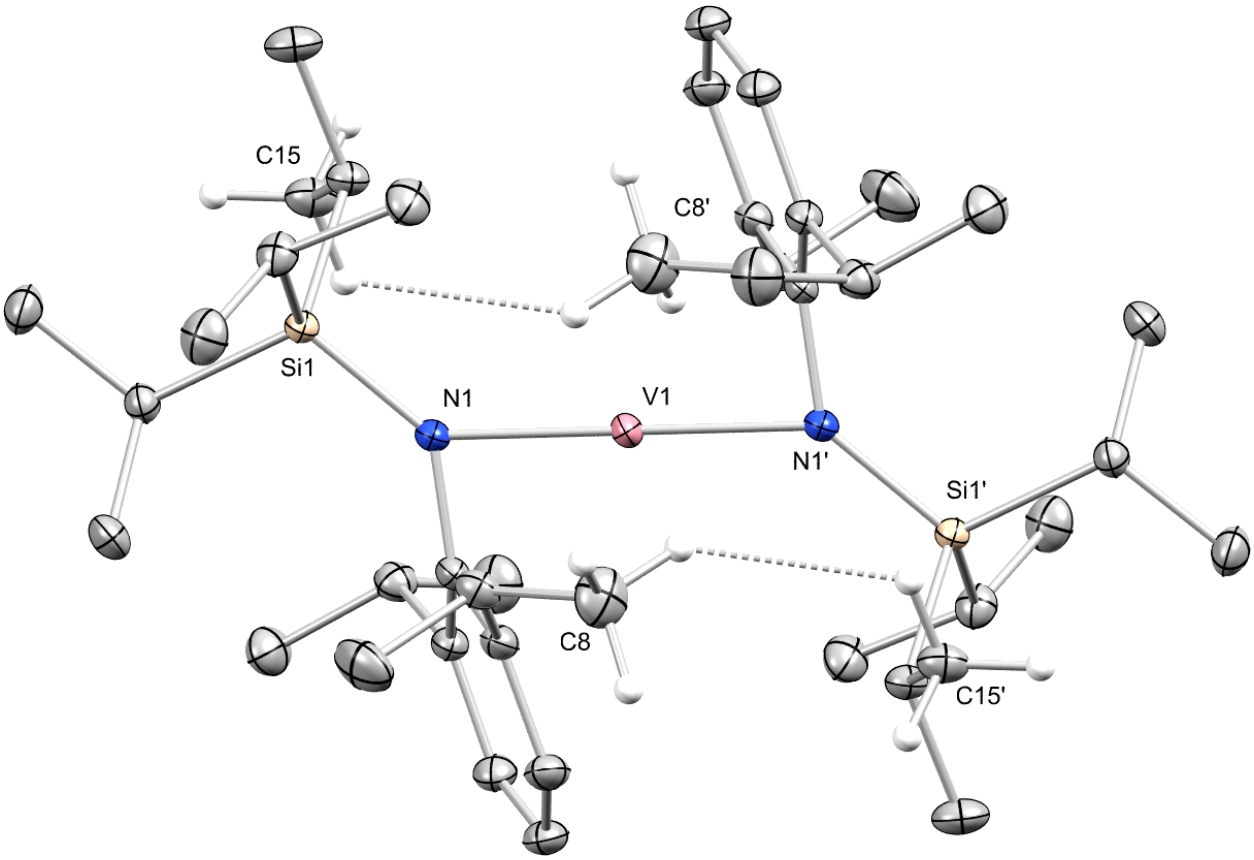

Notes: Thermal ellipsoids shown at 50% probability. Hydrogen atoms have been omitted for clarity, with the exception of hydrogen atoms on C8 and C15, which have been located from the electron density difference map.

Figure S4.2: Solid-state structure of Cr[N(Si^{t}Bu$_2$Me)DIPP]$_2$ as determined by single-crystal X-ray diffraction.

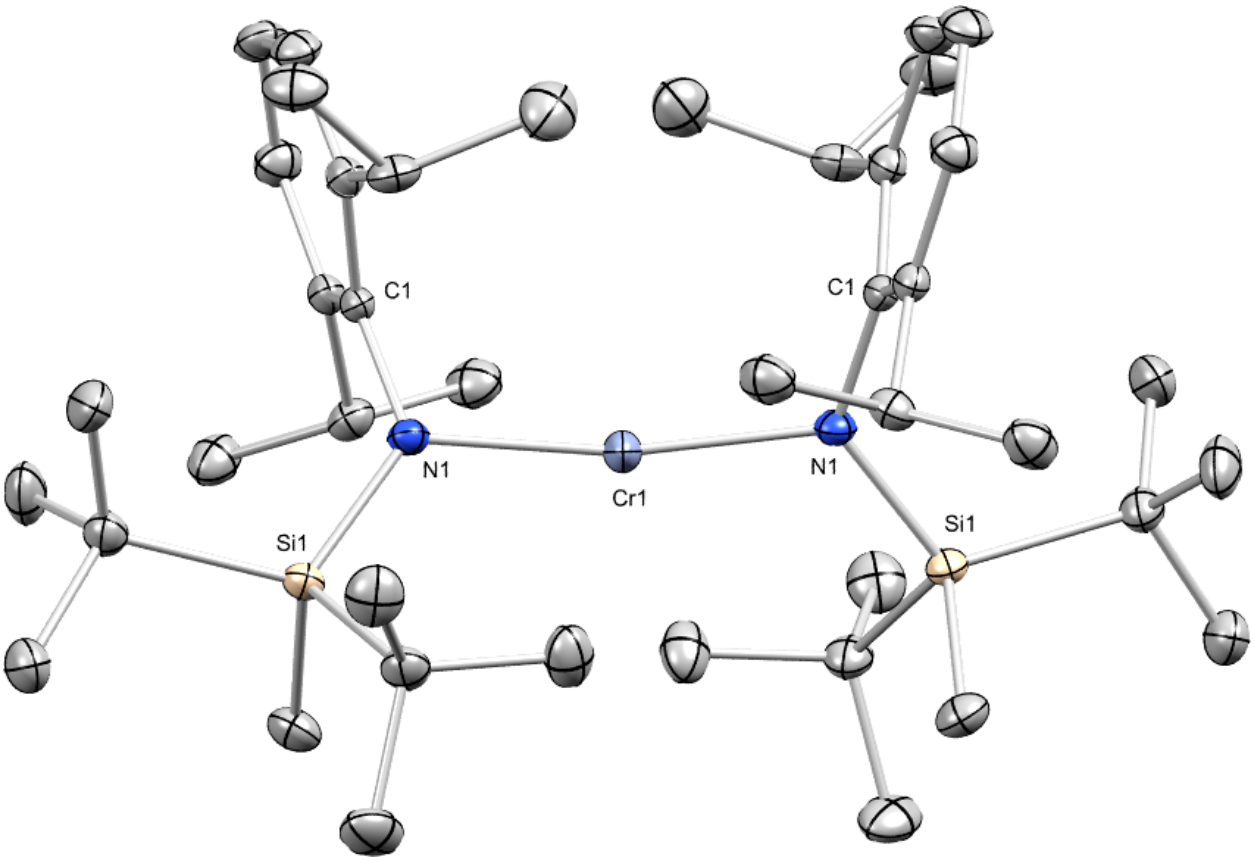

Notes: Thermal ellipsoids shown at 50% probability. Hydrogen atoms have been omitted for clarity. Selected bond distances [Å], angles [°], and torsions [°]: Cr1–N1: 1.979(2), Cr1–C1: 2.830(3), N1–Cr1–N1': 169.80(14), Cr1–N1–C1: 110.97(17), C1–N1–N1'–C1': ±53.0(2).

Figure S4.3: Variable frequency out-of-phase (χ'') molar magnetic susceptibility for V[N(Si^{i}Pr$_3$)(DIPP)]$_2$ (**4.1**, restrained with glass wool) under an applied dc fields of 2000 Oe over the temperature range 2-3 K.

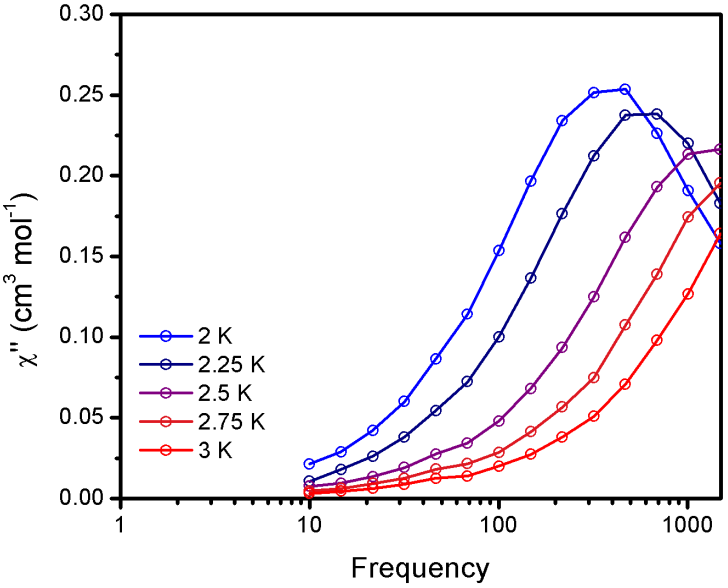

Figure S4.4: Variable frequency out-of-phase (χ'') molar magnetic susceptibility for V[(η^5-DIPP)N(Si^{t}Bu$_2$Me)]$_2$ (**4.2**, restrained with eicosane) under an applied dc fields of 2000 Oe over the temperature range 2-3 K.

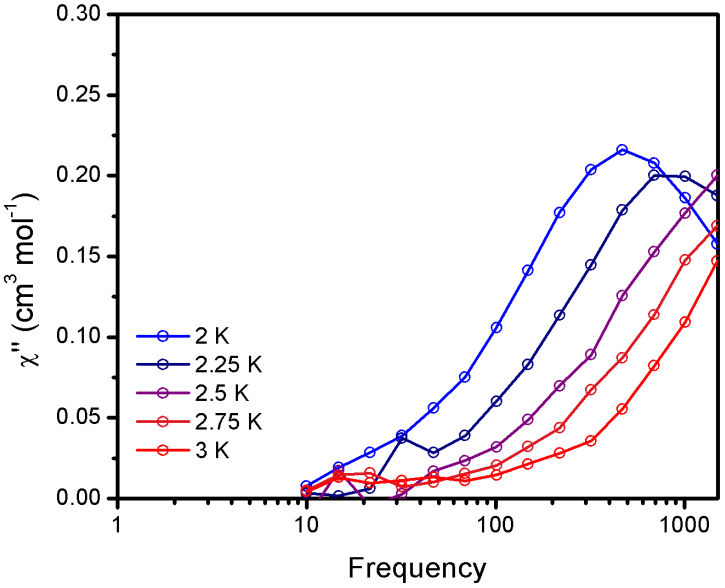

Figure S4.5: X-band EPR spectrum of V[(η^5-DIPP)N(Si^{t}Bu$_2$Me)]$_2$ (**4.2**, solid-state)

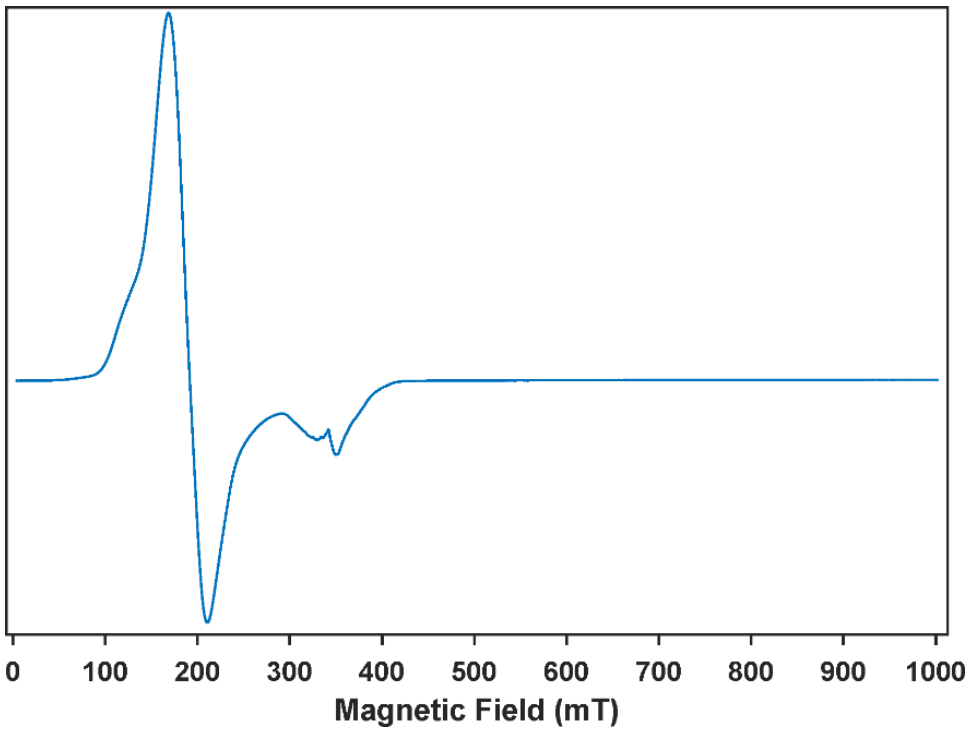

Figure S4.6: X-band EPR spectrum of V[N(Si^{i}Pr$_3$)(DIPP)]$_2$ (**4.1**, solid-state)

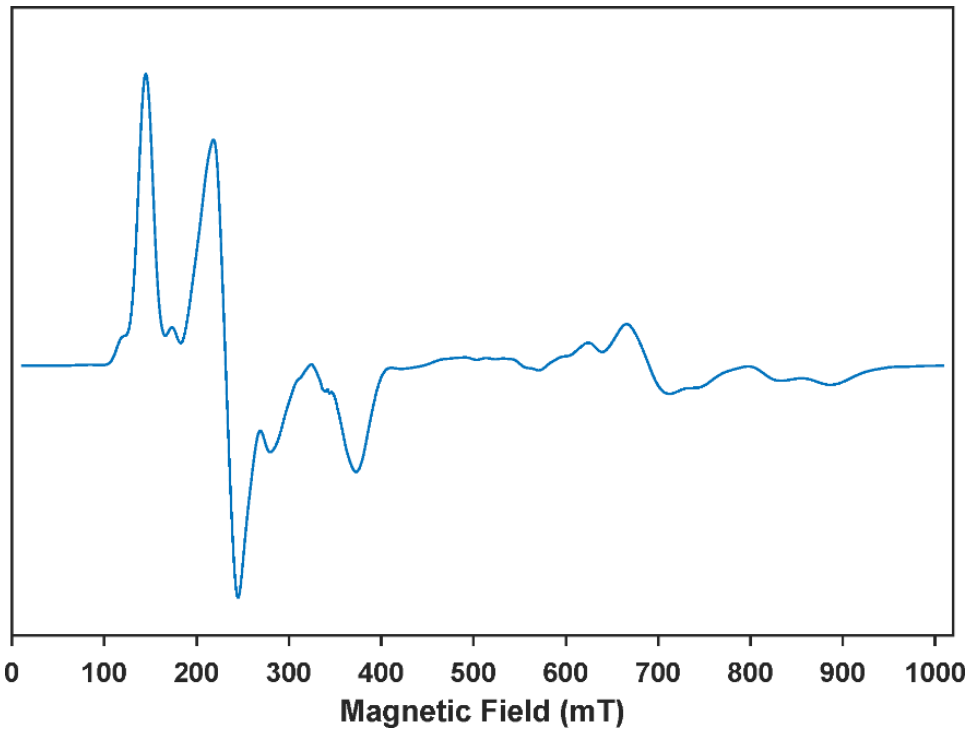

Figure S4.7: X-band EPR spectrum of a 4.0 mM solution of V[N(Si^{i}Pr$_3$)(DIPP)]$_2$ (**4.1**) in pentane, immediately after dissolution

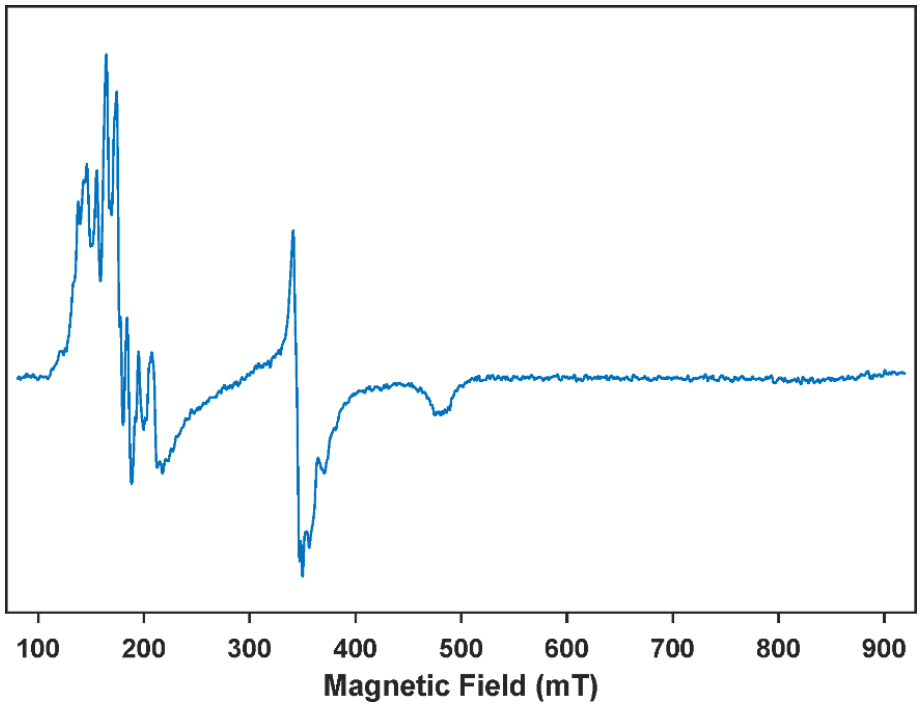

Figure S4.8: X-band EPR spectrum of a 4.0 mM solution of V[N(Si^{i}Pr$_3$)(DIPP)]$_2$ (**4.1**) in pentane, after ca. 1 h standing at 21 °C

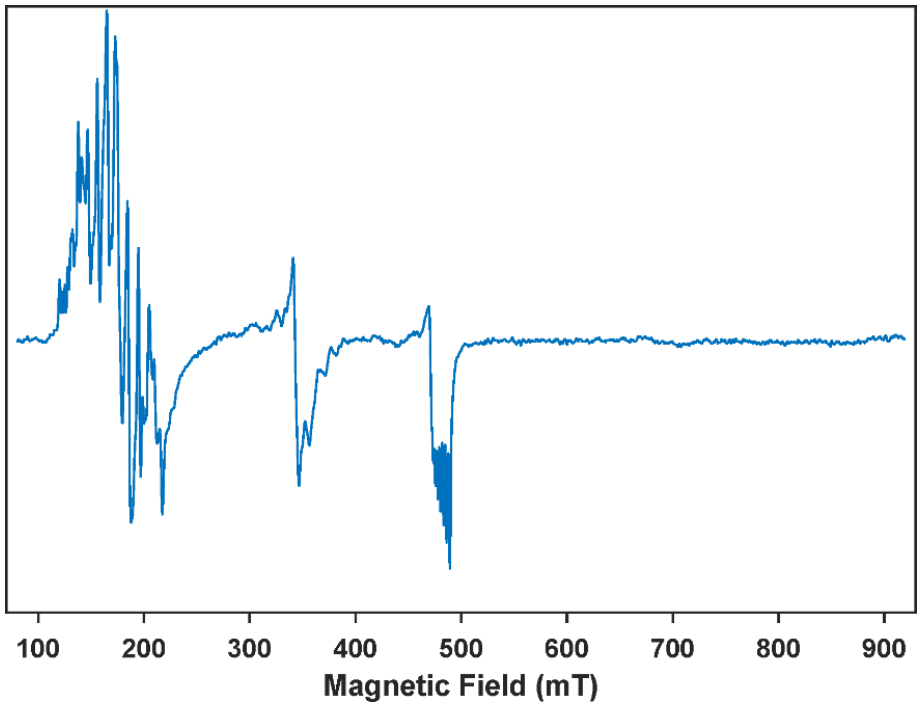

Figure S4.9: ^{1}H NMR of V[N(Si^{i}Pr$_3$)(DIPP)]$_2$ (**4.1**) in benzene-d_6 at various intervals following dissolution

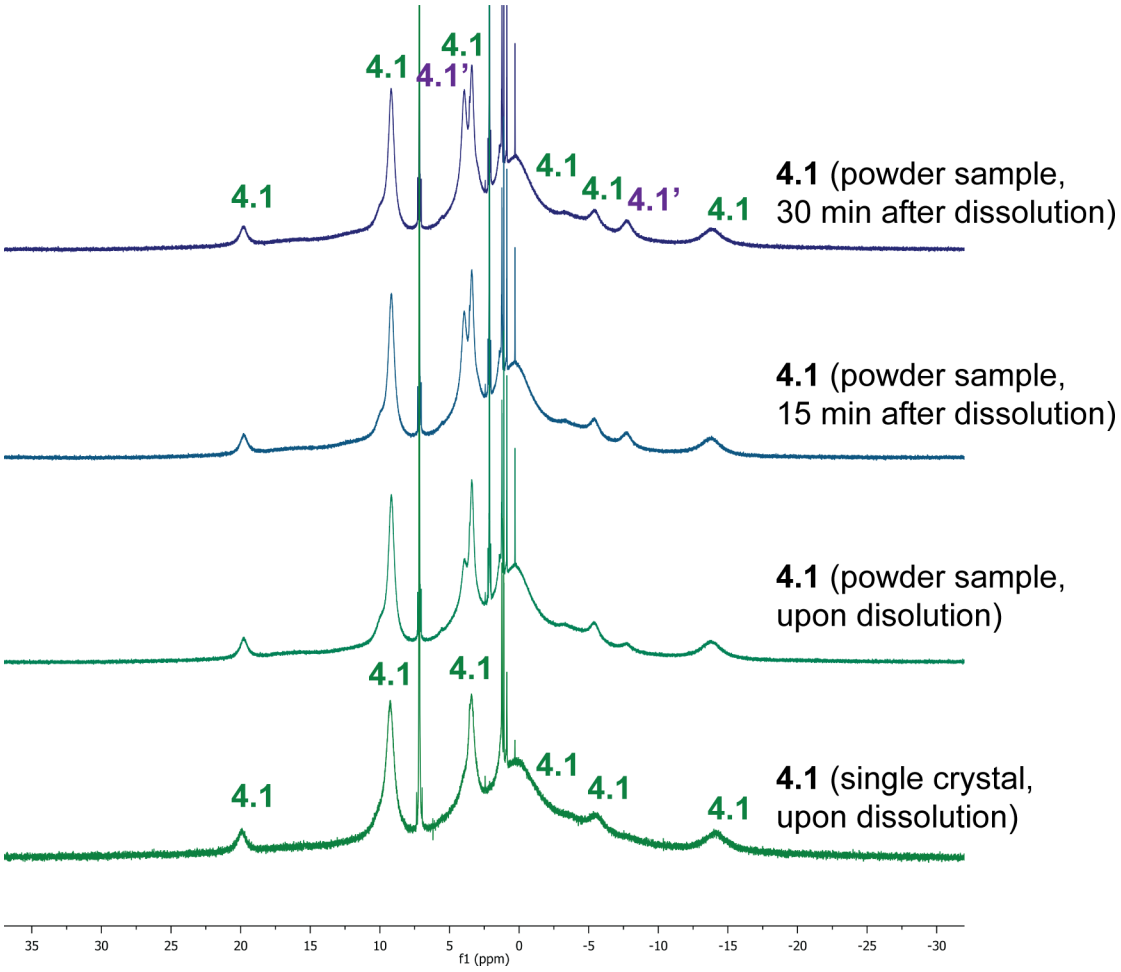

Notes: Hexamethylbenzene added as an internal standard to powder sample of **4.1** in benzene-d_6.

Figure S4.10: UV-Visible spectrum of V[N(Si^{i}Pr$_3$)(DIPP)]$_2$ (**4.1**) in pentane (0.79 mM) at 30 °C, at 5 minute intervals following dissolution and insertion of the sample into the spectrometer ; inset: spectrum of V[N(Si^{i}Pr$_3$)(DIPP)]$_2$ (**4.1**) in pentane (6.7 mM) at 30 °C, at 5 minute intervals following dissolution and insertion of the sample into the spectrometer, from 750 to 1100 nm.

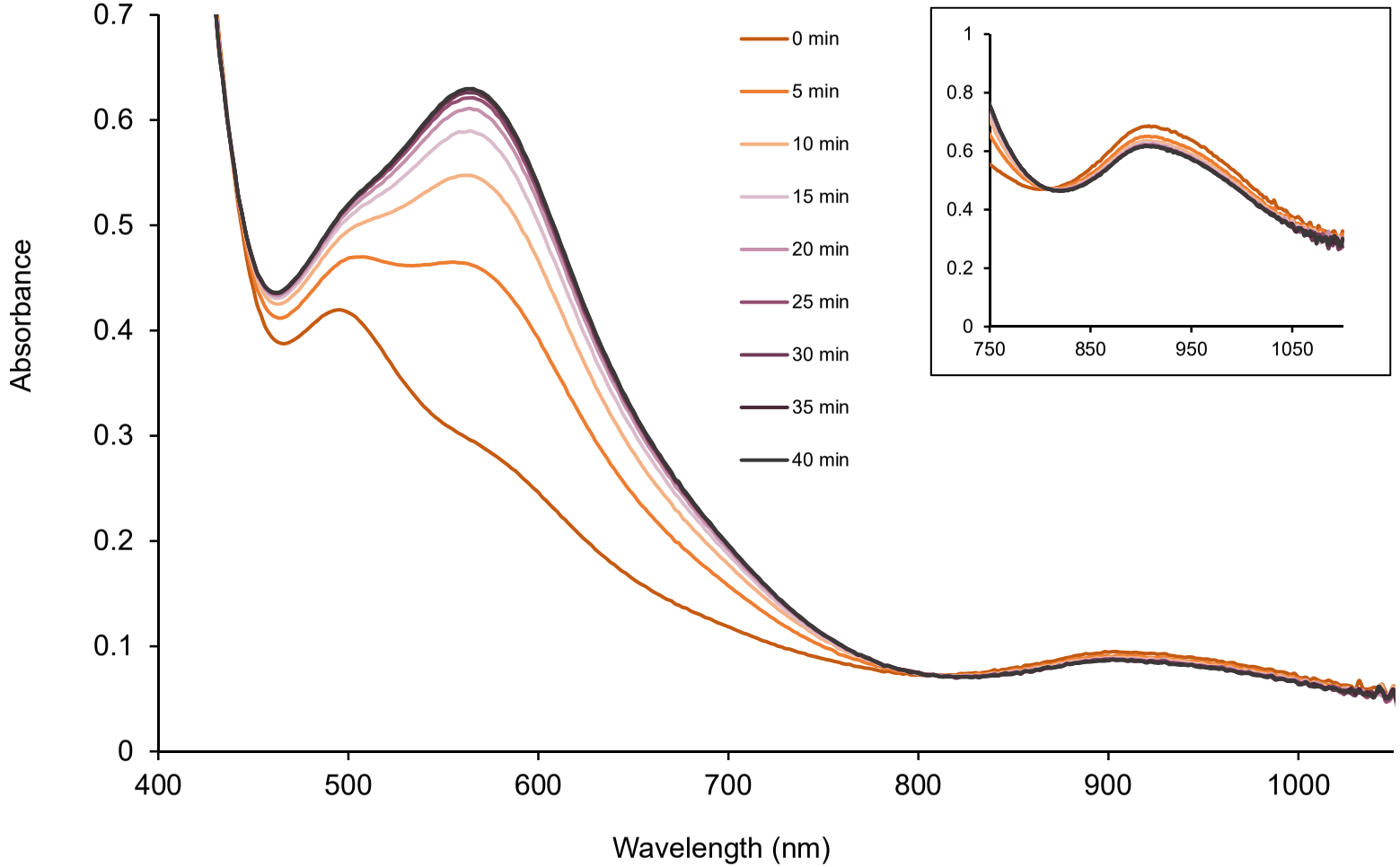

Figure S4.11: IR spectra of V[N(Si^{i}Pr$_3$)(DIPP)]$_2$ (**4.1**, KBr pellet) and V[(η^5-DIPP)N(Si^{t}Bu$_2$Me)]$_2$ (**4.2**, KBr pellet)

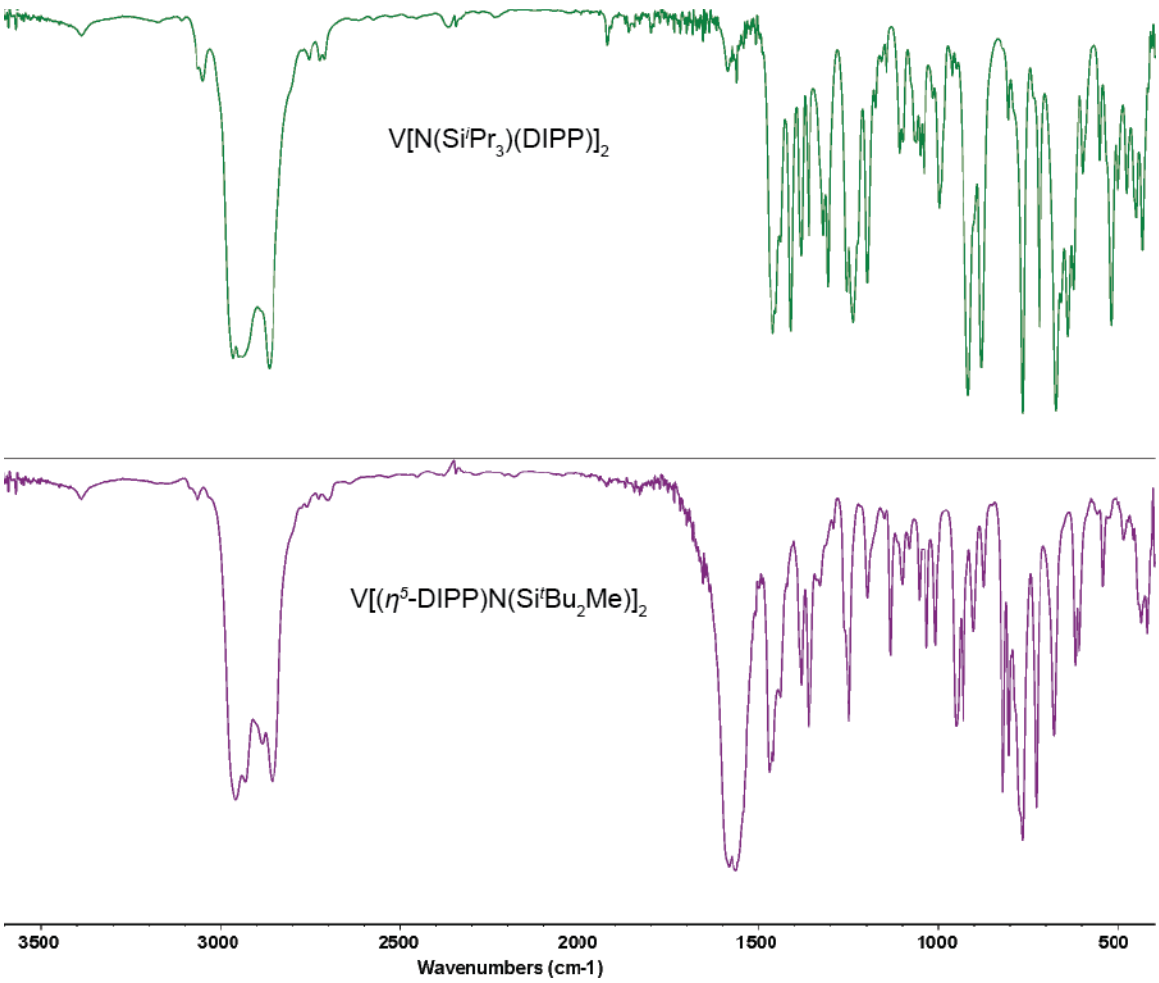

Figure S4.12: ^{1}H NMR of V[N(Si^{i}Pr$_3$)(DIPP)]$_2$ (**4.1**) in benzene-d_6 at various intervals following the addition of 1-cyanoadamantane, 1 h after the dissolution of **4.1**

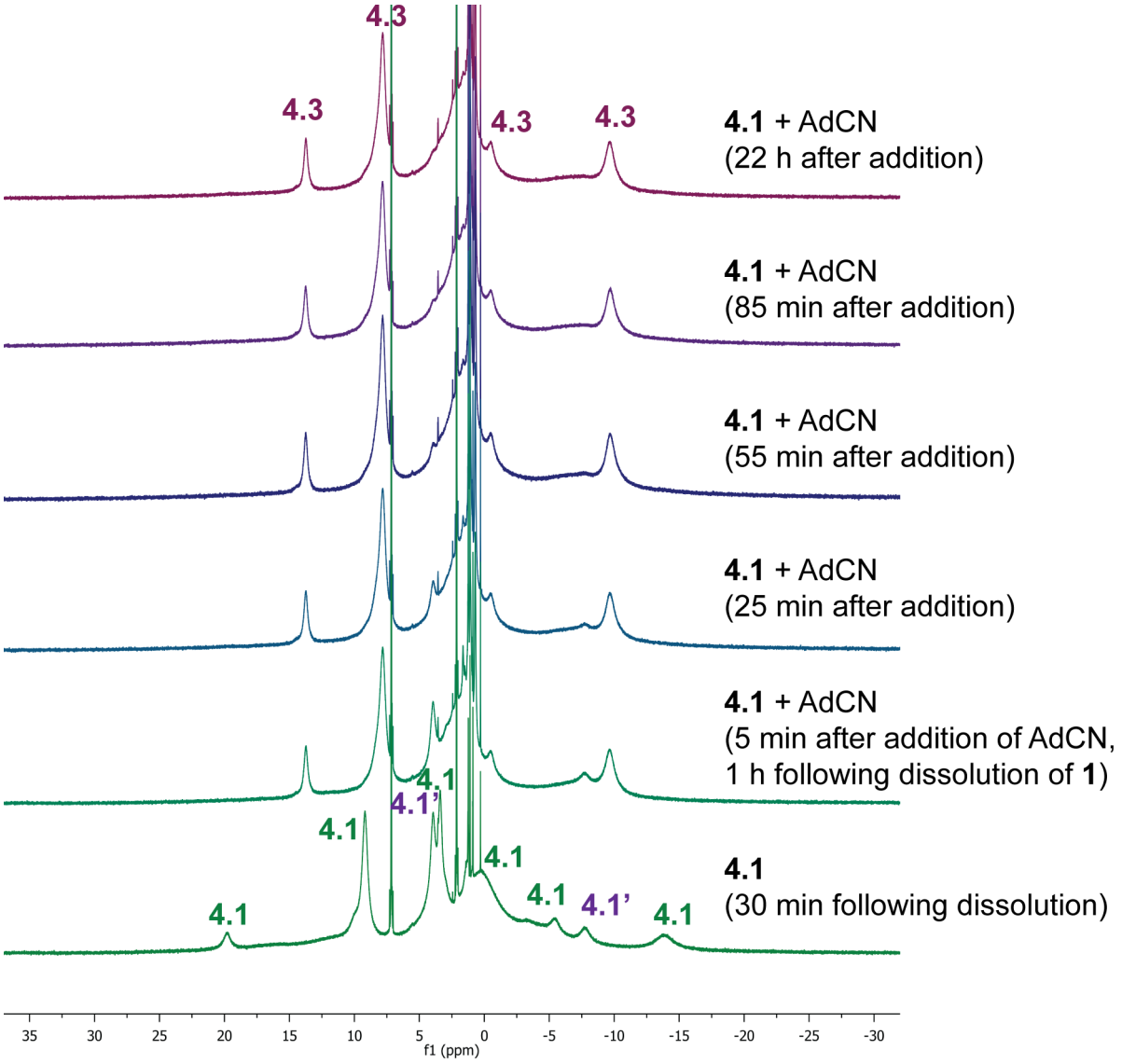

Notes: Hexamethylbenzene added as an internal standard.

Figure S4.13. Solid state structure of complex **4.5** as determined by single-crystal X-ray diffraction

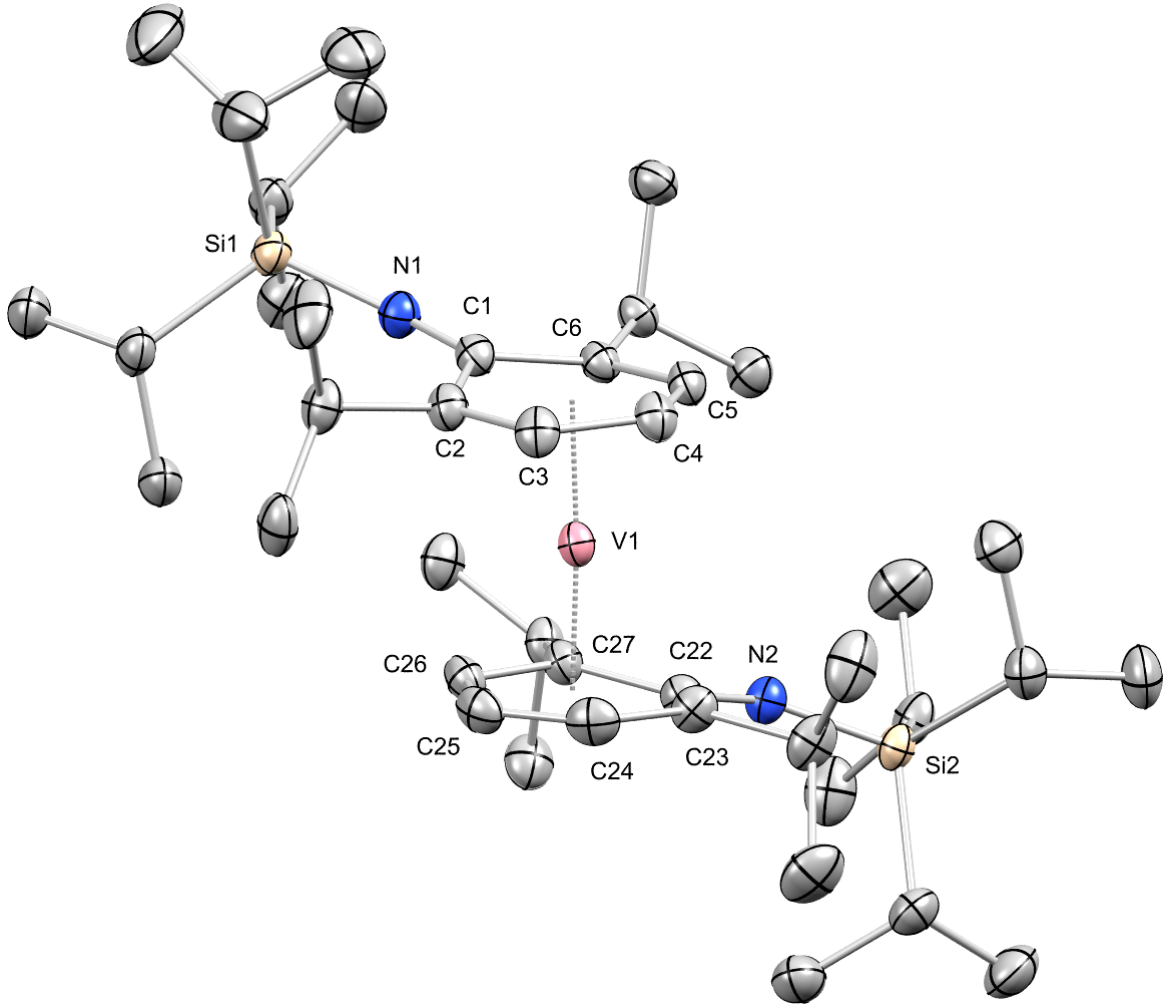

Notes: Thermal ellipsoids shown at 50% probability. Hydrogen atoms, cation, and solvent molecules have been omitted for clarity. Selected bond distances [Å] and angles [°]: N1–C1: 1.313(3), N2–C22: 1.311(3), N1–Si1: 1.671(2), N2–Si2: 1.663(2), distance between V1 and least-squares plane of (C2, C3, C4, C5, C6): 1.755, distance between V1 and least-squares plane of (C23, C24, C25, C26, C27): 1.759, V1–C1: 2.498(2), V1–C22: 2.511(2); C1–N1–Si1: 155.59(18), C22–N2–Si2: 153.02(18).

Figure S4.14: Cyclic voltammogram recorded for a 1.0 mM solution of **4.1** in 1,2-difluorobenzene

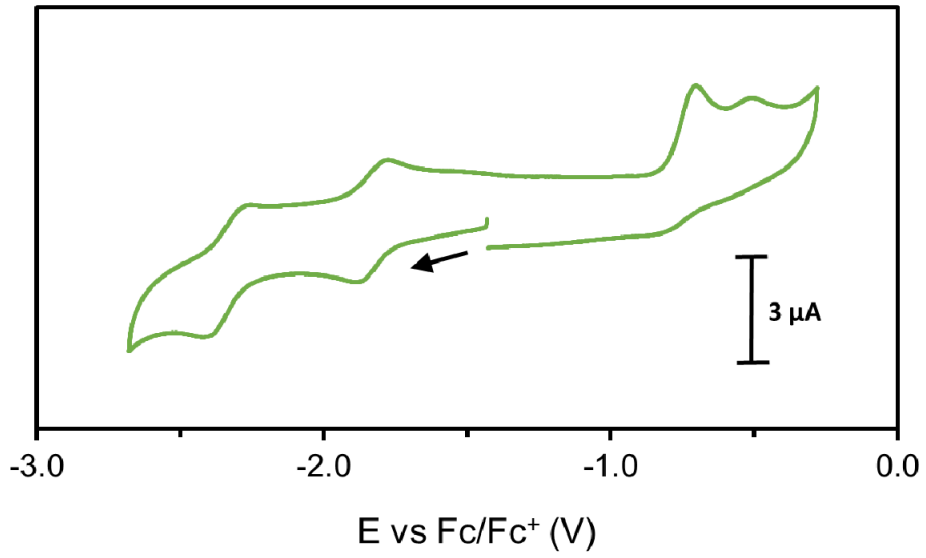

Notes: Solution contained 0.1 M [^{n}Bu$_4$N][PF$_6$] as supporting electrolyte. The arrow indicates the initial potential and scanning direction. The voltammogram displays one complete cycle (3 segments) and was recorded at 100 mV/s.

Figure S4.15: Cyclic voltammogram recorded for a 1.0 mM solution of **4.2** in 1,2-difluorobenzene

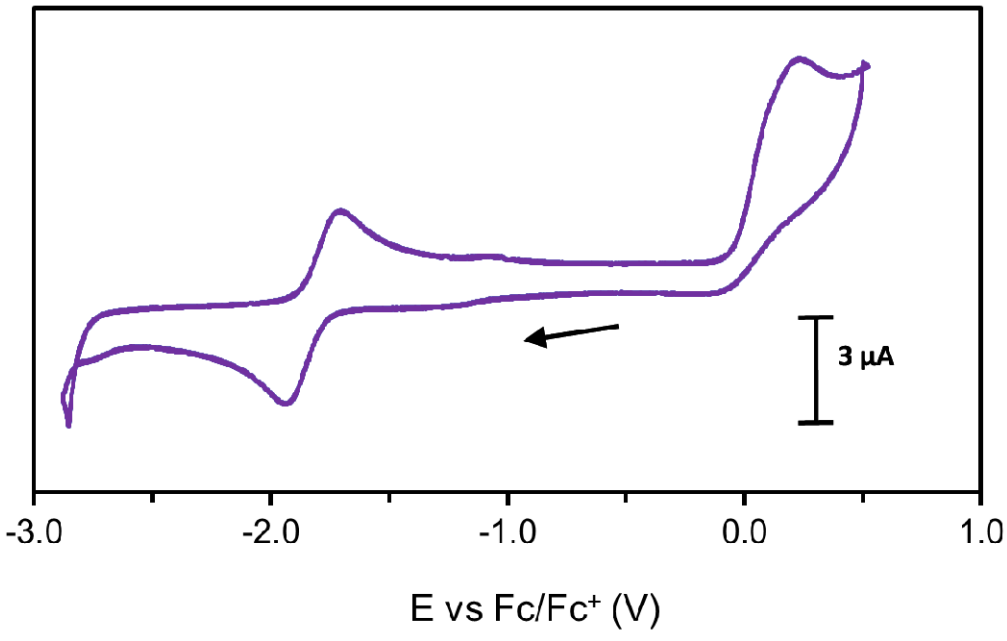

Notes: Solution contained 0.1 M [^{n}Bu$_4$N][PF$_6$] supporting electrolyte. The arrow indicates the initial potential and scanning direction. The voltammogram displays one complete cycle (3 segments) and was recorded at 100 mV/s.

Figure S4.16: Cyclic voltammograms recorded at multiple scan rates for a 1.0 mM solution of **4.2** in 1,2-difluorobenzene

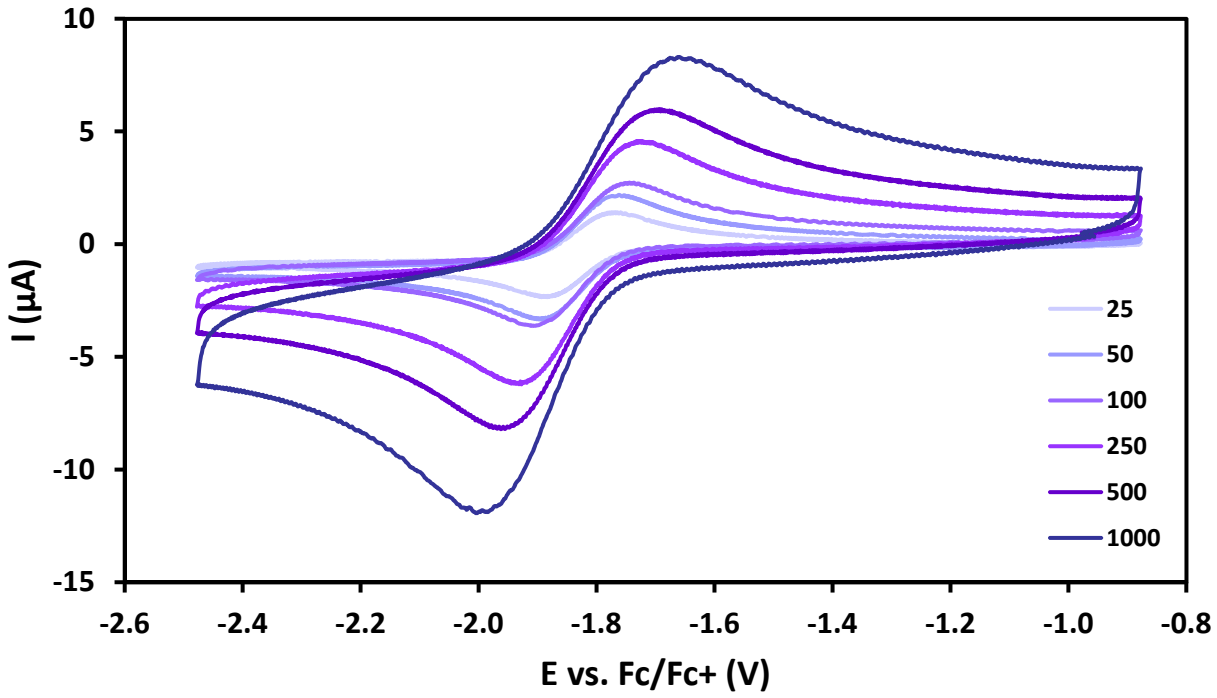

Notes: Solution contained 0.1 M [^{n}Bu$_4$N][PF$_6$] supporting electrolyte. Each voltammogram displays one complete cycle (3 segments).

Figure S4.17: Scan rate dependence of cyclic voltammograms' peak currents of a 1.0 mM solution of **4.2** in 1,2-difluorobenzene

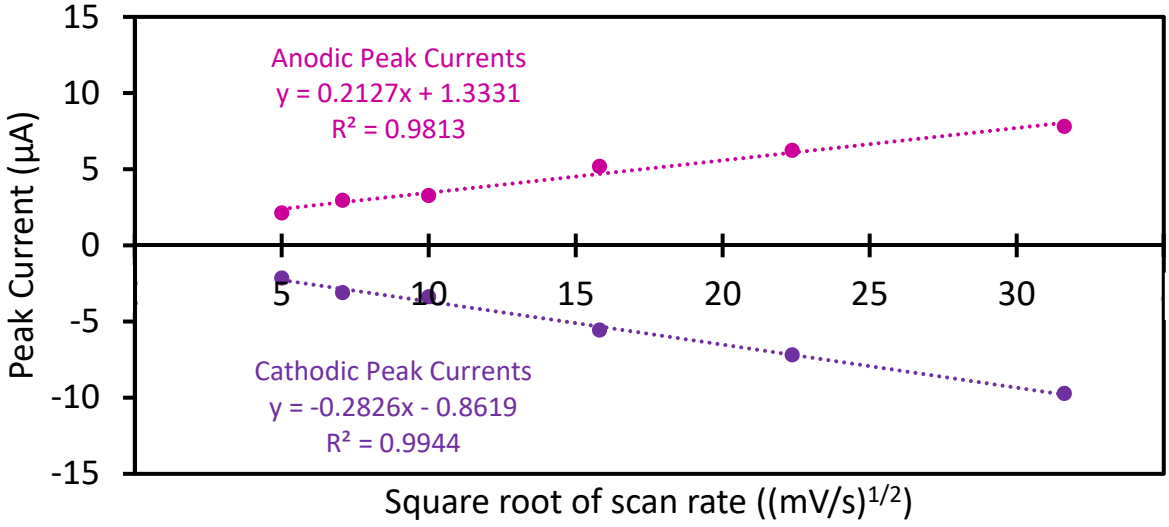

Figure S4.18: Cyclic voltammogram recorded for a 1.0 mM solution of **4.5** in 1,2-difluorobenzene

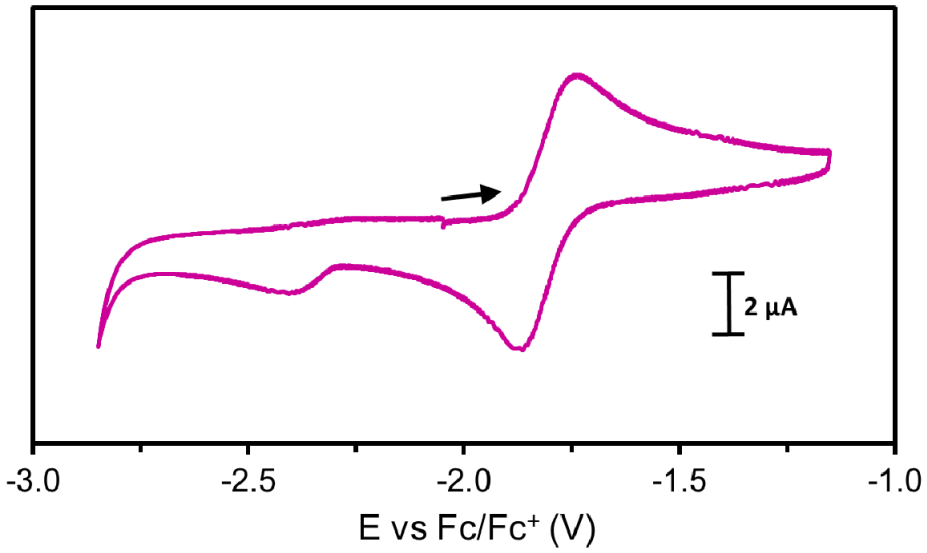

Notes: Solution contained 0.1 M [^{n}Bu$_4$N][PF$_6$] supporting electrolyte. The arrow indicates the initial potential and scanning direction for all scans. The voltammogram displays one complete cycle (3 segments) and was recorded at 100 mV/s.

Figure S4.19: Cyclic voltammograms recorded at multiple scan rates for a 1.0 mM solution of **4.5** in 1,2-difluorobenzene

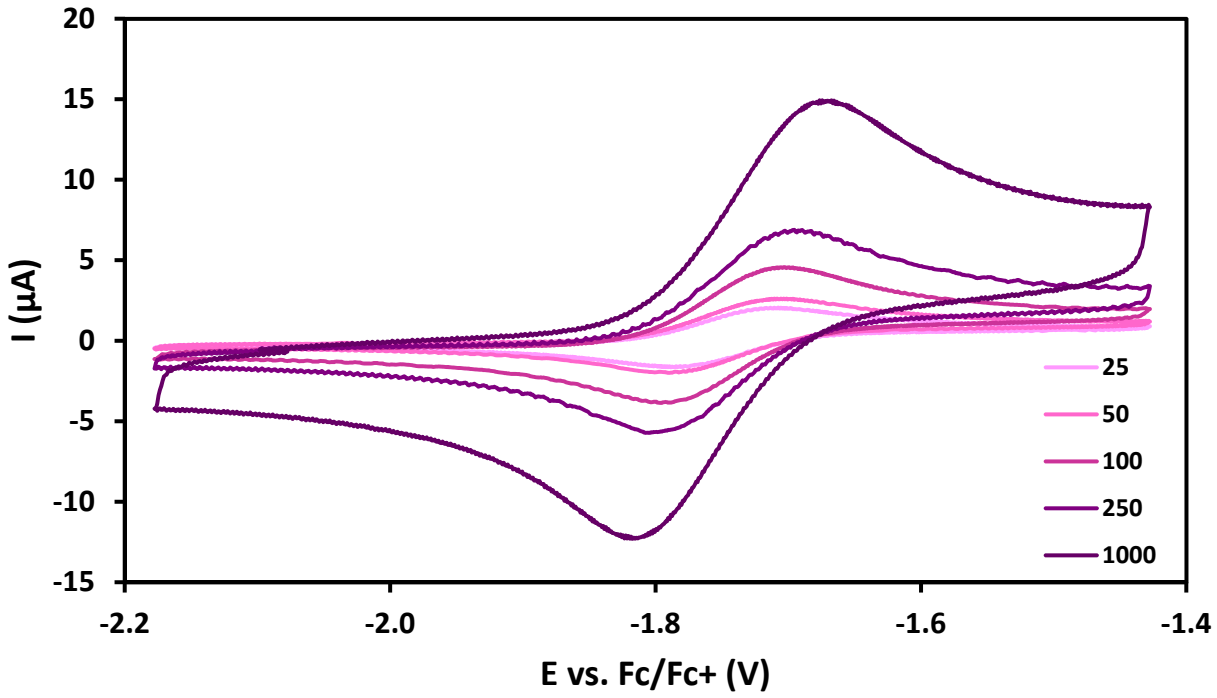

Notes: Solution contained 0.1 M [^{n}Bu$_4$N][PF$_6$] supporting electrolyte. Each voltammogram displays one complete cycle (3 segments).

Figure S4.20: Scan rate dependence of cyclic voltammograms' peak currents of a 1.0 mM solution of **4.5** in 1,2-difluorobenzene

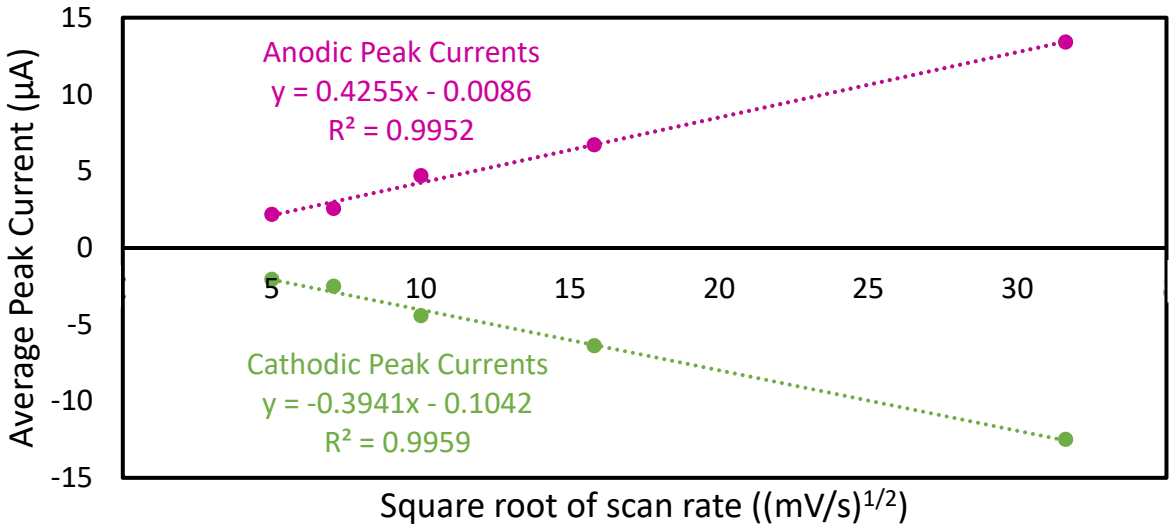

Figure S4.21: ^{1}H NMR of $I_2V[N(DIPP)][N(Si^iPr_3)(DIPP)]$ (**4.8**) in toluene-d_8, from 370 K (top) to 290 K (bottom).

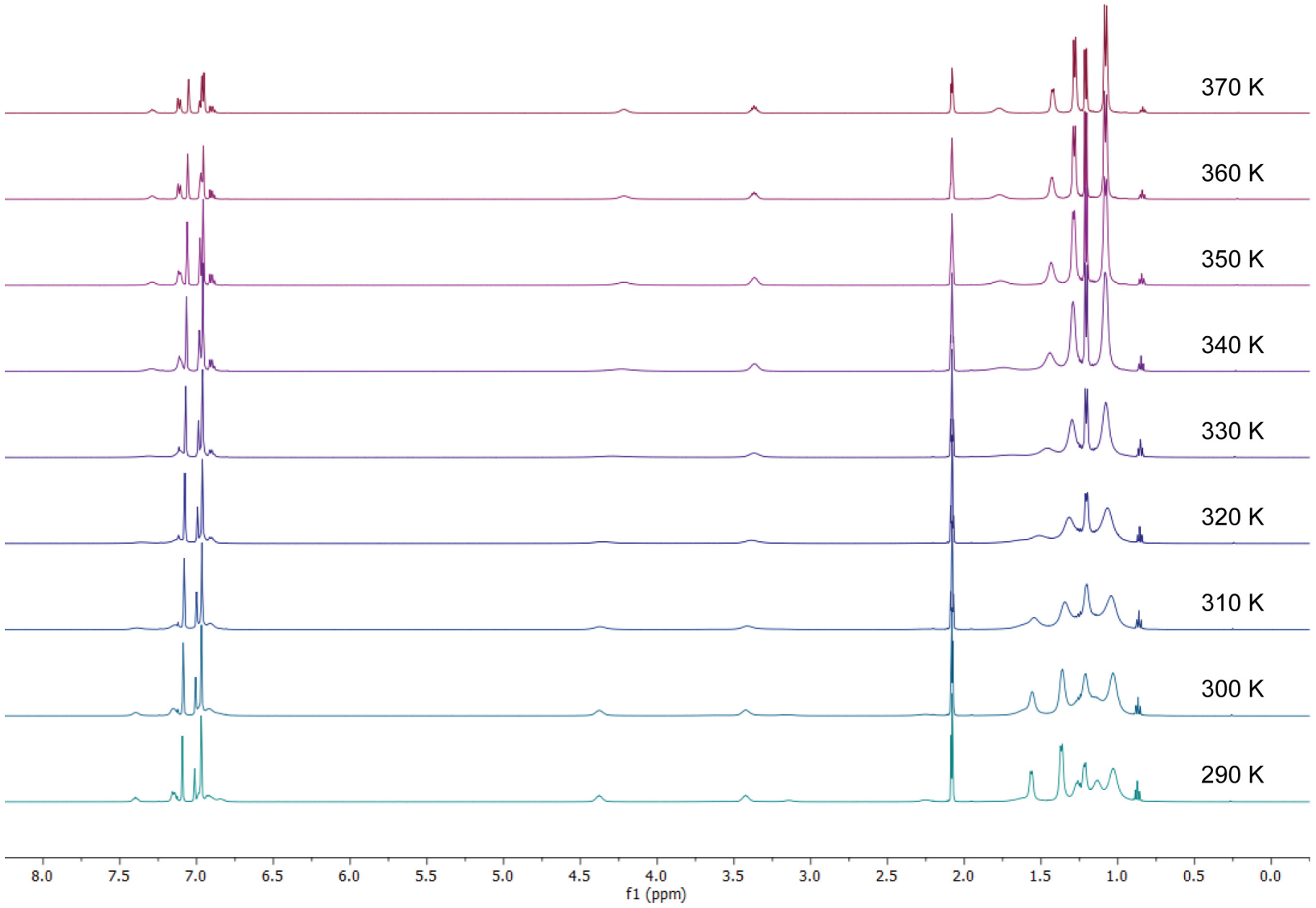

Notes: All spectra were referenced to the residual proton solvent peak (δ 2.08 ppm).

Figure S4.22: ^{1}H NMR of $I_2V[N(DIPP)][N(Si^iPr_3)(DIPP)]$ (**4.8**) in toluene-d_8, from 290 K (top) to 200 K (bottom).

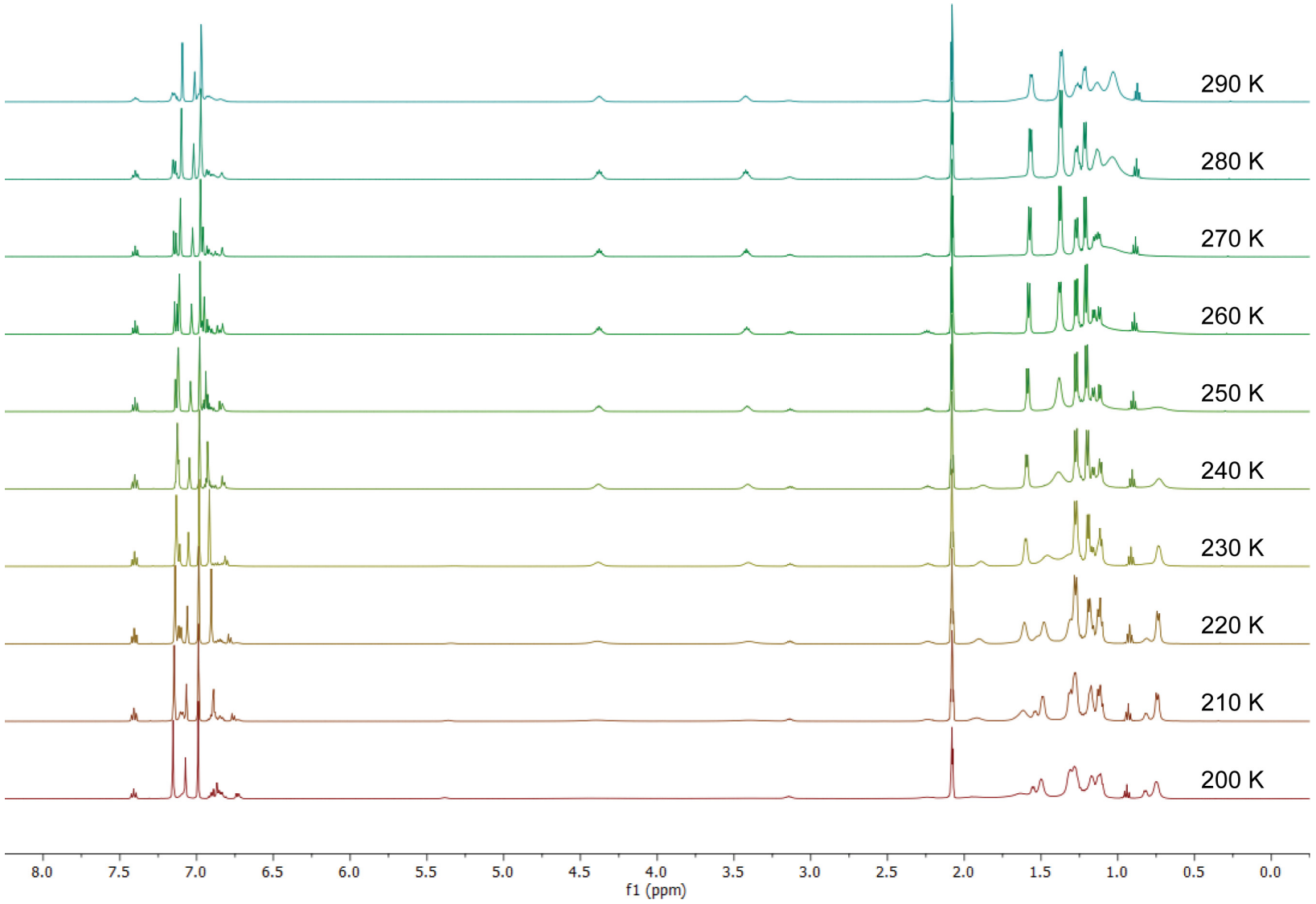

Notes: All spectra were referenced to the residual proton solvent peak (δ 2.08 ppm).

Figure S4.23: IR spectra of crystallized **4.11** (blue trace), crude **4.11** (green trace), and 1,2-difluorobenzene-soluble crude products resulting from the reaction of **4.10** with $Li[B(C_6F_5)_4]$ (orange trace), prepared as KBr pellets.

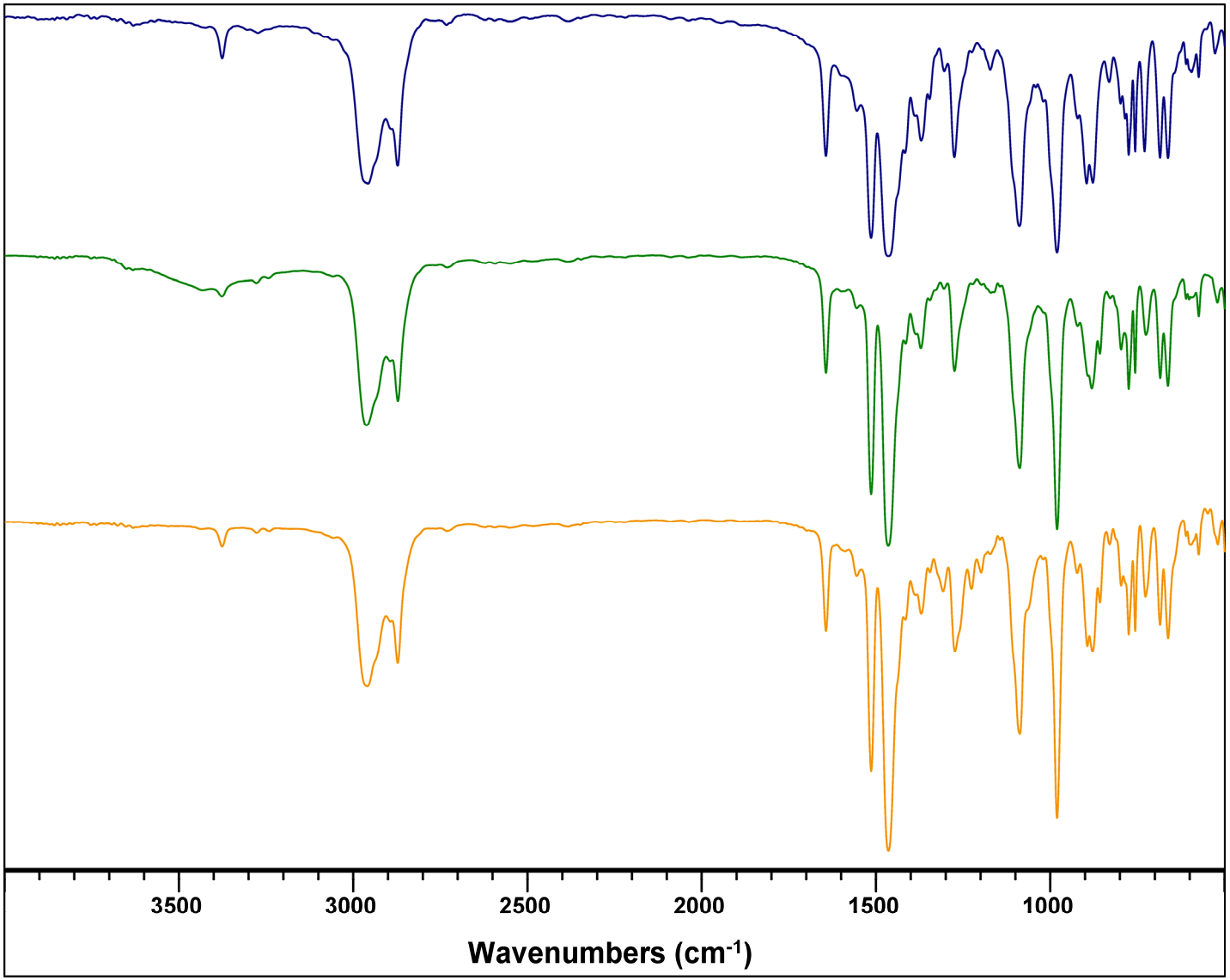

SINGLE-CRYSTAL X-RAY DIFFRACTION CRYSTAL STRUCTURE DETAILS

Figure SX4.1. Solid state structure of complex **4.1** as determined by single-crystal X-ray diffraction

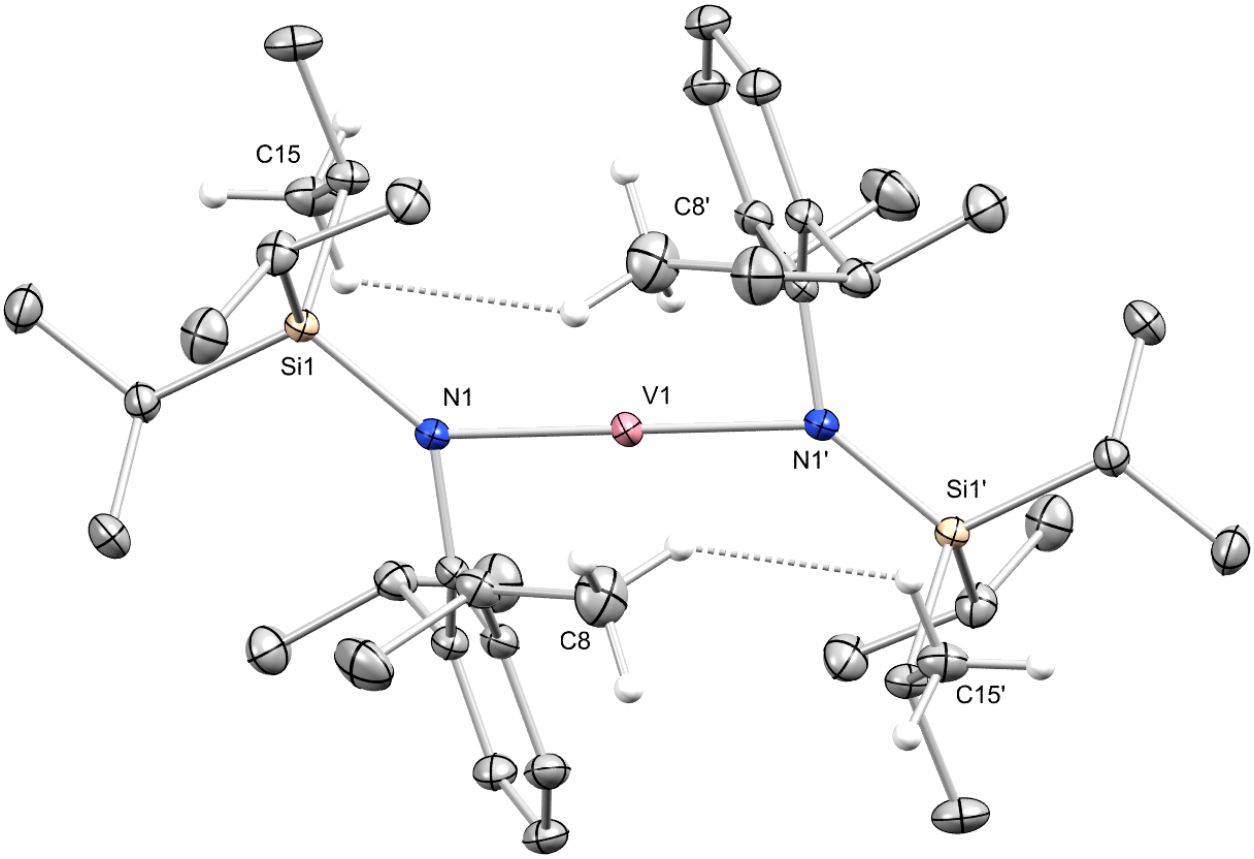

Notes: Thermal ellipsoids shown at 50% probability. Hydrogen atoms have been omitted for clarity, with the exception of hydrogen atoms on C8 and C15, which have been located from the electron density difference map. Selected bond distances [Å], angles [°], and torsions [°]: V1–N1: 1.9824(5), V1–C1: 2.3024(5), N1–Si1: 1.7284(5), N1–C1: 1.4132(7), H(C8)···H(C15'): 2.41233(11); N1–V1–N1': 180.0, V1–N1–C1: 83.59(3); C1–N1–N1'–C1': ±180.00(5).

Table SX4.1. Crystal data and structure refinement for complex **4.1**

Empirical formula	$C_{42}H_{76}N_2Si_2V$
Formula weight	716.16
Temperature	100(2) K
Crystal system	triclinic
Space group	$P\bar{1}$
a	10.7299(5) Å
b	10.8434(5) Å
c	11.5214(5) Å
α	99.297(2)°
β	105.357(2)°
γ	118.904(2)°
Volume	1062.96(9) $Å^3$
Z	1
ρ_{calc}	1.119 g/cm^3
μ	0.400 mm^{-1}
F(000)	393.0
Crystal size	0.21 × 0.126 × 0.084 mm^3
Radiation	synchrotron (λ = 0.7749)
2Θ range for data collection	4.256 to 87.66°
Index ranges	$-19 \leq h \leq 19$, $-19 \leq k \leq 19$, $-20 \leq l \leq 20$
Reflections collected	23310
Independent reflections	12222 [R_{int} = 0.0235, R_{sigma} = 0.0342]
Data/restraints/parameters	12222/0/224
Goodness-of-fit on F^2	1.042
Final R indexes [I>=2σ (I)]	R_1 = 0.0335, wR_2 = 0.0919
Final R indexes [all data]	R_1 = 0.0423, wR_2 = 0.0972
Largest diff. peak/hole	0.59 / –0.61 $e/Å^3$

Figure SX4.2. Solid state structure of complex **4.2** as determined by single-crystal X-ray diffraction

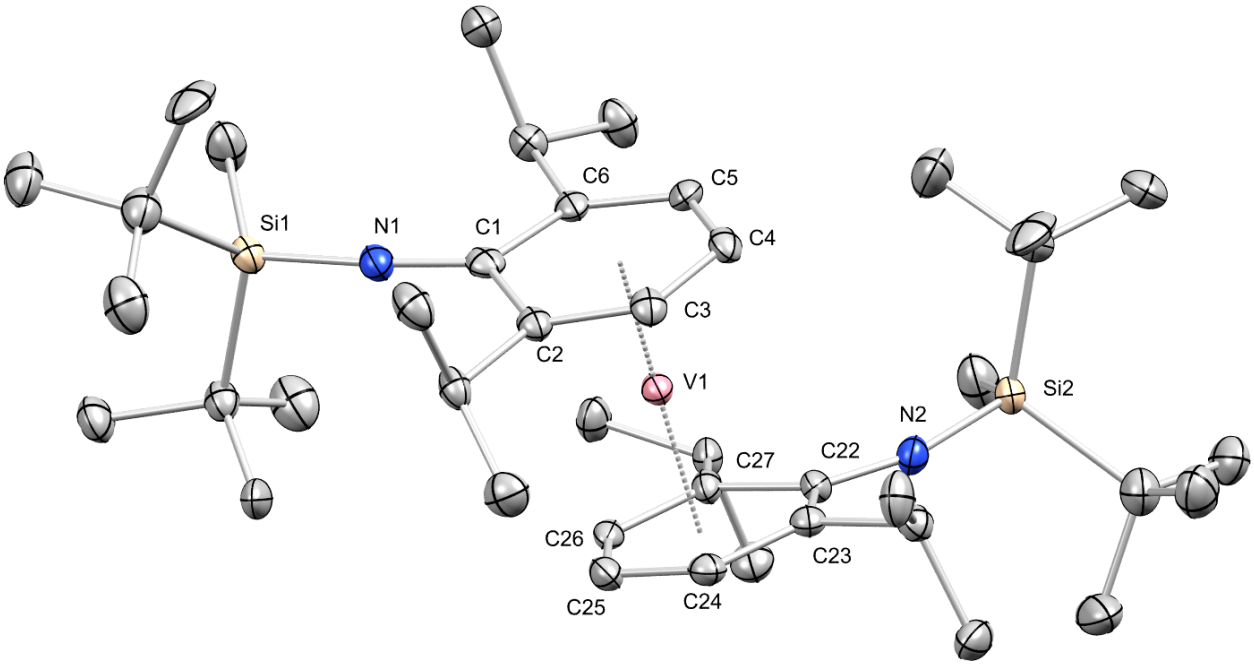

Notes: Thermal ellipsoids shown at 50% probability. Hydrogen atoms, disordered silicon atoms, and pentane molecule have been omitted for clarity. Selected bond distances [Å] and angles [°]: N1–C1: 1.290(7), N2–C22: 1.299(7), N1–Si1: 1.673(5), N1–Si1A: 1.60(2), N2–Si2: 1.685(5), N2–Si2A: 1.638(15), distance between V1 and least-squares plane of (C2, C3, C4, C5, C6): 1.840, distance between V1 and least-squares plane of (C23, C24, C25, C26, C27): 1.851, V1–C1: 2.555(5), V1–C22: 2.534(5); C1–N1–Si1: 164.1(4), C1–N1–Si1A: 166.7(13), C22–N2–Si2: 162.2(4), C22–N2–Si2A: 168.4(8).

Table SX4.2. Crystal data and structure refinement for complex **4.2**

Empirical formula	$C_{47}H_{88}N_2Si_2V$
Formula weight	788.31
Temperature	100(2) K
Crystal system	monoclinic
Space group	$P2_1/c$
a	10.4617(8) Å
b	26.938(2) Å
c	17.3073(13) Å
α	90°
β	100.040(3)°
γ	90°
Volume	4802.8(6) $Å^3$
Z	4
ρ_{calc}	1.090 g/cm^3
μ	0.305 mm^{-1}
F(000)	1740.0
Crystal size	0.18 × 0.09 × 0.09 mm^3
Radiation	synchrotron (λ = 0.7288)
2Θ range for data collection	3.952 to 52.308°
Index ranges	$-12 \leq h \leq 12$, $-32 \leq k \leq 32$, $-20 \leq l \leq 20$
Reflections collected	64559
Independent reflections	8880 [R_{int} = 0.0546, R_{sigma} = 0.0333]
Data/restraints/parameters	8880/0/495
Goodness-of-fit on F^2	1.159
Final R indexes [I>=2σ (I)]	R_1 = 0.0969, wR_2 = 0.2372
Final R indexes [all data]	R_1 = 0.1058, wR_2 = 0.2411
Largest diff. peak/hole	1.04 / –1.55 e/$Å^3$

Figure SX4.3. Solid state structure of complex **4.3** as determined by single-crystal X-ray diffraction

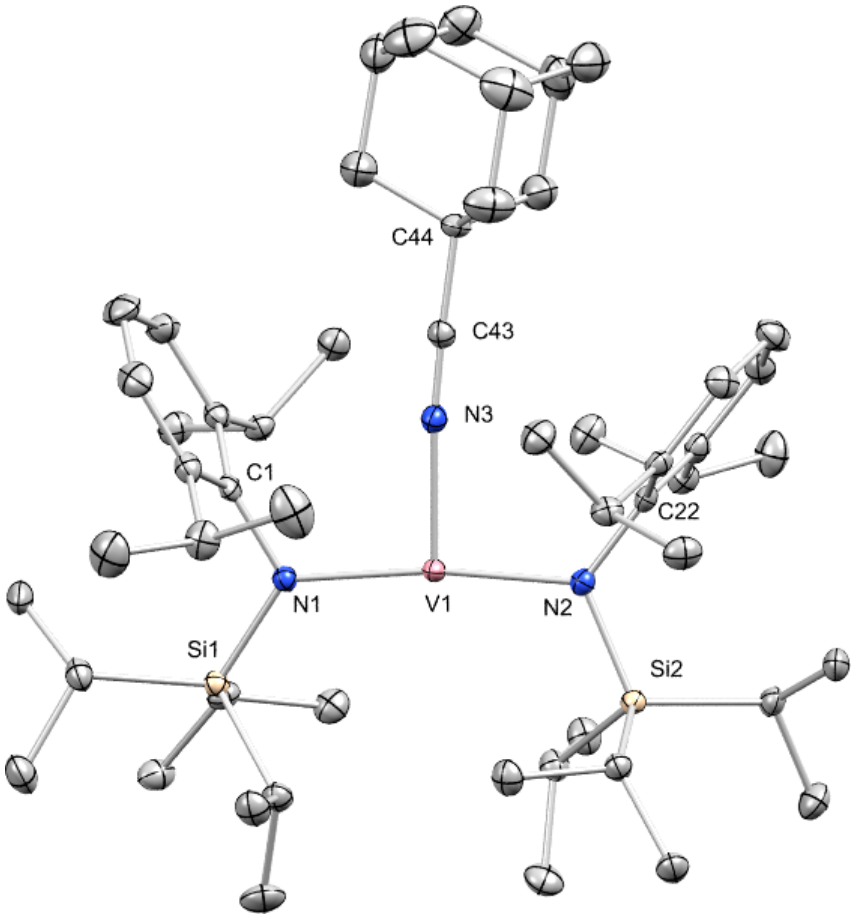

Notes: Thermal ellipsoids shown at 50% probability. Hydrogen atoms have been omitted for clarity. Selected bond distances [Å], angles [°], and torsions [°]: V1–N1: 2.0271(15), V1–N2: 2.0217(15), V1–N3: 2.0641(16), N3–C43: 1.145(2); N1–V1–N2: 172.30(6); C1–N1–N2–C22: ±7.8(2).

Table SX4.3. Crystal data and structure refinement for complex **4.3**

Empirical formula	$C_{53}H_{91}N_3Si_2V$
Formula weight	877.40
Temperature	100(2) K
Crystal system	monoclinic
Space group	$P2_1/c$
a	17.9370(5) Å
b	13.0478(4) Å
c	22.3602(6) Å
α	90°
β	90.860(2)°
γ	90°
Volume	5232.6(3) $Å^3$
Z	4
ρ_{calc}	1.114 g/cm^3
μ	0.271 mm^{-1}
F(000)	1924.0
Crystal size	0.18 × 0.17 × 0.1 mm^3
Radiation	MoKα (λ = 0.71073)
2Θ range for data collection	6.246 to 59.064°
Index ranges	$-24 \leq h \leq 22$, $-18 \leq k \leq 16$, $-30 \leq l \leq 30$
Reflections collected	79747
Independent reflections	12696 [R_{int} = 0.0673, R_{sigma} = 0.0517]
Data/restraints/parameters	12696/0/552
Goodness-of-fit on F^2	1.014
Final R indexes [I>=2σ (I)]	R_1 = 0.0479, wR_2 = 0.1113
Final R indexes [all data]	R_1 = 0.0712, wR_2 = 0.1205
Largest diff. peak/hole	1.30 / –0.41 e/$Å^3$

Figure SX4.4. Solid state structure of complex **4.4** as determined by single-crystal X-ray diffraction

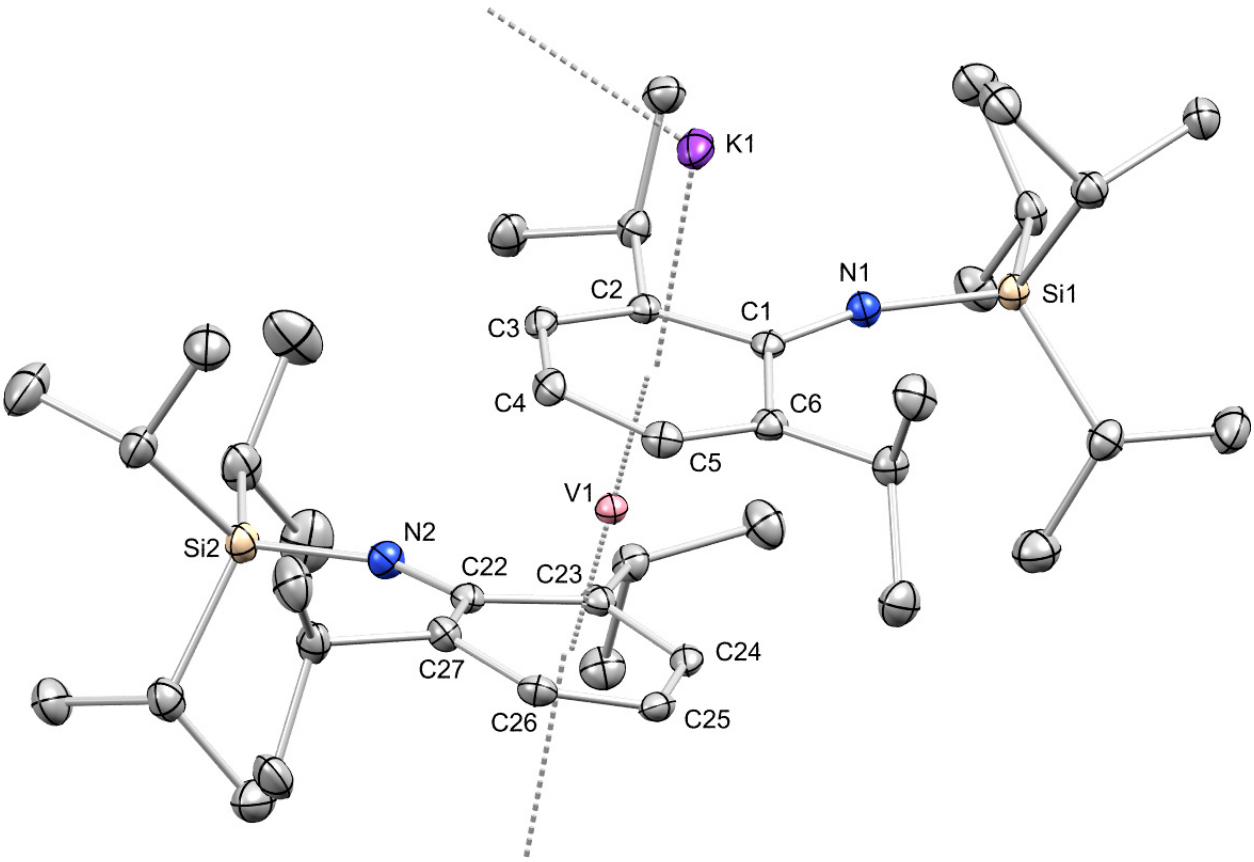

Notes: Thermal ellipsoids shown at 50% probability. The second crystallographically independent molecule of **4.4** has been omitted. Hydrogen atoms and solvent molecules have also been omitted for clarity. Selected bond distances [Å] and angles [°]: N1–C1: 1.316(3), N2–C22: 1.311(3), N3–C43: 1.308(3), N4–C64: 1.312(3), distance between V1 and least-squares plane of (C2, C3, C4, C5, C6): 1.748, distance between V1 and least-squares plane of (C23, C24, C25, C26, C27): 1.756, distance between V2 and least-squares plane of (C44, C45, C46, C47, C48): 1.748, distance between V2 and least-squares plane of (C65, C66, C67, C68, C69): 1.742, V1–C1: 2.482(2), V1–C22: 2.487(2), V2–C43: 2.519(2), V2–C64: 2.498(2); C1–N1–Si1: 155.59(18), C22–N2–Si2: 153.02(18), C43–N3–Si3: 154.19(18), C64–N4–Si5: 156.10(19).

Table SX4.4. Crystal data and structure refinement for complex **4.4**

Empirical formula	$C_{89}H_{164}K_2N_4Si_4V_2$
Formula weight	1582.67
Temperature	100(2) K
Crystal system	monoclinic
Space group	$P2_1$
a	15.0239(9) Å
b	15.4163(9) Å
c	20.4203(12) Å
α	90°
β	103.964(2)°
γ	90°
Volume	4589.8(5) $Å^3$
Z	2
ρ_{calc}	1.145 g/cm^3
μ	0.390 mm^{-1}
F(000)	1732.0
Crystal size	0.1 × 0.1 × 0.1 mm^3
Radiation	MoKα (λ = 0.71073)
2Θ range for data collection	2.794 to 55.08°
Index ranges	$-19 \leq h \leq 19$, $-13 \leq k \leq 20$, $-26 \leq l \leq 26$
Reflections collected	80619
Independent reflections	18698 [R_{int} = 0.0326, R_{sigma} = 0.0347]
Data/restraints/parameters	18698/1/952
Goodness-of-fit on F^2	1.036
Final R indexes [I>=2σ (I)]	R_1 = 0.0307, wR_2 = 0.0693
Final R indexes [all data]	R_1 = 0.0359, wR_2 = 0.0721
Largest diff. peak/hole	0.33 / –0.27 e/$Å^3$
Flack parameter	–0.010(5)

Figure SX4.5. Solid state structure of complex **4.5** as determined by single-crystal X-ray diffraction

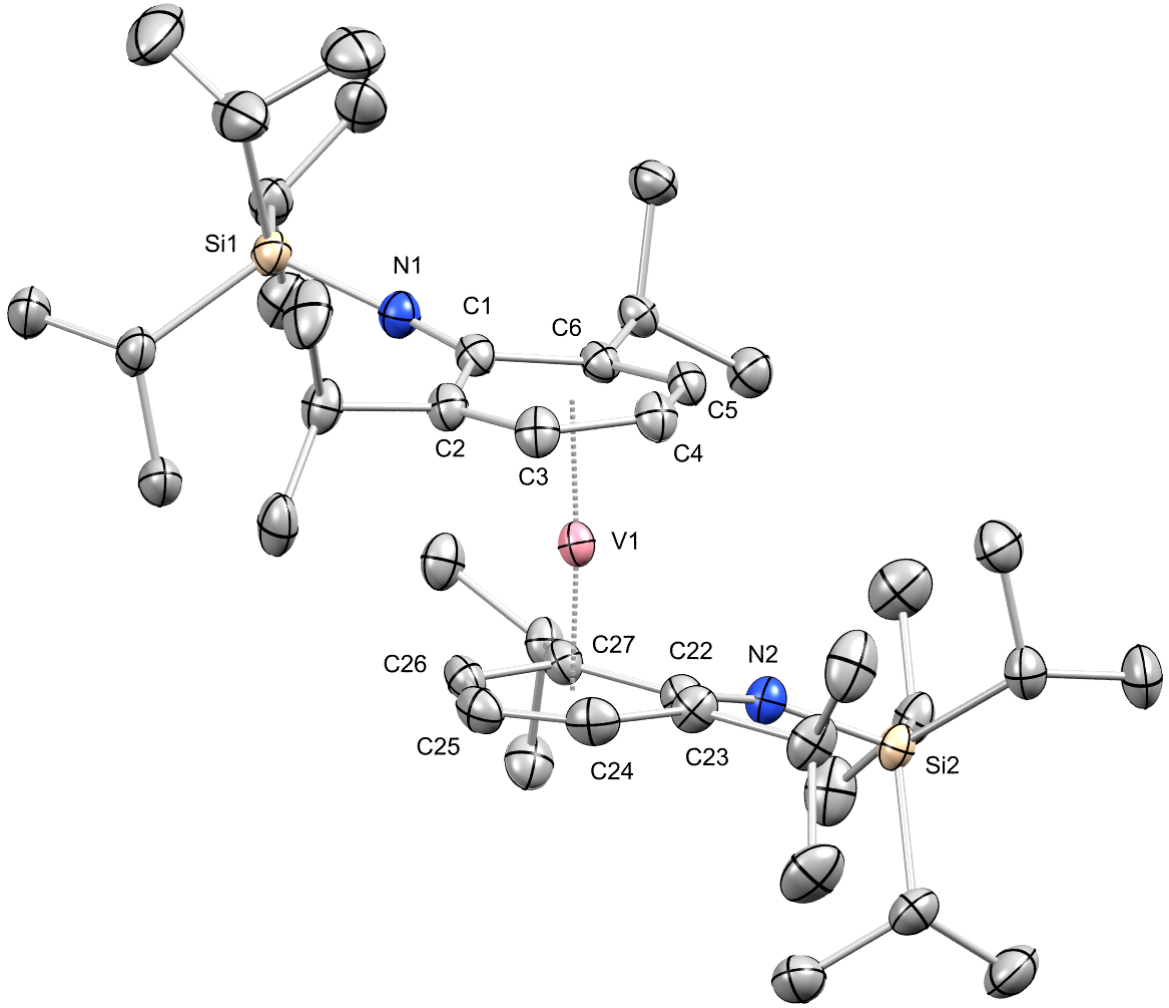

Notes: Thermal ellipsoids shown at 50% probability. Hydrogen atoms, $[K(18\text{-cr-}6)_{1.5}]$ cation, and diethyl ether molecules have been omitted for clarity. Selected bond distances [Å] and angles [°]: N1–C1: 1.313(3), N2–C22: 1.311(3), N1–Si1: 1.671(2), N2–Si2: 1.663(2), distance between V1 and least-squares plane of (C2, C3, C4, C5, C6): 1.755, distance between V1 and least-squares plane of (C23, C24, C25, C26, C27): 1.759, V1–C1: 2.498(2), V1–C22: 2.511(2); C1–N1–Si1: 155.59(18), C22–N2–Si2: 153.02(18).

Table SX4.5. Crystal data and structure refinement for complex **4.5**

Empirical formula	$C_{66}H_{123.5}KN_2O_{10.5}Si_2V$
Formula weight	1259.38
Temperature	100(2) K
Crystal system	triclinic
Space group	$P\bar{1}$
a	14.7693(5) Å
b	16.4391(6) Å
c	18.5577(6) Å
α	65.0500(10)°
β	68.4030(10)°
γ	68.0700(10)°
Volume	3669.0(2) $Å^3$
Z	2
ρ_{calc}	1.140 g/cm^3
μ	0.294 mm^{-1}
F(000)	1375.0
Crystal size	0.181 × 0.09 × 0.045 mm^3
Radiation	synchrotron (λ = 0.7288)
2Θ range for data collection	2.564 to 61.916°
Index ranges	$-20 \leq h \leq 20$, $-23 \leq k \leq 23$, $-26 \leq l \leq 26$
Reflections collected	63882
Independent reflections	21387 [R_{int} = 0.0528, R_{sigma} = 0.0591]
Data/restraints/parameters	21387/48/801
Goodness-of-fit on F^2	1.048
Final R indexes [I>=2σ (I)]	R_1 = 0.0710, wR_2 = 0.1940
Final R indexes [all data]	R_1 = 0.0973, wR_2 = 0.2119
Largest diff. peak/hole	1.26 / –0.83 e/$Å^3$

Figure SX4.6. Solid state structure of complex **4.6** as determined by single-crystal X-ray diffraction

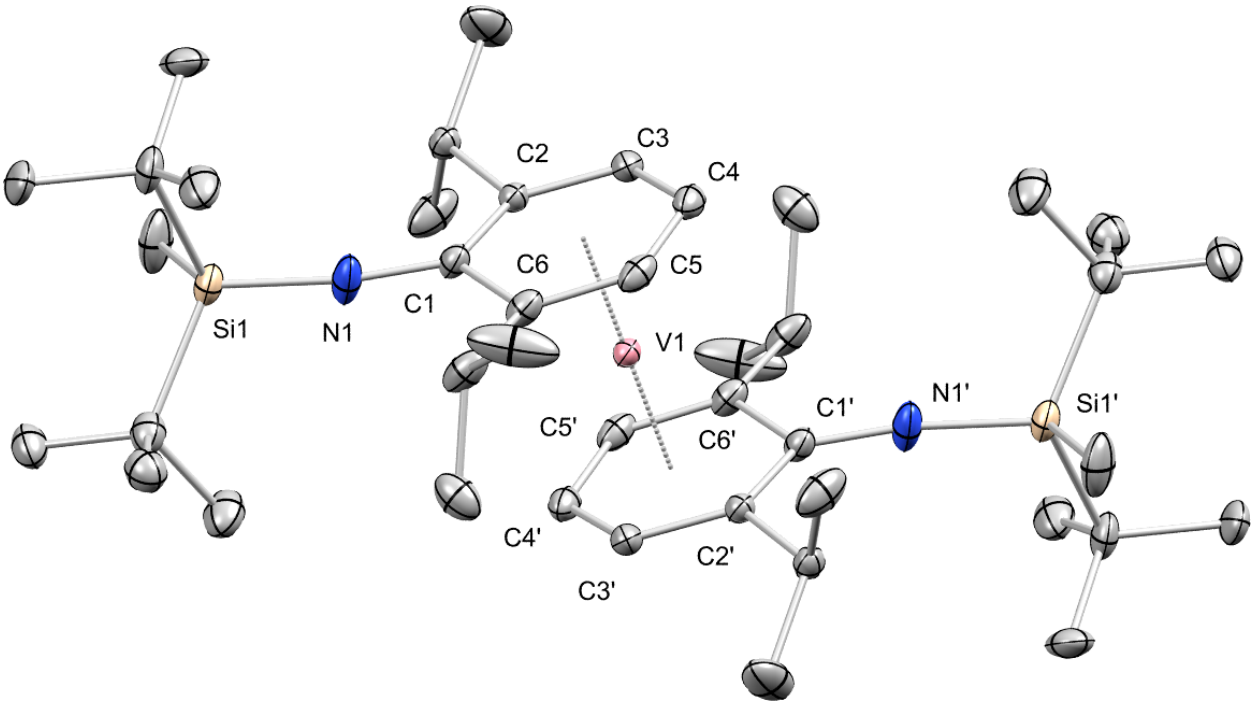

Notes: Thermal ellipsoids shown at 50% probability. Hydrogen atoms, disordered di-*tert*-butylmethylsilyl group, [K(18-cr-6)] cation, and THF molecules of solvation have been omitted for clarity. Selected bond distances [Å] and angles [°]: N1–C1: 1.3064(13), N1–Si1: 1.6798(11), distance between V1 and least-squares plane of (C2, C3, C4, C5, C6): 1.771, V1–C1: 2.4727(9); C1–N1–Si1: 170.00(8), C1–N1–Si1A: 159.64(10).

Table SX4.6. Crystal data and structure refinement for complex **4.6** as determined by single-crystal X-ray diffraction

Empirical formula	$C_{62}H_{116}KN_2O_8Si_2V$
Formula weight	1163.78
Temperature	100(2) K
Crystal system	triclinic
Space group	$P\bar{1}$
a	10.4819(5) Å
b	11.1648(5) Å
c	15.5086(8) Å
α	103.500(2)°
β	104.811(2)°
γ	99.698(2)°
Volume	1655.16(14) $Å^3$
Z	1
ρ_{calc}	1.168 g/cm^3
μ	0.318 mm^{-1}
F(000)	636.0
Crystal size	0.206 × 0.203 × 0.12 mm^3
Radiation	synchrotron (λ = 0.7288)
2Θ range for data collection	2.91 to 81.252°
Index ranges	$-18 \leq h \leq 18$, $-19 \leq k \leq 19$, $-27 \leq l \leq 27$
Reflections collected	37903
Independent reflections	19362 [R_{int} = 0.0616, R_{sigma} = 0.0833]
Data/restraints/parameters	19362/0/455
Goodness-of-fit on F^2	1.065
Final R indexes [I>=2σ (I)]	R_1 = 0.0551, wR_2 = 0.1424
Final R indexes [all data]	R_1 = 0.0832, wR_2 = 0.1598
Largest diff. peak/hole	0.62 / –0.71 $e/Å^3$

Figure SX4.7. Solid state structure of complex **4.7** as determined by single-crystal X-ray diffraction

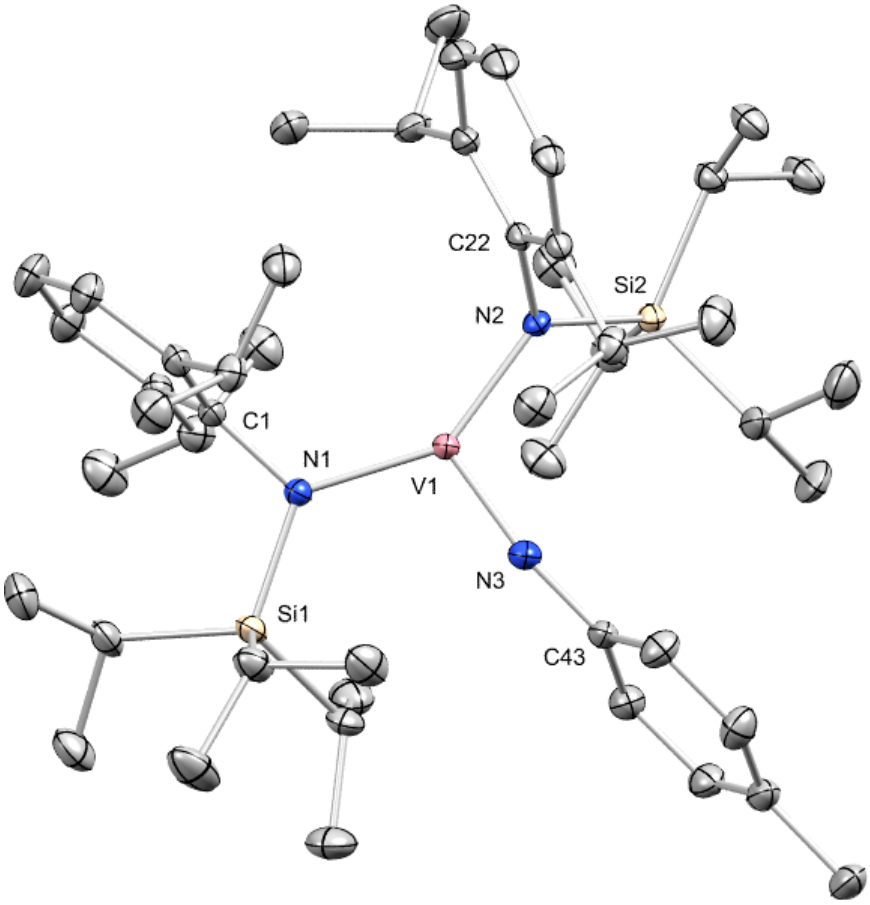

Notes: Thermal ellipsoids shown at 50% probability. Hydrogen atoms and disordered pentane molecule have been omitted for clarity. Selected bond distances [Å], angles [°], and torsions [°]:V1–N1: 1.9175(13), V1–N2: 1.9299(13), V1–N3: 1.6703(13); N1–V1–N2: 142.76(6), V1–N3–C43: 171.56(12); C1–N1–N2–C22: ±47.2(1).

Table SX4.7. Crystal data and structure refinement for complex **4.7**

Empirical formula	$C_{51.5}H_{89}N_3Si_2V$
Formula weight	857.37
Temperature	100 (K)
Crystal system	monoclinic
Space group	C2/c
a	21.3462(8) Å
b	22.0991(8) Å
c	23.8006(8) Å
α	90°
β	114.0220(10)°
γ	90°
Volume	10255.1(6) $Å^3$
Z	8
ρ_{calc}	1.111 g/cm^3
μ	0.292 mm^{-1}
F(000)	3760.0
Crystal size	0.136 × 0.136 × 0.045 mm^3
Radiation	synchrotron (λ = 0.7288)
2Θ range for data collection	2.856 to 57.392°
Index ranges	$-28 \leq h \leq 28$, $-29 \leq k \leq 29$, $-31 \leq l \leq 31$
Reflections collected	75364
Independent reflections	12276 [R_{int} = 0.0992, R_{sigma} = 0.0676]
Data/restraints/parameters	12276/54/564
Goodness-of-fit on F^2	1.027
Final R indexes [I>=2σ (I)]	R_1 = 0.0442, wR_2 = 0.1041
Final R indexes [all data]	R_1 = 0.0645, wR_2 = 0.1146
Largest diff. peak/hole	0.34 / –0.39 e/$Å^3$

Figure SX4.8. Solid state structure of complex **4.8** as determined by single-crystal X-ray diffraction

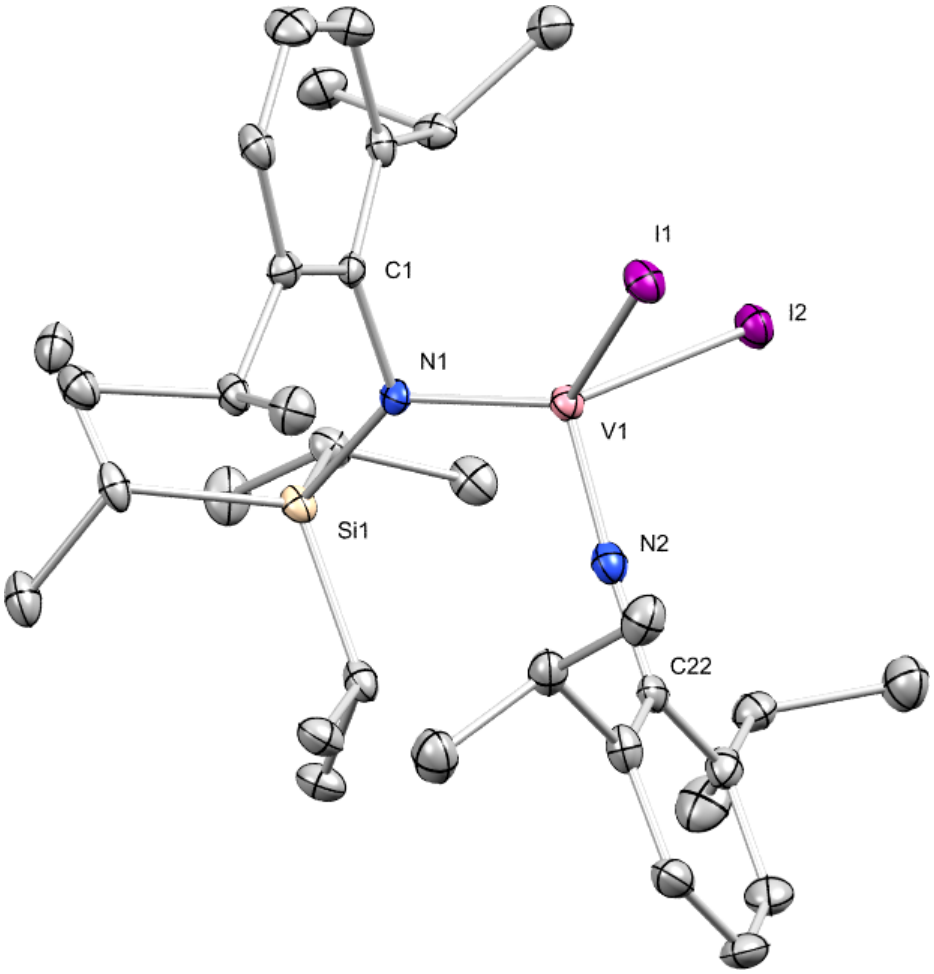

Notes: Thermal ellipsoids shown at 50% probability. Hydrogen atoms and pentane molecule have been omitted for clarity. Selected bond distances [Å] and angles [°]:V1–N1: 1.864(3), V1–N2: 1.658(3), V1–I1: 2.580(6), V1–I2: 2.5879(6); V1–N1–C1: 97.72(19), V1–N2–C22: 174.8(3).

Table SX4.8. Crystal data and structure refinement for complex **4.8**

Empirical formula	$C_{38}H_{67}I_2N_2SiV$
Formula weight	884.76
Temperature	100(2) K
Crystal system	triclinic
Space group	$P\bar{1}$
a	10.0850(7) Å
b	12.9269(9) Å
c	16.6817(11) Å
α	69.741(2)°
β	80.721(3)°
γ	88.267(3)°
Volume	2012.8(2) $Å^3$
Z	2
ρ_{calc}	1.460 g/cm^3
μ	1.943 mm^{-1}
F(000)	904.0
Crystal size	0.084 × 0.042 × 0.017 mm^3
Radiation	synchrotron (λ = 0.7288)
2Θ range for data collection	2.704 to 58.328°
Index ranges	$-13 \leq h \leq 13$, $-17 \leq k \leq 17$, $-22 \leq l \leq 22$
Reflections collected	32491
Independent reflections	10040 [R_{int} = 0.0644, R_{sigma} = 0.0759]
Data/restraints/parameters	10040/0/413
Goodness-of-fit on F^2	1.043
Final R indexes [I>=2σ (I)]	R_1 = 0.0394, wR_2 = 0.0753
Final R indexes [all data]	R_1 = 0.0664, wR_2 = 0.0841
Largest diff. peak/hole	1.33 / –0.80 e/$Å^3$

Figure SX4.9. Solid state structure of complex **4.9** as determined by single-crystal X-ray diffraction

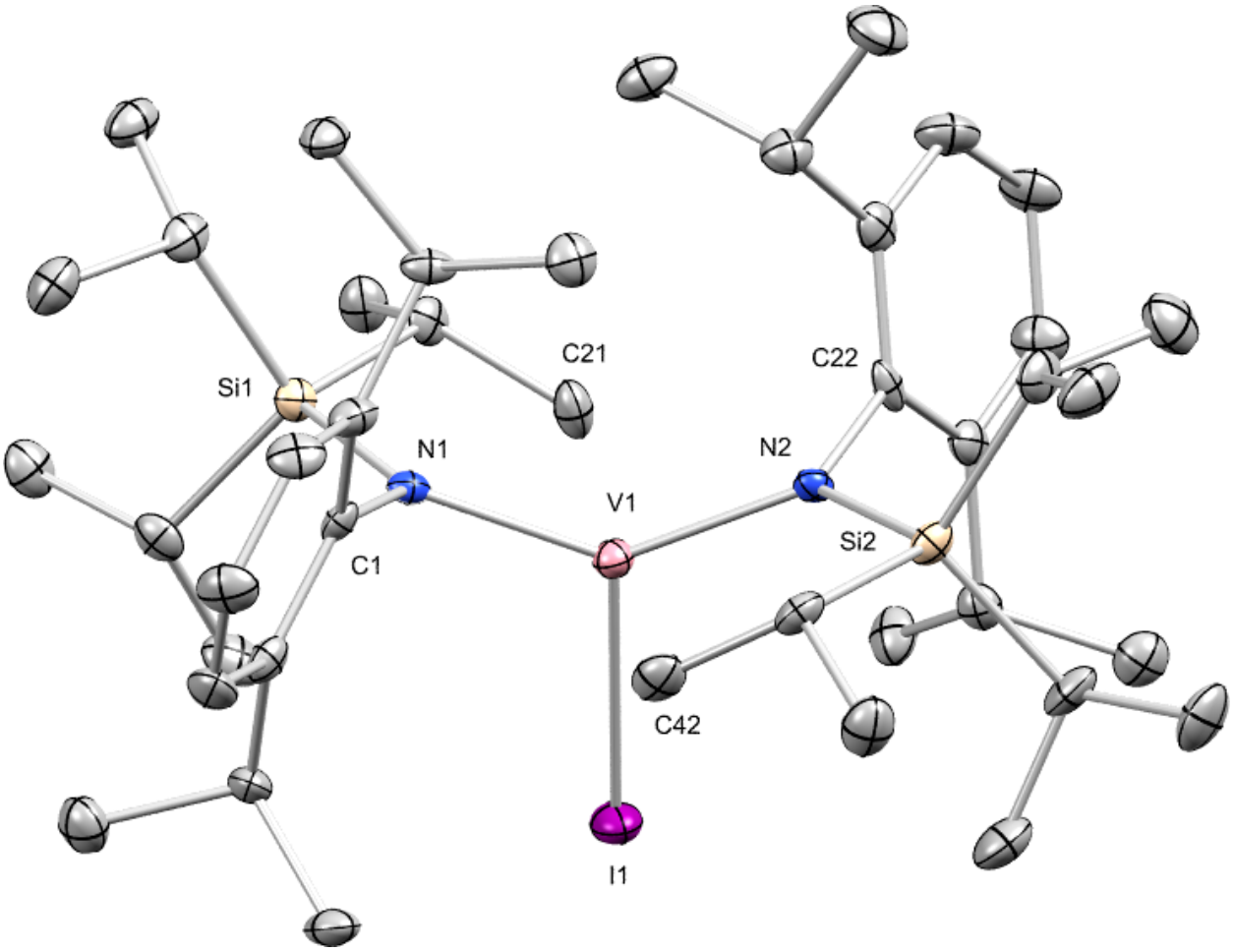

Notes: Thermal ellipsoids shown at 50% probability. Hydrogen atoms have been omitted for clarity. Selected bond distances [Å], angles [°], and torsions [°]:V1–N1: 1.968(4), V1–N2: 1.942(4), V1–I1: 2.6502(9), V1···H(C21): 2.0785(10), V1···H(C42): 2.0581(10); N1–V1–N2: 136.17(17); C1–N1–N2–C22: ±150.4(4).

Table SX4.9. Crystal data and structure refinement for complex **4.9**

Empirical formula	$C_{42}H_{76}IN_2Si_2V$
Formula weight	843.06
Temperature/K	100(2) K
Crystal system	triclinic
Space group	$P\bar{1}$
a	10.5266(5) Å
b	10.7440(5) Å
c	20.7180(9) Å
α	99.5290(10)°
β	92.1560(10)°
γ	107.3630(10)°
Volume	2196.08(17) $Å^3$
Z	2
ρ_{calc}	1.275 g/cm^3
μ	1.072 mm^{-1}
F(000)	892.0
Crystal size	0.05 × 0.049 × 0.041 mm^3
Radiation	synchrotron (λ = 0.7288)
2Θ range for data collection	4.106 to 52.1°
Index ranges	$-12 \leq h \leq 12$, $-12 \leq k \leq 12$, $0 \leq l \leq 24$
Reflections collected	7932
Independent reflections	7932 [R_{int} = ?, R_{sigma} = 0.0819]
Data/restraints/parameters	7932/0/454
Goodness-of-fit on F^2	1.036
Final R indexes [I>=2σ (I)]	R_1 = 0.0474, wR_2 = 0.0877
Final R indexes [all data]	R_1 = 0.0647, wR_2 = 0.0952
Largest diff. peak/hole	0.59 / –0.61 e/$Å^3$

Figure SX4.10. Solid state structure of complex **4.10** as determined by single-crystal X-ray diffraction

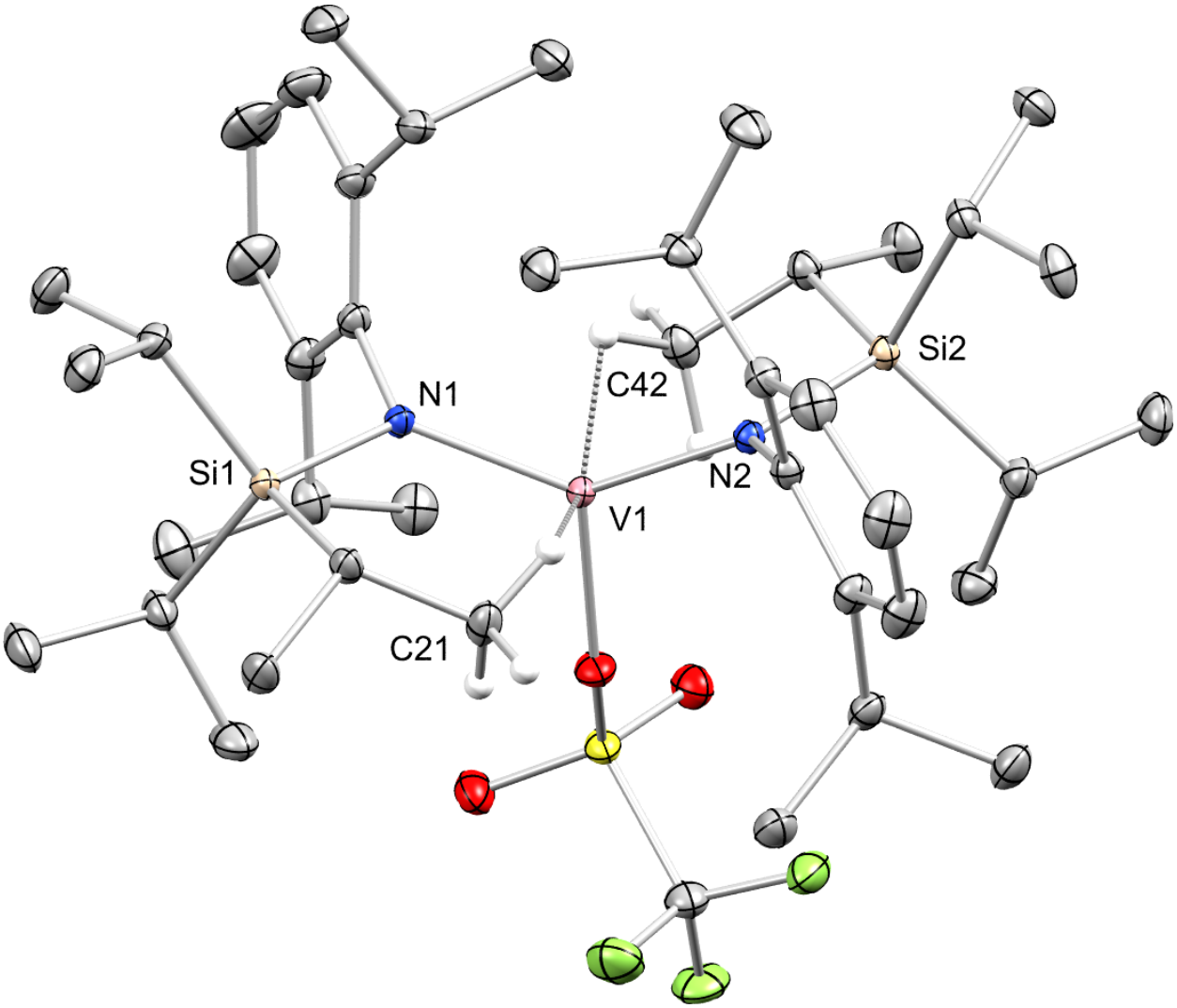

Notes: Thermal ellipsoids shown at 50% probability. Hydrogen atoms have been omitted for clarity, with the exception of hydrogen atoms on C21 and C42, which were located using the electron density difference map. Oxygen atoms shown in red; sulfur atom shown in bright yellow; fluorine atoms shown in green. Selected bond distances [Å], angles [°], and torsions [°]:V1–N1: 1.9384(8), V1–N2: 1.9412(8), V1–O1: 1.9876(7), V1···H(C21): 2.0631(3), V1···H(C42): 2.0540(3); N1–V1–N2: 135.02(3); C1–N1–N2–C22: ±144.30(8).

Table SX4.10. Crystal data and structure refinement for complex **4.10**

Empirical formula	$C_{43}H_{76}F_3N_2O_3SSi_2V$
Formula weight	865.23
Temperature/K	100(2) K
Crystal system	monoclinic
Space group	$P2_1/n$
a	10.7929(4) Å
b	22.9951(9) Å
c	19.1537(8) Å
α	90°
β	101.3550(10)°
γ	90°
Volume	4660.6(3) $Å^3$
Z	4
ρ_{calc}	1.233 g/cm^3
μ	0.381 mm^{-1}
F(000)	1864.0
Crystal size	0.214 × 0.214 × 0.179 mm^3
Radiation	synchrotron (λ = 0.7288)
2Θ range for data collection	2.872 to 74.83°
Index ranges	$-17 \leq h \leq 17$, $-38 \leq k \leq 38$, $-29 \leq l \leq 31$
Reflections collected	105265
Independent reflections	22515 [R_{int} = 0.0675, R_{sigma} = 0.0546]
Data/restraints/parameters	22515/0/516
Goodness-of-fit on F^2	1.021
Final R indexes [I>=2σ (I)]	R_1 = 0.0441, wR_2 = 0.1129
Final R indexes [all data]	R_1 = 0.0544, wR_2 = 0.1188
Largest diff. peak/hole	1.51 / –0.82 e/$Å^3$

Figure SX4.11. Solid state structure of complex **4.11** as determined by single-crystal X-ray diffraction

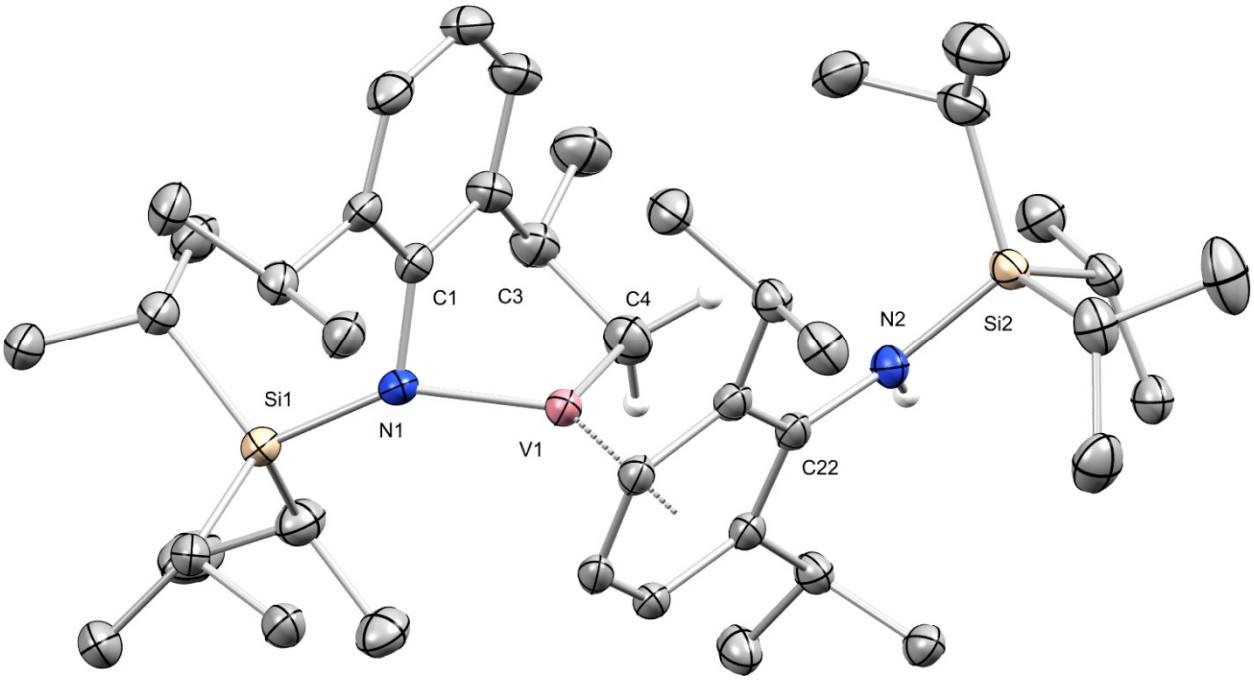

Notes: Thermal ellipsoids shown at 50% probability. Hydrogen atoms, $B(C_6F_5)_4$ anion, and solvent molecules have been omitted for clarity, with the exception of hydrogen atoms on C4 and N2, which were located using the electron density difference map. Selected bond distances [Å] and angles [°]: V1–N1: 1.877(2), V1–C4: 2.097(3), N1–Si1: 1.789(2), N1–C1: 1.435(3), C3–C4: 1.521(5), N2–Si2: 1.777(2), N2–C22:1.381(4), distance between V1 and least-squares plane of (C22, C23, C24, C25, C26, C27): 1.987; V1–N1–C1: 87.6(2), N1–V1–C4: 98.1(1), C22–N2–Si2: 144.2(2).

Table SX4.11. Crystal data and structure refinement for complex **4.11**

Empirical formula	$C_{80}H_{92}BF_{20}N_2Si_2V$
Formula weight	1579.48
Temperature	100(2) K
Crystal system	monoclinic
Space group	$P2_1/c$
a	12.2998(7) Å
b	25.3828(13) Å
c	24.8471(13) Å
α	90°
β	101.216(2)°
γ	90°
Volume	7609.2(7) $Å^3$
Z	4
ρ_{calc}	1.379 g/cm^3
μ	0.271 mm^{-1}
F(000)	3288.0
Crystal size	0.113 × 0.113 × 0.045 mm^3
Radiation	synchrotron (λ = 0.7288)
2Θ range for data collection	2.376 to 52.198°
Index ranges	$-14 \leq h \leq 14$, $-30 \leq k \leq 30$, $-29 \leq l \leq 29$
Reflections collected	99625
Independent reflections	13982 [R_{int} = 0.0755, R_{sigma} = 0.0452]
Data/restraints/parameters	13982/244/992
Goodness-of-fit on F^2	1.048
Final R indexes [I>=2σ (I)]	R_1 = 0.0552, wR_2 = 0.1578
Final R indexes [all data]	R_1 = 0.0696, wR_2 = 0.1680
Largest diff. peak/hole	0.88 / –0.67 e/$Å^3$

Table SX4.12. Crystal data and structure refinement for complex Cr[N(Si^{t}Bu$_2$Me)DIPP]$_2$

Empirical formula	$C_{42}H_{76}N_2Si_2Cr$
Formula weight	717.22
Temperature/K	100(2) K
Crystal system	orthorhombic
Space group	$P2_12_12$
a	12.9547(5) Å
b	15.2924(7) Å
c	10.7545(4) Å
α	90°
β	90°
γ	90°
Volume	2130.56(15) Å^3
Z	2
ρ_{calc}	1.118 g/cm^3
μ	0.354 mm^{-1}
F(000)	788.0
Crystal size	0.08 × 0.04 × 0.01 mm^3
Radiation	MoKα (λ = 0.71073)
2Θ range for data collection	3.788 to 50.85°
Index ranges	$-15 \leq h \leq 15$, $-18 \leq k \leq 16$, $-12 \leq l \leq 12$
Reflections collected	21968
Independent reflections	3930 [R_{int} = 0.0528, R_{sigma} = 0.0457]
Data/restraints/parameters	3930/0/225
Goodness-of-fit on F^2	1.033
Final R indexes [I>=2σ (I)]	R_1 = 0.0353, wR_2 = 0.0726
Final R indexes [all data]	R_1 = 0.0449, wR_2 = 0.0770
Largest diff. peak/hole	0.24 / –0.28 e/Å^3
Flack parameter	0.48(3)

COMPUTATIONAL DETAILS

All calculations were performed with QChem (v. 5.0.1).[14] Starting from the crystallographically determined atomic coordinates of the relevant complexes, any cocrystallized solvent molecules were deleted, the organosilicon groups were modified as necessary, and the geometries of the resulting species were optimized. Calculations employed the ωB97X-D functional[15] and the def2-SVP basis set as specified for all atoms.

Table SC4.1. Atomic coordinates and energy of the calculated linear structure of V[N(Si^{i}Pr$_3$)DIPP]$_2$ with def2-SVP basis set.

Charge = 0, Multiplicity = 4

	x	*y*	*z*
V	-0.00031	-0.00011	-0.00018
Si	-1.20778	1.61667	2.78489
N	-0.50614	0.30177	1.88641
C	-0.23392	-1.05947	2.04414
C	-1.03602	-2.01336	1.33635
C	0.95293	-1.53489	2.70254
C	-0.09555	3.15194	2.48724
H	0.29133	2.97678	1.46795
C	-1.2992	1.21493	4.64217
H	-0.24191	1.16966	4.96164
C	1.30488	-2.87305	2.6064
H	2.21125	-3.2216	3.10832
C	-0.60292	-3.35136	1.23909
H	-1.21763	-4.06667	0.68707
C	-2.92842	2.09503	2.09331
H	-3.09046	3.11231	2.49316
C	-1.92575	-0.14993	4.95292
H	-1.8479	-0.38355	6.02887
H	-1.43425	-0.96773	4.40373
H	-2.99541	-0.17814	4.69384
C	-2.46442	-1.69438	0.90565
H	-2.59671	-0.61152	1.01898
C	0.5518	-3.78379	1.85821
H	0.86937	-4.825	1.77475
C	1.10917	3.22411	3.43316
H	1.79061	4.04274	3.14497
H	1.70352	2.29952	3.43817
H	0.79512	3.4174	4.47234
C	-1.96868	2.33877	5.44241
H	-3.02329	2.47453	5.15217
H	-1.46326	3.30636	5.29804
H	-1.95571	2.12082	6.52383
C	1.82184	-0.59168	3.50932
H	1.40649	0.41093	3.35225
C	-2.87473	2.21301	0.56621
H	-2.74461	1.22742	0.08901
H	-2.04125	2.84282	0.21867
H	-3.80459	2.64208	0.15576
C	-0.81644	4.50582	2.46115
H	-1.31395	4.7307	3.41921
H	-1.57947	4.56186	1.67134
H	-0.0974	5.3217	2.27382
C	1.75354	-0.90202	5.0084
H	0.71708	-0.9131	5.37308
H	2.31179	-0.14819	5.58547
H	2.19574	-1.88703	5.22908
C	3.27484	-0.57368	3.02531
H	3.78502	-1.52682	3.2374
H	3.83936	0.22404	3.53301
H	3.33862	-0.39848	1.94259
C	-4.12636	1.25553	2.54859
H	-5.05523	1.60829	2.06846
H	-4.2812	1.31752	3.63595
H	-4.01578	0.19147	2.29722
C	-3.4481	-2.37265	1.86761
H	-3.38226	-3.46992	1.7944
H	-4.48441	-2.0812	1.6351
H	-3.23693	-2.09192	2.90997
C	-2.7774	-2.04777	-0.54788
H	-2.11577	-1.50803	-1.24255
H	-3.81665	-1.78125	-0.793

H	-2.65562	-3.12363	-0.74997
Si	1.20837	-1.61635	-2.78496
N	0.50529	-0.30197	-1.88685
C	0.23302	1.05929	-2.04454
C	1.03555	2.01346	-1.3377
C	-0.95456	1.53433	-2.7019
C	0.09679	-3.1522	-2.48798
H	-0.29097	-2.97701	-1.46906
C	1.30028	-1.21444	-4.64213
H	0.24306	-1.16998	-4.96195
C	-1.30673	2.87244	-2.60571
H	-2.21367	3.22068	-3.1068
C	0.60227	3.35135	-1.24022
H	1.21725	4.06686	-0.68877
C	2.92906	-2.09387	-2.09287
H	3.09122	-3.1113	-2.49227
C	1.92594	0.15089	-4.95254
H	1.84839	0.38454	-6.02851
H	1.43359	0.96829	-4.4035
H	2.99548	0.17987	-4.69299
C	2.46407	1.69447	-0.90752
H	2.59655	0.61179	-1.02215
C	-0.55312	3.78345	-1.85839
H	-0.87083	4.82461	-1.77479
C	-1.10716	-3.22507	-3.43484
H	-1.78869	-4.04365	-3.14678
H	-1.70164	-2.30056	-3.44082
H	-0.79225	-3.41881	-4.47367
C	1.97091	-2.33774	-5.44218
H	3.02557	-2.47256	-5.1517
H	1.46633	-3.30578	-5.29789
H	1.95799	-2.11985	-6.52361
C	-1.82395	0.59059	-3.50753
H	-1.40869	-0.41192	-3.34954
C	2.87531	-2.21133	-0.56574
H	2.74499	-1.22564	-0.08877
H	2.04192	-2.84122	-0.21812
H	3.8052	-2.64014	-0.15512
C	0.81839	-4.50567	-2.46108
H	1.31662	-4.73059	-3.41877
H	1.58099	-4.56097	-1.6708
H	0.09971	-5.32191	-2.27389
C	-1.75583	0.89951	-5.00692
H	-0.7194	0.9103	-5.37169
H	-2.31408	0.1451	-5.58323
H	-2.19808	1.8843	-5.22846
C	-3.27684	0.57329	-3.02321
H	-3.78701	1.52622	-3.23628
H	-3.84151	-0.22494	-3.52995
H	-3.34044	0.39924	-1.94029
C	4.127	-1.25454	-2.54849
H	5.05593	-1.60736	-2.06852
H	4.28159	-1.31668	-3.63588
H	4.01667	-0.19042	-2.29724
C	3.44766	2.37407	-1.86861
H	3.38163	3.47124	-1.79418
H	4.48401	2.08258	-1.63633
H	3.23666	2.09447	-2.91131
C	2.77697	2.04609	0.54647
H	2.11533	1.50546	1.24048
H	3.81622	1.77932	0.79134
H	2.6551	3.12169	0.74989

Final Energy: -3276.85737241208 Ha

Table SC4.2. Atomic coordinates and energy of the calculated (hypothetical) sandwich structure of V[(DIPP)N(Si^{i}Pr$_3$)]$_2$ with def2-SVP basis set.

Charge = 0, Multiplicity = 4

	x	*y*	*z*
V	0.01957	0.00699	0.68905
Si	2.63439	-4.04803	-0.74916
Si	-2.71157	3.8648	-0.94433
N	1.20962	-3.29482	-0.23231
N	-1.26998	3.07955	-0.51991
C	0.30416	-2.51662	0.228
C	0.18224	-2.15592	1.66363
C	-0.31194	2.43903	0.04881
C	-0.18887	2.21193	1.51278

C	-0.67246	-1.81895	-0.64733
C	-1.78798	-1.16872	-0.10734
C	1.85211	1.16381	-0.13774
C	0.76125	1.78827	-0.7462
C	-1.93386	-0.9684	1.27847
C	1.95081	1.02469	1.26142
C	3.96984	-2.67564	-0.78951
C	-0.94829	-1.48713	2.14097
C	4.04527	-1.90137	0.53019
C	-0.56786	-2.04285	-2.14071
C	-4.14801	2.62104	-0.7014
C	-1.1673	2.88623	2.45337
C	-1.27499	-0.98029	-2.98062
C	1.1482	-2.77663	2.65316
C	0.94378	1.59762	2.05914
C	0.76019	2.04575	-2.23545
C	-1.10073	-3.43878	-2.48761
C	1.55769	1.04898	-3.06955
C	-2.9876	5.49787	0.02808
C	-3.75209	5.42257	1.35275
C	1.26593	3.4757	-2.48103
C	3.16161	-5.53321	0.34432
C	0.45408	-3.93092	3.38795
C	-1.78064	1.96257	3.50475
C	-0.49274	4.08976	3.12434
C	2.47875	-4.75032	-2.52481
C	-4.1202	1.97598	0.68557
C	1.75833	-1.78893	3.64582
C	-2.76173	4.50412	-2.75703
C	-4.11798	1.5291	-1.77855
C	-1.65535	6.23922	0.19124
C	3.68509	-1.69868	-1.93421
C	1.94697	-6.31536	0.85855
C	4.12022	-5.22087	1.49805
H	-2.53741	-0.73639	-0.77247
H	2.63614	0.72765	-0.75909
H	-2.80512	-0.44895	1.67162
H	2.81113	0.5306	1.70853
H	-1.04943	-1.31252	3.21586
H	4.77175	-1.07191	0.46645
H	4.33642	-2.53172	1.38141
H	3.06293	-1.46584	0.76934
H	0.50984	-2.03731	-2.37615
H	-1.97556	3.26472	1.81723
H	-2.37032	-1.08822	-2.93248
H	-0.98925	-1.07934	-4.03824
H	-1.02639	0.04004	-2.65725
H	1.95826	-3.20538	2.04797
H	1.01947	1.4997	3.14562
H	-0.29353	2.01248	-2.54808
H	-2.18783	-3.48873	-2.31418
H	-0.61414	-4.20167	-1.86897
H	-0.91065	-3.67846	-3.54523
H	2.64302	1.14758	-2.9081
H	1.373	1.22779	-4.13924
H	1.27843	0.00999	-2.85028
H	-4.74185	4.95557	1.23144
H	-3.9143	6.43113	1.77049
H	-3.20624	4.84857	2.11781
H	2.31069	3.57592	-2.14531
H	0.65263	4.2088	-1.93954
H	1.23256	3.72122	-3.55387
H	-0.3013	-3.55324	4.09671
H	1.18189	-4.52717	3.95945
H	-0.05826	-4.60131	2.68325
H	-1.0157	1.53201	4.17194
H	-2.33425	1.13481	3.04399
H	-2.48411	2.52479	4.13762
H	0.26262	3.76277	3.85757
H	-1.23187	4.70629	3.65882
H	0.01457	4.72876	2.38818
C	3.84491	-5.05506	-3.15354
H	2.00278	-3.93949	-3.10754
C	1.58016	-5.98844	-2.62665
H	-4.92062	1.22364	0.798
H	-4.23711	2.70492	1.49997
H	-3.15719	1.46676	0.83799
H	0.98976	-1.2891	4.25853
H	2.34105	-1.01279	3.13289
H	2.43488	-2.31444	4.3368
C	-4.19497	4.88409	-3.16328
C	-2.11424	3.63689	-3.83938
H	-4.34505	1.91962	-2.78036
H	-4.85258	0.73327	-1.56384
H	-3.12288	1.05838	-1.83446
H	-1.14828	6.3953	-0.77436

H	-0.96331	5.66901	0.82775
H	-1.79678	7.23063	0.65434
H	3.71878	-2.17409	-2.92527
H	4.40669	-0.86261	-1.94491
H	2.68018	-1.26417	-1.81984
H	1.27868	-6.64227	0.0493
H	1.34645	-5.69474	1.53837
H	2.25908	-7.21518	1.41588
H	5.03917	-4.72253	1.15336
H	4.42438	-6.14598	2.01707
H	3.6504	-4.57124	2.25536
H	4.94653	-3.16175	-0.97082
H	-5.09088	3.18888	-0.80632
H	-3.61171	6.10225	-0.65463
H	3.71103	-6.19094	-0.35602
H	3.73426	-5.44094	-4.18139
H	4.38565	-5.82727	-2.58048
H	4.49886	-4.17184	-3.20432
H	1.39241	-6.25827	-3.68
H	0.60166	-5.84572	-2.14548
H	2.05597	-6.86221	-2.15173
H	-2.24579	4.09178	-4.83643
H	-2.54939	2.62637	-3.88544
H	-1.03699	3.5247	-3.6749
H	-2.18161	5.44602	-2.71461
H	-4.82363	3.9913	-3.31192
H	-4.20179	5.44227	-4.11459
H	-4.70076	5.51378	-2.4148

Final energy: -3276.8274802554 Ha

Table SC4.3. Atomic coordinates and energy of the calculated sandwich structure of V[(DIPP)N(Si^{t}Bu$_2$Me)]$_2$ with def2-SVP basis set.

Charge = 0, Multiplicity = 4

	x	*y*	*z*
V	0.01838	0.02793	0.84894
Si	2.64376	-3.84644	-0.88325
Si	-2.67481	3.77667	-1.06785
N	1.40294	-3.12019	0.01119
N	-1.40174	3.10929	-0.17236
C	0.40967	-2.42992	0.43556
C	0.27785	-2.06605	1.86981
C	-0.39352	2.4507	0.26638
C	-0.21072	2.19308	1.71839
C	-0.64515	-1.85515	-0.43273
C	-1.77087	-1.22775	0.11359
C	1.77597	1.22613	-0.04144
C	0.63025	1.81073	-0.59394
C	-1.8944	-0.9793	1.49492
C	1.94916	1.08051	1.34942
C	4.13661	-2.62043	-0.82399
C	-0.87781	-1.44853	2.35334
C	4.26909	-1.9778	0.56349
C	-0.5815	-2.17362	-1.91006
C	-4.15504	2.54614	-0.89455
C	-1.21964	2.79045	2.67699
C	-1.39239	-1.23452	-2.7987
C	1.31622	-2.59999	2.83426
C	0.96309	1.61391	2.20607
C	0.51883	2.02119	-2.08803
C	-5.4954	3.19038	-1.27304
C	-1.01804	-3.62873	-2.13372
C	1.30292	1.02024	-2.93259
C	-2.98601	5.55017	-0.38077
C	-3.59563	5.5016	1.02721
C	0.94591	3.45599	-2.42998
C	2.96461	-5.58059	-0.10552
C	0.83586	-3.94601	3.39029
C	-1.56916	1.90482	3.87096
C	-0.72444	4.16777	3.13403
C	5.46062	-3.29639	-1.20428
C	2.30207	-4.1667	-2.72355
C	-4.24137	1.98209	0.53002
C	1.6969	-1.64178	3.96079
C	-2.38489	3.9956	-2.93152
C	-3.90151	6.37515	-1.29918
C	-3.87799	1.37746	-1.85432
C	-1.61696	6.24834	-0.30482

C	3.83974	-1.50452	-1.83952
C	1.59429	-6.26396	0.04519
C	3.61118	-5.45764	1.28133
C	3.8519	-6.46154	-0.99913
H	-2.55656	-0.86271	-0.54961
H	2.53819	0.81081	-0.70227
H	-2.77171	-0.46736	1.88906
H	2.84158	0.5998	1.74893
H	-0.96634	-1.25463	3.42526
H	5.102	-1.25087	0.57458
H	4.46866	-2.71968	1.3515
H	3.34682	-1.4447	0.83956
H	0.48014	-2.0969	-2.19275
H	-2.13034	2.94773	2.08383
H	-2.47634	-1.38172	-2.66942
H	-1.1643	-1.42704	-3.85746
H	-1.17053	-0.17863	-2.59177
H	2.21012	-2.79479	2.22684
H	1.08758	1.49655	3.28558
H	-0.5508	1.92593	-2.33256
H	-5.46648	3.65072	-2.27386
H	-5.79321	3.96984	-0.5551
H	-6.29973	2.4328	-1.28495
H	-2.08684	-3.74633	-1.8931
H	-0.44462	-4.3182	-1.50053
H	-0.8693	-3.92123	-3.18427
H	2.39024	1.17515	-2.84861
H	1.04177	1.13827	-3.99465
H	1.08955	-0.01871	-2.64638
H	-4.61329	5.08063	1.02047
H	-3.66415	6.51704	1.4576
H	-2.9853	4.89386	1.71018
H	2.0216	3.5896	-2.23234
H	0.39187	4.18965	-1.83027
H	0.76317	3.67255	-3.49345
H	-0.06319	-3.81658	4.0148
H	1.61524	-4.41644	4.00947
H	0.5877	-4.64069	2.57577
H	-0.70125	1.70863	4.52167
H	-1.97545	0.93749	3.54488
H	-2.33218	2.39623	4.49291
H	0.19049	4.07665	3.74196
H	-1.48711	4.67885	3.74162
H	-0.49622	4.80882	2.27113
H	5.39876	-3.81198	-2.17623
H	5.77449	-4.03679	-0.45274
H	6.26911	-2.54742	-1.28424
H	3.22904	-4.47222	-3.23567
H	1.92007	-3.27333	-3.2394
H	1.56676	-4.9731	-2.86626
H	-5.06283	1.24605	0.60637
H	-4.43052	2.76463	1.2805
H	-3.30477	1.47721	0.81042
H	0.84981	-1.41458	4.62861
H	2.08354	-0.69164	3.56678
H	2.48482	-2.08958	4.5847
H	-3.32594	4.26937	-3.43575
H	-2.01085	3.07709	-3.40734
H	-1.65742	4.79605	-3.13487
H	-3.47491	6.49231	-2.3074
H	-4.04116	7.38974	-0.88452
H	-4.90049	5.9272	-1.40815
H	-3.94943	1.67995	-2.91025
H	-4.60675	0.56117	-1.69585
H	-2.87043	0.96223	-1.69834
H	-1.14747	6.34205	-1.29791
H	-0.91847	5.694	0.3395
H	-1.7235	7.26866	0.10532
H	3.89013	-1.86251	-2.87914
H	4.57051	-0.68088	-1.73915
H	2.83483	-1.08171	-1.68562
H	1.09696	-6.40568	-0.92846
H	0.91743	-5.67163	0.67881
H	1.7056	-7.26239	0.50484
H	4.62792	-5.03806	1.22591
H	3.69202	-6.44932	1.76195
H	3.01769	-4.81554	1.94757
H	3.40236	-6.62941	-1.99007
H	3.99265	-7.45368	-0.53363
H	4.85169	-6.02919	-1.1537

Final energy: -3276.84758640603 Ha

Table SC4.4. Atomic coordinates and energy of the calculated (hypothetical) linear structure of V[N(Si^{t}Bu$_2$Me)DIPP]$_2$ with def2-SVP basis set.

Charge = 0, Multiplicity = 4

	x	*y*	*z*
V	-0.00452	-0.00209	-0.00078
Si	-0.98848	1.18886	2.92078
N	-0.38436	-0.14837	1.95529
C	0.01062	-1.41715	2.44035
C	-0.87047	-2.52763	2.28569
C	1.31382	-1.64355	2.96522
C	0.40027	2.39364	3.38374
H	0.91926	2.74948	2.47949
C	-1.85487	0.69955	4.57884
C	-0.79162	0.22641	5.58547
C	1.68472	-2.93659	3.34528
H	2.6848	-3.10474	3.7547
C	-0.44233	-3.80216	2.66295
H	-1.11468	-4.65338	2.53795
C	-2.13144	2.18781	1.71664
C	-2.22018	3.67291	2.10533
C	-2.8775	-0.43601	4.43735
H	-3.40206	-0.58708	5.39774
H	-2.37879	-1.38186	4.18806
H	-3.64392	-0.24012	3.67398
C	-2.26203	-2.3516	1.683
H	-2.56319	-1.31726	1.89187
C	0.8233	-4.0158	3.19857
H	1.13606	-5.01904	3.49518
C	-2.55961	1.93308	5.17117
H	-3.41857	2.25534	4.56333
H	-1.88128	2.79387	5.28109
H	-2.94734	1.6949	6.17752
C	2.34807	-0.52964	3.08724
H	1.89105	0.37828	2.67439
C	-1.48535	2.11382	0.32776
H	-1.69348	1.12549	-0.13828
H	-0.40898	2.35441	0.33434
H	-1.9318	2.81612	-0.39543
C	2.72844	-0.25128	4.54576
H	1.84951	-0.03133	5.1636
H	3.41444	0.60814	4.61032
H	3.23881	-1.11867	4.99419
C	3.62101	-0.80292	2.2749
H	4.13612	-1.71224	2.62253
H	4.32622	0.03598	2.38236
H	3.41837	-0.92712	1.20373
C	-3.54894	1.60766	1.61055
H	-4.12598	2.13728	0.83163
H	-4.10747	1.70771	2.55251
H	-3.53585	0.53878	1.34108
C	-3.31474	-3.27762	2.29991
H	-3.18055	-4.32379	1.98222
H	-4.32208	-2.97022	1.97956
H	-3.28627	-3.2544	3.39884
C	-2.27483	-2.51679	0.15803
H	-1.69882	-1.72914	-0.35839
H	-3.30136	-2.45422	-0.23582
H	-1.85212	-3.4884	-0.14532
Si	0.98305	-1.18937	-2.92189
N	0.38038	0.14776	-1.95543
C	-0.00818	1.41907	-2.43906
C	0.87786	2.52503	-2.28017
C	-1.30908	1.65249	-2.96656
C	-0.40926	-2.38924	-3.38653
H	-0.92876	-2.7447	-2.48239
C	1.85306	-0.70105	-4.57859
C	0.79329	-0.22513	-5.58754
C	-1.67236	2.94801	-3.34578
H	-2.67049	3.12181	-3.75761
C	0.45715	3.80222	-2.65661
H	1.13343	4.64985	-2.52838
C	2.12335	-2.19271	-1.71854
C	2.20745	-3.6778	-2.10828
C	2.87815	0.43202	-4.43464
H	3.40383	0.5833	-5.39438
H	2.3814	1.37867	-4.18429
H	3.64354	0.23327	-3.67099
C	2.26673	2.34083	-1.67382
H	2.56318	1.30544	-1.88437

C	-0.806	4.02272	-3.19534
H	-1.11315	5.02792	-3.4912
C	2.55582	-1.93602	-5.17035
H	3.41294	-2.2609	-4.56139
H	1.87543	-2.79495	-5.28214
H	2.94589	-1.69811	-6.17585
C	-2.3488	0.54411	-3.09343
H	-1.8987	-0.3663	-2.67836
C	1.47726	-2.11775	-0.32973
H	1.68549	-1.12913	0.1354
H	0.40082	-2.35789	-0.33687
H	1.92329	-2.8198	0.39401
C	-2.72339	0.26774	-4.55385
H	-1.84294	0.04095	-5.16694
H	-3.41548	-0.58652	-4.6218
H	-3.22493	1.13879	-5.00517
C	-3.62478	0.82441	-2.28816
H	-4.13366	1.73561	-2.63995
H	-4.33337	-0.0112	-2.39875
H	-3.42759	0.94899	-1.21604
C	3.54264	-1.61717	-1.61143
H	4.11712	-2.14843	-0.83174
H	4.1018	-1.71918	-2.55278
H	3.5329	-0.54825	-1.34209
C	3.32575	3.26304	-2.28547
H	3.19558	4.30915	-1.96589
H	4.33053	2.95005	-1.96253
H	3.30063	3.24229	-3.38453
C	2.27598	2.50249	-0.14839
H	1.69435	1.71708	0.36519
H	3.30101	2.43359	0.2483
H	1.85774	3.4758	0.15572
H	0.00903	3.2774	3.91048
H	1.15302	1.92843	4.03418
H	-0.24593	-0.65583	5.21649
H	-1.27631	-0.06326	6.53485
H	-0.06022	1.01421	5.82248
H	-2.885	4.20966	1.40583
H	-1.23851	4.16797	2.06346
H	-2.62361	3.818	3.11777
H	-0.02163	-3.27346	-3.91518
H	-1.1609	-1.91996	-4.03536
H	1.28063	0.06	-6.53694
H	0.25146	0.66057	-5.22124
H	0.05842	-1.00998	-5.82362
H	2.61064	-3.82354	-3.12069
H	1.2241	-4.16961	-2.06714
H	2.87029	-4.21724	-1.40897

Final energy: -3276.86128533836 Ha

REFERENCES FOR EXPERIMENTAL DETAILS, SUPPLEMENTARY FIGURES, SINGLE-CRYSTAL X-RAY DIFFRACTION CRYSTAL STRUCTURE DETAILS, AND COMPUTATIONAL DETAILS

(1) Calderazzo, F., De Benedetto, G. E., Pampaloni, G., Mössmer, C. M., Strähle, J., Wurst, K. *J. Organomet. Chem.* **1993**, *451* (1), 73–81.
(2) Cai, I. C., Lipschutz, M. I., Tilley, T. D. *Chem. Commun.* **2014**, *50* (86), 13062–13065.
(3) Bergbreiter, D. E., Killough, J. M. *J. Am. Chem. Soc.* **1978**, *100* (7), 2126–2134.
(4) Maruani, A., Alom, S., Canavelli, P., Lee, M. T. W., Morgan, R. E., Chudasama, V., Caddick, S. *Chem. Commun.* **2015**, *51* (25), 5279–5282.
(5) Spinney, H. A., Clough, C. R., Cummins, C. C. *Dalton Trans.* **2015**, *44* (15), 6784–6796.
(6) Kuprat, M., Lehmann, M., Schulz, A., Villinger, A. *Organometallics* **2010**, *29* (6), 1421–1427.
(7) Fulmer, G. R., Miller, A. J. M., Sherden, N. H., Gottlieb, H. E., Nudelman, A., Stoltz, B. M., Bercaw, J. E., Goldberg, K. I. *Organometallics* **2010**, *29* (9), 2176–2179.
(8) Evans, D. F. *J. Chem. Soc. Resumed* **1959**, No. 0, 2003–2005.
(9) Sur, S. K. *J. Magn. Reson. 1969* **1989**, *82* (1), 169–173.
(10) Grant, D. H. *J. Chem. Educ.* **1995**, *72* (1), 39–40.
(11) Dolomanov, O. V., Bourhis, L. J., Gildea, R. J., Howard, J. a. K., Puschmann, H. *J. Appl. Crystallogr.* **2009**, *42* (2), 339–341.
(12) Sheldrick, G. M. *Acta Crystallogr. Sect. Found. Adv.* **2015**, *71* (1), 3–8.
(13) Sheldrick, G. M. *Acta Crystallogr. Sect. C Struct. Chem.* **2015**, *71* (1), 3–8.
(14) Shao, Y., Gan, Z., Epifanovsky, E., Gilbert, A. T. B., Wormit, M., Kussmann, J., Lange, A. W., Behn, A., Deng, J., Feng, X., Ghosh, D., Goldey, M., Horn, P. R., Jacobson, L. D., Kaliman, I., Khaliullin, R. Z., Kuś, T., Landau, A., Liu, J., Proynov, E. I., Rhee, Y. M., Richard, R. M., Rohrdanz, M. A., Steele, R. P., Sundstrom, E. J., III, H. L. W., Zimmerman, P. M., Zuev, D., Albrecht, B., Alguire, E., Austin, B., Beran, G. J. O., Bernard, Y. A., Berquist, E., Brandhorst, K., Bravaya, K. B., Brown, S. T., Casanova, D., Chang, C.-M., Chen, Y., Chien, S. H., Closser, K. D., Crittenden, D. L., Diedenhofen, M., Jr, R. A. D., Do, H., Dutoi, A. D., Edgar, R. G., Fatehi, S., Fusti-Molnar, L., Ghysels, A., Golubeva-Zadorozhnaya, A., Gomes, J., Hanson-Heine, M. W. D., Harbach, P. H. P., Hauser, A. W., Hohenstein, E. G., Holden, Z. C., Jagau, T.-C., Ji, H., Kaduk, B., Khistyaev, K., Kim, J., Kim, J., King, R. A., Klunzinger, P., Kosenkov, D., Kowalczyk, T., Krauter, C. M., Lao, K. U., Laurent, A. D., Lawler, K. V., Levchenko, S. V., Lin, C. Y., Liu, F., Livshits, E., Lochan, R. C., Luenser, A., Manohar, P., Manzer, S. F., Mao, S.-P., Mardirossian, N., Marenich, A. V., Maurer, S. A., Mayhall, N. J., Neuscamman, E., Oana, C. M., Olivares-Amaya, R., O'Neill, D. P., Parkhill, J. A., Perrine, T. M., Peverati, R., Prociuk, A., Rehn, D. R., Rosta, E., Russ, N. J., Sharada, S. M., Sharma, S., Small, D. W., Sodt, A., Stein, T., Stück, D., Su, Y.-C., Thom, A. J. W., Tsuchimochi, T., Vanovschi, V., Vogt, L., Vydrov, O., Wang, T., Watson, M. A., Wenzel, J., White, A., Williams, C. F., Yang, J., Yeganeh, S., Yost, S. R., You, Z.-Q., Zhang, I. Y., Zhang, X., Zhao, Y., Brooks, B. R., Chan, G. K. L., Chipman, D. M., Cramer, C. J., III, W. A. G., Gordon, M. S., Hehre, W. J., Klamt, A., III, H. F. S., Schmidt, M. W., Sherrill, C. D., Truhlar, D. G., Warshel, A., Xu, X., Aspuru-Guzik, A., Baer, R., Bell, A. T., Besley, N. A., Chai, J.-D., Dreuw, A., Dunietz, B. D., Furlani, T. R., Gwaltney, S. R., Hsu, C.-P., Jung, Y., Kong, J., Lambrecht, D. S., Liang, W., Ochsenfeld, C., Rassolov, V. A., Slipchenko, L. V., Subotnik, J. E.,

Voorhis, T. V., Herbert, J. M., Krylov, A. I., Gill, P. M. W., Head-Gordon, M. *Mol. Phys.* **2015**, *113* (2), 184–215.
(15) Chai, J.-D., Head-Gordon, M. *Phys. Chem. Chem. Phys.* **2008**, *10* (44), 6615–6620.

CONCLUSION

Prior to this work, few efforts had been focused on the synthesis of two-coordinate complexes of early first-row transition metals, let alone understanding the reactivity of these species. Although the easily accessible silylarylamido ligand –N(SiMe$_3$)DIPP readily supported low-coordinate complexes of metals such as manganese, iron, cobalt, and nickel, this specific ligand platform appeared to be less amenable to supporting stable two-coordinate complexes of chromium, an earlier transition metal. The challenges of accessing such a species, however, also highlighted the potential reactivity that could be mediated by a coordinatively unsaturated early transition metal center.

To circumvent the undesirable C–H bond activations previously reported for the addition of LiN(SiMe$_3$)DIPP to chromium(II) chloride, nucleophilic methyl groups were substituted for more sterically demanding isopropyl groups. The corresponding silylarylamido ligand, –N(Si^{i}Pr$_3$)DIPP, was then used to support two-coordinate complexes of chromium in the +1, +2, and +3 oxidation states. Furthermore, the neutral chromium(II) bis(amido) complex could be used to access a three-coordinate chromium(III) methyl species, *via* an isolable chromium(III) bis(amido) iodide complex. This initial study demonstrated the feasibility of accessing two-coordinate silylarylamido complexes of chromium, as well as low-coordinate derivatives.

Consequently, the syntheses of the chromium(III) iodide and methyl complexes supported by –N(Si^{i}Pr$_3$)DIPP prompted a reinvestigation into the use of –N(SiMe$_3$)DIPP, albeit in the context of chromium(III) species. Addition of the lithium amide salt to CrCl$_3$·3(THF) readily afforded the chromium bis(amido) chloride complex, (Cl)Cr[N(SiMe$_3$)DIPP]$_2$, which not only provided access to the chromium(III) bis(amido) methyl complex but also the analogous benzyl derivative. Despite the lack of previously reported mononuclear chromium(II) species supported by the silylarylamido ligand –N(SiMe$_3$)DIPP, these chromium(III) bis(amido) alkyl complexes could be reduced to their anionic chromium(II) analogs. Similarly, the chromium(III) chloride complex provided access, *via* an isolable base-stabilized chromium(II) bis(amido) intermediate, to a two-coordinate anionic chromium(I) species. Upon reduction of the chromium(III) chloride complex in the presence of a bulky base, C–H bond activation was induced. This wide range of low-coordinate chromium complexes supported by –N(SiMe$_3$)DIPP, in comparison with the few complexes supported by –N(Si^{i}Pr$_3$)DIPP, demonstrates the resulting trade-offs between reactivity and stability in the context of two-coordinate chemistry.

Similar comparisons were also observed for manganese bis(amido) complexes supported by –N(SiMe$_3$)DIPP and –N(Si^{i}Pr$_3$)DIPP. Although both bis(amido) complexes of manganese readily support a pyridine N-oxide adduct, the bulkier amido ligand enforces linearity within the pyridine N-oxide ligand; this geometry is not observed for the less bulky amido ligand. These differences in steric bulk have a much more profound effect on the coordination chemistry of anionic manganese(I) species. While –N(SiMe$_3$)DIPP and –N(Si^{i}Pr$_3$)DIPP could both be used to access two-coordinate complexes of manganese(I), the less sterically demanding amido ligand provides access to a dinitrogen-bound manganese dimer with arene-bound potassium cations. Although the impacts of steric bulk can often be predicted, it remains to be seen how structure and reactivity are affected by the participation of alkali metals in low-coordinate transition metal chemistry.

Although a number of two-coordinate complexes have already been reported for chromium and manganese, there have been relatively few reports of two- and three-coordinate complexes of vanadium. Gratifyingly, the silylarylamido ligand –N(Si^{i}Pr$_3$)DIPP was found to support a two-

coordinate complex of vanadium(II). However, an alternative binding mode was observed upon the reduction of this species, resulting in a vanadium(I) metal center sandwiched between arene rings. These complexes were characterized and compared to vanadium sandwich species supported by the silylarylamido isomer –N(Si^{t}Bu$_2$Me)DIPP. Although –N(Si^{t}Bu$_2$Me)DIPP readily supports two-coordinate chromium(II), this ligand does not readily support a two-coordinate amido-bound complex of vanadium. Despite the challenges observed with synthesizing two-coordinate vanadium species, the bulky amido ligand –N(Si^{i}Pr$_3$)DIPP can still be used to access several low-coordinate derivatives. Moreover, upon oxidation of V[N(Si^{i}Pr$_3$)DIPP]$_2$ in the presence of a non-coordinating anion, ligand C–H bond activation can be observed. The bulky ligand –N(Si^{i}Pr$_3$)DIPP provides access to a stable vanadium(II) complex that is two-coordinate in the solid-state, in addition to a wide range of reactivity.

These studies demonstrate the relationship between structure and reactivity for low-coordinate silylarylamido complexes of early first-row transition metals. The challenges of working with these paramagnetic species necessitates an iterative process, in which stable species supported by sterically demanding ligands are often synthesized as proof-of-concept before a more reactive (and often more interesting) analog supported by a less bulky analog can be investigated. Although silylarylamido ligands can formally be described as X-type ligands, the ability of silylarylamido ligands to support low-coordinate species should not be underestimated. For complexes of chromium, manganese, and vanadium, the arene moiety within the silylarylamido ligand likely plays an important role in complex stabilization. The approaches taken in this work will hopefully inspire further investigations in two-coordinate chemistry, of existing species and perhaps even those of earlier first-row transition metals.